



PHD

**Crystal growth and characterization of I-IV2-V3 semiconductor compounds and alloys based thereon.**

Omar, Mustafa Saeed

*Award date:*  
1985

*Awarding institution:*  
University of Bath

[Link to publication](#)

## Alternative formats

If you require this document in an alternative format, please contact:  
[openaccess@bath.ac.uk](mailto:openaccess@bath.ac.uk)

### General rights

Copyright and moral rights for the publications made accessible in the public portal are retained by the authors and/or other copyright owners and it is a condition of accessing publications that users recognise and abide by the legal requirements associated with these rights.

- Users may download and print one copy of any publication from the public portal for the purpose of private study or research.
- You may not further distribute the material or use it for any profit-making activity or commercial gain
- You may freely distribute the URL identifying the publication in the public portal ?

### Take down policy

If you believe that this document breaches copyright please contact us providing details, and we will remove access to the work immediately and investigate your claim.

CRYSTAL GROWTH AND CHARACTERIZATION OF I-IV<sub>2</sub>-V<sub>3</sub> SEMICONDUCTOR  
COMPOUNDS AND ALLOYS BASED THEREON

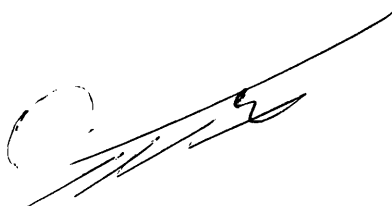
submitted by Mustafa Saeed Omar  
for the degree of Doctor of Philosophy  
of the University of Bath

1985

Copyright

Attention is drawn to the fact that copyright of this thesis rests with its author. This copy of the thesis has been supplied on condition that anyone who consults it is understood to recognise that its copyright rests with its author and that no quotation from the thesis and no information derived from it may be published without the prior written consent of the author.

This thesis may be made available for consultation within the University Library and may be photocopied or lent to other libraries for the purpose of consultation.

A handwritten signature or scribble, possibly in ink, consisting of several overlapping, diagonal lines and a small circular mark on the left side.

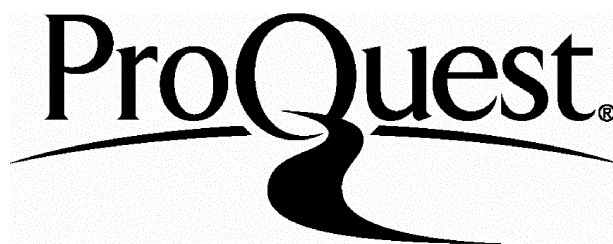
ProQuest Number: U362245

All rights reserved

INFORMATION TO ALL USERS

The quality of this reproduction is dependent upon the quality of the copy submitted.

In the unlikely event that the author did not send a complete manuscript and there are missing pages, these will be noted. Also, if material had to be removed, a note will indicate the deletion.



ProQuest U362245

Published by ProQuest LLC(2015). Copyright of the Dissertation is held by the Author.

All rights reserved.

This work is protected against unauthorized copying under Title 17, United States Code.  
Microform Edition © ProQuest LLC.

ProQuest LLC  
789 East Eisenhower Parkway  
P.O. Box 1346  
Ann Arbor, MI 48106-1346

*To my Family*

## ACKNOWLEDGEMENTS

The author wishes to express his sincere appreciation and gratitude to Dr. B.R. Pamplin for his interest, inspiration and guidance throughout this investigation. The author would also like to thank all the staff and researchers in the School of Physics; particularly Dr. W.C. Clark for many useful discussions and Prof. G.A. Saunders for providing the facilities.

I am especially grateful to Mr. R.C.J. Draper and Mr. B. Chapman in overcoming many technical difficulties. Thanks also to Mrs. W.A. Lambosn for cutting the crystals.

The author would also like to thank Dr. R.A.L. Sullivan for many crystallographic explanations; and Mr. F.S. Hasoon and Dr. J.E. MacDonald for thir assistance. Thanks also to Dr. A.A. Woolf of the School of Chemistry for the chemical analysis and Mr. H. Perrott of the School of Materials Science for the EPMA.

I am indebted to my cousin, M.A. Hamad and my dear friends S.S. Karim and F.H. Ahmed, for their endless assistance and encouragement whilst working towards this degree.

Mrs. Paula Keilthy has patiently typed this thesis - it is a pleasure to thank her.

This work has been entirely supported by the General Secretariat for Higher Education in Arbil, Iraq, which grant is gratefully acknowledged.

## ABSTRACT

The existence of various ternary adamantine compounds is discussed. Normal and defect ternary adamantine compounds have been a subject of discussion, particularly from a structural point of view. Rules for the formation of adamantine compounds are explained and related to each other.

A home-made DTA apparatus was operated to detect the melting point and phase change from room temperature up to 1300 °C for the materials investigated.

The group I-IV<sub>2</sub>-V<sub>3</sub> compounds were the main subject of this research. CuGe<sub>2</sub>P<sub>3</sub> and CuSi<sub>2</sub>P<sub>3</sub> were the only compounds found to grow in this family. The first was chosen for study in more detail, mainly because of its lower melting point.

CuGe<sub>2</sub>P<sub>3</sub> was compared to other compounds, particularly structural aspects, and solid solutions were tried for twenty-two different materials. This investigation shows similarity with group I<sub>2</sub>-IV-V<sub>3</sub> compounds, such as Cu<sub>2</sub>GeS<sub>3</sub>, and new alloys were found with Cu<sub>2</sub>GeS<sub>3</sub>. Stoichiometric Cu<sub>2</sub>GeS<sub>3</sub> does not form good material, but alloys containing 10% CuGe<sub>2</sub>P<sub>3</sub> produced good material with a zincblend structure.

As well as alloys with ternary compounds, about 33% Ge per mole could be dissolved in CuGe<sub>2</sub>P<sub>3</sub>. This result showed similarity with the compounds Cu<sub>2</sub>GeSe<sub>3</sub> and ZnGeAs<sub>2</sub>, which also dissolve a considerable quantity of Ge.

In this investigation, only a maximum of 33% Si per mole in CuSi<sub>2</sub>P<sub>3</sub> was prepared, although it is likely that even more Si can be dissolved.

Attention was also given to  $\text{AgGe}_2\text{P}_3$ . Chemical analysis of single crystals grown from  $\text{AgGe}_2\text{P}_3$  composition showed the existence of only the  $\text{Ag}_6\text{Ge}_{10}\text{P}_{12}$  compound.

Single crystals were grown for all single phase materials. A new modification of the directional freeze technique was employed, which was capable of controlling the pressure and having a steep temperature gradient. This method improved the growth to produce large single crystals of cm dimensions.

The  $\text{CuGe}_2\text{P}_3$  crystals doped with Zn, S, Sn, Se and ZnIn were prepared. Single crystals of  $\text{CuGe}_2\text{P}_3$  were also annealed with Cu-P and  $\text{CuGe}_2\text{P}_3$  powder.

Room temperature lattice parameters were determined for all the compounds and alloys, while variations of the lattice parameters with temperatures up to the melting point of  $\text{CuGe}_2\text{P}_3$  were studied using a high temperature X-ray camera.

Measurements of optical properties were not successful in this investigation, although electrical properties were successfully measured. These measurements were carried out for all materials in a single crystal form. Hall mobility and conductivity measurements were carried out from liquid nitrogen to 450 °K. Carrier concentration was very high for phosphide compounds and alloys, whilst it was lower for sulphides.

Flash evaporation was used for preparing thin films of compounds  $\text{CuGe}_2\text{P}_3$  and  $\text{Ag}_6\text{Ge}_{10}\text{P}_{12}$ . Single phase films were the result for  $\text{Ag}_6\text{Ge}_{10}\text{P}_{12}$ , whilst a particular treatment was employed for producing films of  $\text{CuGe}_2\text{P}_3$  after evaporation.

A final investigation of the compound  $\text{CuGe}_2\text{P}_3$  was made into its lattice matching with other compounds. The  $p$ - $n$  junctions were produced with  $n$ -type GaP, using epitaxial growth, while results were negative with CdS and Si.



## CONTENTS

	<u>Page</u>	
CHAPTER 1	General introduction	1
CHAPTER 2	Formation of Ternary Adamantine Compounds	3
	2.1 Introduction	3
	2.2 General Characteristics for Adamantine Compounds	3
	2.3 The Third Rule for Adamantine Structure Compounds	8
	2.4 Extending the Adamantine Family	9
	2.5 Ternary Normal Adamantine Compounds	10
	2.6 Crystal Structure of I-IV <sub>2</sub> -V <sub>3</sub> Type Compounds	17
CHAPTER 3	Crystal Growth	29
	3.1 Introduction	29
	3.2 Primary Considerations for the Synthesis of Ternary Compounds	29
	3.3 Preparation of Ampoules	32
	3.4 Crystal Growth from Melt	32
	3.5 Solution Growth	45
	3.6 Iodine Transport	45
CHAPTER 4	Differential Thermal Analysis and High Temperature Lattice Parameters	53
	4.1 Introduction	53
	4.2 DTA Apparatus	54
	4.3 Differential Thermal Analysis for CuGe <sub>2</sub> P <sub>3</sub>	56
	4.4 DTA for CuGe <sub>2</sub> P <sub>3</sub> -Ge System	63
	4.5 High Temperature Lattice Parameter	68
	4.6 Coefficient of Thermal Expansion	70
	4.7 Discussion	76

## CONTENTS (continued)

	<u>Page</u>
CHAPTER 5 Solid Solutions Based on $\text{CuGe}_2\text{P}_3$	78
5.1 Introduction	78
5.2 X-Ray Crystal Analysis	78
5.3 Electron Probe Microanalysis (EPMA)	80
5.4 Phase Relationships in Ag-Ge-P and Chemical Analysis	80
5.5 Phase Relationships in Cu-Ge-P Systems	84
5.6 The Compound $\text{CuSi}_2\text{P}_3$ and the $\text{CuSi}_2\text{P}_3$ -Si System	99
5.7 Solid Solutions of the $\text{CuGe}_2\text{P}_3$ -I <sub>2</sub> -IV-VI <sub>3</sub> Systems	104
5.8 Other Solid-Solution Systems based on $\text{CuGe}_2\text{P}_3$	116
5.9 Discussion	121
CHAPTER 6 Electrical Properties of I-IV <sub>2</sub> -V <sub>3</sub> Compounds	123
6.1 Introduction	123
6.2 The Measuring System	123
6.3 The Hall Effect	128
6.4 Hall Effect for $\text{Ag}_6\text{Ge}_{10}\text{P}_{12}$	129
6.5 Hall Effect and Conductivity Measurements for $\text{CuGe}_2\text{P}_3$ - $\text{Cu}_2\text{GeS}_3$ System	143
6.6 The Hall Effect and Conductivity Measurements for the $\text{CuSi}_2\text{P}_3$ -Si System	153
6.7 Annealing and Doping Studies of $\text{CuGe}_2\text{P}_3$	157
6.8 Electrical Properties of the $\text{CuGe}_2\text{P}_3$ -Ge System	169
6.9 Electrical Measurement for 80% $\text{CuGe}_2\text{P}_3$ - 20% ${}^{6/7}\text{Ge}_3\text{P}_4$	170
CHAPTER 7 Thin Film Preparation of $\text{CuGe}_2\text{P}_3$ and $\text{Ag}_6\text{Ge}_{10}\text{P}_{12}$	172
7.1 Operation	172
7.2 Film Evaporation Procedure	172
7.3 Annealing Procedure	174
7.4 X-Ray Powder Photography	175
7.5 EPMA and Scanning Electron Microscopy	176

## CONTENTS (continued)

	<u>Page</u>
CHAPTER 8 The $p$ - $n$ Junction of $\text{CuGe}_2\text{P}_3$ -GaP	182
8.1 Introduction	182
8.2 Preparation of the Junction	182
8.3 A Study of Interface Alloying	184
CHAPTER 9 Conclusions and Suggestions for Further Work	189
9.1 Conclusions	189
9.2 Suggestions for Further Work	192
REFERENCES	195

## CHAPTER 1

### General Introduction

Since the discovery of light-emitting diodes and laser beam devices, *etc.*, researchers have tried to investigate new semi-conductors with a wider range of energy gaps and hoped for higher mobilities to replace the traditional silicon and germanium.

Binary compounds of III-V and II-VI types are the first choice for serving in the above-mentioned areas, but the complications involved in preparing some of these binary compounds in a suitable form have delayed their use.

For a wider range of applications, scientists have moved to ternary and multinary compounds. Since binary compounds have higher mobilities than elemental semi-conductors, scientists thought that higher mobilities in ternary compounds might be found in preference to binary compounds. However, some of the ternary compounds were found to be more difficult to grow than their parents. For example, most I-IV<sub>2</sub>-V<sub>3</sub> compounds have not so far been grown successfully, even though their melting points are lower than most other ternary compounds.

Most of the group II-IV-V<sub>2</sub> and I-III-VI<sub>2</sub> compounds were found to be more interesting for the new technology and they have been thoroughly investigated. Their structures are more complicated than the simpler cubic compounds and consequently, their physical properties - particularly their bond structures - are slightly different from their parents. However, these ternary compounds are promising for applications in the areas of visible and infrared light-emitting diodes, infrared detectors, hetero-junction lasers and far infrared generation, *etc.*

Due to the need for particular wavelengths in light-emitting diodes and laser detectors, *etc.*, scientists have realised the importance of investigating new solid-solutions between binary, as well as ternary compounds. Such solid-solutions could produce high conductivity semi-conductors, which are applicable for thermal applications as well.

This thesis is divided into nine chapters. Chapter 2 includes a theoretical explanation of the formation of the ternary adamantine family of semi-conductors. In Chapter 3, the methods of crystal growth are explained, including novel methods developed to grow new single crystals. Three different techniques of crystal growth were used. Chapter 4 contains the temperature dependence of lattice parameters and the differential thermal analysis (DTA) of some of the materials prepared. Both DTA and high temperature X-ray photographs are used for characterising the materials. X-Ray structural analyses of these materials are described in Chapter 5. The formation of the ternary compound  $\text{CuGe}_2\text{P}_3$  and its solid-solutions with other semi-conductors is also described in this chapter. In Chapter 6, a description is given of the Hall effect investigation of the compounds and alloys prepared in this thesis, and the results are compared with theoretical calculations. Chapter 7 contains a description of the development of techniques for the preparation of thin films of  $\text{CuGe}_2\text{P}_3$  and  $\text{Ag}_6\text{Ge}_{10}\text{P}_{12}$ . Chapter 8 gives an account of epitaxial growth of a p-n junction between a p-type  $\text{CuGe}_2\text{P}_3$  on single crystals of n-type GaP.

## CHAPTER 2

### Formation of Ternary Adamantine Compounds

#### 2.1 Introduction

The composition and structural features of tetrahedral structures can be predicted by using two electron rules, the first having as the important parameter the electron-to-atom ratio  $N_E/N$  (also known as valence electron concentration, VEC), and the second using the electron-to-anion ratio,  $N_E/N_A$  [also known as partial valence electron concentration of the anion  $(VEC)_A$ ].

The object of this chapter is to review the general characteristics of the adamantine family of compounds, and systematic prediction of their formation, especially considering the ternary compounds. This group is divided into two sub groups, the normal ternary adamantine compounds and the defect ternary adamantine compounds, which crystallise in zincblende wurtzite, or related structures. All known ternary adamantine compounds with related structures and VEC are shown in Table 2.5.

There is a new crystal structure, related to the diamond lattice, which has been found for the compound  $Ag_6Ge_{10}P_{12}$ . Table 2.4 summarises all compounds having this crystal structure.

#### 2.2 General Characteristics for Adamantine Compounds

The isolated atoms of group IV elements have the  $s^2p^2$  electron configuration in the ground state. If these atoms combine to form a crystal, their electronic configuration changes to a quadrivalent  $sp^3$

state, which is obtained by uncoupling the  $s$  electron pair and transferring one electron from the  $s$  to  $p$  orbitals to form  $sp^3$  hybridisation. The four equivalent  $sp^3$  hybrid orbitals form tetrahedral angles of  $109.4^\circ$  with each other. That is the case of diamond and its analogues, *viz.* silicon, germanium and gray-tin. All four substances have one and the same crystal structure, which consists of two inter-penetrating face centred cubic sub lattices, in which each atom has tetrahedral bonding with its four nearest neighbours.

There is another form of silicon [1] and carbon [2] which is also tetrahedrally bonded to four neighbours. This is the rare Lonsdaleite structure, which consists of two inter-penetrating hexagonal, close packed lattices (symmetry  $P6_3/mmc$  or  $D_{6h}^4$ ).

A perfect  $sp^3$  hybrid should occur only if one atom is bonded to four equal ligand atoms. If the ligands are not identical, the tetrahedrons are most probably slightly distorted and the tetrahedral bonds are bent (as in the case of chalcopyrite). This deviation from the ideal tetrahedral bond angle is made by the wave function of the hybrid orbitals with different amounts of  $s$  wave functions. Further complications arise if  $d$  and  $f$  wave functions also participate in the hybridisation.

It is interesting to use cross-substitution to extend the diamond lattice, following the Grimm-Sommerfeld rule [3] to form new ternary and quaternary compounds. This is done by replacing one atomic species in the structure with two atoms having more or less electrons than the replaced species respectively, in order to keep the electron-to-atom ratio constant.

Two ideal tetrahedral structures for elements are known. Namely the normal, cubic diamond structure and the hexagonal diamond structure.

The crystal structure of compounds where the composition can be derived by cross-substitution should be essentially cubic or hexagonal diamond structures, with ordered atomic arrangements. Examples are well known for structure types geometrically derived from the normal diamond, as shown in Figure 2.1, which brings out the close relationship between the zincblend chalcopyrite, famatinite and stannite structures.

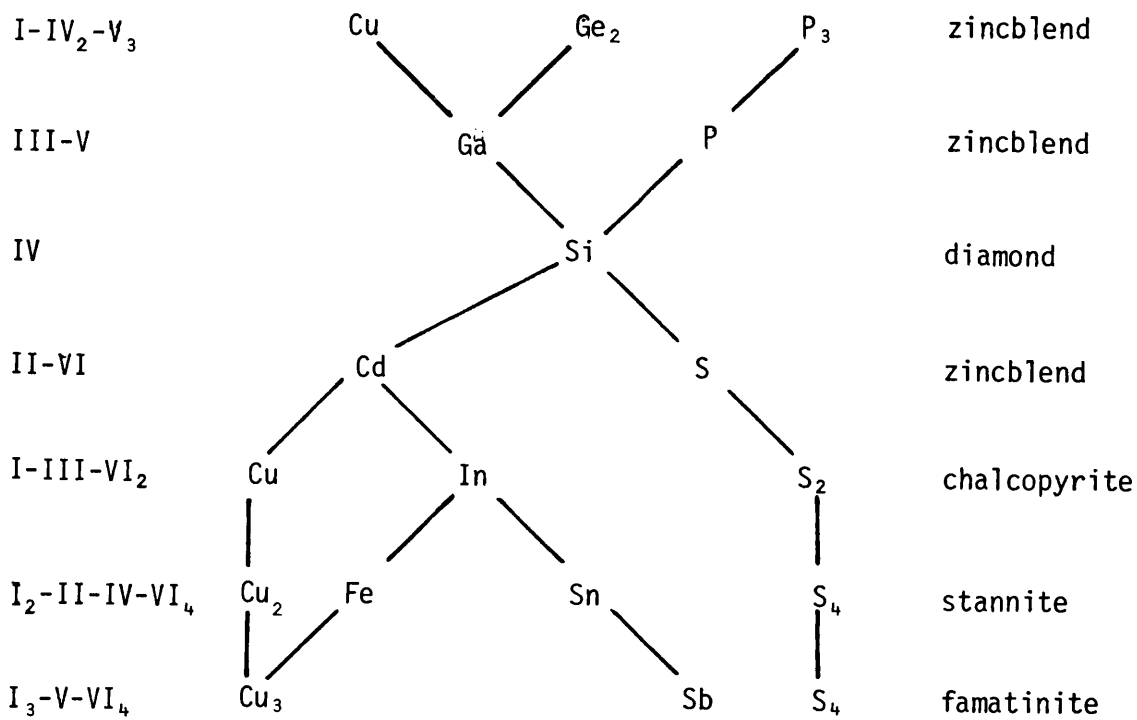


Figure 2.1 Relationship between diamond and normal tetrahedral structures by the cross-substitution rule.

For all adamantine compounds, the average number of valence electrons per site equals four, and there must be equal numbers of cation and anion sites. This definition for tetrahedral structures was originally devised by Pamplin in 1960 [4], in the general form:



$$\frac{\sum_i n_i v_i}{\sum_i n_i} = 4 \quad (2.1)$$

where  $n_i$  is the number of atoms of the  $i^{\text{th}}$  kind, with  $v_i$  electrons in the outer shell,  $v_i$  being zero for vacant sites.

There are two kinds of tetrahedral structures, namely normal and defective. In normal tetrahedral structures, every atom, without exception, is tetrahedrally surrounded by four tetrahedrally co-ordinated atoms. Every atom in such a structure has  $sp^3$  hybridised orbitals for which one needs an average of four valence electrons per atom.

For defective tetrahedral structures, every atom again has four tetrahedral orbitals, but not every orbital is used for bonding. Thus in defective tetrahedral structures, some atoms have fewer than four neighbours. All these orbitals, which are not used for bonding, obtain one extra electron each and become non-bonding orbitals. An example of the normal tetrahedral structure is the ordered ternary  $\text{Cu}_3\text{SbS}_4$  (the mineral famatinite). It is a tetragonal analogue of the zinc-blend structure. By applying equation (2.1), it is possible to obtain

$$\frac{(3)(1) + (1)(5) + (4)(6)}{3 + 1 + 4} = \frac{32}{8} = 4$$

Applying equation (2.1) for defect tetrahedral structures, such as the compound  $\text{ZnAl}_2\text{□Se}_4$

$$\frac{(1)(2) + (2)(3) + (1)(0) + (4)(6)}{1 + 2 + 1 + 4} = \frac{32}{8} = 4$$

The geometrical features of tetrahedral structures and their rules have been studied by Parthe in 1963 [5]. These were shown mathematically by the general tetrahedral structure equation:

$$\text{VEC} = 4\left(1 + \frac{1}{y}\right) \quad (2.2)$$

where VEC is the electron-to-atom ratio and  $y$  is the number of atoms in a structure in which four non-bonding orbitals occur and is

$$y = \frac{n + m + \dots}{p}$$

where  $p$  denotes the number of vacancies and  $(n + m + \dots)$  denotes the number of atoms in the compound. So if the VEC value is four, we have a normal tetrahedral structure, but if it is larger than four, it is a defect tetrahedral structure. Compounds with a VEC value smaller than four cannot crystallise with a tetrahedral structure.

Applying equation (2.2) to ternary  $\text{Cu}_3\text{SbS}_4$  and  $\text{ZnAl}_2\text{□Se}_4$  gives VEC equal to 4 and 4.57 respectively. Thus, the first structure is normal tetrahedral, whilst the latter is defective tetrahedral. In 1972, Parthé [6] found that adamantine structures are listed only with  $4.0 \leq \text{VEC} \leq 4.92$  and that with a VEC value larger than 4.92, no adamantine structure can occur. Carbon, most of whose chemistry is based on tetrahedral bonding, is present in very few tetrahedral compounds, in fact, only in  $\text{Al}_2\text{CO}$  and  $\text{BeCN}_2$ . This can be accounted for by a consideration of its small atomic size. The other elements of the second period also have small radii and so the structures of their compounds are frequently not tetrahedral. Elements in the third period show a markedly higher tendency to enter into tetrahedral co-ordination. Most of the tetrahedral compounds so far investigated are compounds of the fourth and fifth periods.

In compounds involving elements from the sixth period, tetrahedral bonding is largely absent, mercury being the notable exception. Group III-V compounds involving Tl and Bi are not formed and group III<sub>2</sub>□-VI<sub>3</sub>

compounds involving Tl are only formed in solid solution with other  $\text{II}_2\text{-VI}_3$  compounds to well under 5% [7]. Au, Tl and Bi all show an aversion to  $sp^3$  hybridisation.

### 2.3 The Third Rule for Adamantine Structure Compounds

Mooser and Pearson [8,9] have studied the occurrence of the different structure types among the normal valence compounds and have found that if they plotted different compounds of one composition in a diagram with average principal quantum number  $\bar{n}$  as ordinate and electronegativity difference of the components  $\Delta\chi$  as abscissa, all compounds with a particular structure type have their plots in a special area of the diagram in which they are sharply separated from the other compounds having other structures. These results were formulated analytically by Parthe [6], which, to the first approximation, resulted in the finding that an adamantine structure will occur when

$$\bar{n} + 2\Delta\chi \leq 6 \quad (2.3)$$

Goryunova [10] has stated a similar approximation of adamantine structure, depending on specific electron affinity of cation ( $E_C$ ) and specific electron affinity of anion ( $E_A$ ) in the form

$$E_C - 0.1 E_A \geq 6 \quad (2.4)$$

There are two different influences which may prevent the occurrence of the adamantine structure. One is a strong tendency to draw the bonding electrons closer to one atom than the other. This condition is characterised by a large ( $\Delta\chi$ ) value and leads to the formation of ions and the occurrence of typically ionic structures. Another disturbance is found when ( $\bar{n}$ ) becomes large. Then the ionisation energies of all

elements decrease. Compounds with large values of  $(\bar{n})$  will show metallic properties and will crystallise with metallic crystal structures.

#### 2.4 Extending the Adamantine Family

The search for new inorganic semi-conducting compounds should not be guided by luck and intuition alone, but follow rational principles. Guidelines for the search for these compounds have been published (see, for example, Pamplin [4,11], Goryunova (10), and Parthe [6]); however, they should be studied again from time to time to incorporate new theoretical viewpoints, as well as new experimental data.

The adamantine family can be extended by considering pseudo-binary (or pseudo-ternary) systems of known adamantine phases. Frequently, when atomic radii and electronegativity difference allow, solid solutions are obtained. Some of these notably mixed III-V and mixed II-VI, are now commercially important. In other cases, for example  $\text{HgTe-In}_2\text{-Te}_3$ , a complete solid solution is broken up by compound formation at certain simple element ratios.

Parthe [6] fixed the idea of extending new adamantine compounds geometrically, depending on the general tetrahedral equation and the equation for normal valence compounds. The difficulty arises with some ternary and multicomponent adamantine structure compounds because, on first sight, it seems difficult to decide which elements are cations and which are anions. For example, in the adamantine structure compound  $\text{Cu}_3\text{AsS}_4$  ( $\text{I}_3\text{-V-VI}_4$ ) both Cu and As have to be considered as cations, whereas in the defect adamantine structure compound  $\text{Zn}_3\text{AsI}_3$  ( $\text{II}_3\text{-V-VII}_3$ ) the As atoms are counted as anions. This difficulty can be overcome if we remember that the anion sites of wurtzite or zincblend must always be completely occupied with electronegative atoms and, further, that the

number of electrons provided by the atoms on the Zn or cation sites must be just right to complete the octet shell of the atoms on the s or anion sites.

## 2.5 Ternary Normal Adamantine Compounds

Ternary normal adamantine structure compounds fall into two groups: those in which the third element replaces some of the A atoms and those in which it replaces some of the R atoms, when the binary compounds are denoted by AR. These elements never go into both sub lattices at once, except when it is a Group IV element, as in compounds of the type  $Ag_8IV-VI_6$ . Thus there are two separate cases, the "two-cation" phase and the "two-anion" phase [12-14].

### (1) "Two-cation" phases $(C_m D_n)_o A_o$ :

The two different kinds of cation, C and D, occupy the Zn sites, whereas the S sites are filled with the third component, A. Combining equation (2.1) for the ternary normal tetrahedral structure, we can write

$$\frac{me_C + ne_D + oe_A}{m + n + o} = 4 \quad (2.5)$$

With the equation for normal valence compounds [6]

$$me_C + ne_D = o(8 - e_A) \quad (2.6)$$

we obtain

$$o = m + n \quad (2.7)$$

It is advantageous to introduce a new parameter R, at this point, which is the ratio of m over n.

$$\text{If} \quad R = \frac{m}{n} \quad (2.8)$$

Inserting equations (2.7) and (2.8) into equation (2.5) gives

$$R = \frac{e_D + e_A - 8}{8 - e_C - e_A} \quad (2.9)$$

There are only five solutions for R, which are neither zero, infinite, nor negative. They correspond to compositions of I-III-VI<sub>2</sub>, I-IV<sub>2</sub>-V<sub>3</sub>, I<sub>2</sub>-IV-VI<sub>3</sub>, I<sub>3</sub>-V-VI<sub>4</sub> and II-IV-V<sub>2</sub>.

(2) "Two-anion" phases C<sub>m</sub>(A<sub>o</sub>B<sub>p</sub>):

The C atoms occupy the cation sites, whereas A and B atoms are distributed over the anion sites of a wurtzite or zincblend. The equation for normal valence compounds can be written as follows for this case:

$$me_C = o(8 - e_A) + p(8 - e_B) \quad (2.10)$$

which, combined with equation (2.5) gives

$$m = o + p \quad (2.11)$$

Introducing again a parameter  $R = \frac{m}{o}$  leads to

$$R = \frac{e_B - e_A}{e_C + e_B - 8} \quad (2.12)$$

which has five solutions for  $R > 1$  corresponding to II<sub>2</sub>-V-VII, III<sub>3</sub>-IV<sub>2</sub>-VII, II<sub>3</sub>-IV-VII<sub>2</sub>, II<sub>4</sub>-III-VII<sub>3</sub> and III<sub>3</sub>-IV-VI.

As a matter of fact, only two of these anionic ternary compounds have been clearly identified, namely Al<sub>2</sub>CO, a III<sub>2</sub>-IV-VI compound, which has a structure based on wurtzite, showing some statistical occupancy of octahedral sites [15], and Zn<sub>2</sub>NF, a II<sub>2</sub>-V-VII compound, which was discovered by Marchand and Lang [12]. This fact shows that adamantine compounds with mixed anions are true compounds.

The same electron equation can be used to calculate the composition of possible quaternary and multicomponent compounds. Goryunova [10] has obtained thirty-seven different quaternary compositions. The number of possible compositions increases accordingly if quinary phases are considered.

### 2.5.1 Structure types for ternary normal adamantine compounds

The arrangement of the different atoms on the zincblend or wurtzite structure sites may be ordered or not ordered, but the "cations" are always on the zinc sites and the "anions" on the sulphur sites. Theoretical calculations have been made [4,16,17] to determine what kind of super cells would occur if all atoms arranged themselves in an orderly fashion. However, only four super cells of ternary normal adamantine structure have been found in nature. Two are related to zincblend, chalcopyrite observed with I-III-VI<sub>2</sub> and II-IV-V<sub>2</sub> compounds and famatinite with I<sub>3</sub>-V-VI<sub>4</sub> compounds. Two superstructures can be derived from wurtzite, the BeSiN<sub>2</sub> type, which has not yet been observed with other compounds, and enargite, another structure type for I<sub>3</sub>-V-VI<sub>4</sub> compounds.

There are three other superstructures for quaternary adamantine structure compounds. Two superstructures can be derived from zincblend, stannite with I<sub>2</sub>-II-IV-VI<sub>4</sub> compounds, *e.g.*, Cu<sub>2</sub>FeSnS<sub>4</sub>, and the new structure which has recently been discovered by Schafer [18], which is Cu<sub>4</sub>NiSi<sub>2</sub>S<sub>7</sub>. One superstructure can be derived from wurtzite, the wurtz-stannite of compound I<sub>2</sub>-II-IV-VI<sub>4</sub>, *e.g.*, Cu<sub>2</sub>CdGeS<sub>4</sub>.

#### (a) Ternary adamantine structures related to sphalerite

(1) Ternary chalcopyrite structure.-In the zincblend structure, each S atom is at the centre of a tetrahedron with four Zn atoms at each corner. The four bonds all have the same length and are symmetrically equivalent.

In the case of ternary compounds of chalcopyrite, for example the mineral CuFeS<sub>2</sub> as a superstructure, Zn atoms are replaced by Fe, then the four bonds are no longer identical, the distance between S and Cu not being equal to the distance between S and Fe. The atomic arrangement of CuFeS<sub>2</sub>

is shown in Figure 2.2, with space group  $I\bar{4}2d(D_2d^{12})$ , the unit cell of chalcopyrite  $CuFeS_2$  is ( $E1_1$  type), tetragonal with  $C/a \approx 2$ , and point positions as shown below:-

$CuFeS_2$	$I\bar{4}2d(D_2d^{12})$		
atoms	x	y	z
4 Cu in (4a)	0,0	$0, \frac{1}{2}$	$0, \frac{1}{4}$
4 Fe in (4b)	0,0	$0, \frac{1}{2}$	$0, \frac{3}{4}$
8 S in (8d)	$x, \bar{x}$	$\frac{1}{2}, \frac{3}{4}$	$\frac{1}{8}, \frac{7}{8}$
	$\frac{3}{4}, \frac{1}{4}$	$x, \bar{x}$	$\frac{7}{8}, \frac{1}{8}$

(2) Famatinite type structure related to sphalerite.-The mineral  $Cu_3SbS_4$  ternary compound is a good example found to crystallise in the famatinite structure. The atomic arrangement of  $Cu_3SbS_4$  is shown in Figure 2.2, with space group  $I\bar{4}2m(D_2d^{11})$  and point positions as shown below:-

$Cu_3SbS_4$	$I\bar{4}2m(D_2d^{11})$		
atoms	x	y	z
2 Sb in (2a)	0	0	0
2 Cu in (2b)	0	0	$\frac{1}{2}$
4 Cu in (4d)	$0, \frac{1}{2}$	$\frac{1}{2}, 0$	$\frac{1}{4}, \frac{3}{4}$
8 S in (8i) with $xx\bar{x}, \bar{x}\bar{x}z,$ $xx\bar{z}, \bar{x}\bar{x}\bar{z}$			

The unit cell is tetragonal with  $C/a \approx 2$  and  $c \sim 2a_{Zb\ell}$ . Every sulphur atom is surrounded by 3 Cu and one Sb. This ordering leads to a tetragonal super cell, with  $a_{fam} \approx a_{Zb\ell}$ .

(b) Ternary adamantine structures related to wurtzite

(1) Structures of the enargite type.-The ternary compounds  $Cu_3AsS_4$  and  $Cu_3PS_4$  are known as enargite ( $H2_5$ -type), related to wurtzite and the



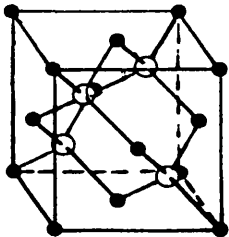
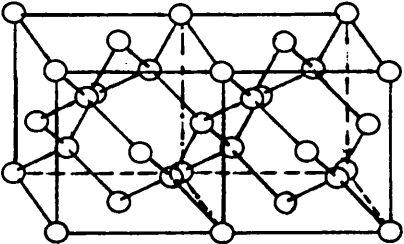
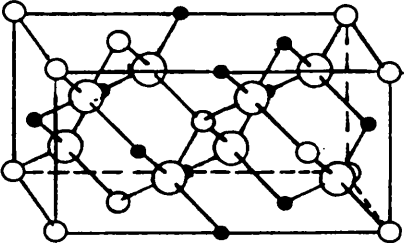
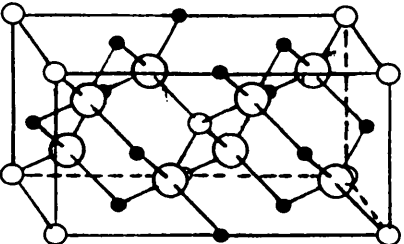
	A	ABC2	A3BC4
 <p>zincblende related structures</p>	 <p>diamond C<sub>D</sub> A<sub>4</sub></p>	 <p>chalcopyrite CuFeS<sub>2</sub> E<sub>1</sub></p>	 <p>famatinite Cu<sub>3</sub>SbS<sub>4</sub></p>
<ul style="list-style-type: none"> <li>● Zn</li> <li>○ S</li> </ul>	<p>O→C and Si</p>	<ul style="list-style-type: none"> <li>● Cu</li> <li>○ Fe</li> <li>○ S</li> </ul>	<ul style="list-style-type: none"> <li>● Cu</li> <li>○ Sb</li> <li>○ S</li> </ul>

Figure 2.2 Zincblende related structure types of ternary normal adamantine structures

BeSiN<sub>2</sub> structure. The atomic arrangement of Cu<sub>3</sub>AsS<sub>4</sub> is shown in Figure 2.3, with space group (C<sub>2v</sub><sup>7</sup>-Pmm2<sub>1</sub>), axial ratio a:b:c 2:√3:√8/√3, and point positions as shown below:-

Cu <sub>3</sub> AsS <sub>4</sub> Pmm2 <sub>1</sub> (C <sub>2v</sub> <sup>7</sup> )			
atoms	x	y	z
2 As in (2a)		5/6	0
2 Cu in (2a)		1/6	1/2
4 Cu in (4b)	1/4	1/3	0
2 S in (2a)		5/6	3/8
2 S in (2a)		1/6	7/8
4 S in (4b)	1/4	1/3	3/8

(2) Structure of the type BeSiN<sub>2</sub>.-Rabenau and Eckerlin [19] have shown that BeSiN<sub>2</sub> has the wurtzite structure and they conclude that BeSiN<sub>2</sub> can be regarded as an analogue of aluminium, gallium, or indium nitride. Eckerlin [20] has shown that BeSiN<sub>2</sub> is analogous to chalcopyrite and has the space group (Pna2<sub>1</sub>-C<sub>2v</sub><sup>9</sup>) with axial ratio a:b:c √3:2:2√2/√3 and a ~ √3a<sub>w</sub>, b ~ 2a<sub>w</sub>, c = c<sub>w</sub>. The atomic arrangement of BeSiN<sub>2</sub> (E1<sub>a</sub> type) are shown in Figure 2.3 and the point positions of BeSiN<sub>2</sub> are as shown below:-

BeSiN <sub>2</sub> Pna2 <sub>1</sub> (C <sub>2v</sub> <sup>9</sup> )			
atoms	x	y	z
4 Be in (4a)	1/12	7/8	0
4 Si in (4a)	1/12	3/8	0
4 N in (4a)	1/12	7/8	3/8
4 N in (4a)	1/12	3/8	3/8

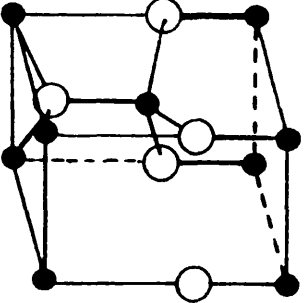
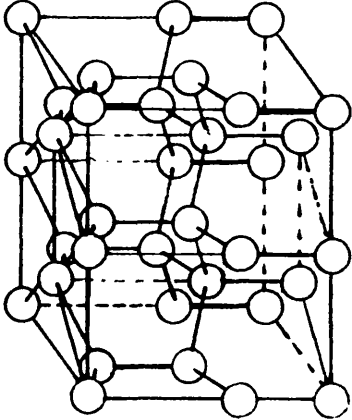
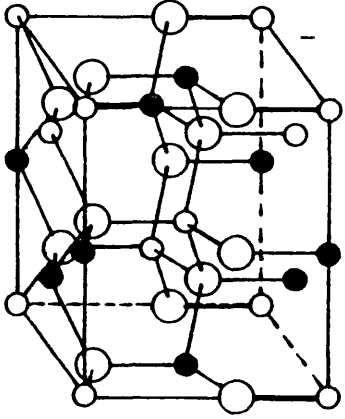
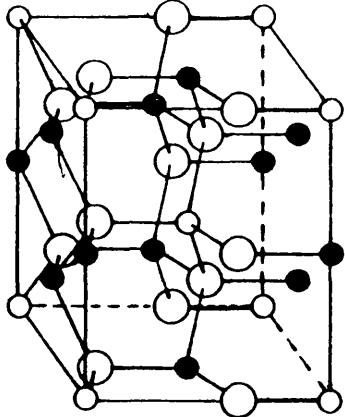
 <p>wurtzite related structures</p> <p>● Zn ○ S</p>	<p>A</p>  <p>wurtzite-silicon</p> <p>○ Si</p>	<p>ABC2</p>  <p>BeSiN<sub>2</sub></p> <p>● Be ○ Si ○ N</p>	<p>A<sub>3</sub>BC4</p>  <p>Enorgite Cu<sub>3</sub>AsS<sub>4</sub> H<sub>2</sub>S</p> <p>● Cu ○ As ○ S</p>
--	--	--	---

Figure 2.3 Wurtzite related structure types of ternary normal adamantine structures

### 2.5.2 Ternary defect adamantine compounds

There are only three possible compositions stated by Parthe [6] for ternary defect adamantine structure compounds in the form of  $C_m D_n \square_s A_4$ . This is derived from the same mathematical calculations which were used for finding the possible compositions of non defect compounds, as explained earlier. In the three ordered structure types, the anion partial structure is the same as in zincblend, but two kinds of "cations" in the ratio 2:1 occupy three out of every four former zinc sites in ordered fashion. The three compositions are  $I_2 II - \square - VII_4$ ,  $II - III_2 - \square - VI_4$  and  $II_2 - IV - \square - VI_4$ . Examples of all three composition formulae are known and these are shown in Table 2.5.

There are two other ternary defect compositions which can be derived from the ternary phase diagram. This series of compositions appears as lines. For example, the alloys of the series  $(III_2 - \square - VI_2)_x (II - VI)_{1-x}$  and  $(III_2 - \square - VI_3)_x (III - V)_{1-x}$  are the possible ternary adamantine structure compositions in the ternary systems II-III-VI and III-V-VI. However, all the possible compositions may not have an adamantine structure [21,22], while in the ternary system Ga-As-Se, an adamantine structure is formed throughout a compound line which starts at GaAs and extends all the way to  $Ga_2Se_3$ . Compounds  $HgGa_2Te_4$ ,  $CdIn_2Se_4$ ,  $CdGa_2S_4$  and  $BCu_2HgI_4$  form in four different structure types of  $II - III_2 - \square - VI_4$  and  $I_2 II - \square - VII$ , related to sphalerite, while  $ZnAl_2S_4$  is the only structure known that is related to wurtzite [6].

### 2.6 Crystal Structure of I-IV<sub>2</sub>-V<sub>3</sub> Type Compounds

The least known ternary compounds are the I-IV<sub>2</sub>-V<sub>3</sub> group. The first data on this group were reported by Goryunova and Sokolova [23]. In the work reported by Sokolova and Tsvetkova in 1964 [24], attempts were made

to prepare substances of this group. Table 2.1 lists all the possible combinations in this group. They investigated the combinations of elements which are formed in Table 2.1. They discovered that the combination containing lead and bismuth gave off free bismuth. The alloy of tin with antimony or arsenic revealed the presence of the NaCl structure, corresponding to the formation of the binary compounds SnSb and SnAs respectively. Alloys based on germanium and containing antimony or arsenic usually contained pure germanium. In all these cases, two or more phases were present. The reaction with silicon required high temperatures and were not completed under the conditions used by these workers. Only the phase  $\text{CuSi}_2\text{P}_3$ , crystallising with the ZnS structure and the parameter  $a = 5.25 \text{ \AA}$ , was obtained. Their initial attempts to introduce gold into compounds with a tetrahedral structure were not successful.

Alloys containing phosphorus consisted of a single phase in two cases:  $\text{CuGe}_2\text{P}_3$  and  $\text{AgGe}_2\text{P}_3$ . The other composition,  $\text{AgSn}_2\text{P}_3$ , was reported in a quite complex phase. The main phase was crystallised in a complex structure.

A new form of  $\text{Cu}_4\text{SnP}_{10}$  was found for the Cu-Sn-P system with a bcc lattice and a parameter of  $a = 10.260 \text{ \AA}$  [25]. This compound crystallises in the cubic space group  $I\bar{4}3m(T_d^3)$  [26]. The point position of the atoms is shown in Table 2.4.

The substance represented by  $\text{CuGe}_2\text{P}_3$  crystallised in the zincblend structure with a lattice parameter  $a = 5.370 \text{ \AA}$  and with the presence of 3-5% of a second phase. The thermal analysis was also reported to show the presence of two transformations, one at  $800^\circ \text{C}$  and a second at  $759^\circ \text{C}$  [23].

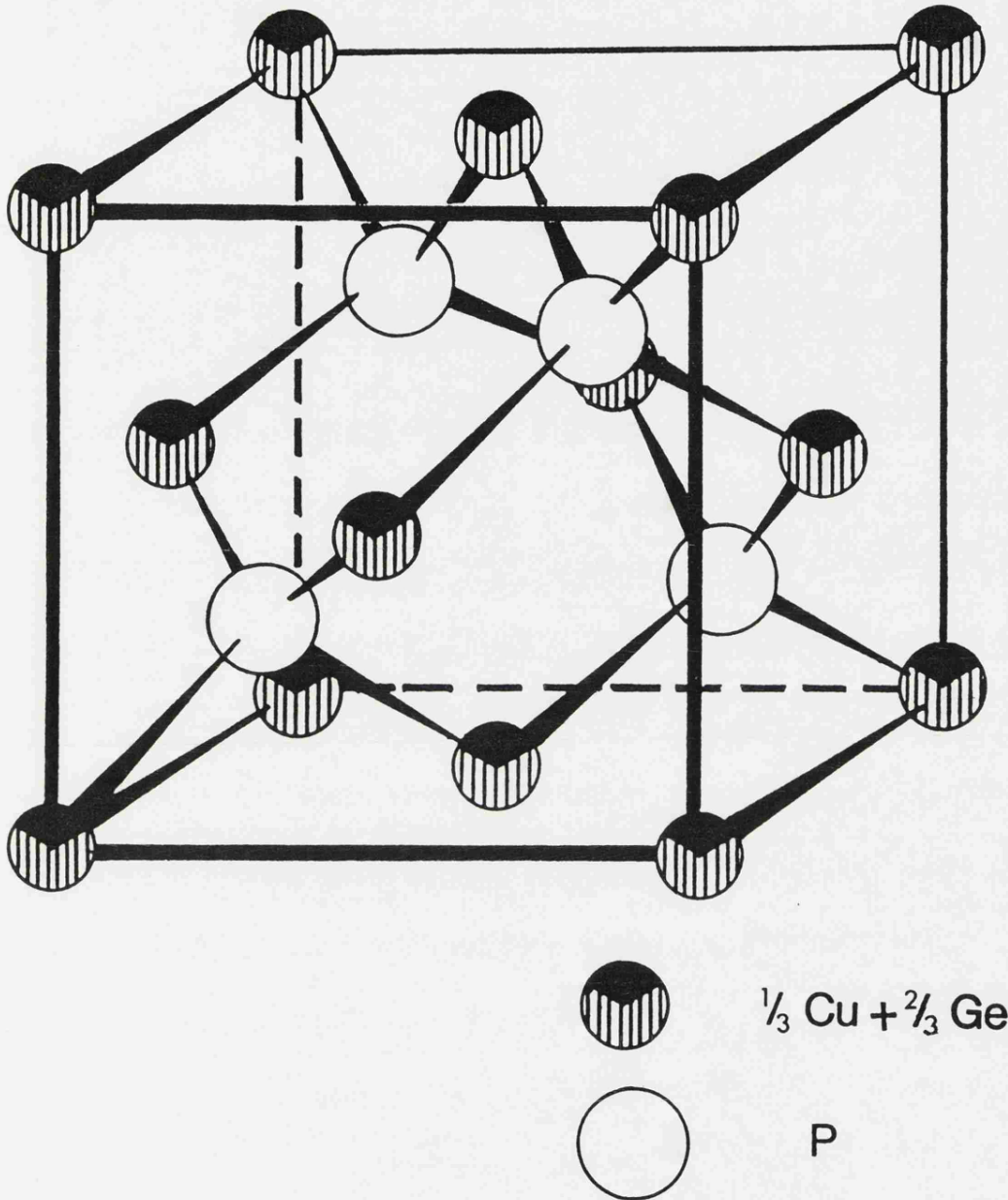
Table 2.1

Possible combinations of group I-IV<sub>2</sub>-V<sub>3</sub> compounds

* CuSi <sub>2</sub> P <sub>3</sub>	* AgSi <sub>2</sub> P <sub>3</sub>	AuSi <sub>2</sub> P <sub>3</sub>
* CuGe <sub>2</sub> P <sub>3</sub>	* AgGe <sub>2</sub> P <sub>3</sub>	AuGe <sub>2</sub> P <sub>3</sub>
* CuSn <sub>2</sub> P <sub>3</sub>	* AgSn <sub>2</sub> P <sub>3</sub>	AuSn <sub>2</sub> P <sub>3</sub>
* CuPb <sub>2</sub> P <sub>3</sub>	* AgPb <sub>2</sub> P <sub>3</sub>	AuPb <sub>2</sub> P <sub>3</sub>
* CuSi <sub>2</sub> As <sub>3</sub>	AgSi <sub>2</sub> As <sub>3</sub>	AuSi <sub>2</sub> As <sub>3</sub>
* CuGe <sub>2</sub> As <sub>3</sub>	* AgGe <sub>2</sub> As <sub>3</sub>	* AuGe <sub>2</sub> As <sub>3</sub>
* CuSn <sub>2</sub> As <sub>3</sub>	* AgSn <sub>2</sub> As <sub>3</sub>	AuSn <sub>2</sub> As <sub>3</sub>
* CuPb <sub>2</sub> As <sub>3</sub>	* AgPb <sub>2</sub> As <sub>3</sub>	AuPb <sub>2</sub> As <sub>3</sub>
CuSi <sub>2</sub> Sb <sub>3</sub>	* AgSi <sub>2</sub> Sb <sub>3</sub>	AuSi <sub>2</sub> Sb <sub>3</sub>
* CuGe <sub>2</sub> Sb <sub>3</sub>	* AgGe <sub>2</sub> Sb <sub>3</sub>	AuGe <sub>2</sub> Sb <sub>3</sub>
* CuSn <sub>2</sub> Sb <sub>3</sub>	* AgSn <sub>2</sub> Sb <sub>3</sub>	AuSn <sub>2</sub> Sb <sub>3</sub>
* CuPb <sub>2</sub> Sb <sub>3</sub>	AgPb <sub>2</sub> Sb <sub>3</sub>	AuPb <sub>2</sub> Sb <sub>3</sub>
CuSi <sub>2</sub> Bi <sub>3</sub>	AgSi <sub>2</sub> Bi <sub>3</sub>	AuSi <sub>2</sub> Bi <sub>3</sub>
* CuGe <sub>2</sub> Bi <sub>3</sub>	AgGe <sub>2</sub> Bi <sub>3</sub>	AuGe <sub>2</sub> Bi <sub>3</sub>
* CuSn <sub>2</sub> Bi <sub>3</sub>	AgSn <sub>2</sub> Bi <sub>3</sub>	AuSn <sub>2</sub> Bi <sub>3</sub>
* CuPb <sub>2</sub> Bi <sub>3</sub>	AgPb <sub>2</sub> Bi <sub>3</sub>	AuPb <sub>2</sub> Bi <sub>3</sub>

---

\* These compounds have been investigated [24].



Figure(2.4):-The atomic arrangement of  $\text{CuGe}_2\text{P}_3$  compound. Showing Cu and Ge are distributed randomly in Zn sites and P in S sites.

AgGe<sub>2</sub>P<sub>3</sub>, unlike CuGe<sub>2</sub>P<sub>3</sub>, does not crystallise in the zincblend structure. The lattice of AgGe<sub>2</sub>P<sub>3</sub> belongs to the cubic system, its unit cell being a body-centred cube [27]. The same lattice spaces were reported for Ag<sub>6</sub>Ge<sub>10</sub>P<sub>12</sub> [28].

Werner [29] reported the structure of Cu<sub>3</sub>As for the compounds CuGe<sub>2</sub>As<sub>3</sub> and CuGe<sub>2</sub>Sb<sub>3</sub>, in a new form of Cu<sub>75</sub>Ge<sub>15</sub>As<sub>10</sub> and Cu<sub>75</sub>Ge<sub>12.5</sub>Sb<sub>12.5</sub> with the lattice parameters of a = 4.165 Å, c = 7.475 Å for the latter.

Figure 2.4 illustrates the atomic arrangements for the compound CuGe<sub>2</sub>P<sub>3</sub>, which showed Cu and Ge randomly distributed in Zn sites and the P atom in S sites.

### 2.6.1 Crystal structure of the compound Ag<sub>6</sub>Ge<sub>10</sub>P<sub>12</sub>

The compound Ag<sub>6</sub>Ge<sub>10</sub>P<sub>12</sub> crystallises in the cubic space group I $\bar{4}3m$  [28]. The point position of the atoms is shown in Table 2.2.

The most important interatomic distance and the binding angle are placed together in Table 2.3. Figure 2.5 shows the substantial sections of this structure with the co-ordinates for all the atoms.

Table 2.2

The point position of Ag<sub>6</sub>Ge<sub>10</sub>P<sub>12</sub> atoms [28]

Ag <sub>6</sub> Ge <sub>10</sub> P <sub>12</sub> I $\bar{4}3m$ (T <sub>d</sub> <sup>3</sup> )			
atoms	x	y	z
Ag in 12(e)	0.19540 (13)	0	0
Ge(1) in 8(c)	0.28850 (15)	x	x
Ge(2) in 12(d)	$\frac{1}{4}$	$\frac{1}{2}$	0
P in 24(g)	0.12832 (23)	x	0.30605 (32)



Table 2.3

The binding intervals (distance) and binding angles of the compound  $\text{Ag}_6\text{Ge}_{10}\text{P}_{12}$  [28]

Binding intervals (distance)			Binding angles			
Atom-atom	Interval distance (Å)	Number	Atom-atom	Angle	Number	Mean
Ag-Ag	2.852(3)	4x	P-Ag-P	95,4(2)	1x	
Ag-P	2.532(4)	2x				
Ag-Ge(1)	3.092(4)	2x	P-Ge(1)-P	84,4(1)	3x	} 89.2°
Ge(1)-P	2.454(4)	3x	P-Ge(1)-Ag	107,3(1)	6x	
Ge(1)-Ag	3.092(4)	3x	Ag-Ge(1)-Ag	54,9(1)	3x	
Ge(2)-P	2.325(4)	4x				
P-Ag	2.532(4)	1x	P-Ge(2)-P	107,0(1)	4x	} 109.5°
P-Ge(1)	2.454(4)	1x	P-Ge(2)-P	114,6(2)	2x	
P-Ge(2)	2.325(4)	2x	Ge(1)-P-Ag	120,1(1)	1x	} 109.2°
P-P	3.389(7)	2x	Ge(2)-P-Ag	113,7(1)	2x	
P-P	3.737(5)	4x	Ge(2)-P-Ge(1)	102,0(1)	2x	
P-P	3.746(6)	1x	Ge(2)-P-Ge(2)	103,4(1)	1x	

Table 2.4

Space group and point position of compounds isotopic to  $\text{Ag}_6\text{Ge}_{10}\text{P}_{12}$  [26]

Compounds	Space group	Point position
$\text{Ag}_6\text{Sn}_4\text{Si}_6\text{P}_{12}$	$I\bar{4}3m(T_d^3)$	12 Ag in 12(e), 8 Sn in 8(c), 12 Si in 12(d), 24 P in 24(g)
$\text{Ag}_6\text{Sn}_4\text{Ge}_6\text{P}_{12}$	$I\bar{4}3m(T_d^3)$	12 Ag in 12(e), 8 Sn in 8(c), 12 Ge in 12(d), 24 P in 24(g)
$\text{Cu}_4\text{SnP}_{10}$	$I\bar{4}3m(T_d^3)$	4 Cu(1) in 4(a), 16 P(1) in 16(e), 24 P(2) in 24(g), 12 Cu(2) in 16(e) and 4 Sn in 16(e)

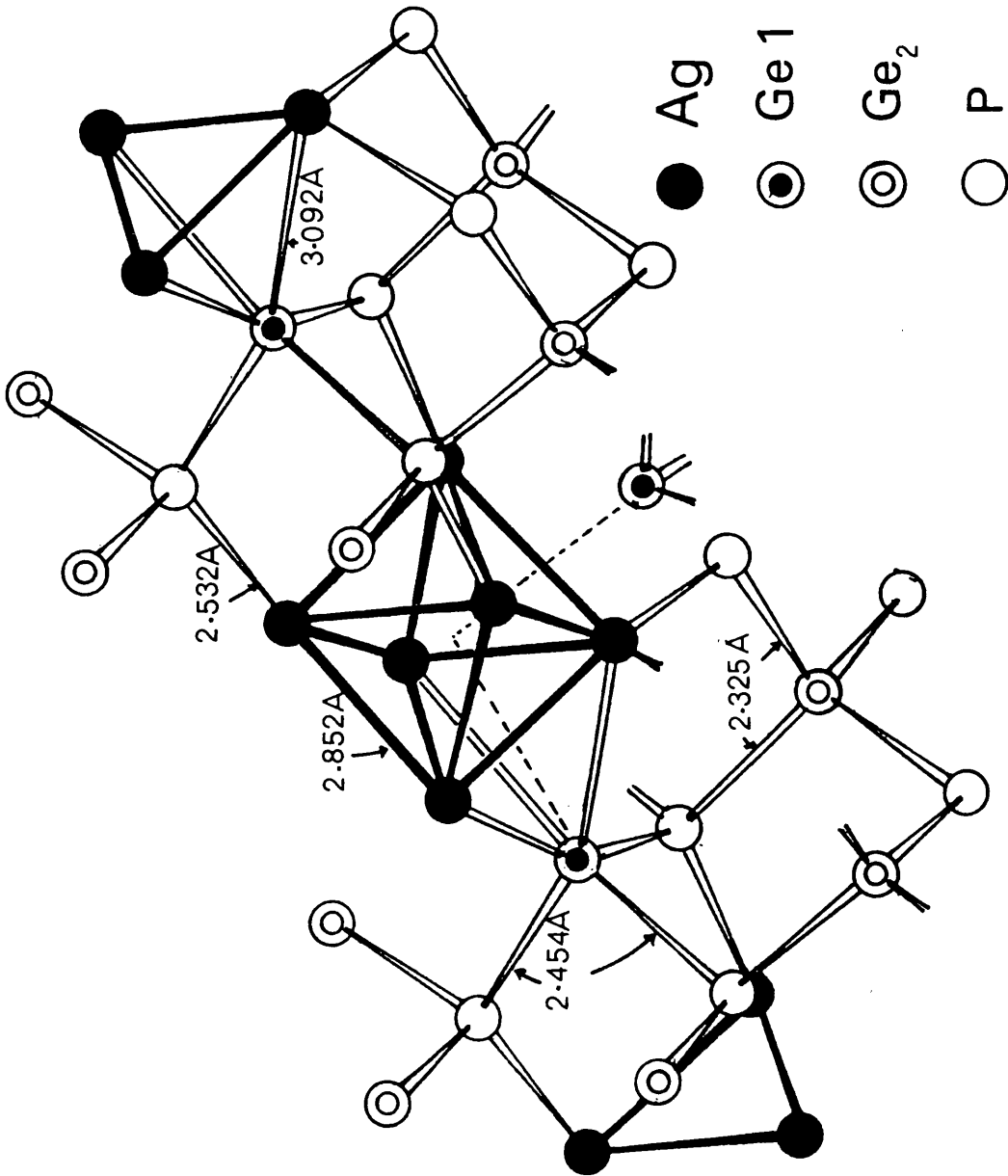


Figure 2.5 Extract from the  $\text{Ag}_6\text{Ge}_{10}\text{P}_{12}$  structure lengthwise [111]; for each atom Ag, Ge(1), Ge(2) and P, the connection at one point with the bond intervals is indicated [28].

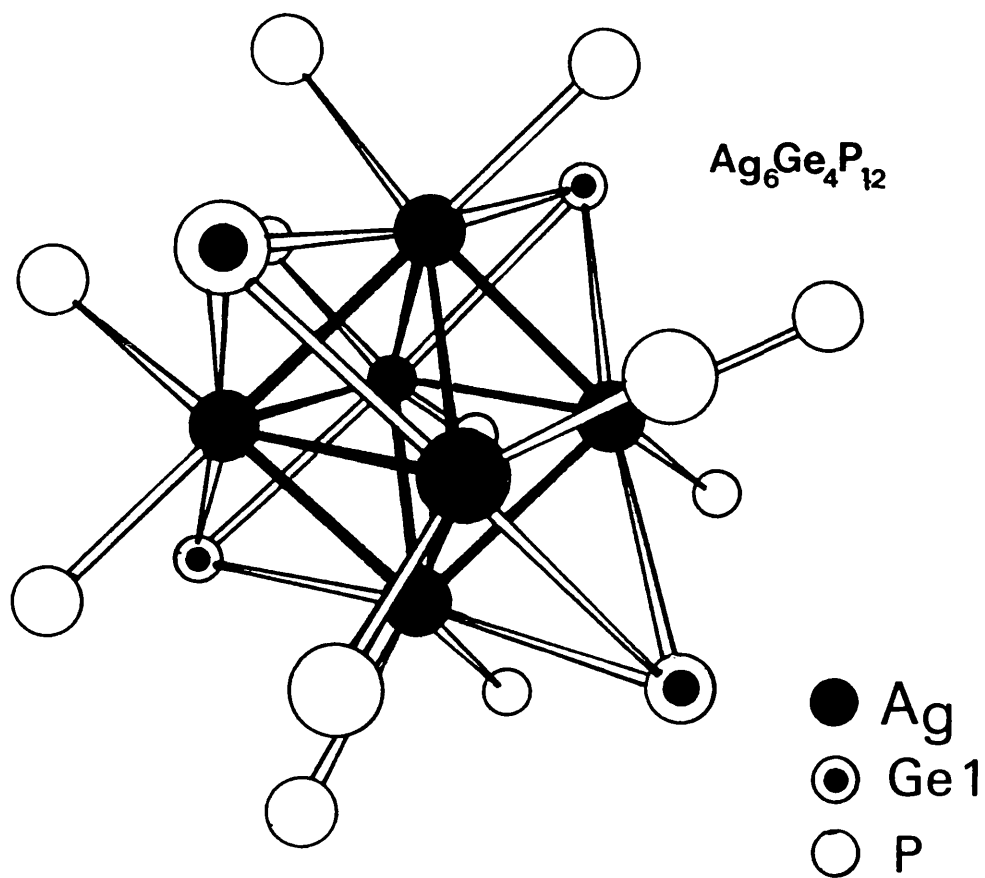


Figure 2.6 The atomic arrangement of group  $[\text{Ag}_6\text{Ge}_4]\text{P}_{12}$ , the structure of this group being identical to that of the  $\text{Rh}_6(\text{CO})_{16}$  molecule, the building groups  $[\text{Ag}_6\text{Ge}_4]\text{P}_{12}$  are connected in the crystal shown in Figure 2.5 to the atom Ge(2) [28].

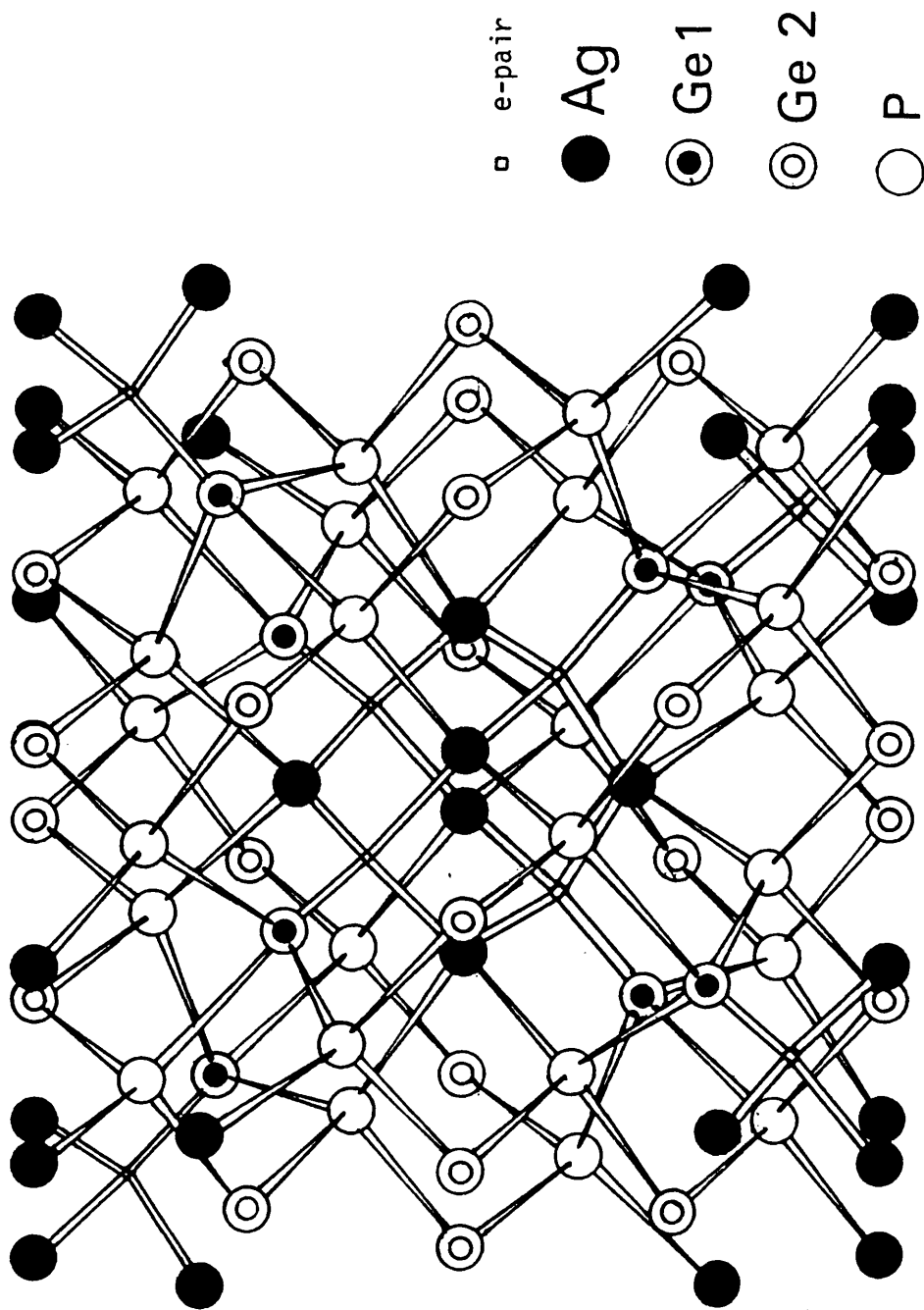


Figure 2.7 Diamond-analogous tetrahedral structure of  $[Ag_6Ge_{10}P_{12}]$  [28]

The occupation of the different positions by the atoms Ag, Ge(1), Ge(2) and P like the mutual arrangement allows the formula  $[\text{Ag}_6\text{Ge}_4\text{P}_{12}]\text{Ge}_6$  for this structure. Each P atom is tetrahedrally bound to an Ag atom, Ge(1) and two atoms of Ge(2). The bond intervals are as shown in Figure 2.5, and shown in Table 2.3. The bond angle P-Ge(2)-P amounts on average to the tetrahedral co-ordination value ( $109.5^\circ$ ). For Ge(1), the bond angle P-Ge-P is similar to that in the  $\text{Rh}_6(\text{CO})_{16}$  cluster, see Figures 2.5-2.7. The atoms Ge(1) are enclosed in the  $\text{Ag}_6$ -octahedron in the form of a tetrahedron.

Table 2.5

List of known ternary adamantine structure compounds\*

Composition	VEC	Wurtzite or related structures	Zincblend or related structures.
I-III-VI <sub>2</sub>	4.0	AgInS <sub>2</sub> , β-LiGaO <sub>2</sub> [33], LiGaS <sub>2</sub> [30], LiInS <sub>2</sub> [30], NaGaO <sub>2</sub> [30]	CuBSe <sub>2</sub> , CuAlS <sub>2</sub> , CuAlSe <sub>2</sub> , CuAlTe <sub>2</sub> , CuGaS <sub>2</sub> , CuGaSe <sub>2</sub> , CuGaTe <sub>2</sub> , CuInS <sub>2</sub> , CuInSe <sub>2</sub> , CuInTe <sub>2</sub> , CuTlS <sub>2</sub> , CuTlSe <sub>2</sub> , CuFeS <sub>2</sub> , CuFeSe <sub>2</sub> , AgAlS <sub>2</sub> , AgAlSe <sub>2</sub> , AgAlTe <sub>2</sub> , AgGaS <sub>2</sub> , AgGaSe <sub>2</sub> , AgGaTe <sub>2</sub> , AgInS <sub>2</sub> , AgInSe <sub>2</sub> , AgInTe <sub>2</sub> , AgFeS <sub>2</sub>
II-IV-V <sub>2</sub>	4.0	BeSiP <sub>2</sub>	HgGeP <sub>2</sub> , ZnSiP <sub>2</sub> , ZnSiAs <sub>2</sub> , ZnGeP <sub>2</sub> , ZnGeAs <sub>2</sub> , ZnSnP <sub>2</sub> [10], ZnSnAs <sub>2</sub> , CdSiP <sub>2</sub> [31], CdSiAs <sub>2</sub> [10]. CdGeP <sub>2</sub> , CdGeAs <sub>2</sub> , CdSnP <sub>2</sub> [10]. CdSnAs <sub>2</sub> , ZnSnSb <sub>2</sub> [32]
I <sub>3</sub> -V-VI <sub>4</sub>	4.0	Cu <sub>3</sub> PS <sub>4</sub> , Cu <sub>3</sub> AsS <sub>4</sub>	Cu <sub>3</sub> AsS <sub>4</sub> , Cu <sub>3</sub> AsSe <sub>4</sub> , Cu <sub>3</sub> SbS <sub>4</sub> , Cu <sub>3</sub> SbSe <sub>4</sub>
I <sub>2</sub> -IV-VI <sub>3</sub>	4.0	Cu <sub>2</sub> SiS <sub>3</sub> [33]	Cu <sub>2</sub> SiS <sub>3</sub> [33], Cu <sub>2</sub> SiTe <sub>3</sub> , Cu <sub>2</sub> GeS <sub>3</sub> , Cu <sub>2</sub> GeSe <sub>3</sub> , Cu <sub>2</sub> GeTe <sub>3</sub> , Cu <sub>2</sub> SnS <sub>3</sub> , Cu <sub>2</sub> SnSe <sub>3</sub> , Cu <sub>2</sub> SnTe <sub>3</sub>
I-IV <sub>2</sub> -V <sub>3</sub>	4.0		CuSi <sub>2</sub> P <sub>3</sub> , CuGe <sub>2</sub> P <sub>3</sub>
II <sub>5</sub> -III <sub>2</sub> -□-VI <sub>8</sub>	4.27		Hg <sub>5</sub> Ga <sub>2</sub> Te <sub>8</sub> , Hg <sub>5</sub> In <sub>2</sub> Te <sub>8</sub>
I <sub>2</sub> -II-□-VI <sub>4</sub>	4.57		Cu <sub>2</sub> HgI <sub>4</sub> , Ag <sub>2</sub> HgI <sub>4</sub>
II-III <sub>2</sub> -□-VI <sub>4</sub>	4.57	ZnAl <sub>2</sub> S <sub>4</sub>	ZnAl <sub>2</sub> Se <sub>4</sub> , ZnAl <sub>2</sub> Te <sub>4</sub> , ZnGa <sub>2</sub> S <sub>4</sub> , ZnGa <sub>2</sub> Se <sub>4</sub> , ZnGa <sub>2</sub> Te <sub>4</sub> , ZnIn <sub>2</sub> Se <sub>4</sub> , ZnIn <sub>2</sub> Te <sub>4</sub> , CdAl <sub>2</sub> S <sub>4</sub> , CdAl <sub>2</sub> Se <sub>4</sub> , CdAl <sub>2</sub> Te <sub>4</sub> , CdGa <sub>2</sub> S <sub>4</sub> , CdGa <sub>2</sub> Se <sub>4</sub> , CdGa <sub>2</sub> Te <sub>4</sub> , CdIn <sub>2</sub> Se <sub>4</sub> , CdIn <sub>2</sub> Te <sub>4</sub> , HgAl <sub>2</sub> S <sub>4</sub> , HgAl <sub>2</sub> Se <sub>4</sub> , HgAl <sub>2</sub> Te <sub>4</sub> , HgGa <sub>2</sub> S <sub>4</sub> , HgGa <sub>2</sub> Se <sub>4</sub> , HgGa <sub>2</sub> Te <sub>4</sub> , HgIn <sub>2</sub> Se <sub>4</sub> , HgIn <sub>2</sub> Te <sub>4</sub>
II <sub>2</sub> -IV-□-VI <sub>4</sub>	4.57		Zn <sub>2</sub> GeS <sub>4</sub> [34], Zn <sub>2</sub> GeSe <sub>4</sub> [34], Hg <sub>2</sub> GeSe <sub>4</sub> [23]
II <sub>3</sub> -□-V-VI <sub>3</sub>	4.57		Zn <sub>3</sub> PI <sub>3</sub> , Zn <sub>3</sub> AsI <sub>3</sub>
III <sub>2y+z</sub> -□-V <sub>z</sub> -VI <sub>3y</sub>	4.0-4.80		Complete solid solution between III-V and III <sub>2</sub> -□-VI <sub>3</sub> found with Ga <sub>2y+x</sub> P <sub>x</sub> S <sub>3y</sub> [10], Ga <sub>2y+x</sub> As <sub>x</sub> Se <sub>3y</sub> [10], In <sub>2y+x</sub> As <sub>x</sub> Te <sub>3y</sub> [10]
III <sub>4</sub> -IV-□ <sub>3</sub> -VI <sub>8</sub>	4.923		Ga <sub>4</sub> GeSe <sub>8</sub> [35]

\*If not specifically marked, the literature reference to all compounds can be found in references [6,36,37].

## CHAPTER 3

### Crystal Growth

#### 3.1 Introduction

A limited amount of work was done (mainly in Russia) twenty-four years ago, on compounds of the type I-IV<sub>2</sub>-V<sub>3</sub>. CuGe<sub>2</sub>P<sub>3</sub> and CuSi<sub>2</sub>P<sub>3</sub> were the only compounds which were successfully prepared and these were only in polycrystalline form. In the same period, the alloys of CuGe<sub>2</sub>P<sub>3</sub>-Ge were prepared with a certain degree of success [23,27,32,38].

In this work, some ternary I-IV<sub>2</sub>-V<sub>3</sub> compounds were prepared. The ternary compound CuGe<sub>2</sub>P<sub>3</sub> was the main material of interest in this investigation. Attempts at preparing solid solutions based on this compound with single component semiconductors, binary and ternary compounds, were also tried. Melt growth was the main method used to grow the above-mentioned materials. Tin solution and iodine transport growth were used as well, to overcome the particular difficulties which were encountered.

Large single crystals of CuGe<sub>2</sub>P<sub>3</sub>, Ag<sub>6</sub>Ge<sub>10</sub>P<sub>12</sub> and all single phase alloys were prepared by the slow cooling method of Bridgman.

#### 3.2 Primary Considerations for the Synthesis of Ternary Compounds

Only a few of the phase diagrams of ternary systems, in which ternary compounds with tetrahedral co-ordination are formed, have been investigated, especially those containing volatile components. Consequently, the development of the synthesis methods for ternary compounds containing volatile components is greatly complicated by the fact that the dependence of the phase composition on pressure, temperature, and chemical composition is not well known. It must thus be concluded that the majority of ternary compounds prepared by direct synthesis from the component elements, using



the available techniques and the very limited information on the phase diagrams, cannot be perfect with respect to their composition and homogeneity.

Analysis of T-X phase diagrams of binary systems, in which binary tetrahedral phases can be formed, can yield some information on the departures of the stability of the  $sp^3$  electron configuration which results, in the end, in the disappearance of chemical interaction when the principal quantum numbers of the atoms forming part of the system are increased. Figure 3.1(a) shows the Gibbs triangles involved in the formation of ternary two-cation valence compounds in the I-IV<sub>2</sub>-V<sub>3</sub> system. A close study of this diagram, in which ternary tetrahedral structures can form, reveals that the formation of ternary phases is governed by the chemical interaction in I-V and IV-V binary systems.

The nature of the interaction in I-IV and I-V systems is obviously not decisive, although it may be of some importance. If there is no chemical interaction in the basic systems, tetrahedral phases are not formed. The same statement can also be made by considering the crystallochemical concept of valence ternary tetrahedral compounds, consisting of cations and anions held in the structure by covalent, as well as fairly strong ionic, forces.

Compounds of the type I-IV<sub>2</sub>-V<sub>3</sub> are difficult to analyse, because of their complexity. However, only two of these compounds are known to exist in this composition, which are CuGe<sub>2</sub>P<sub>3</sub> and CuSi<sub>2</sub>P<sub>3</sub> [24]. In spite of the considerable complexity of the processes of synthesis of ternary compounds, compared with binary materials, the earliest investigations have already established that ternary compounds have many advantages over binary ones, particularly with respect to their much lower melting points.

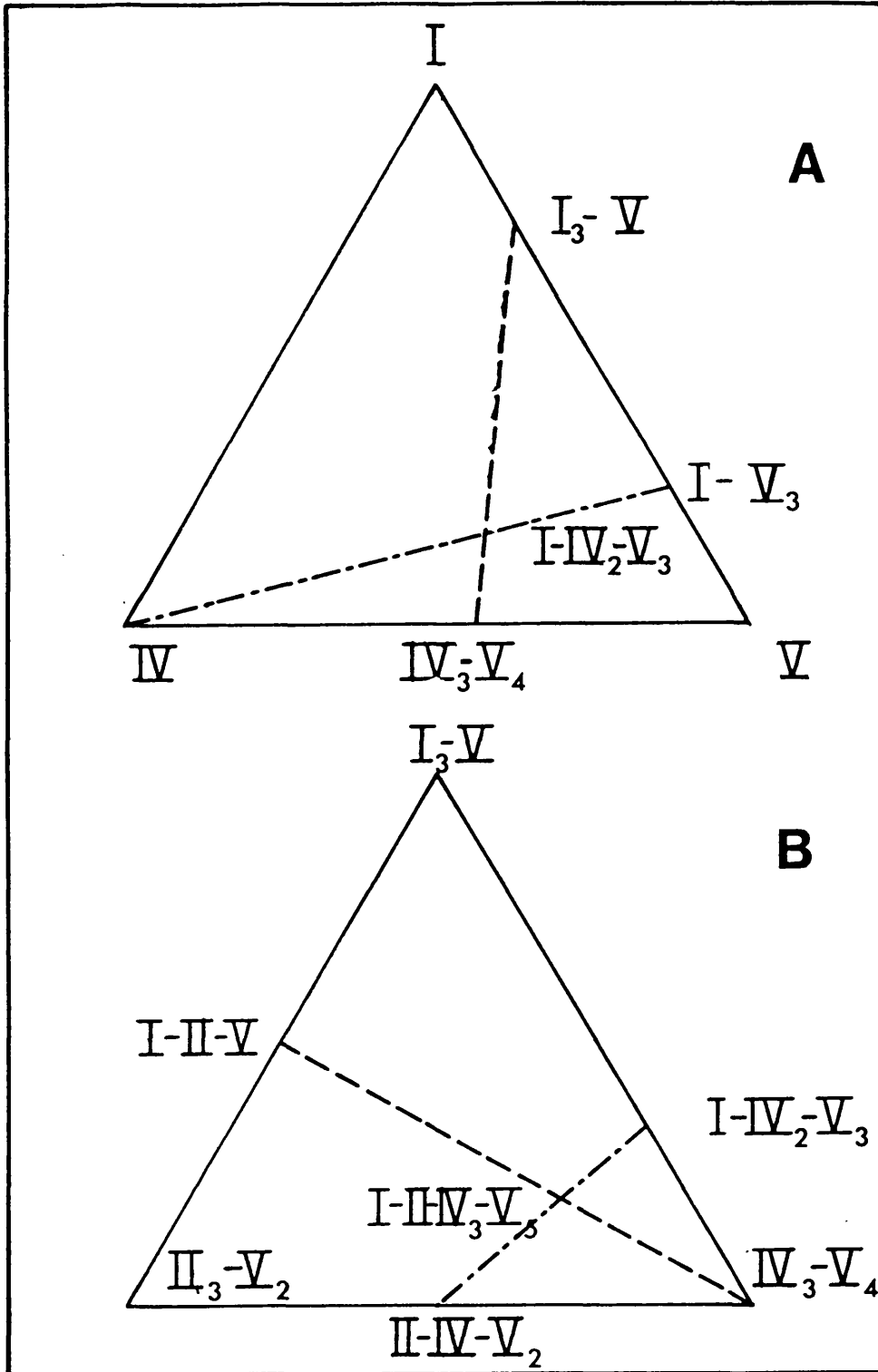


Figure 3.1 A - Gibbs triangles for the ternary compound  $I-IV_2-V_3$  two cation system  
 B - Gibbs triangles for quaternary alloy  $I-II-IV_3-V_5$   
 (Thick lines represent the basic systems, the dashed lines represent valence compounds and alloys and the chain lines compounds with four electrons per atom.)

The low melting temperature not only makes it easier to prepare them, but also provides an opportunity to reduce the contamination during synthesis. Table 4.1 contains the melting points of some ternary materials investigated in this work. The melting points of some other ternary compounds are given in references 10, 36 and 37. The vapour pressure of the volatile compound should also be controlled. The selection of a particular synthesis technique should be based on the total vapour pressure of all the elements in the compound.

### 3.3 Preparation of Ampoules

After the tube was sealed, the ampoules were cleaned, using a standard procedure each time. HCl and HNO<sub>3</sub> solution was used for about 24 hours. This was washed with demineralised water and cleaned ultrasonically for about 20 minutes. The tubes were then outgassed under a low pressure of about  $10^{-5}$  torr or less, at a temperature of about 1000°C for 8-10 hours. These conditions were the same for all ampoules used in the preparation of compounds in this work.

### 3.4 Crystal Growth from Melt

#### 3.4.1 Theoretical considerations

The growth of single crystals from the melt is well known now. In 1953 Chalmers [39] stated three ways in which the essential requirement that growth shall proceed from a single nucleus is fulfilled:

- (1) A small seed crystal is used in the base of the mould.
- (2) Only a small volume of material is maintained in the temperature range in which nucleation can take place.
- (3) Several nuclei are allowed to form, but only one is allowed to survive to form a single crystal.

In most successful melt methods of growing crystals, the second requirement is satisfied by slow cooling from one end of the mould, which is usually pointed. Unidirectional solidification is ensured by maintaining a steep temperature gradient along the mould. So crystallisation consists mainly of directional deposition of atoms, originating from a molten phase, onto a solidifying interface.

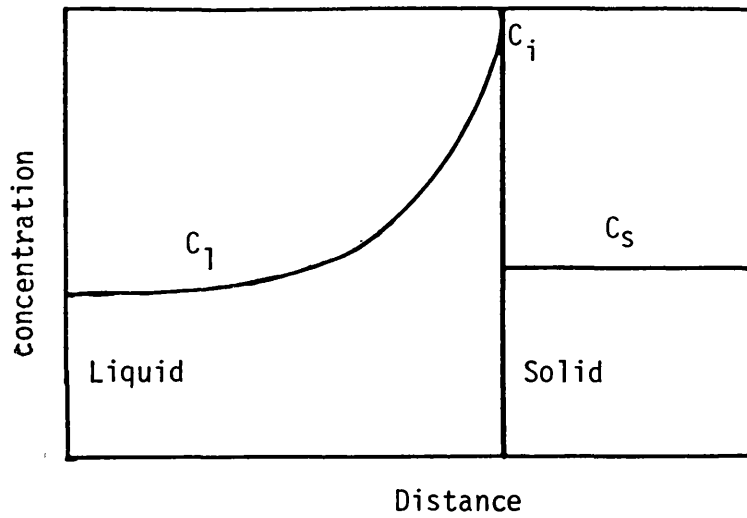
The raising of temperature above the melting point without phase transfer of the solid is termed superheating and supercooling is the reverse phenomenon.

When growth is from a system including a second component or solute impurity, there will be a build-up of the components rejected from the solid close to the growth interface, as shown in Figure 3.2(a), where  $C_l$  is the liquid concentration,  $C_i$  is the interface concentration, and  $C_s$  is the solid concentration. The difference in composition of the three regions of the system give the result shown in Figure 3.2(b). In this figure, the dashed lines A, A' represent the temperature gradients along the system. The CB is supercooled corresponding to gradient A' [40-42]. The condition for supercooling is given by Tiller [43] as:

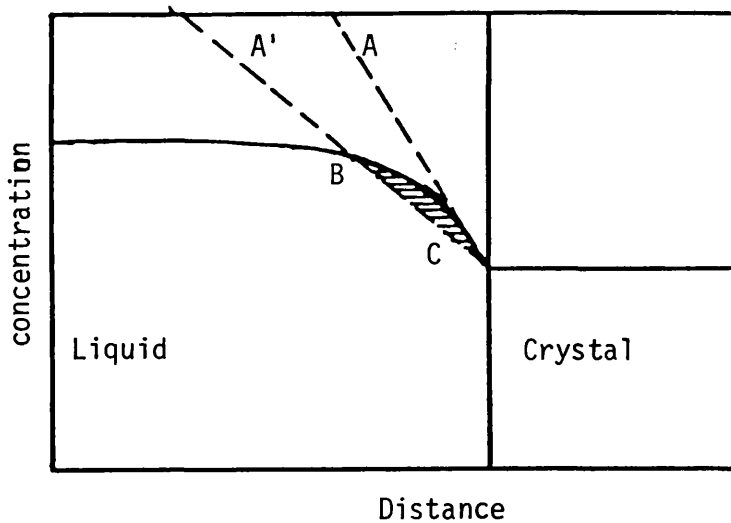
$$\frac{G}{V} \leq \frac{mC_s(0)(1-k_0)}{k_0D_L}$$

where  $G$  is the temperature gradient of the interface,  $V$  is the growth rate,  $C_s(0)$  is the solute concentration in the solid at the interface,  $k_0$  is the partition coefficient in the slope of the slope of the liquids and  $D_L$  is the solute diffusion coefficient,  $m$  is the liquidus slope.

As can be seen from this equation, conditions involving steep gradient and slow growth rates are best, to avoid constitutional supercooling.



(a)



(b)

Figure 3.2 Constitutional supercooling - (a) distribution of solution; (b) liquidus and temperature gradient. In each case, the abscissa represents the distance along the specimen (Rutte and Chalmers, 1953).

A = normal growth.

A' = constitutional supercooling.

### 3.4.2 Polycrystalline growth

Stoichiometric amounts of a high purity element (99.999%) were used for all materials prepared. The preparation of every sample material resulted initially in the polycrystalline form being produced. The elements were introduced into prepared tubes. After evacuating the tube and sealing it off at a pressure of less than  $10^{-6}$  torr, the loaded tube was placed in the temperature gradient of a two zone tubular resistance furnace. Some problems arose from the high pressure inside the phosphide ampoules, especially below the melting point of the material. This caused some samples to explode before the melting point was reached. This problem was solved as described in section 3.4.3. The sample was heated rapidly to about 50° C above the melting point of the materials, maintaining it at this temperature for more than 20 hours, then cooling it down at a rate of 6° C/h to about 600° C and then 20° C/h to room temperature.

A continuous vibration was used for heating to assist in mixing the elements and reducing the pressure for the phosphide samples. The whole procedure took about one week for each experiment. The tubes were removed from the furnace and in all the phosphide samples there was more than 5% in volume of unreacted phosphorus present. This problem was solved as described in the next section. A list of all the compounds and alloys prepared is given in Tables 3.1 and 5.12.

All the samples prepared were tested by electron probe microanalysis, X-ray powder photographic investigation, and DTA measurement.

### 3.4.3 Growth of single crystals using a modified Bridgman technique

There are several laboratory techniques which are used to grow single crystals, the liquid-solid method being that most widely used. The most

important experimental schemes which have evolved in this region are:

- (a) directional solidification;
- (b) cooled seed;
- (c) crystal pulling; and
- (d) zone melting.

The directional solidification method was the main procedure used in the present work. This method was used for the first time in 1925 by Bridgman in the USA [44] and others [45-48] for the growth of large metal single crystals, and later by Stockbarger [49,50] for the growth of optical quality alkali halide crystals for prisms and lenses. It was also developed independently in Europe [51,52].

Many of the compounds of current technological interest in the field of semiconductors and electro-optical application such as GaAs, InP, ZnTe, ZnSiP<sub>2</sub>, *etc.*, are difficult to prepare in bulk form from the melt. Because of the high vapour pressure and dissociation, CuGe<sub>2</sub>P<sub>3</sub> and Ag<sub>6</sub>Ge<sub>10</sub>P<sub>12</sub> are materials with the same problems. The dominant difficulty is that of controlling the vapour pressure. If it is sufficiently high to cause evaporation, then serious problems can occur during crystal growth. These problems range from loss of visibility to melt non-stoichiometry, a concomitant effect due to constitutional supercooling. Crystal contamination by impurities is another intrinsic problem.

The main purpose of the present technique is to show how a simple technique of pressure balancing can be used to solve some of these outstanding problems, as well as the temperature gradient. It is clear that control of dissociation is the central problem encountered during the growth of the above-mentioned compounds. Without that, single crystals cannot be prepared from the melt. In order to reduce the evaporation loss, 10% extra phosphorus was added to the compound [53].

This method of controlling dissociation allows the melt to equilibrate in a closed environment which is capable of standing the dissociation pressure. Another important problem was that of explosions caused by the high pressure of phosphorus (about 100 atm at 600° C, as calculated from the extrapolation of the pressure data, taken from the Handbook of Chemistry and Physics (1974). This was solved by using a double zone furnace, as shown in Figures 3.3(a) and (b).

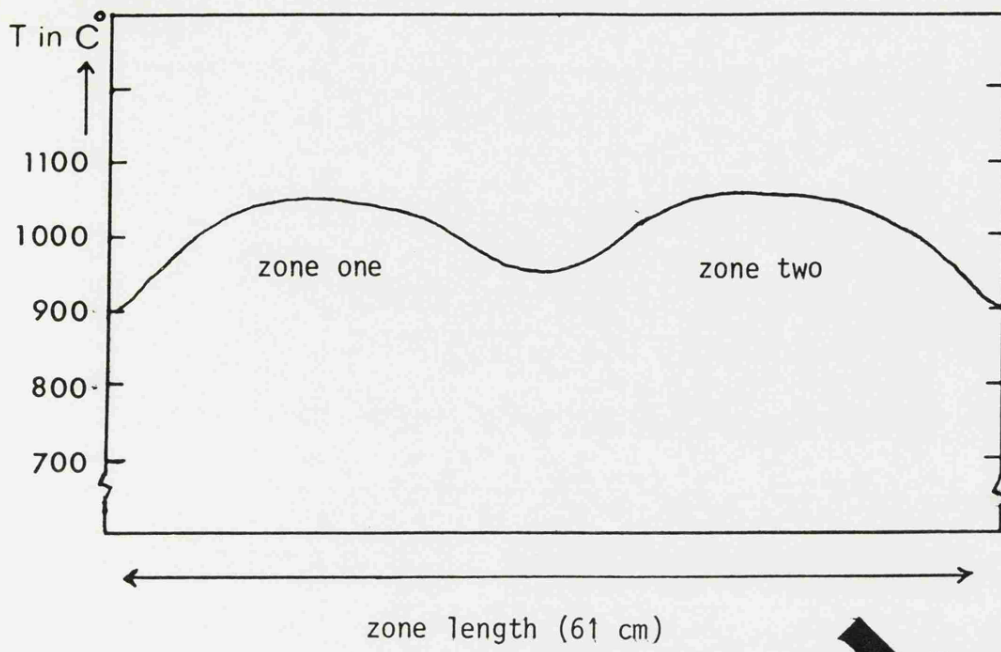
The furnace position was 10° to the vertical. The ampoule was placed in the furnace where the source material was fixed in zone one. The temperature of this zone was increased above the melting point of the compound, keeping zone two at room temperature. In this case, the compound temperature was about 950° C, thus the material was reacted under insufficient phosphorus, caused by the low pressure in the other side of the ampoule. However, the pressure is due to the compound, not to the phosphorus, which has a higher pressure [54].

In the next stage, the temperature of zone two was increased to the same degree, or above, to balance the phosphorus pressure inside the ampoule. By these procedures, the problem of dissociation was solved.

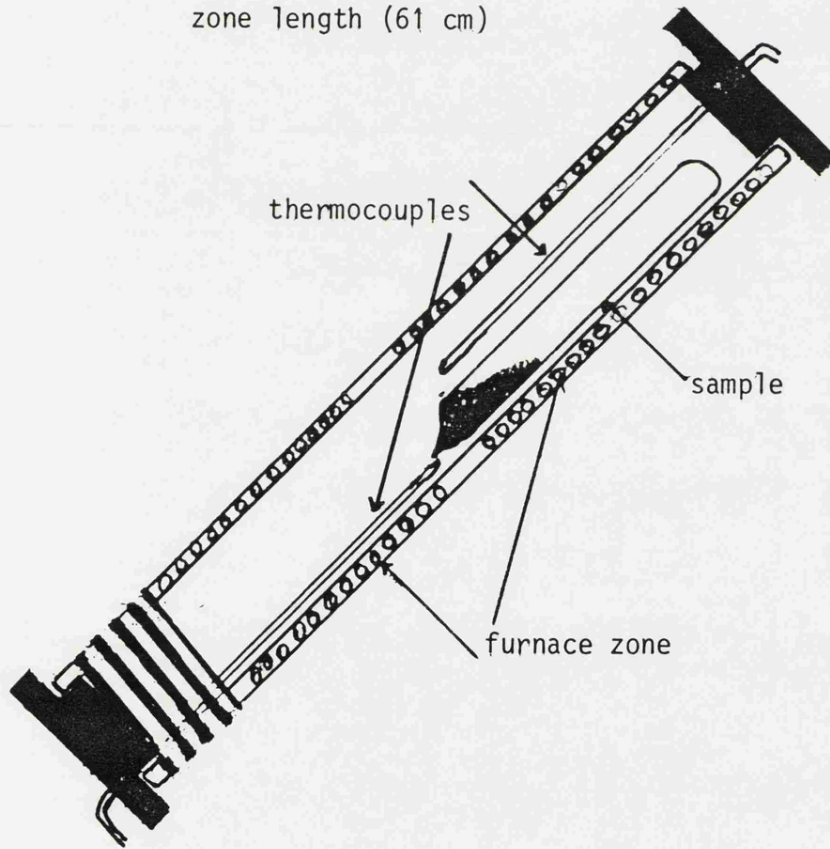
The final problem, that of having a suitable temperature gradient, was solved by carefully moving the ampoule to zone two, allowing the end of the sample to be fixed in the region of the air gap between the two zones, where the best temperature gradient could be obtained, as shown in Figures 3.3(a), (b) and (c).

The two outer ends of the zones were closed, in order to minimise the flow of the air inside the furnace. The fume cupboard was closed as a precaution against any external disturbance.





(a)



(b)

Figure 3.3 (a) Temperature gradient of double zone furnace  
(b) Ampoule position inside the furnace

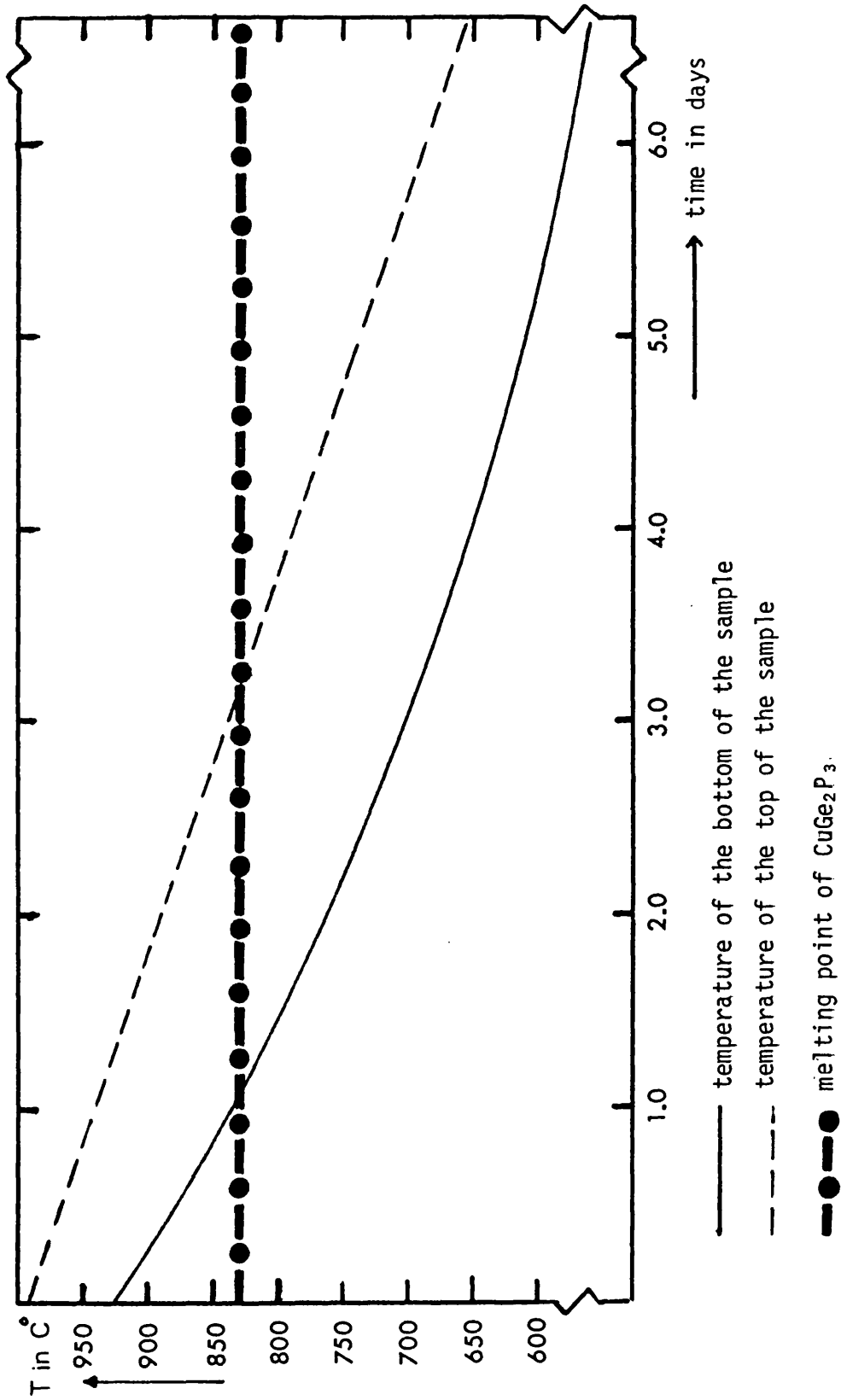


Figure 3.3 (c) Cooling temperature gradient of the two ends of the sample (time dependent) inside the furnace zone, showing reasonable gradient for crystal growing

Cooling started with zone one at 2° C per hour and only when the temperature reached 500° C, was the cooling of zone two started at 2° C per hour, to about 400° C. The sample was taken out after fast cooling at this temperature. The result of all these procedures was the formation of single crystals of several compounds and alloys, as shown in Table 3.1.

The photograph of single crystals of  $\text{CuGe}_2\text{P}_3$  is shown in Figures 3.4(a) and (b), and the Laue photograph can be seen in Figure 3.5(a) and that for  $\text{Ag}_6\text{Ge}_{10}\text{P}_{12}$  in Figure 3.5(b).

All these procedures took no more than two weeks. The crystals were tested and studied by using X-ray powder and Laue method photographs. The direction of growth can be observed for  $\text{CuGe}_2\text{P}_3$  as shown in Figures 3.4(a) and (b).

### 3.5 Solution Growth

The main reason for growing crystals from solution is to reduce the temperature at which crystallisation takes place. In the case of  $\text{CuSi}_2\text{P}_3$ , this method of growth was useful, because of the high melting point of the compound and the high vapour pressure due to the phosphorus. However, this growth technique was also of value for compounds in which phase transitions take place below the melting point, for example the transition from disordered structures to ordered ones, such as some chalcopyrite structures.

There are, however, disadvantages to solution growth, such as solute diffused into the crystal surface. Since the growth takes place over a considerable range of temperature, then the doping and composition of the crystal will change along the growth directions of the crystal.

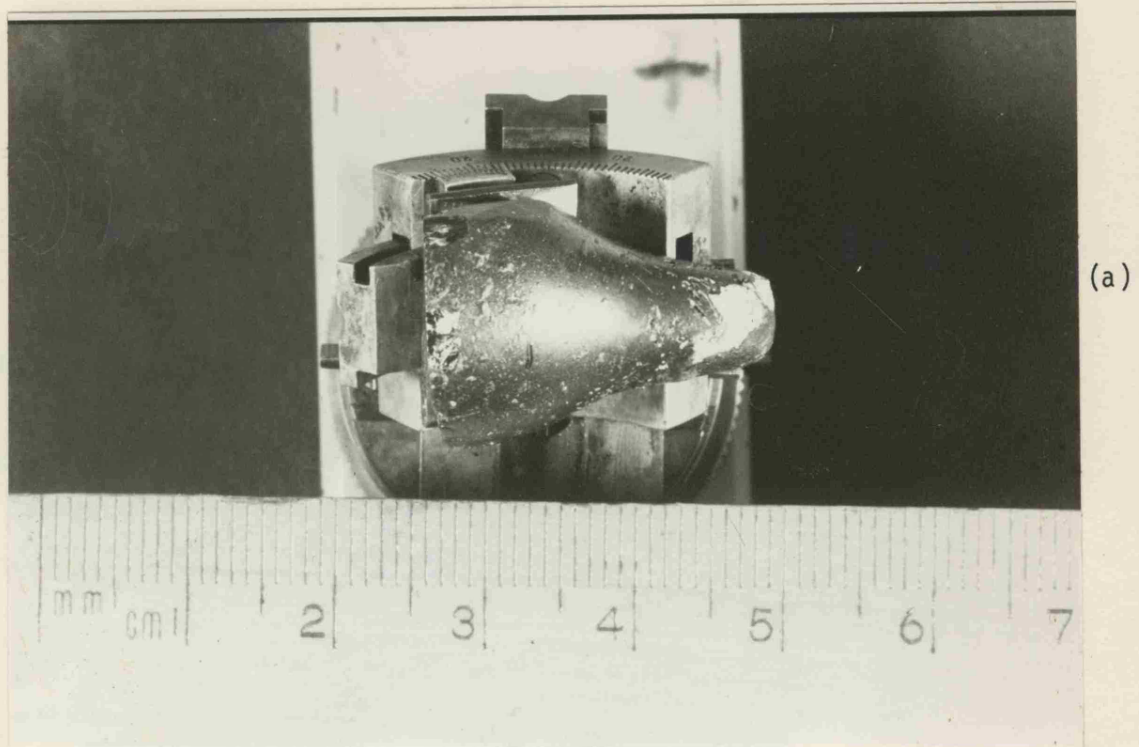
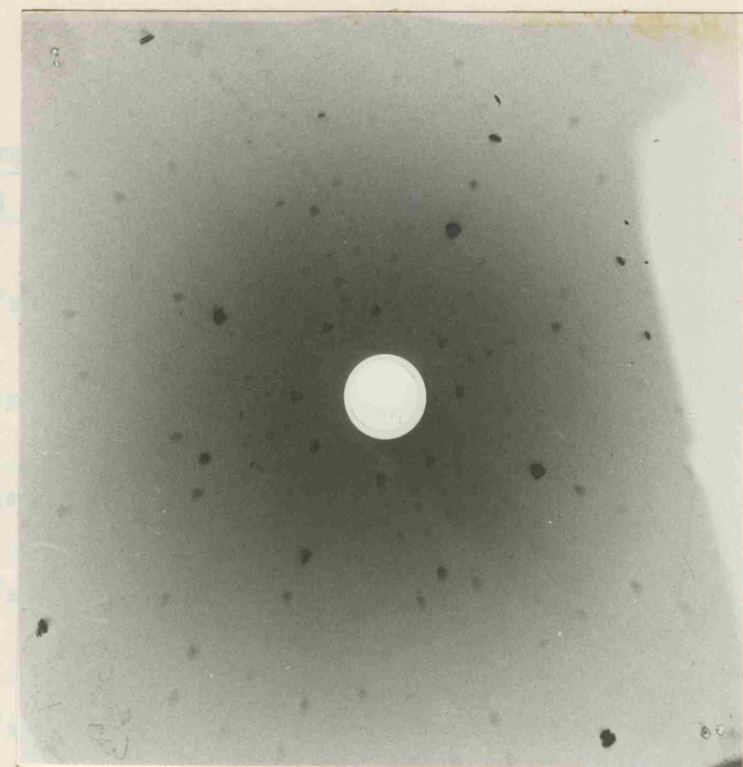
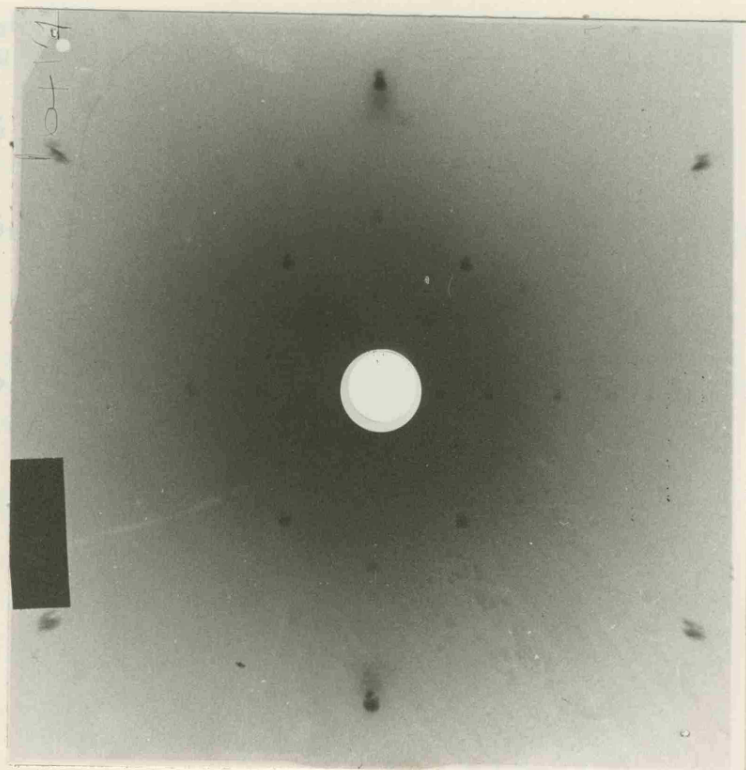


Figure 3.4 Single crystal of  $\text{CuGe}_2\text{P}_3$ : (a)  $\langle 100 \rangle$  surface;  
(b)  $\langle 110 \rangle$  surface



(b)



(a)

Figure 3.5 Laue back-reflection photographs: (a) for  $\text{CuGe}_2\text{P}_3$  crystals ( $\langle 110 \rangle$  surface);  
(b) for  $\text{Ag}_6\text{Ge}_{10}\text{P}_{12}$  crystals

Table 3.1

Single crystals grown using a modified Bridgman method

<u>Compounds and alloys</u>	<u>Dimensions in cm</u>		<u>Notes</u>
	<u>Length</u>	<u>Diameter</u>	
CuGe <sub>2</sub> P <sub>3</sub>	2.5	1.5	
CuGe <sub>2+x</sub> P <sub>3</sub>	2.5	0.5	six crystals of different composition up to x = 3
Ag <sub>6</sub> Ge <sub>10</sub> R <sub>12</sub>	2.5	0.5	
CuSi <sub>2</sub> P <sub>3</sub>			crystals as large as 0.02 x 0.1 x 0.5 cm in dimension were produced by using tin solution growth
CuSi <sub>3</sub> P <sub>3</sub>	3.0	0.5	
CuSi <sub>4</sub> P <sub>3</sub>	3.0	0.5	
CuSi <sub>5</sub> P <sub>3</sub>	3.0	0.5	
(CuGe <sub>2</sub> P <sub>3</sub> ) <sub>1-x</sub> -(Cu <sub>2</sub> GeS <sub>3</sub> ) <sub>x</sub>	2.5	0.5	single crystal for every x when x = 0.1 - 0.9
CuGePS	2.0	1.5	
Cu <sub>2</sub> GeS <sub>3</sub>			small ingots were produced as large as 0.2 x 0.4 x 0.8
CuGe <sub>2</sub> P <sub>3</sub> -Ge <sub>3</sub> P <sub>4</sub>	2.5	0.5	two single crystals for 20% and 35% of Ge <sub>3</sub> P <sub>4</sub>

The type of solvent used could be very active for some physical properties such as band structure or general electrical properties, so a solvent with a very low solid solubility must be used.

Apart from the properties mentioned above, the solvent should have a low melting point, to allow the material to grow at a lower temperature and be easily decanted from the crystal in order to avoid damage to the crystal which would result from the contraction of the metal during cooling.

Tin and zinc were the most successful solvents used in this field. Most of the II-IV-V<sub>2</sub> group compounds were grown successfully using these materials, whilst other materials were avoided, such as cadmium, gallium, indium and mercury, due to their high impurity, or solid solutions resulting from the use of indium and gallium [55]. Some solvents have a very high vapour pressure, which is unsuitable for practical application, such as mercury [56].

Since group IV elements such as tin and lead should be electrically neutral in compounds containing group IV, these elements were the most widely used ones in this regard. However, tin is the most common material in this case, and is used for growing almost all group II-IV-V<sub>2</sub> materials successfully, particularly the ones containing tin and silicon as group IV [55,57].

Group V elements, such as antimony and bismuth, have been used, but so far with no success [55].

The most difficult compound to grow in this work, due to its high melting point and pressure, is CuSi<sub>2</sub>P<sub>3</sub>. However, the melt growth method failed to prepare this compound. Tin solution growth was chosen for the

reasons mentioned earlier. Such a method of growth could control the pressure and crystallise the material at a lower temperature than its melting point. Tin was chosen as a solvent for the above reasons, although information on this compound is limited. The compound was reported to be grown by fusion, in poor polycrystalline form, when the lattice parameter is much higher than expected [32]. The melting point of the compound was measured with no sign of phase transition, using DTA curves, the details of which are given in Chapter 4.

With tin as the solvent, an ampoule of 1 cm diameter and 15 cm length was used. Then 1:5 of  $\text{CuSi}_2\text{P}_3:\text{Sn}$  were mixed as raw materials, sealed off under about  $10^{-7}$  torr and fixed in a double zone furnace, which is suitable for growing crystals by the fusion method. The temperature gradient could be as much as  $40\text{-}60^\circ \text{C/cm}$  in the growth region. The material was heated quite quickly to  $1100^\circ \text{C}$ , then held for one day at this temperature and cooled at about  $2^\circ \text{C/h}$  down to  $600^\circ \text{C}$ , then the furnace was inverted to allow the tin to separate from the grown crystals. Crystals as large as  $0.02 \times 0.3 \times 0.5 \text{ cm}$  were grown. The remaining tin was removed by polishing techniques and a rectangular shape was made for some electrical measurements.

These crystals were analysed by X-ray techniques. The possibility of replacing silicon by tin is rather small<sup>\*</sup>, since the latter exists in bcc form and there was no sign of this for crystals tested so far [25].

### 3.6 Iodine Transport

#### 3.6.1 General considerations

Vapour transport growth is a reliable method of growing compounds with either a high melting point or high pressure of the volatile component at the melting point, which undergo peritectic decomposition. However,

---

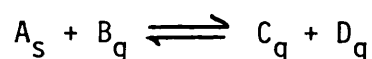
\* in  $\text{CuSi}_2\text{P}_3$



special care must be taken to avoid uncontrollable nucleation and poor crystalline quality [58].

The conditions required for chemical transport of elements are as follows:- all compounds produced in the reaction must be volatile, and the transport agent must be chosen such that the equilibrium constant has a suitable value at a convenient temperature for crystal growth. When the chemical transport of a compound is considered, then the partial pressure of compounds such as  $AY_a$  and  $BY_b$  should be approximately in the stoichiometric ratio of the compound required, when the A and B component elements of  $Y_a$  and  $Y_b$  are transporting agents. In addition, the chemical potential of A and B must have suitable values at the points where the compound is to be volatilised and deposited [59].

Chemical transport occurs throughout a heterogeneous reaction which can be written schematically as:



The subscripts g and s refer to the gaseous and solid compounds respectively. This reaction occurs in a temperature gradient, which is the driving force, resulting in a "chemical transport" of  $A_s$ . This takes place either in a closed or open system. A steady state of transport of  $A_s$  is built up and a concentration gradient of the gaseous phase is created.

When the transport is rate-limiting, the speed of deposition can be calculated, mass transport by diffusion resulting from the concentration gradients in the gas phase. Thermal convection and bulk flow of the vapour (Stephen's law) takes place. Further details of the theoretical calculations of the speed of deposition can be found in references 60-62.

### 3.6.2 Nucleation

Systematic investigation of the speed of deposition of Si and GaAs has been carried out [63]. Two temperature regions can be distinguished: a high-temperature region, where the process is limited by the chemical transport of matter, and a low temperature region, where the growth rate is determined by surface reaction.

Crystal growth starts by nucleation, *i.e.*, formation of the first tiny single crystal. Supersaturation is an important parameter controlling the nucleation, which is defined as

$$p/p_0 = \alpha$$

where  $\alpha - 1 \rightarrow$  is the supersaturation;  $p_0 \rightarrow$  is the equilibrium pressure of gases and  $p \rightarrow$  the actual pressure. The difference in free energy per atom,  $G_V$ , between a molecule in the gas phase and in equilibrium with the solid is:

$$G_V = -kT \ln \alpha$$

To determine the surface free energy, we write:

$$G_i = G_V(i) + G_S(i)$$

Where  $G_S(i)$  is the energy expended in creating the surface of the nuclei with  $i$  atoms. In a closed system, nucleation occurs at random, preferentially at a defect in the wall. In general, two factors in the control of nucleation are very important - the supersaturation  $\alpha - 1$ , and the surface free energy,  $G_S$  [64].

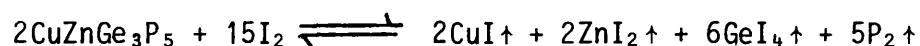
### 6.3.6 Experimental

Silica ampoules are often used to grow ternary and quaternary semiconductors in closed systems. Ampoules were prepared and cleaned, the elements were cleaned and put into the prepared tubes, and sealed off at a pressure of less than  $10^{-6}$  torr, with the end containing the source material cooled down to decrease the iodine evaporation, then placed in the double zone furnace. During stage one, both zones were heated up quite fast, but the deposition zone was kept hotter. This reverse temperature gradient cleaned the deposition zone. This zone was kept at the required temperature for about 10 hours, then in stage two, the deposition zone was cooled slowly to the required temperature until it was at a lower temperature than the source zone.

This was the primary nucleation period. Finally, the source zone was held constant at the chosen temperature of about  $70^{\circ}$  C above that of the deposition zone. Figures 3.6(a) and (b) show the temperature programmes of the two zones in the case of  $\text{CuZnGe}_3\text{P}_5$ .

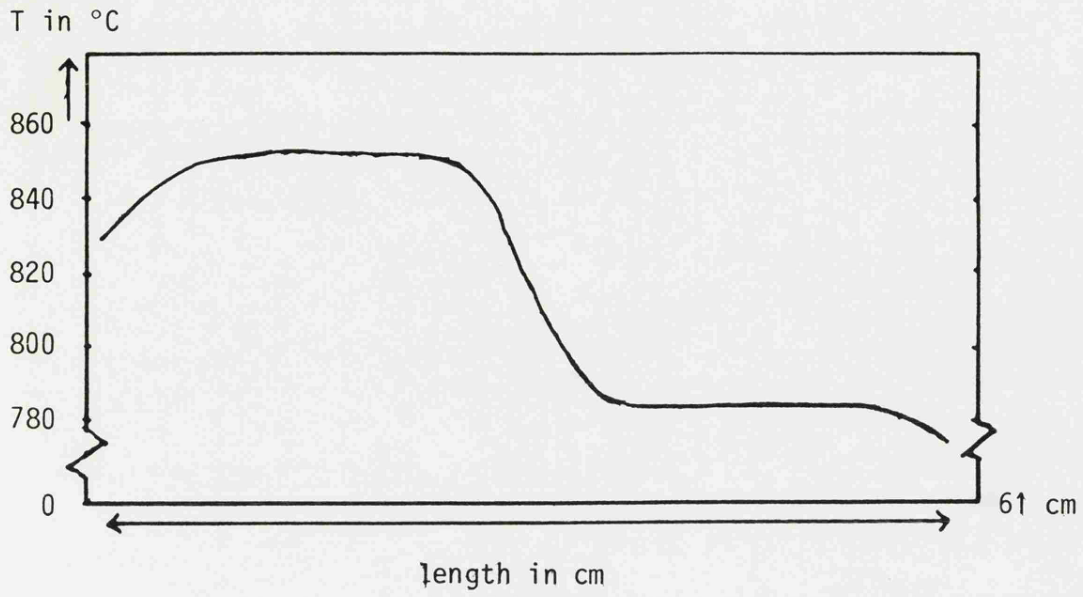
The growth period takes two to three weeks. This method is used for growing compounds which are shown in Table 3.2.

The transferring mechanism equation of compound  $\text{CuZnGe}_3\text{P}_5$  can be shown as:

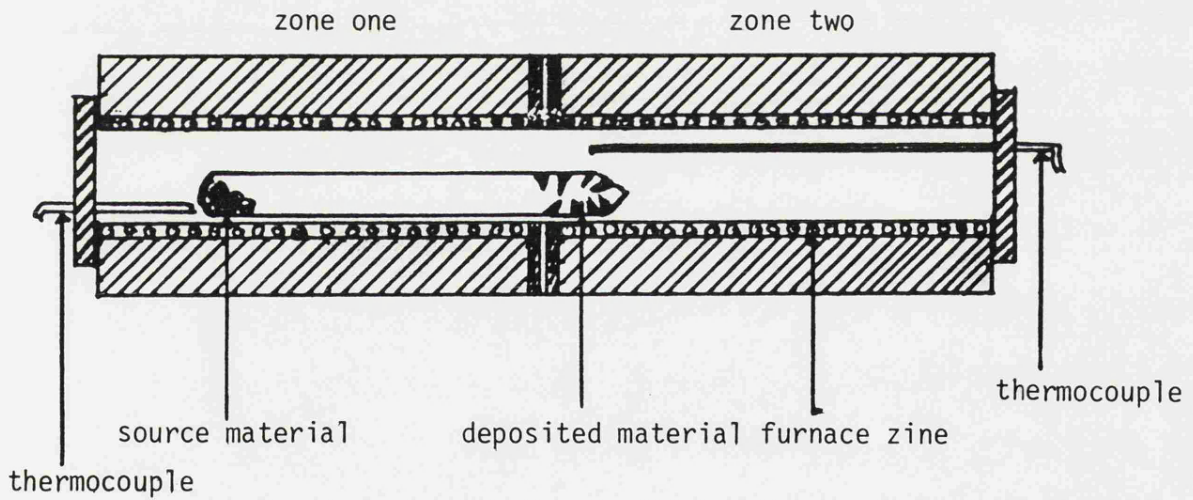


The equation goes to the right in the hot zone and to the left in the cold zone.

A schematic diagram of the two-zone furnace is shown in Figure 3.6(b). This is the same double zone furnace which was used for growing single crystals of  $\text{CuGe}_2\text{P}_3$  and  $\text{Ag}_6\text{Ge}_{10}\text{P}_{12}$  from melt using the modified Bridgman method mentioned in section 3.4.3.



(a)



(b)

Figure 3.6 (a) Temperature profile of the two zone furnace

(b) Schematic drawing of the crystal growth furnace in cross-section and ampoule position inside the zone tube

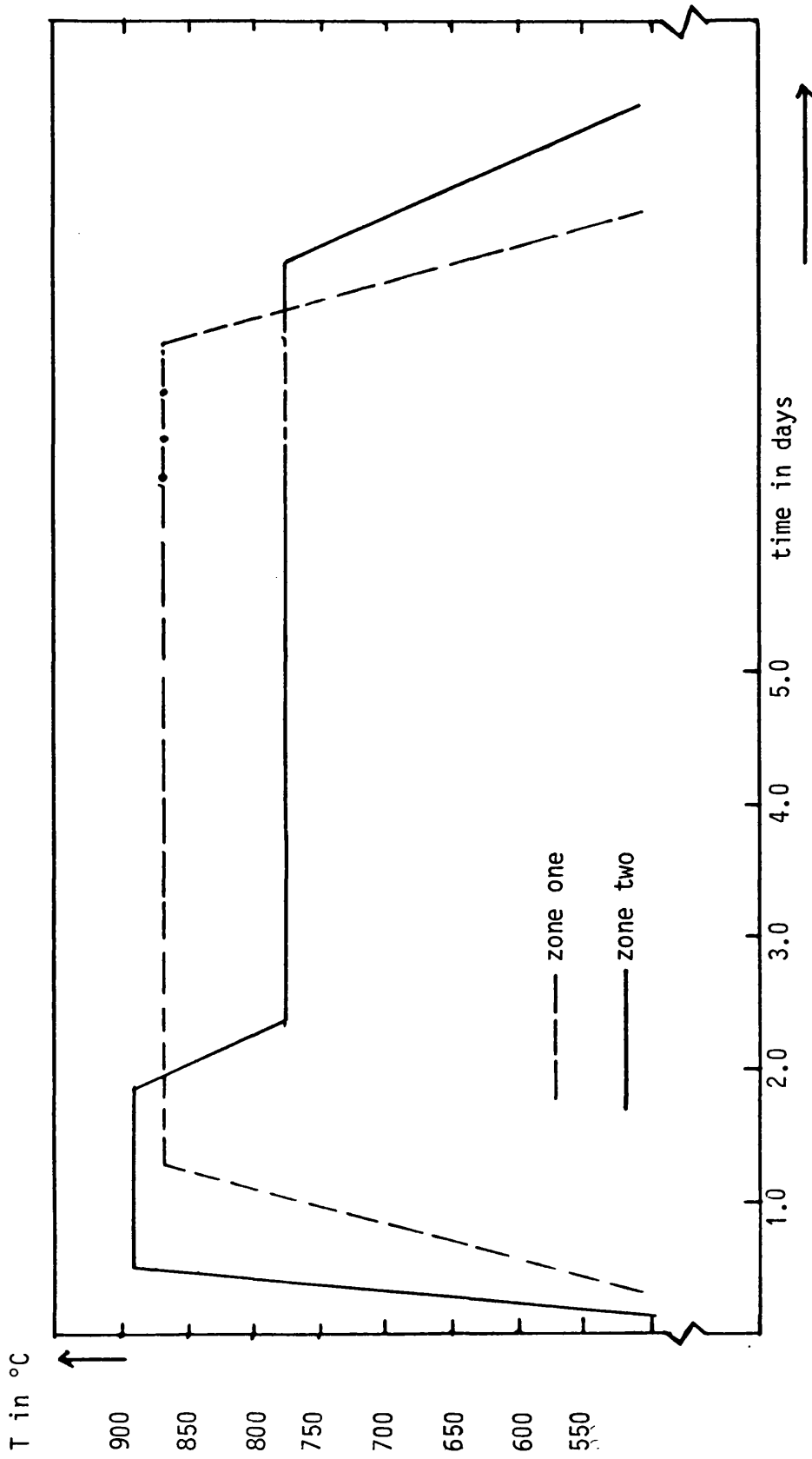


Figure 3.6 (c) Temperature programmes for source and deposition zone for growing  $\text{CuZnGe}_3\text{P}_5$

The rate of transport was studied by the mean transfer rate  $M$  in mg/h, which was assessed from the weight of the transported crystal in relation to the residence time. The rate of transport for  $\text{CuZnGe}_3\text{P}_5$ , using 8 g of material with an iodine concentration of 6.5 mg/cc, tube diameter of 2.5 cm and 19.5 cm in length and a temperature difference of 70° C between the two zones, is 25.48 mg/h.

The rate of transport is dependent on the capsule's internal diameter and is independent of the residence time [65]. The size deposition in the crystalliser decreases with increasing mass transfer, due to the increasing capsule diameter. The proportion of hollow crystals increases and the proportion of the largest crystals decreases simultaneously [65,66].

Table 3.2

Iodine transport growth of some ternary compounds and alloys investigated in this work

<u>Compounds</u>	<u>X-ray investigation</u>	<u>EPMA</u>	<u>Results</u>
$\text{CuGe}_2\text{P}_3$	Unknown and complicated structure	Uniform of all elements as single crystal	
$\text{CuZnGe}_3\text{P}_5$	Two different single crystals of $\text{CuGe}_2\text{P}_3$ and $\text{ZnGeP}_2$ and single phase in a polycrystalline form of $\text{CuZnGe}_3\text{P}_5$	Uniform of all elements in a polycrystalline form	Successful compound
$\text{CuGe}_2\text{As}_3$	Unknown structure and very complicated	Not uniform as polycrystalline	Unsuccessful compound
$\text{CuZnGe}_3\text{As}_5$	Single crystals of $\text{ZnGeP}_2$ and unknown second phases	Not uniform as polycrystalline	Unsuccessful compound
$\text{AgGe}_2\text{P}_3$			No transport
$\text{AgZnGe}_3\text{P}_5$			No transport

CHAPTER 4

Differential Thermal Analysis and High Temperature  
Lattice Parameters

---

4.1 Introduction

The discovery of differential thermal analysis (DTA) is usually credited to Le Chatelier in 1887 [67,68]. Twelve years later, Sir Robert Austen [69] published a description of the DTA apparatus which forms the essential basis of all modern differential thermal analysers.

The use of differential thermal analysis has been established for some time in the field of ceramics, minerals and clays [67,70] and, to a lesser extent, in metallic alloy systems, is recognised as an essential technique for studying phase transformation occurring in compounds and mixtures of semi-conductor interest. In general, the phase diagram of the binary system in which the III-V and II-VI compounds occur is known [71], as it is for ternary compounds [37]. However, the expansion of semi-conductor work into lesser known regions of chemical composition has made the determination of phase diagrams an essential part of semi-conductor research. This arises firstly in the study of new and possibly complex semi-conducting compounds, where even the melting point may be unknown. Further, these compounds are sometimes deliberately prepared to be non-stoichiometric and in addition, often exhibit solid state phase transitions of great importance from the point of view of their electrical and thermal properties.

Secondly, DTA is invaluable in the examination of semi-conducting solid solutions between known pure compounds. A knowledge of the phase diagram is essential for the production of material of predetermined



composition by zone melting, particularly where the ternary section containing the solid solution is not pseudo-binary. In this case, chemical analysis and X-ray examination are usually also necessary.

However, the DTA results are due to physical or chemical processes, and therefore, if these do not occur, a steady differential temperature normally develops between the test and reference material. This is due primarily to differences in the heat capacity and thermal conductivity of two materials [72], but is also influenced by many other factors, such as sample mass and packing density [73].

#### 4.2 DTA Apparatus

The modern differential thermal analyser is a sophisticated piece of equipment, utilising many of the advantages made possible by the advent of solid-state electronics. However, the simple DTA contains mainly a sample holder with measuring system, a furnace as the heat source having a large uniform temperature zone and a recording system for indicating and/or recording the e.m.f. (suitably amplified) from the differential and temperature measuring thermocouples.

##### 4.2.1 Sample Holder-Measuring System

Recent improvements have resulted in better methods of amplifying the  $\Delta T$  signal, so that increased sensitivity can be obtained by using a small sample holder. A rectangular shaped ceramic sample holder measuring 1.5 x 3.7 x 7.3 cm was used. The DTA ampoules (0.5 cm diameter x 4 cm length) were fixed in the sample holder by means of two holes 1.0 cm in diameter. The ampoules are fixed in this manner in order to make good contact with differential Cr/Al thermocouples and only minimal contact with the sample holder. The differential Cr/Al thermocouple was in contact with the bottom of samples, as shown in Figure 4.1, in order to

detect temperature differences between the sample and inert material. The temperature of the system was registered by fixing another Cr/Al thermocouple between the samples by means of a small hole and opened to the two samples by two other holes, to make the temperature between the junction and the temperature record thermocouple more uniform (see Figure 4.1). The sample holder and its container were moved to the inside of the furnace zone by means of a motor driver, in order to obtain the same position in every cycle of the experiments. The sample holder was screened by a looped, earthed wire, to minimise pick-up of stray currents by the thermocouple. The Cr/Al thermocouple which was used was 0.056 cm in diameter. Boersma [74] found that the diameter of thermocouple wires should be as small as possible, to keep the thermal capacity and leak down to a minimum, but other workers [70] detected no difference in sensitivity when using thermocouples of 0.013 inches diameter.

#### 4.2.2 Furnaces

In order to assist in maintaining uniform heating, the furnace should have the following characteristics:

low heat capacity of the active furnace space for rapid response of the furnace temperature to variations in heat input;

high coefficient of heat transfer to the sample holder, *i.e.*, sufficiently large heating elements arranged in such a way that thermal gradients in the active space are minimised; and

adequate closing to prevent the air current from disturbing the heating process [75-78].

Although it is usually assumed that a furnace has a relatively large amount of packed insulation to minimise heat loss, Whitehead and Berger [79] described a furnace for vacuum DTA in which radiation shielding was used

instead of conventional packing. After analysis, the furnace could be cooled very quickly and be ready for another heating. Use of conventional techniques in winding furnaces, such as closer wire spacing near the ends of the furnace, assists in maintaining a uniform heat zone in the active space. In some cases, non-inductive winding has been used to minimise pick-up of stray currents by the thermocouple.

Figure 4.1 illustrates the DTA furnace which was used in this work. It was a two-zone furnace, in which the first zone was 60 cm long and 5.2 cm in diameter, fixed inside the second zone, which was 40.0 c.m. long and 8.0 cm in diameter, maintaining a gap between the two zones. The two zones were connected to the main power in series. No insulation was used between the second zone and the furnace wall. This new technique makes for a more uniform temperature and helps to attain higher temperatures up to about 1300 °C, where the heat rate was between 10-15 °C/min and cooling at about the same rate, down to about 600 °C, which was followed by cooling at a slower rate. Connecting the two zones in series also reduces some pick-up problems.

#### 4.3 Differential Thermal Analysis for $\text{CuGe}_2\text{P}_3$

The DTA for  $\text{CuGe}_2\text{P}_3$  was carried out in the range 20-1100 °C, under the above-mentioned conditions. The materials used were polycrystalline containing the second phase and single crystal (single phase). The DTA curve for polycrystalline  $\text{CuGe}_2\text{P}_3$  containing the second phase as shown by X-ray photography (Figure 4.2a) is illustrated in Figure 4.5a. On raising the temperature of the sample, a small but steady temperature difference developed between the test and reference materials. This was due to the fact that although the temperature at the centres of both materials was lagging behind that of the furnace, the magnitude of the lag depended

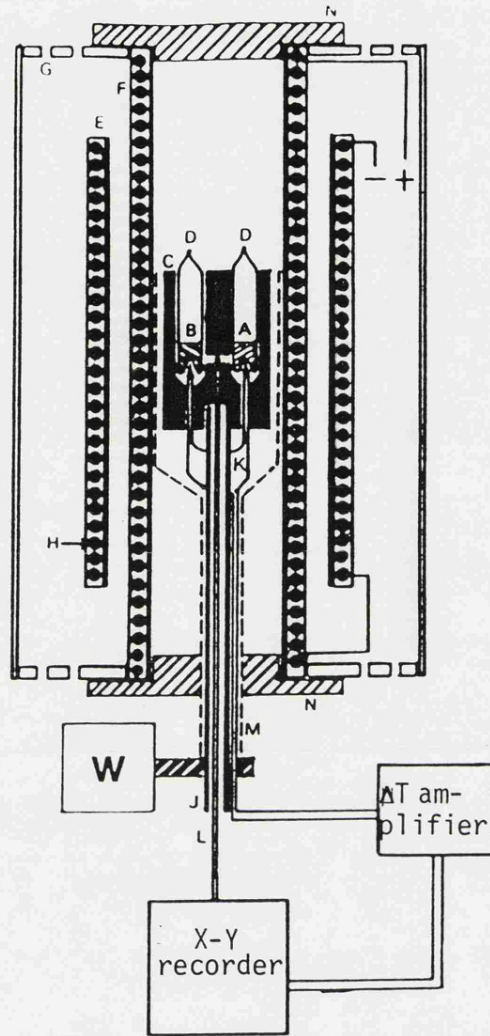


Figure 4.1 Cross section diagram of a complete apparatus of DTA used in this work.

- A - crucible (sample)
- B - reference (Ag)
- C - ceramic sample holder
- D - silica ampoules
- E - second zone
- F - first zone
- G - air cooling holes
- H - furnace winding
- J - ceramic road (sample holder, holder)
- K - differential Cr/Al thermocouple
- L - temperature recorder Cr/Al thermocouple
- M - earth shield
- N - air movement control
- W - sample holder motor driver

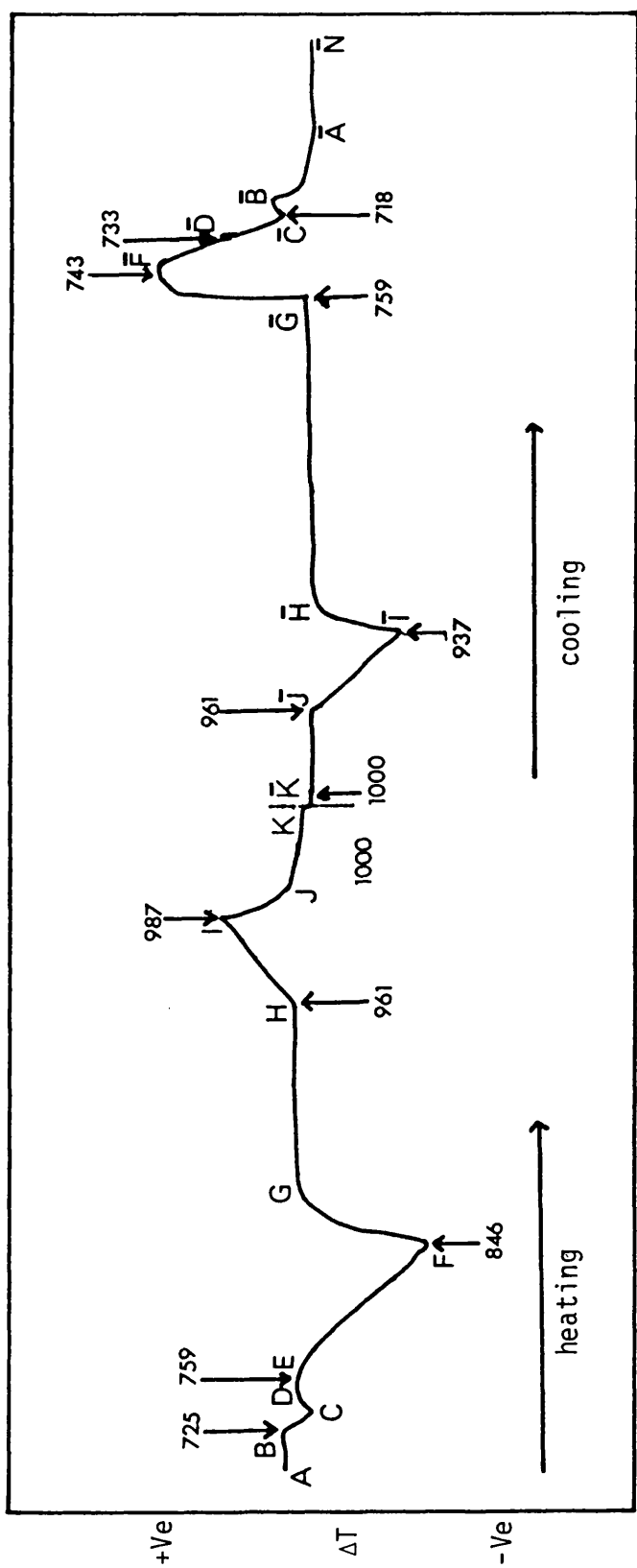
primarily on the thermal conductivity and heat capacity of each substance. Accordingly, the DTA curve continued in an approximately rectilinear manner, until the test material underwent some physical or chemical change (AB). At B (725 °C), the curve began to deviate from the base line, due to an endothermic process occurring within the test sample. This point, B, will hereafter be referred to as the onset temperature of the reaction, or phase transition, since it represents the temperature at which the process was first detected by DTA. The endothermic peak temperature, C, corresponds to the maximum rate of heat evolution detected by the differential thermocouples. At D, the curve returns to a new base line, due to the completion of the endothermic process. Generally, the peak temperature tended to show a much greater variation with the heating rate and other experimental factors than the onset of temperature, although the peak temperature was more easily measured. The endothermic process giving rise to the peak BCD was completed at the same temperature between points C and D. At E (759 °C), the curve began a new deviation from the base line, due to another endothermic process occurring within the test sample. This point will hereafter be referred to as the onset temperature of the second reaction, or phase transition, as it represents the temperature at which the process is detected for a second time by DTA. Thus E is the melting point of the sample and F is the second endothermic peak temperature. The endothermic process giving rise to the peak EFG is completed at the same temperature between points F and G. No further evolution of heat is detectable above G and the sample dissolved, so the curve returned to a new base line, GH. The heights of DE and GH above the abscissa normally differed, reflecting the change in heat capacity of the sample as a result of the endothermic process.

Another endothermic process took place, which is shown in the curve. This began at H, with a peak HIJ due to the reference sample of Ag. Completion of this process and formation of a new, thermally stable, phase, was confirmed when all the reference sample melted and the curve was then in a new horizontal portion of the curve JK. This all occurred in the heating process of the DTA experiment for the sample  $\text{CuGe}_2\text{P}_3$  with the reference material, Ag.

In cooling, the exothermic process J'I'H' occurred at J' (961 °C) and ended at H', when all the Ag as a reference, was frozen. The second exothermic process, G'F'A', occurred at G' (759 °C) and ended at A', with a secondary evolution at the peak at C' (733 °C) and E' (718 °C). At A', the curve returned to a new base line again, with no further evolution of heat being detected below A'.

In DTA experiments on  $\text{CuGe}_2\text{P}_3$ , as indicated by the curves shown in Figure 4.2, the peaks were reasonably sharp and well separated. It is important to remember that the peaks on a DTA can arise from both physical and chemical changes. The former includes melting, boiling and solid-solid structure transition. In Figure 4.2a, the first peak, BCD, was due to a chemical change in the compound as a solid. This may be the appearance of  $\text{Cu}_3\text{P}$  as a second phase in the sample, with increasing percentage of Ge in the compound. The second peak, which began at 759 °C, was due to the compound itself melting, and the third peak was due to the reference sample.

On cooling, the first peak resulted from the outcome of the reference sample. It began at 961 °C. The second peak was due to the compound and commenced at 759 °C, which was the freezing point of the compound. At this point there were two more small peaks at 733 °C and 718 °C, associated with some chemical changes, or possibly related to changes of  $\text{Cu}_3\text{P}$  and  $\text{CuGe}_2\text{P}_3 + \text{Ge}$  to  $\text{CuP}_2$  and  $\text{CuGe}_2\text{P}_3$ .



Temperature in  $^{\circ}\text{C}$

Figure 4.2(a) DTA curves of heating and cooling of  $\text{CuGe}_2\text{P}_3$  (polycrystalline sample containing second phase)

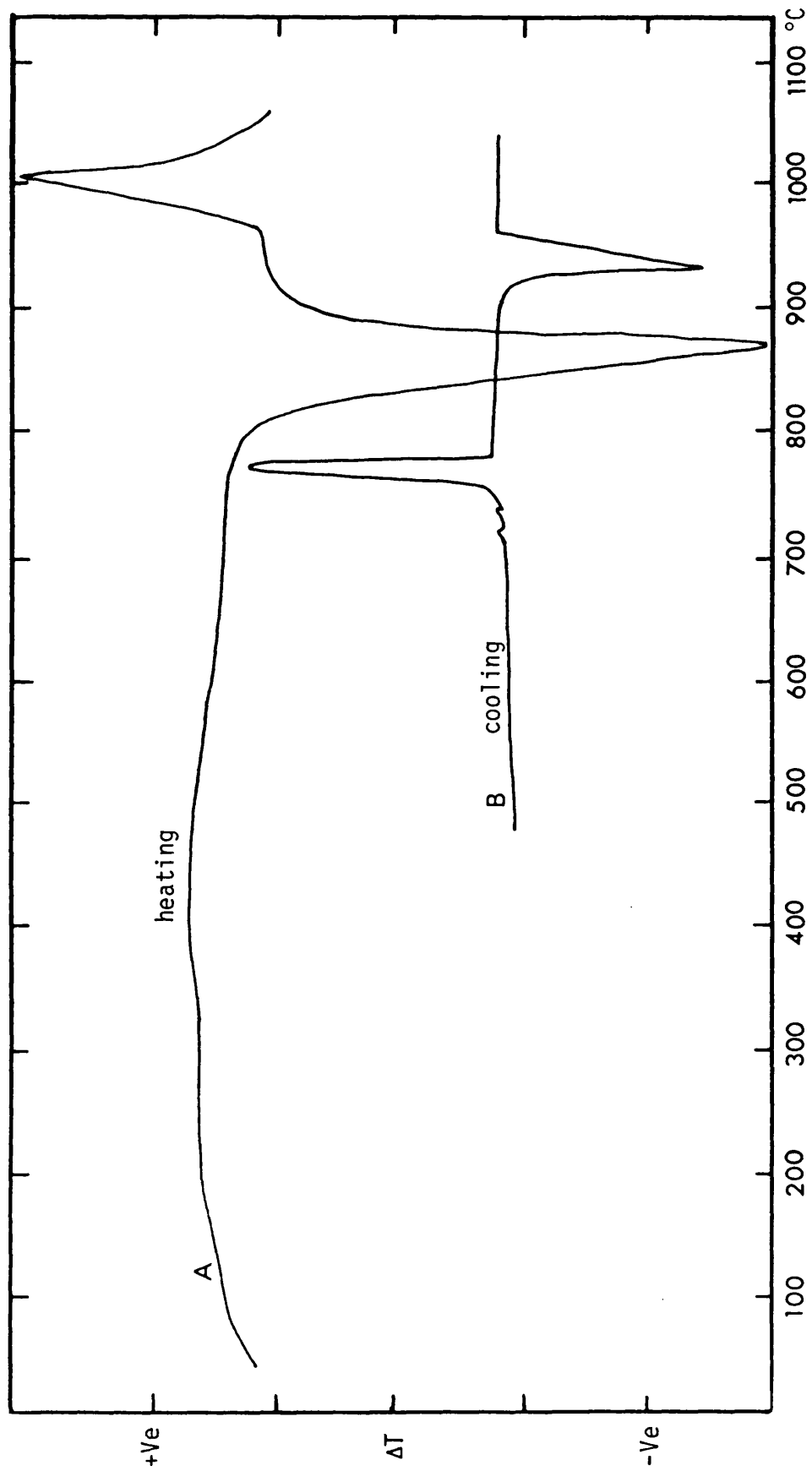


Figure 4.2(b) DTA curves for  $\text{CuGe}_2\text{P}_3$  (single phase material) first run, showing no second phase at heating, but secondary peaks appeared on cooling



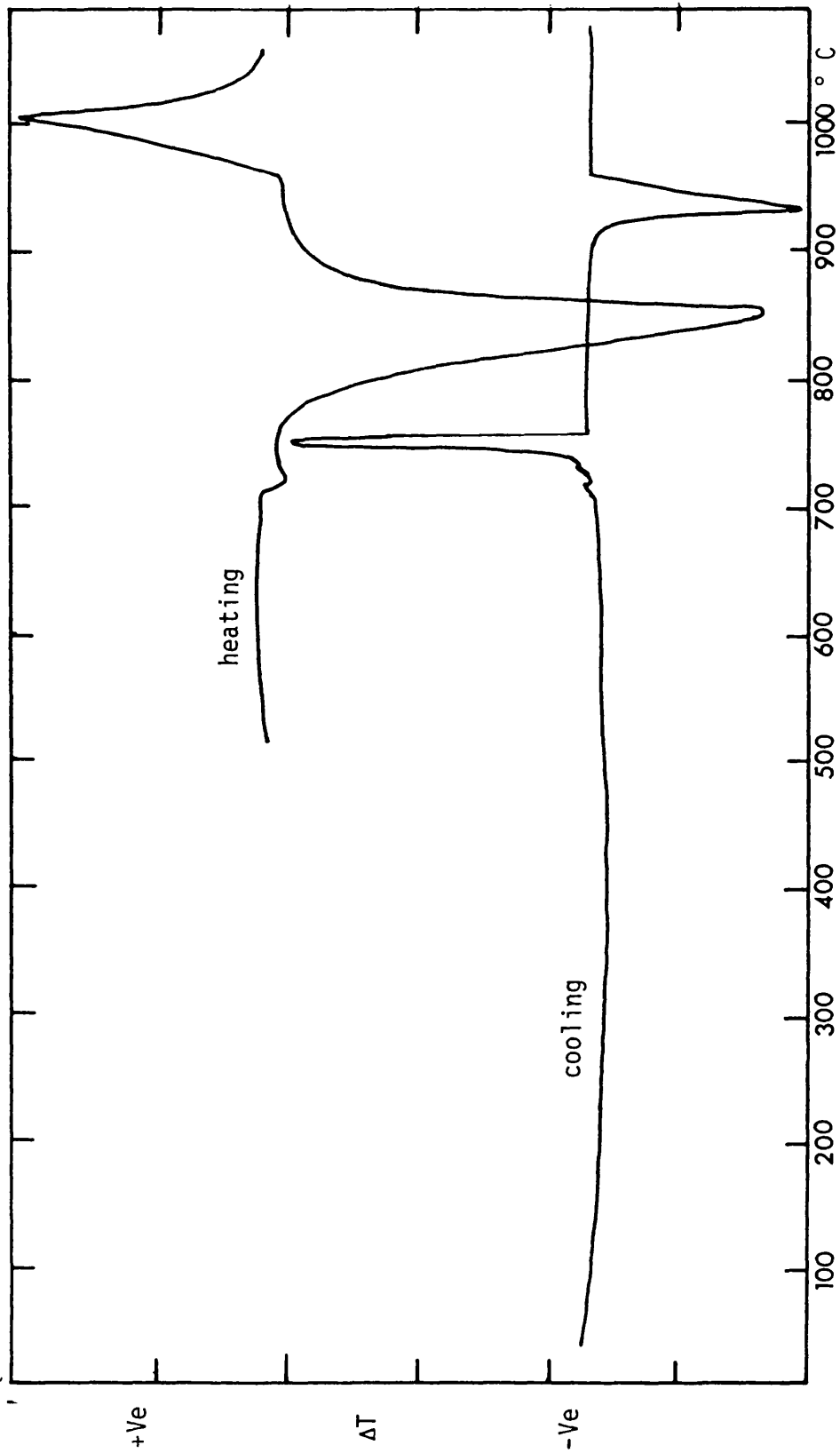


Figure 4.2(c) DTA curves for  $\text{CuGe}_2\text{P}_3$  (second run of single crystal), showing second phase appearing as in Figure 4.2(a).

The DTA for single phase materials of single crystal  $\text{CuGe}_2\text{P}_3$  showed no phase transition before the melting point of the compound was reached (about 830 °C). On cooling, however, the second phase appeared at the same temperature mentioned earlier. In the second cycle for this sample, the result was the same as for polycrystalline material, showing second phase peaks [see Figure 4.2(b) and (c)].

The DTA curve for  $\text{AgGe}_2\text{P}_3$  showed first evolution at 680 °C, with three main peaks, the last of which started at about 760 °C. The cooling process showed one main evolution at about 660 °C, with two other small peaks appearing at lower temperatures. The  $\text{Ag}_6\text{Ge}_{10}\text{P}_{12}$  curve, however, showed only one evolution on cooling and one on heating, at 738 and 780 °C respectively [see Figure 4.3 (a) and (b)].

The DTA curves for the  $\text{CuSi}_2\text{P}_3$  zinc blend structure showed only one transition on heating and one on cooling, without revealing any phase changes or second phases.

DTA results for these compounds and others are listed in Table 4.1.

#### 4.4 DTA for $\text{CuGe}_2\text{P}_3$ -Ge System

DTA measurements were made on fifteen samples within the Cu-Ge-P ternary systems, with compositions can be seen in Figure 4.4.

Figure 4.4(A) illustrates the melting point of the  $\text{CuGe}_2\text{P}_3$ -Ge section. The composition of  $\text{CuGe}_3\text{P}_3$  revealed the lowest melting point in the system, at 784 °C. For other compositions, the melting point began to increase slowly and became stable after the composition of  $\text{CuGe}_5\text{P}_3$ , at about 805 °C. In the cooling curve [Figure 4.4(B)], the solidification was almost in the same temperature region and below the melting point for the single phase composition region, which ends at  $\text{CuGe}_5\text{P}_3$ . For other compositions, however,

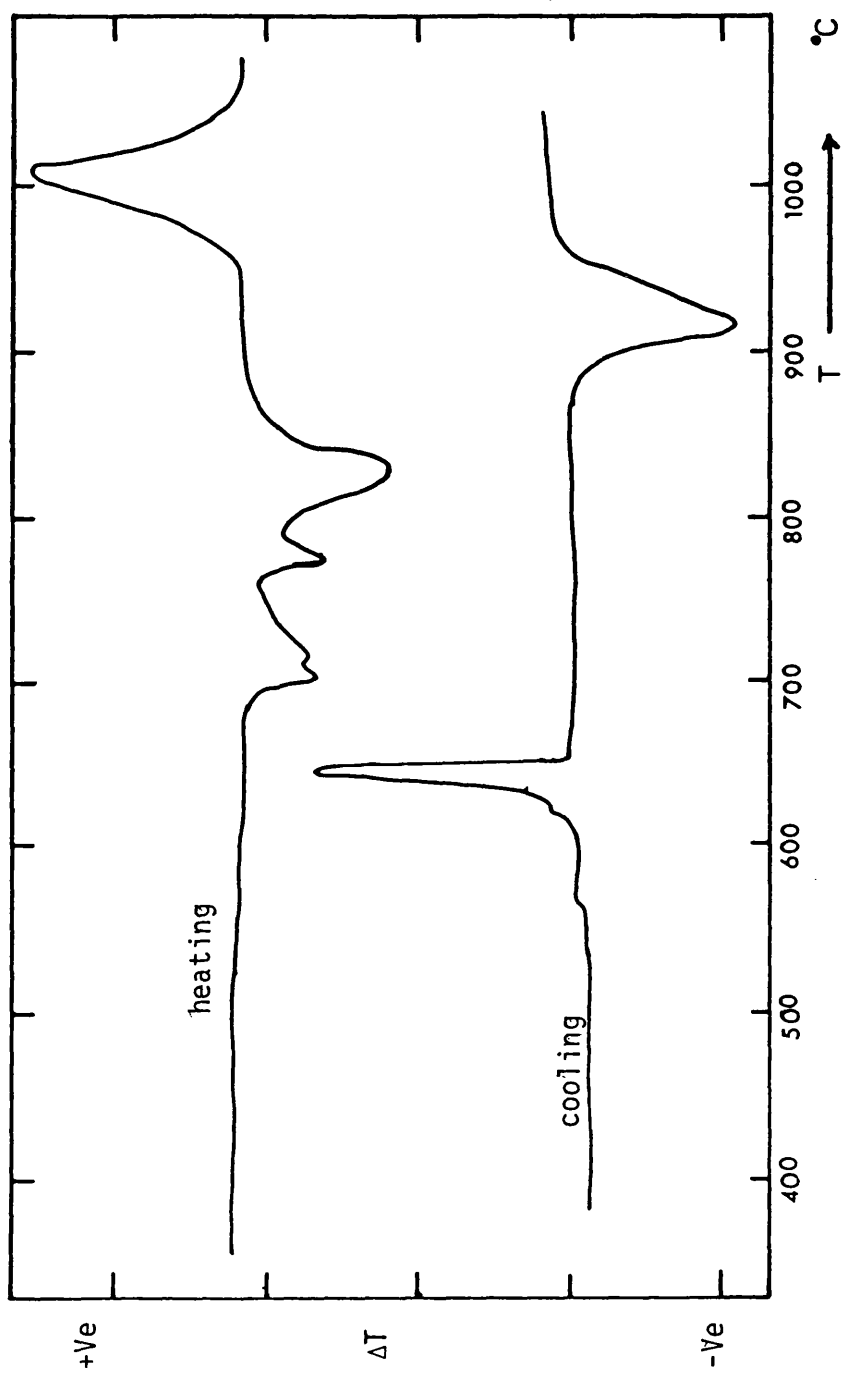


Figure 4.3(a) DTA curves for  $\text{AgGe}_2\text{P}_3$  (first run), showing more than one phase

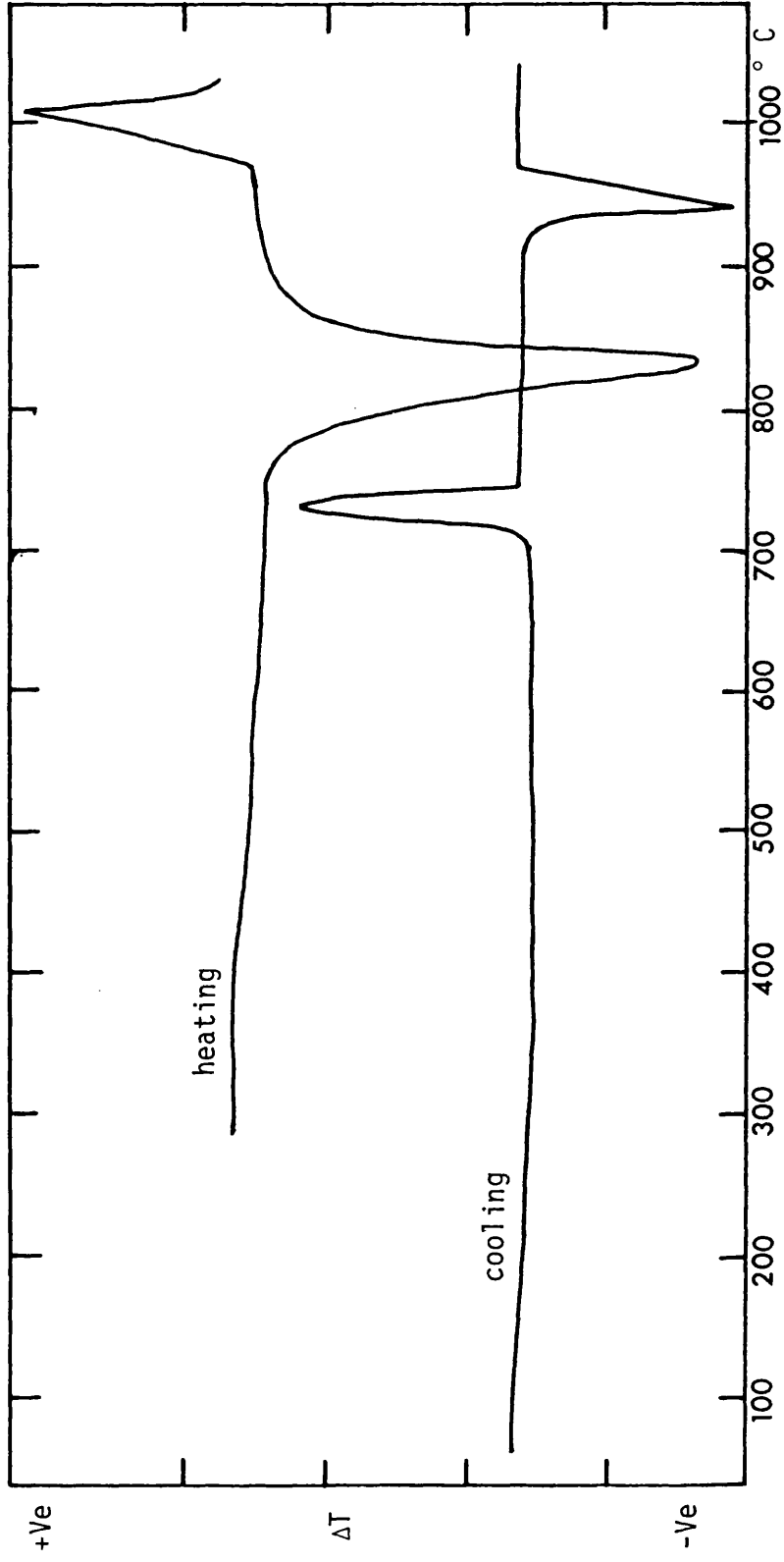


Figure 4.3(i)(b) DTA curves of heating and cooling of  $\text{Ag}_6\text{Ge}_{10}\text{P}_{12}$

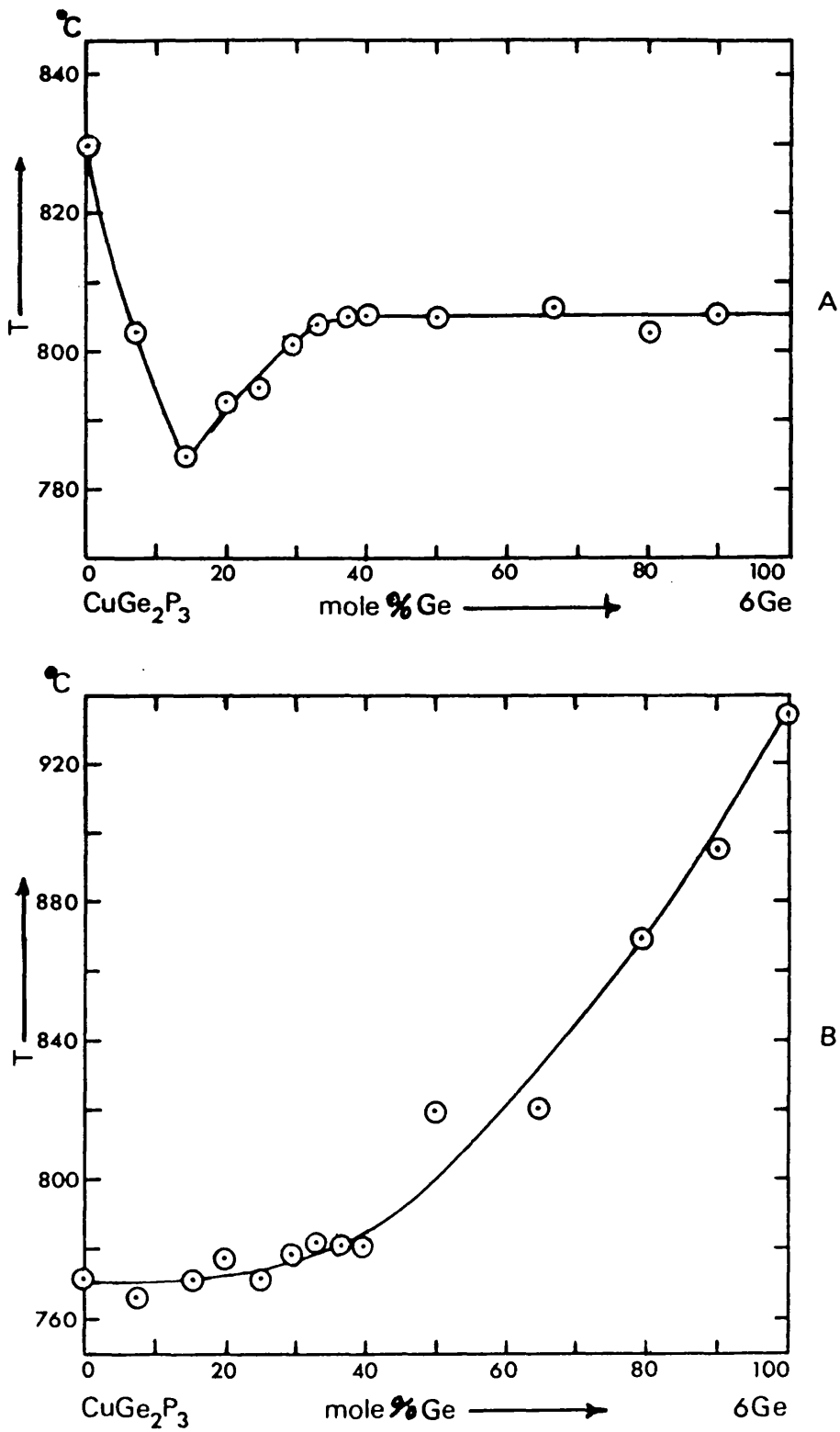


Figure 4.4 Section  $\text{CuGe}_2\text{P}_3$ -Ge of the system Cu-Ge-P.  
A - heating, B - cooling

Table 4.1

DTA results (heating and cooling) of some compounds and alloys of types I-IV<sub>2</sub>-V<sub>3</sub>, I-II-IV<sub>3</sub>-V<sub>5</sub> and I<sub>2</sub>-II-IV<sub>3</sub>-V<sub>8</sub>

Compounds	Heating peaks (T → °C)	Cooling peaks (T → °C)	Melting points (T → °C)
CuSi <sub>2</sub> P <sub>3</sub>	1178	1155	1178
AgGe <sub>2</sub> P <sub>3</sub>	625, 710, 750, 790	650, 625	
Ag <sub>6</sub> Ge <sub>10</sub> P <sub>12</sub>	780	738	780
CuZnGe <sub>3</sub> P <sub>5</sub>	725, 780	815	780
Cu <sub>2</sub> ZnGe <sub>5</sub> P <sub>8</sub>	725, 760	840, 760, 718	
AgZnGe <sub>3</sub> P <sub>5</sub>	700, 740	730	
Ag <sub>2</sub> ZnGe <sub>5</sub> P <sub>8</sub>	700, 738	727	
CuGe <sub>2</sub> As <sub>3</sub>	600, 720	719, 691	
CuZnGe <sub>3</sub> As <sub>5</sub>	583, 675, 775	800, 675, 638	

it began to increase slowly towards the Ge solidification temperature. The temperature of solidification of this system in the single phase region, was the main problem in drawing the phase diagram. This resulted from the phosphorus over-pressure due to decomposition after the compound melted, and a second phase in the system (see section 4.3), which lowers the solidification temperature.

This has always been the main problem when studying the phase diagrams of compounds containing volatile components such as P, S, Se, Zn, *etc.* [80-83]. For this reason, a special DTA apparatus was designed [84-91].

#### 4.5 High Temperature Lattice Parameter

Several methods have been used for measuring thermal expansion, including the optical method [92], interferometric diameter, or macroscopic thermal expansion [93], and X-ray powder photography. The latter is the most widely used method. These measurements are necessary due to epitaxial layers in which plastic deformation can occur, such as epitaxial Ge layers growing on single crystal GaAs substrates [94]. This created a need to know precisely, the coefficient of thermal expansion of both materials. Accordingly, Ge and GaAs ranges from room temperature to epitaxial deposition. Another reason for the use of thermal expansion data is the need to determine the match or mis-match of the dimensions of semi-conductor elements and substrates when cycled over large temperature ranges. A third method can be used widely to find out whether there are any phase changes in the structure or decomposition of materials in the compound

The linear thermal expansion of a solid is usually measured in terms of the change in length  $l$  with respect to the length  $l_0$  at some fixed temperature  $T_0$ . Usually  $T_0$  is taken at 273, 298, or 300 °K, or room temperature. The data are then usually given in terms of  $(l/l_0 - 1)$  versus

T. Here these data are converted into values of the true linear thermal expansion coefficient  $\alpha$ , where

$$\alpha = \frac{d(\ln \bar{\lambda})}{dT}$$

To a very good approximation,  $\alpha$  is given by

$$\alpha = \frac{1}{d_0} \cdot \frac{d\lambda}{dT}$$

It has been shown that the thermal generation of Schottky defects in solids gives rise to a difference between the macroscopic length change  $[(\frac{\lambda}{\lambda_0}) - 1]$  and the X-ray lattice parameter change  $[(\frac{a}{a_0}) - 1]$ . This work has been reviewed by Scloknecht and Simmons [95]. This difference has been measured in several solids (Al, Cu, *etc.*) [95]. It showed the two types of measurements given the same thermal expansion coefficients, as shown in Ag, Cl [96,97].

The lattice parameters of  $\text{CuGe}_2\text{P}_3$  were measured using a 19 cm Pye Unicam S150 high temperature powder camera, with a Van-Arkel film mounting. The following arrangement was used.

The film was in two sections, one on each side of the X-ray beam and their positions were marked by a series of pins, which cast shadows on the film. The positions of the pins were calibrated using the room temperature powder pattern of  $\text{K}\alpha\text{-Au}$ . It was verified that the lattice parameters of  $\text{CuGe}_2\text{P}_3$  at room temperature measured with this camera agreed with those obtained using a conventional camera.

The sample was contained in a sealed silica tube, 0.7 mm in diameter, which was mounted in the centre of the camera. Except for a narrow gap which allowed the X-ray to pass, the sample was surrounded by a heating



element. The temperature was measured with a Pt/Pt 13% Rh thermocouple near the sample and the inside of the camera was evacuated for thermal insulation.

Copper K $\alpha$  radiation filtered with Ni was used for the high temperature work, because the high power available makes for short exposure times (4 h at 40 kv and 20 mA) and any effects of decomposition should be minimised. All the lines which appeared at room temperature also appeared at higher temperatures. This experiment was done on the polycrystalline material of CuGe<sub>2</sub>P<sub>3</sub> containing the second phase of CuP<sub>2</sub> and the single crystal grown by slow cooling of the Bridgman method.

Photographs taken ranging from room temperature to just below the melting point are shown in Figure 4.5 (a) and (b).

#### 4.6 Coefficient of Thermal Expansion

A graphical method was used to evaluate the coefficient of thermal expansion at various temperatures, from a large scale graph drawn between the temperature and the cell constant, as shown in Figure 4.6 (b). Table 4.3 lists lattice parameters along various temperatures for compound CuGe<sub>2</sub>P<sub>3</sub>. The change in the lattice constant (a) is read in the range ( $\Delta t$ ) of about 100 °C temperature intervals. The  $\alpha_a$  was evaluated using the following equation.

$$\alpha_a = \frac{1}{a_0} \frac{da}{dT}$$

where  $\alpha_a$  is the coefficient of linear expansion. The coefficient of linear expansions are shown in Table 4.2 and compared with GaP.

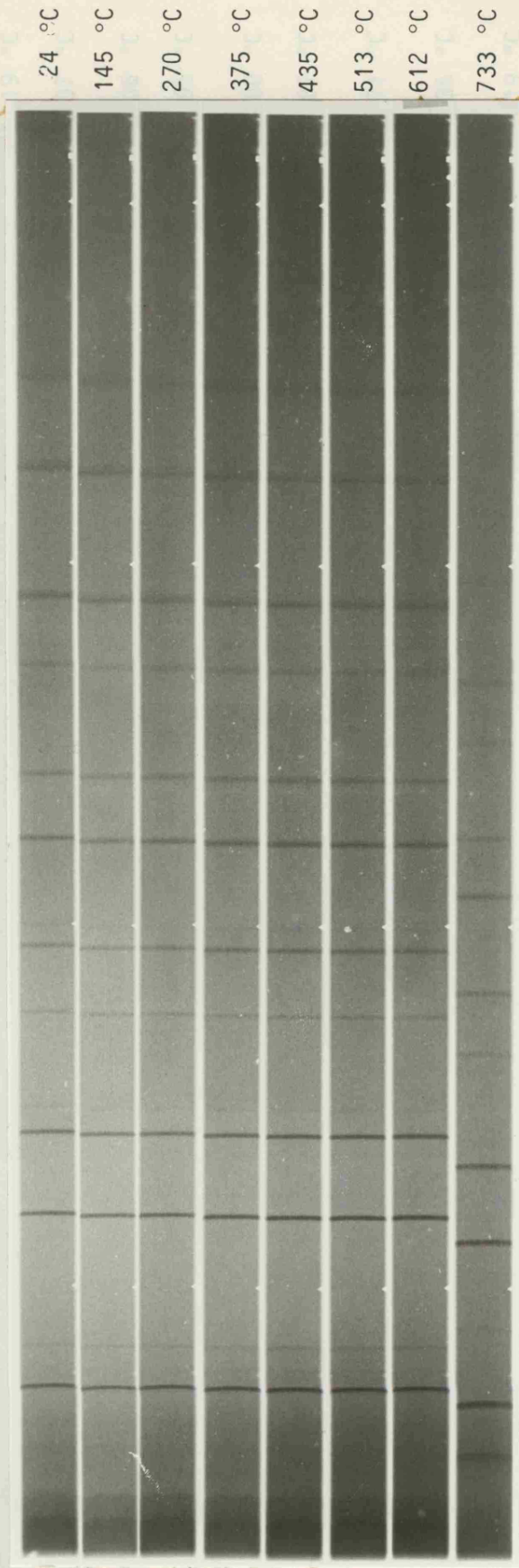


Figure 4.5 (a) Powder photographs of  $\text{CuGe}_2\text{P}_3$  (polycrystalline) containing a second phase at various temperatures, showing decomposition at high temperature

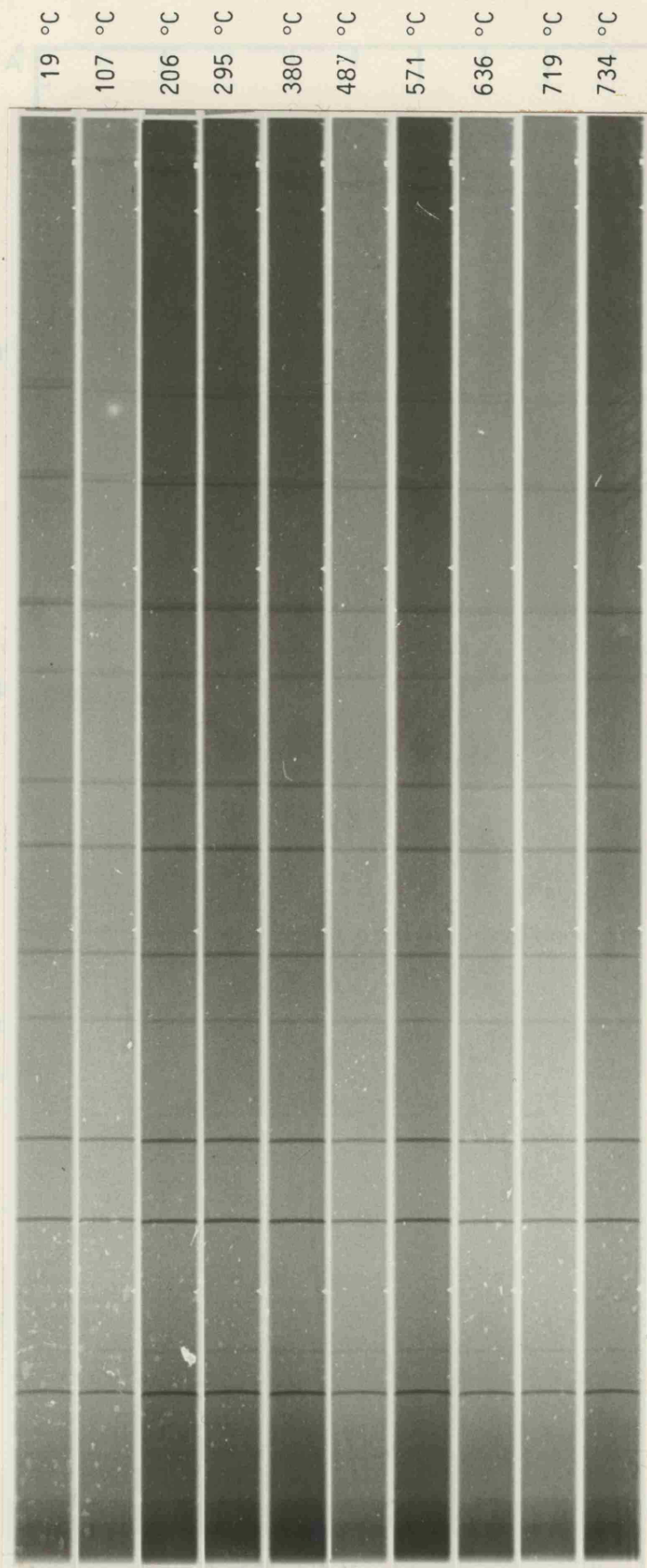


Figure 4.5 (b) Powder photographs of  $\text{CuGe}_2\text{P}_3$  (single crystal) at various temperatures

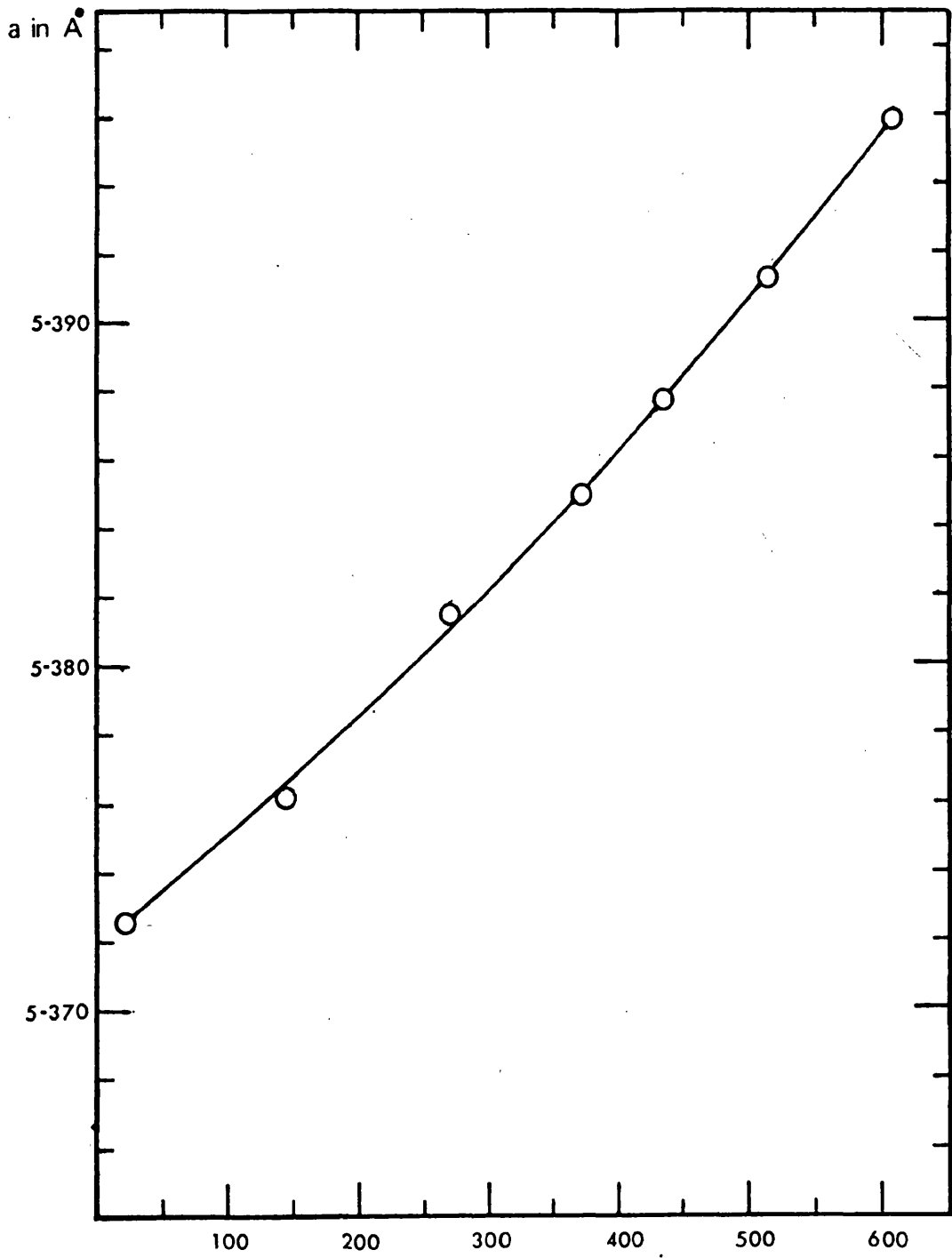


Figure 4.6.(a) Temperature dependence of the lattice parameters of  $\text{CuGe}_2\text{P}_3$  (polycrystalline containing second phase)

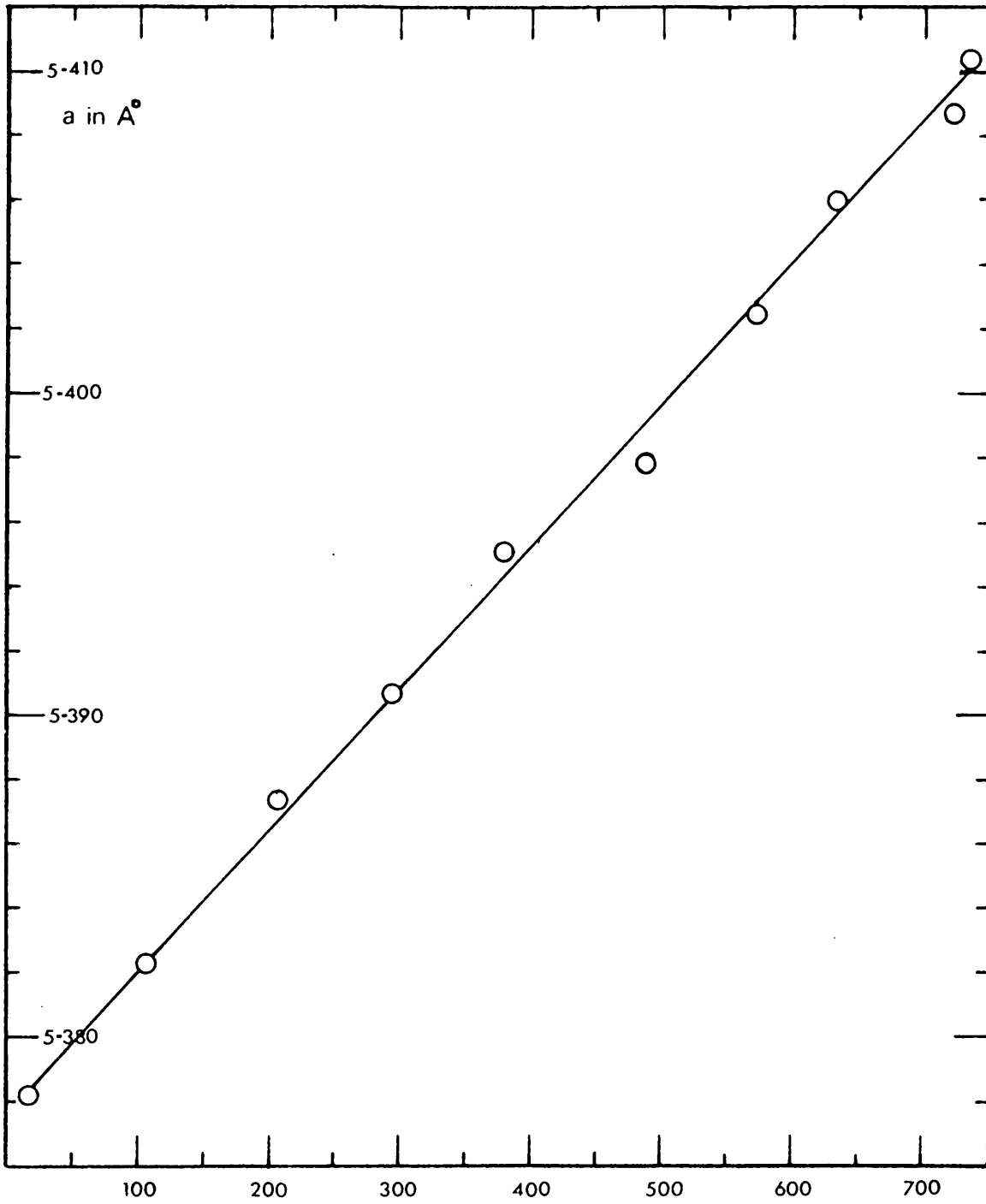


Figure 4.6(b) Temperature dependence of the lattice parameters of  $\text{CuGe}_2\text{P}_3$  (single crystal)

Table 4.3

Coefficient thermal expansion (mean) between 24-830 °C

$\text{CuGe}_2\text{P}_3$  and GaP

Compound	$\alpha_1 \times 10^{-6} \frac{1}{^\circ\text{C}}$ (mean)	$\Delta a$ from 24-830 °C	$\Delta v$ from 24-830 °C	Ref.
$\text{CuGe}_2\text{P}_3$	8.2	0.035 Å	3.071 Å <sup>3</sup>	
GaP	5.23	0.023 Å	2.052 Å <sup>3</sup>	98-101

Table 4.4

High temperature lattice parameters and unit cell volume  
for single crystal material of  $\text{CuGe}_2\text{P}_3$

T → °C	Lattice parameters in Å	Unit cell volume in Å <sup>3</sup>
19	5.3781	155.55595
107	5.3823	155.92067
206	5.3874	156.36432
295	5.3907	156.65184
380	5.3951	157.03574
487	5.3979	157.28036
571	5.4025	157.6828
636	5.4060	157.98946
719	5.4087	158.2263
734	5.4104	158.37555

#### 4.7 Discussion

High temperature lattice parameters were measured for  $\text{CuGe}_2\text{P}_3$  as a single phase (single crystal) and polycrystalline material containing the second phase of  $\text{CuP}_2$ , by using X-ray powder photography.

The former is linearly temperature-dependent of lattice parameters. No phase changes, or any phosphorus decomposition were apparent in the range room temperature to just below melting point. Thermal expansion for polycrystalline material containing the second phase of  $\text{CuP}_2$  changes non-linearly from room temperature to about  $725^\circ\text{C}$ . Then the material changed by increasing the lattice parameters from  $5.396 \text{ \AA}$  to  $5.682 \text{ \AA}$  at a very fast rate. Extra lines appeared after attainment of this temperature at  $\theta^\circ$  values of about  $10.725^\circ$ , and  $17.682^\circ$ , which may belong to  $\text{Cu}_3\text{P}$ . At this temperature, the lines belonging to  $\text{CuP}_2$  disappeared.

The most probable explanation of the increasing lattice parameters is  $\text{CuGe}_2\text{P}_3 + \text{excess Ge}$ , which is due to the shortage of copper and phosphorus in the compound, resulting from the formation of  $\text{Cu}_3\text{P}$ . These results of the X-ray are matched by DTA for  $\text{CuGe}_2\text{P}_3$ , as single phase and polycrystalline material containing second phase. There was always a small peak at  $725^\circ$  [see Figure 4.2 (a)-(c)]. In conclusion, it can be said that this compound will show a phase transition and decomposition at  $725^\circ\text{C}$ , when containing a second phase, but the compound is stable at all temperatures up to the melting point, when it is a single phase (or single crystal). Higher thermal expansion coefficient is shown in this compound, as compared with their derivatives III-V, such as GaP and GaAs and other semi-conductors such as Si and Ge.

Non-linear thermal expansions were shown for most cubic semi-conductor materials in some temperatures ranging from room temperature to melting point [102-104]. Covalent bonds are strong short range forces which

characteristically have low coefficients of thermal expansion, whereas ionic bonds have a much longer range. For example, the mean coefficient of thermal expansion of Si between 0 and 600 °C is  $2.0 \times 10^{-6} \text{ } ^\circ\text{C}^{-1}$  [105], while that for NaCl is about  $50 \times 10^{-6} \text{ } ^\circ\text{C}^{-1}$ . Generally, it is considered that the integrated thermal expansion from absolute zero to melting point is of the order of 0.7% for the covalently bonded crystals, and is three to four times larger than this for the ionic and metallic crystals [103]. This consideration makes it clear that decreasing thermal expansion with the presence of a second phase in  $\text{CuGe}_2\text{P}_3$  decreases the ionicity in the compound, which, in turn, is due to the excess Ge. In other words, it can be said that the  $\text{CuGe}_2\text{P}_3$  compound has more ionicity than its derivatives III-V and other IV semi-conductors such as Ge and Si.



## CHAPTER 5

### Solid Solutions Based on $\text{CuGe}_2\text{P}_3$

#### 5.1 Introduction

Standard X-ray photographic procedures were used throughout this experimental work. Samples were analysed by X-ray powder photographs. The conditions under which X-ray experiments were performed are described in detail.

Electron probe microanalysis was also used to study the component distribution in the grown materials. Alloys based on the compound  $\text{CuGe}_2\text{P}_3$  were investigated with their components, binary and ternary compounds. The Gibbs triangle was one of the reasons for this investigations, which may yield information about the nature of the formation of these ternary compounds, *i.e.*, the information which would be essential in the development of techniques for preparing particular compounds. Another interest in solid solutions based on this compound is that they may have properties which differ from the original.

#### 5.2 X-Ray Crystal Analysis

The use of X-ray diffraction as a technique for crystal structure analysis dates from van Laue's discovery of the X-ray diffraction effect for single crystal samples, in 1912 [105].

The experimental observation of X-ray diffraction patterns was greatly simplified by the introduction of the powder method, by Debye and Scherrer [106] in 1916. In this method, a parallel monochromatic beam of X-rays is allowed to pass through a very finely powdered specimen. Chance orientation of some of the microcrystals of the powdered specimen will be at the correct diffraction angle for a particular set of planes (hkl).

Since the diffraction condition can be satisfied for any possible angular orientation of the normal to the scattering planes around the incident beam axis, and since there will always be microcrystals oriented to produce the (hkl) diffraction for possible angular orientation, the diffracted beam will have the form of a cone, rather than just a pencil of rays.

The materials were ground in an agate mortar and pestle and attached with silicon grease to a thin glass rod giving typical sample dimensions of about 10 x 0.2 mm. The sample was centrally located in a Phillips 114.6 mm diameter X-ray diffraction camera and exposed to  $\text{CuK}\alpha$  radiation for about 24 hours. In all cases, narrow collimators were used, giving well defined diffraction lines enabling the lattice parameters to be determined accurately. The positions of the lines on the film were measured with a Vernier rule capable of measuring to 0.05 mm. The Straumanis film mounting had the advantage that the camera radius did not need to be known, since the position corresponding to  $\theta = 0^\circ$  and  $\theta = 90^\circ$  could be determined directly from the measured positions of the lines. It is assumed that the camera was cylindrical. The interplanar spacing  $d$  between {hkl} plane for cubic systems is shown by:

$$\frac{1}{d^2} = \frac{h^2 + k^2 + l^2}{a^2} = \frac{4 \sin^2 \theta}{\lambda}$$

where  $\lambda$  is the X-ray wave length, and  $\theta$  is the Bragg angle. Values of  $\theta$ ,  $d$  and  $a$  were calculated.

Errors arising from the absorption of X-rays by the sample and from displacement of the sample from the centre of the camera along the line of the X-ray beam both disappear for back scattering ( $\theta = 90^\circ$ ). The measured values of the lattice parameters were extrapolated to  $\theta = 90^\circ$  [107-109].

This extrapolation function  $[\frac{1}{2}(\frac{\cos^2\theta}{\sin\theta} + \frac{\cos^2\theta}{\theta})]$  was calculated and plotted as a graph against the observed measured lattice parameters. The extrapolation to  $\theta = 90^\circ$  from the real lattice parameters. The error in these calculations was estimated as  $\pm 0.003 \text{ \AA}$  for polycrystalline materials and  $\pm 0.0005 \text{ \AA}$  for single crystal materials.

### 5.3 Electron Probe Microanalysis (EPMA)

EPMA was used to analyse the distribution of elements in the compound and to show if it was a single phase or not. For this purpose a polished slice of a sample was used. The results of this analysis on some prepared compounds and alloys are given in Table 5.1.

Table 5.1  
EPMA results of the ternary and quaternary compounds

Compound	EPMA result	Method of preparation
$\text{CuGe}_2\text{As}_3$	Non uniform distribution of elements	fusion and iodine transport
$\text{CuZnGe}_3\text{As}_5$	Non uniform distribution of elements	fusion and iodine transport
$\text{Cu}_2\text{ZnGe}_5\text{As}_8$	Non uniform distribution of elements	fusion
$\text{CuZnGe}_3\text{P}_5$	Uniform distribution of all elements	fusion and iodine transport
$\text{Cu}_2\text{ZnGe}_5\text{P}_8$	Uniform distribution of all elements	fusion

### 5.4 Phase Relationships in Ag-Ge-P and Chemical Analysis

The compound  $\text{AgGe}_2\text{P}_3$ , like other compounds of I-IV<sub>2</sub>-V<sub>3</sub> groups, does not appear as this composition. An  $\text{AgGe}_2\text{P}_3$  compound with a lattice parameter of  $10.20 \text{ \AA}$  as a body centred cube was reported [27]. More

details were reported on its melting point and relationship with other compounds of  $\text{CuGe}_2\text{P}_3$ , which the authors thought to be changing from *fcc* to *bcc* in these compounds [24]. Schnering [28] reported a new composition, which was  $\text{Ag}_6\text{Ge}_{10}\text{P}_{12}$  with a lattice parameter of  $a = 10.32 \text{ \AA}$  and crystal structure of *bcc*, with a complicated atomic distribution, as shown in Figure 2.7. He thought that the latter was similar to the compound found by Sokolova [24]. More details of a similar composition were reported later by Honle [26]. A similar structure was reported by Goryunova [25] for the compound  $\text{CuSn}_2\text{P}_3$  in the composition  $\text{Cu}_4\text{SnP}_{10}$ .

Attempts to grow  $\text{AgGe}_2\text{P}_3$  were carried out by using the methods mentioned in Chapter 3. The grown sample always had phosphorus inclusions distributed between layers of crystalline material of thickness no more than 1 mm. X-Ray powder photographs of crystalline material taken from the sample were shown to be in *bcc* with good line intensities up to the highest angles. The same X-ray lines were produced for powder taken from various parts along the grown sample.

A modified Bridgman method was used to grow this compound and for other ternary compounds produced in this work. Several single crystals were grown, with different dimensions from 1-3 cm in length and 0.5-1.5 cm in diameter. The crystals were always grown from the bottom of the ampoule. The first to freeze end of the sample was good single crystal material, but the last to freeze end was poor crystalline material. X-Ray powder photographs showed the same lines for the single crystals as those investigated by Schnering [28], whilst the top material indicated very weak lines, which were found to be for Ge-P phases having a different composition, which may depend on the applied pressure [119]. However, some very weak lines for the compound itself were observed. Because the calculated

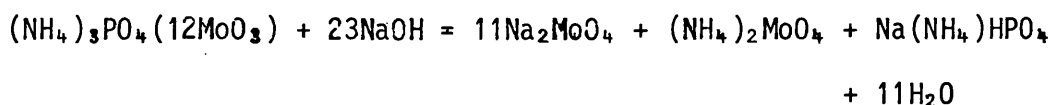
lattice parameters were the same as those reported for  $\text{Ag}_6\text{Ge}_{10}\text{P}_{12}$ , more consideration was given to this compound. The latter composition was prepared and single crystals were grown. However, the lattice parameters showed no difference from the previous preparation.

In order to investigate further, chemical analysis was used for the single crystal and polycrystalline regions of  $\text{AgGe}_2\text{P}_3$ . Figure 5.1 shows X-ray lines for  $\text{Ag}_6\text{Ge}_{10}\text{P}_{12}$  and the X-ray data are given in Table 5.3.

The crystalline part (single crystal) was dissolved in 1:1  $\text{HNO}_3$ , with a few drops of HF (20% w/v) and warmed in a teflon beaker. For separating Ag, a slight excess of KCl was added to form AgCl. This was filtered into a crucible and dried at  $140^\circ\text{C}$ .



To precipitate P, a few drops of  $\text{H}_2\text{SO}_4$  were added to remove HF, then ammonium phosphomolybdate precipitated, and was filtered and titrated with NaOH (0.1 M). The phosphorus was calculated from the following equation:



The P was calculated from  $\text{Na}(\text{NH}_4)\text{HPO}_4$ , so the remaining material was Ge, which was calculated from Ag and P. The Ge percentage was almost the same for both compositions, namely  $\text{AgGe}_2\text{P}_3$  and  $\text{Ag}_6\text{Ge}_{10}\text{P}_{12}$ .

Analysis showed that from the polycrystalline material from the top of the specimen was deficient in Ag and contained an excess of phosphorus and germanium. Table 5.2 shows the results of this analysis.

These results agreed well with the DTA analysis, which showed more than one transition for  $\text{AgGe}_2\text{P}_3$ , but only one transition for  $\text{Ag}_6\text{Ge}_{10}\text{P}_{12}$  for

Ag <sub>6</sub> Ge <sub>10</sub> P <sub>12</sub>		Ag <sub>6</sub> Ge <sub>10</sub> P <sub>12</sub>	
Theoretical (%)		Theoretical (%)	
Ag	31.126	31.093	
Ge	41.952	41.602	
P	26.922	21.302	

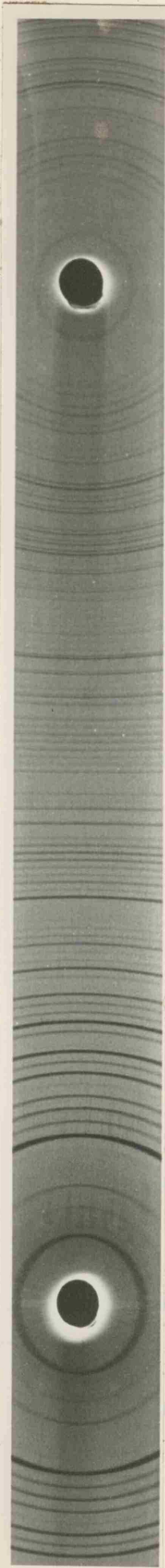


Figure 5.1 X-Ray powder photograph for the compound Ag<sub>6</sub>Ge<sub>10</sub>P<sub>12</sub>.

heating and cooling (see Chapter 5.1).

Chemical analysis results are given in Table 5.1.

single-crystal part of the sample.

### 5.5 Phase Relationships in Cu-Ge-P System

#### 5.5.1 CuGe<sub>2</sub>P<sub>3</sub>-bGe system

There are at least two reasons for the interest in the solubility of germanium in semiconducting materials. Firstly, it is interesting to study the possibility of dissolving various semiconductors in other semiconductors to form alloys with interesting properties.

interest in the solubility of germanium in semiconducting materials. Some of these materials have diamond-like structures, and the possibility of alloying germanium with various semiconductors is of interest to investigate the possibility of dissolving various semiconductors in semiconductors to form alloys with interesting properties.

It is a well-known fact that the position of germanium in the Periodic Table causes this element to form a large number of compounds. An instance of this is the fact that it can occupy interstitial positions in the crystal lattice of a semiconductor (for example, Mg<sub>2</sub>Ge).

position of germanium in the Periodic Table causes this element to form a large number of compounds. An instance of this is the fact that it can occupy interstitial positions in the crystal lattice of a semiconductor (for example, Mg<sub>2</sub>Ge).

Study has shown that small amounts of germanium (up to 0.5 atomic %) can be alloyed with gallium arsenide, substituting for either the gallium atoms or the arsenic atoms and giving rise to either donor or acceptor levels.

Study has shown that small amounts of germanium (up to 0.5 atomic %) can be alloyed with gallium arsenide, substituting for either the gallium atoms or the arsenic atoms and giving rise to either donor or acceptor levels.

heating and cooling (see Chapter 4 for the details).

Table 5.2

Chemical analysis results for the single crystal part of  $\text{AgGe}_2\text{P}_3$

		$\text{AgGe}_2\text{P}_3$		$\text{Ag}_6\text{Ge}_{10}\text{P}_{12}$
		Theoretical (%)	Experimental (%)	Theoretical (%)
Ag	31.178		37.06	37.093
Ge	41.963		40.44	41.603
P	26.858		22.5	21.302

## 5.5 Phase Relationships in Cu-Ge-P Systems

### 5.5.1 $\text{CuGe}_2\text{P}_3$ -6Ge system

There are at least two reasons for the interest in the solubility of germanium in semiconducting compounds which have diamond-like structures. Firstly, it is interesting to explore the possibility of alloying germanium with various semiconductors and secondly, it is of interest to investigate the possibility of dissolving macro quantities of germanium in semiconductors to form alloys with intermediate properties.

It is a well-known fact that the position of germanium in the Periodic Table causes this element to show amphoteric properties in certain of its compounds. An instance of the amphoteric character of germanium appears in the fact that it can occupy either "anodic" or "cathodic" positions in the crystal lattice of a semiconducting compound which contains it as a component (for example,  $\text{Mg}_2\text{Ge}$ , and  $\text{GeTe}$ ).

Study has shown that small quantities of germanium (up to 0.5 atomic %) can be alloyed with gallium arsenide, substituting for either the gallium atoms or the arsenic atoms and thereby giving rise to either donor or

Table 5.3

X-Ray powder data of  $\text{Ag}_6\text{Ge}_{10}\text{P}_{12}$ 

<u>hkl</u>	<u><math>\sin^2\theta</math> (obs.)</u>	<u><math>\sin^2\theta</math> (calc.)</u>	<u><math>d \rightarrow \text{\AA}</math></u>	<u><math>1/I_0</math></u>
110	0.0111	0.0111	7.2933	86.44
200	0.0224	0.0223	5.1715	8.53
211	0.0335	0.0335	4.2107	27.48
220	-	0.0446	3.6466	5.68
310	-	0.0558	3.2616	00.00
222	0.0671	0.0670	2.9774	100.00
321	0.0782	0.0782	2.7566	40.19
400	0.0898	0.0893	2.5785	53.65
411,330	0.1010	0.1005	2.4311	64.45
420	-	0.1117	2.3063	9.48
332	0.1231	0.1229	2.1990	79.62
422	0.1344	0.1340	2.1054	32.22
510,431	0.1458	0.1452	2.0228	91.75
521	0.1683	0.1676	1.8831	33.17
440	0.1794	0.1787	1.8233	90.05
530,433	0.1904	0.1899	1.7688	27.96
600,442	0.2012	0.2011	1.7190	26.54
611,532	0.2144	0.2123	1.6732	52.60
620	-	0.2234	1.6308	00.00
541	0.2318	0.2346	1.5915	12.79
622	0.2467	0.2458	1.5549	60.19
631	0.2575	0.2569	1.5207	12.32
444	-	0.2681	1.4887	6.63
710,550,543	0.2800	0.2797	1.4586	35.54
640	0.2907	0.2904	1.4303	16.11
721,633,552	0.3020	0.3016	1.4036	16.90
642	-	0.3128	1.3783	00.00
730	-	0.3240	1.3543	00.00
732,651	0.3472	0.3463	1.3099	62.56
800	0.3581	0.3575	1.2893	15.17
811,741,554	0.3694	0.3687	1.2696	29.10
820,644	0.3809	0.3798	1.2508	12.79
623	0.3920	0.3910	1.2328	18.48
822,660	0.4032	0.4022	1.2155	38.38
831,750,743	0.4140	0.4134	1.9901	36.77
662	0.4254	0.4245	1.1831	31.18
752	0.4363	0.4357	1.1678	10.23
840	-	0.4469	1.1531	00.00
910,833	0.4588	0.4580	1.1390	35.07
842	-	0.4692	1.1254	3.31
921,761,655	0.4808	0.4804	1.1122	26.07
664	-	0.4916	1.0995	2.84
930,851,754	0.5030	0.5027	1.0872	13.27
932,763	-	0.5251	1.0638	2.84
844	0.5369	0.5363	1.0527	22.27
941,853,770	0.5480	0.5474	1.0419	8.53
1000,860	0.5589	0.5586	1.0314	12.32
1011,772	0.5698	0.5698	1.0212	21.80
1020,862	0.5811	0.5810	1.0114	18.48
950,943	0.5932	0.5921	1.0018	18.01
1022,666	0.6035	0.6033	0.9925	9.00
1031,952,765	0.6147	0.6145	0.9834	14.50



Table 5.3 (cont.)

hkl	$\sin^2 \theta$ (obs.)	$\sin^2 \theta$ (calc.)	$d \rightarrow \text{\AA}$	$I/I_0$
871,855,774	0.6372	0.6368	0.9660	16.59
1040	0.6483	0.6480	0.9577	25.19
1033,961	0.6600	0.6598	0.9495	9.00
1042	-	0.6703	0.9415	6.16
1110,954,873	0.6818	0.6815	0.9338	21.80
1121,1051,963	0.7043	0.7039	0.9189	35.07
880	-	0.7150	0.9117	8.53
1130,970	-	0.7262	0.9046	2.84
1044,882	0.7376	0.7374	0.8977	11.37
1132,1053,972,776	-	0.7485	0.8910	4.74
1060,866	-	0.7597	0.8844	2.84
1141,875	-	0.7709	0.8780	2.84
1062	-	0.7821	0.8717	6.63
965	0.7937	0.7932	0.8655	13.27
1200,884	-	0.8044	0.8595	4.74
1211,1150,1143, 981,974	0.8149 $\alpha_1$	0.8155	0.8536	18.20
1220	-	0.8267	0.8478	4.74
1152,1071,1055	0.8366 $\alpha_1$	0.8379	0.8421	37.53
1222,1064	0.8478 $\alpha_1$	0.8491	0.8366	20.85
1231,983	0.8591 $\alpha_1$	0.8608	0.8311	23.69
1161,1073	0.8814 $\alpha_1$	0.8826	0.8205	21.33
1240	0.8924 $\alpha_1$	0.8938	0.8154	14.22
1233,1154,990, 877	0.9036 $\alpha_1$	0.9049	0.8104	34.88
1242,1080,886	-	0.9161	0.8054	00.00
1163,992,976	0.9257 $\alpha_1$	0.9273	0.8005	11.37
1082	-	0.9385	0.7957	7.58
1310,1251,1170, 985	0.9484 $\alpha_1$	0.9496	0.7916	12.79
1066	0.9597 $\alpha_1$	0.9608	0.7864	15.16
1321,1172,1075	0.9709 $\alpha_1$	0.9720	0.7819	7.58
1244	-	0.9832	0.7775	00.00
1330,1253,994	0.9931 $\alpha_1$	0.9943	0.7731	8.05

acceptor levels, all depending on the working conditions [111]. Other studies of alloyed germanium and gallium arsenide have led to the conclusion that the dissolved germanium atoms can simultaneously occupy both "anodic" and "cathodic" positions in the lattice.

On the other hand, attempts at dissolving considerable quantities of germanium in compounds of the type III-V have not been successful, possibly, as Folberth has suggested [112], because the difference in the chemical bonding of III-V and IV is too great.

Analysis of the available data has led the author to the conclusion that macro quantities of germanium could be brought into solution by using as a solvent a compound in which the chemical bonding was more similar to that of germanium than is the case in those III-V compounds which have been studied thus far. As work in Goryunova's laboratories first showed, the chemical bonding in ternary II-IV-V<sub>2</sub> compounds is intermediate to the bonding in the crystal chemical analogues IV and III-V [113].

Earlier observations had shown that the isomorphic heterovalent substitutions are characteristic of elements of the germanium series (see, for example, reference 114). The bonding in the ternary compounds of the I-IV<sub>2</sub>-V<sub>3</sub> type were expected to be approximately the same as the bonding in IV types. It is unfortunately true that only two compounds of this type have diamond-like structures (CuSi<sub>2</sub>P<sub>3</sub> and CuGe<sub>2</sub>P<sub>3</sub>).

The compound ZnGeAs<sub>2</sub> is an isoelectronic analogue of germanium, which dissolves about 25 mole % germanium, changing from chalcopyrite to zinc-blend structure [115].

The compounds represented by the general formula I<sub>2</sub>-IV-VI<sub>3</sub> are ternary crystallochemical analogues of group IV elements having tetrahedral bonding. It has been reported that Ge compounds of this type, particularly

$\text{Cu}_2\text{GeSe}_3$ , dissolve substantial amounts of Ge (up to 14%) and the unit cell becomes cubic in the process, the excess Ge atoms going substitutionally into the  $\text{Cu}_2\text{GeSe}_3$  lattice [116].

Synthesis of samples from the  $\text{CuGe}_2\text{P}_3$ -6Ge section of the Cu-Ge-P system was carried out by fusion methods which are well known and described in Chapter 3. The samples take the form of single crystals for the range  $\text{CuGe}_2\text{P}_3$  to  $\text{CuGe}_5\text{P}_3$ , then for greater excess of Ge the samples formed single crystals for  $\text{CuGe}_5\text{P}_3$  and germanium. A study of twelve alloys revealed the formation of solid solution over a wide interval of concentration. The  $\text{CuGe}_2\text{P}_3$  always crystallise in the zincblend structure with parameters in the range 5.3678 to 5.375 Å, depending on the growth conditions. Figure 5.2 shows X-ray photographs for the alloys of the system Cu-Ge-P from  $\text{CuGe}_{2.5}\text{P}_3$  to  $\text{CuGe}_6\text{P}_3$ .

Such results were reported in 1961 [24], where the physico-chemical investigation of alloys of the  $\text{CuGe}_2\text{P}_3$ -Ge system confirmed the existence of solid solutions with the sphalerite structure and a lattice constant of the homogeneous alloys varying with the concentration in accordance with Vegard's law [116].

To prepare these alloys, cooling was carried out under directional crystallisation of single phase materials which always formed single crystals. Alloys of germanium with  $\text{CuGe}_2\text{P}_3$  always had the zincblend structure, but with decreasing zincblend X-ray lines from the relative intensity of 20% for  $\text{CuGe}_2\text{P}_3$  to only 2.7% for  $\text{CuGe}_5\text{P}_3$ , and the change of lattice parameters from 5.3678 Å for  $\text{CuGe}_2\text{P}_3$  to 5.458 Å for  $\text{CuGe}_5\text{P}_3$ , as in materials which form single crystals. A second phase of Ge appeared in sections of alloys containing an excess of >33.3% Ge. This phase of Ge separated from the alloy materials and the lattice parameter of Ge was the same as reported ( $\alpha = 5.657$  Å).

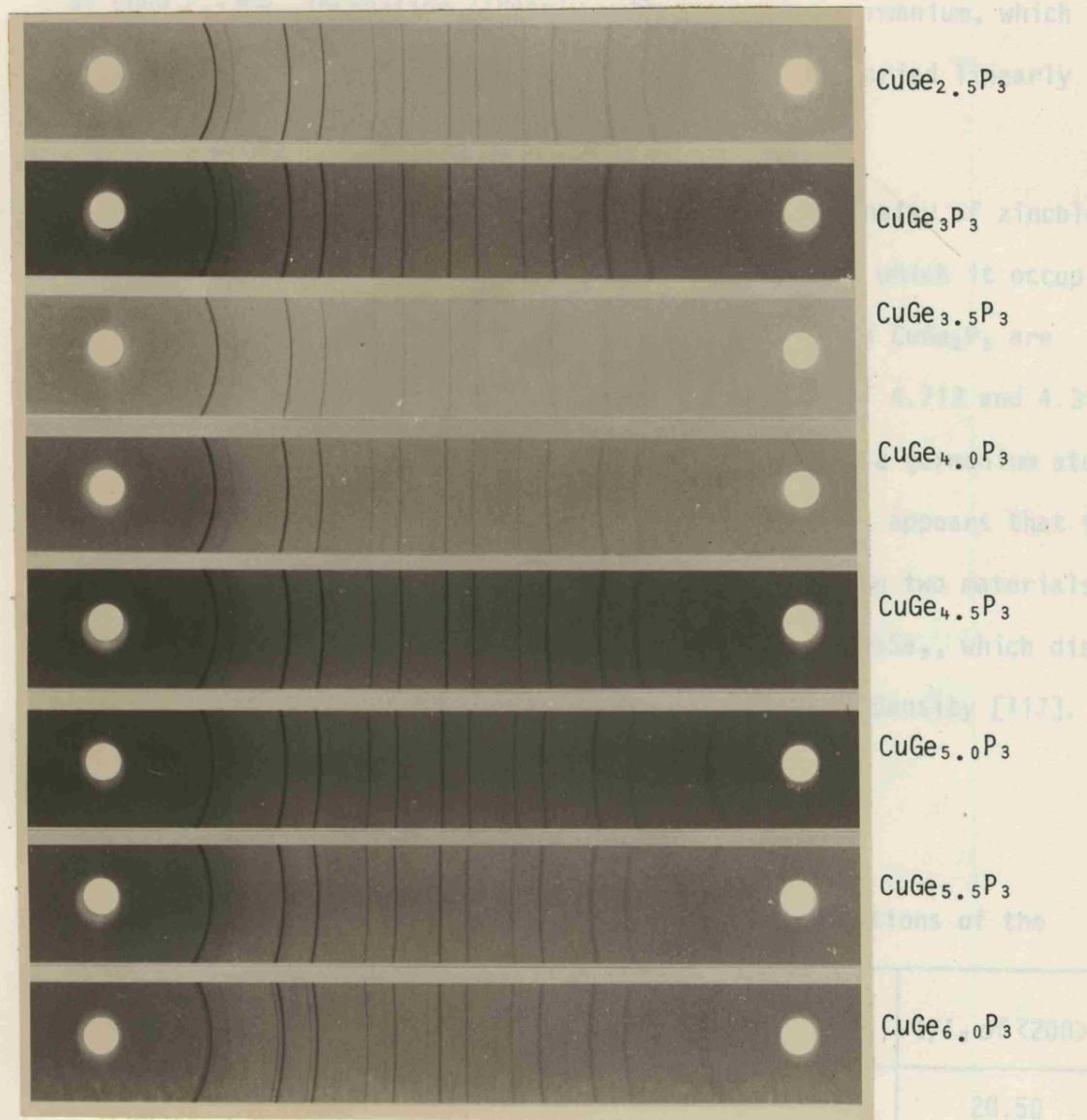


Figure 5.2 X-Ray powder photographs of  $\text{CuGe}_2\text{P}_3\text{-Ge}$  alloys showing single phase near the  $\text{CuGe}_{5.5}\text{P}_3$  alloy. It shows the increase of lattice spacing and change of the lattice towards the diamond structure.

$\text{CuGe}_{2.5}\text{P}_3$	08.50	4.3815	4.4301	20.50
$\text{CuGe}_3\text{P}_3$	14.25	4.4808	4.508	15.10
$\text{CuGe}_{3.5}\text{P}_3$	20.00	4.5301	4.590	12.22
$\text{CuGe}_4\text{P}_3$	25.75	4.5815	4.6556	09.10
$\text{CuGe}_{4.5}\text{P}_3$	31.50	4.6308	4.7135	04.20
$\text{CuGe}_5\text{P}_3$	37.25	4.6815	4.7135	02.77

Figure 5.3(a) shows the lattice parameters of various compositions of  $\text{CuGe}_2\text{P}_3\text{-3Ge}$ , increasing linearly with increasing germanium, which obeys Vegard's law. The density of the alloys also varied linearly with increasing Ge [see Figure 5.3(b)].

To understand how excess of Ge decreases the intensity of zincblend lines, it seemed useful to have some idea of the sites which it occupies in the lattice. The unit cell volumes for  $\text{CuGe}_5\text{P}_3$  and  $\text{CuGe}_2\text{P}_3$  are 162.60 and 154.66  $\text{\AA}^3$  respectively, and bulk densities of 4.713 and 4.319 g/cc respectively. It can easily be seen that the mass of a germanium atom is more than the average mass per atom for  $\text{CuGe}_2\text{P}_3$ . It appears that the average mass of  $\text{CuGe}_2\text{P}_3\text{-Ge}$  alloys were always between the two materials. This differs from other ternary compounds, such as  $\text{Cu}_2\text{GeSe}_3$ , which dissolve about 14% Ge without changing its unit cell volume and density [117].

Table 5.4

Lattice parameters and density for various compositions of the system Cu-Ge-P

Cu-Ge-P section	Mole % Ge	$a \rightarrow \text{\AA}$	$\rho \rightarrow \text{gm/cc}$	$I/I_0$ of $\langle 200 \rangle$
$\text{CuGe}_2\text{P}_3$	00.00	5.3678	4.319	20.50
$\text{CuGe}_{2.5}\text{P}_3$	07.69	5.3815	4.4301	15.10
$\text{CuGe}_3\text{P}_3$	14.28	5.4002	4.508	12.22
$\text{CuGe}_{3.5}\text{P}_3$	20.00	5.4103	4.5900	08.00
$\text{CuGe}_4\text{P}_3$	25.00	5.4316	4.628	05.00
$\text{CuGe}_{4.5}\text{P}_3$	29.41	5.4428	4.6556	04.20
$\text{CuGe}_5\text{P}_3$	33.33	5.4581	4.7135	02.77

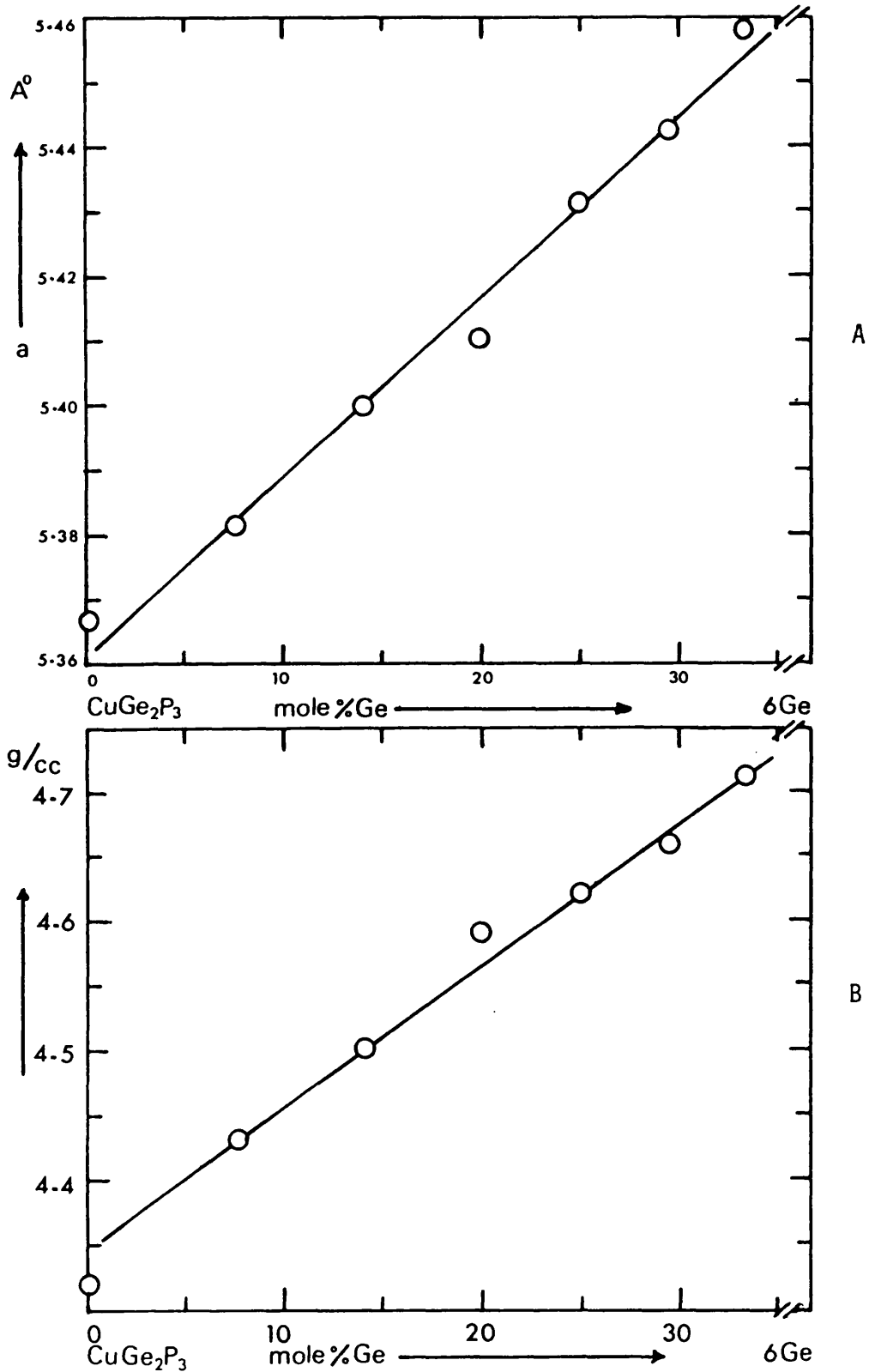


Figure 5.3 Section  $\text{CuGe}_2\text{P}_3$ -Ge of the system Cu-Ge-P.  
A-lattice parameter of various compositions  
B-density of various compositions

As mentioned earlier, there are two lattice sites in  $\text{CuGe}_2\text{P}_3$ , one occupied by P atoms ("anions"), the other shared by Cu and Ge atoms ("cations"). The structure of pure Ge is also similar, the difference being that both sites are now occupied by identical atoms. Therefore, if excess Ge goes substitutionally into the  $\text{CuGe}_2\text{P}_3$  lattice, it must be replacing atoms on both sites with equal probability, half of the Ge atoms replacing P atoms, while the other half occupy sites formerly occupied by Cu and Ge atoms. Since all atoms are tetrahedrally coordinated, a direct linkage of Ge-Ge atoms with a high probability of pure  $sp^3$  bonding is now possible. This direct Ge-Ge bonding should help to stabilise the diamond structure. Final confirmation of this conclusion can be obtained by examining the relative line intensities of the X-ray powder pattern of  $\text{CuGe}_2\text{P}_3$ -Ge. This intensity distribution approximates to that of a diamond lattice. The atomic scattering factors for Cu and Ge are very close, but twice that of P, and hence the intensity pattern in  $\text{CuGe}_5\text{P}_3$  should be similar to the one found in Ge. The relative intensity for the plane  $\langle 200 \rangle$  is shown in Figure 5.4 for the system  $\text{CuGe}_2\text{P}_3$ -Ge.

#### 5.5.2 Non-stoichiometric composition along the tie-line $\text{Cu}_3\text{P}$ - $\text{Ge}_3\text{P}_4$ for the compound $\text{CuGe}_2\text{P}_3$

The deviation from stoichiometry in the compound  $\text{CuGe}_2\text{P}_3$  along the tie-line  $\text{Cu}_3\text{P}$ - $\text{Ge}_3\text{P}_4$  in the system Cu-Ge-P was investigated.\* Several samples close to  $\text{Ge}_3\text{P}_4$  and one sample close to  $\text{Cu}_3\text{P}$  were used. A modified Bridgman method of slow cooling was used for the preparation of all the samples. Samples were all analysed by X-ray powder diffraction (Figure 5.6). It was found that alloys containing 10% (3/2)  $\text{Cu}_3\text{P}$  appear mainly with a zincblend structure and  $a = 5.379 \text{ \AA}$  with excess of

---

\* See Figure 3.1, Chapter 3.

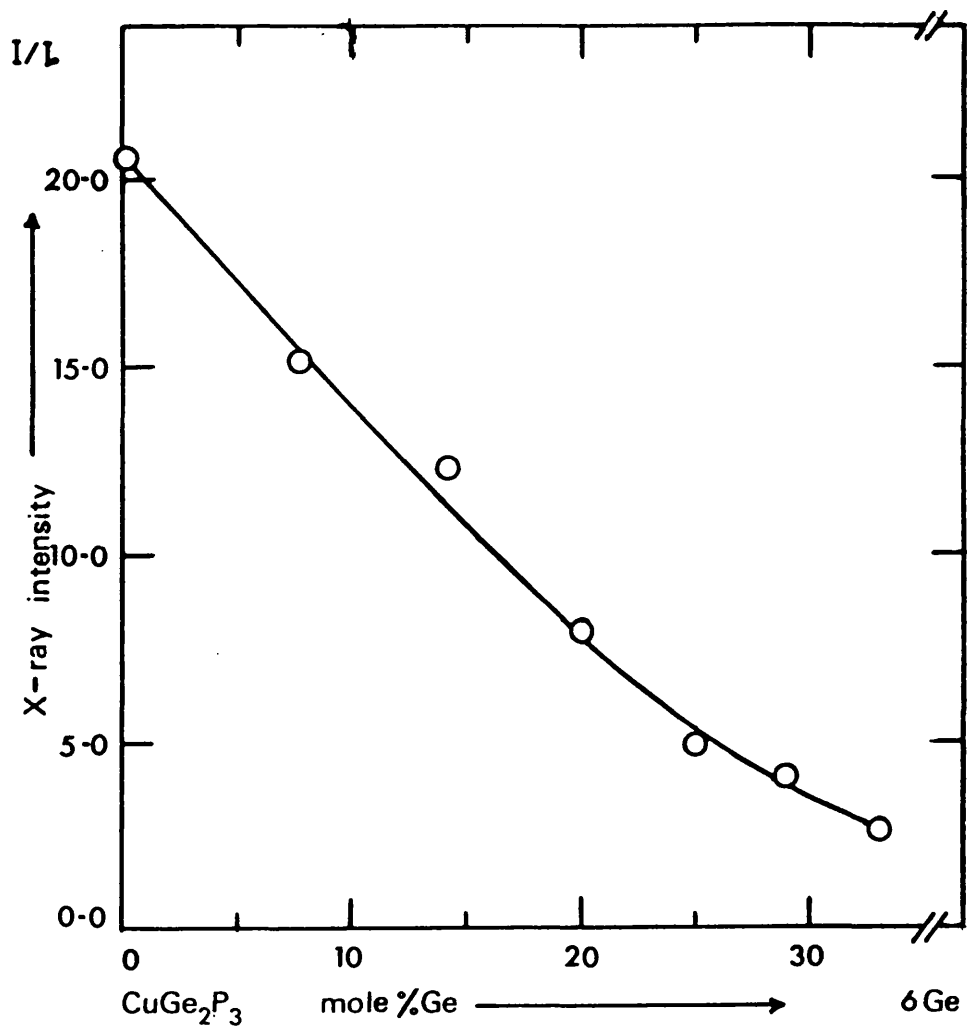


Figure 5.4 Relative X-ray intensity of the line  $\langle 200 \rangle$  for the section  $\text{CuGe}_2\text{P}_3$ -Ge of the system Cu-Ge-P showing the changes with the percentage of Ge.



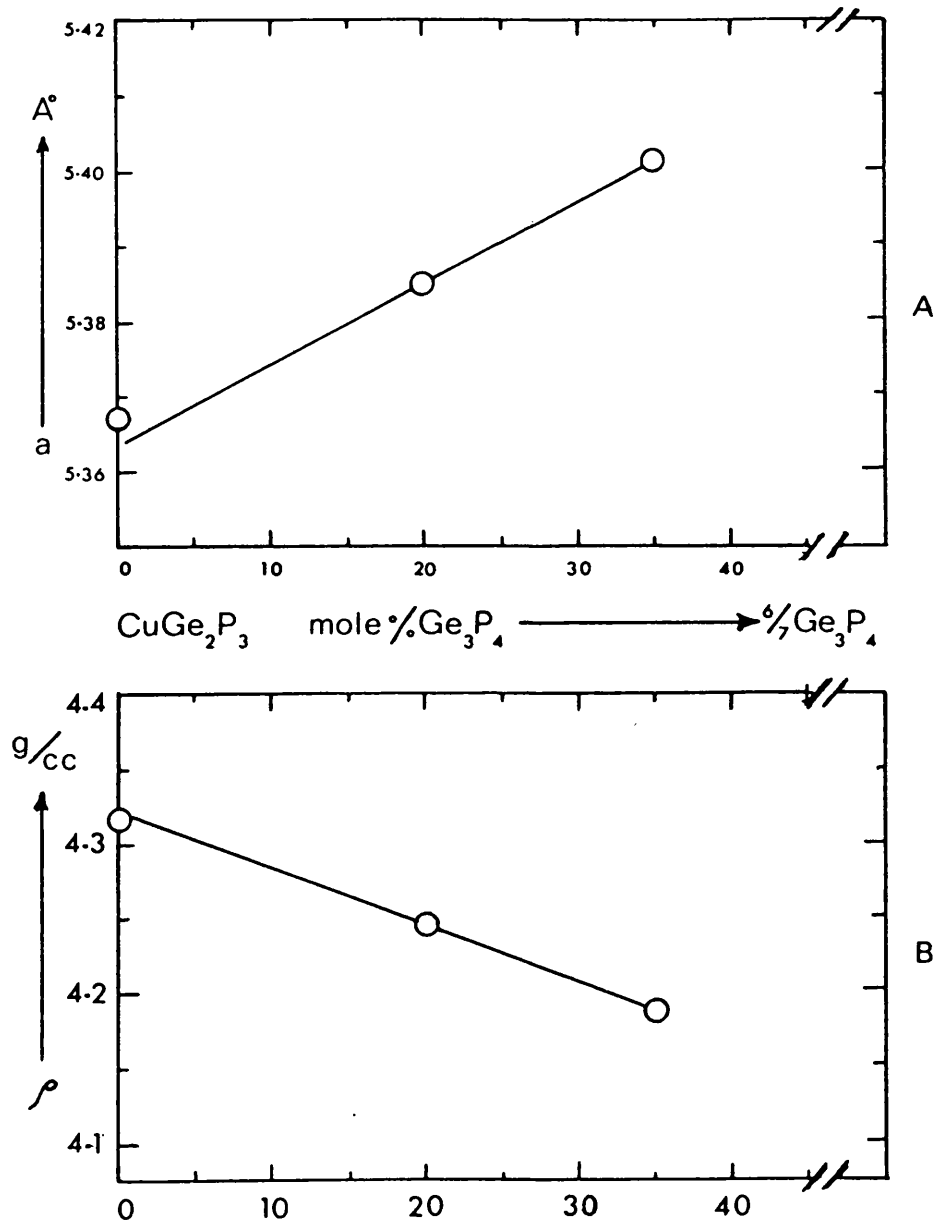


Figure 5.5 Section  $\text{CuGe}_2\text{P}_3\text{-Ge}_3\text{P}_4$  of the system Cu-Ge-P  
A - lattice parameter for various compositions  
B - density of various compositions

$x$

0.00

0.20

0.35

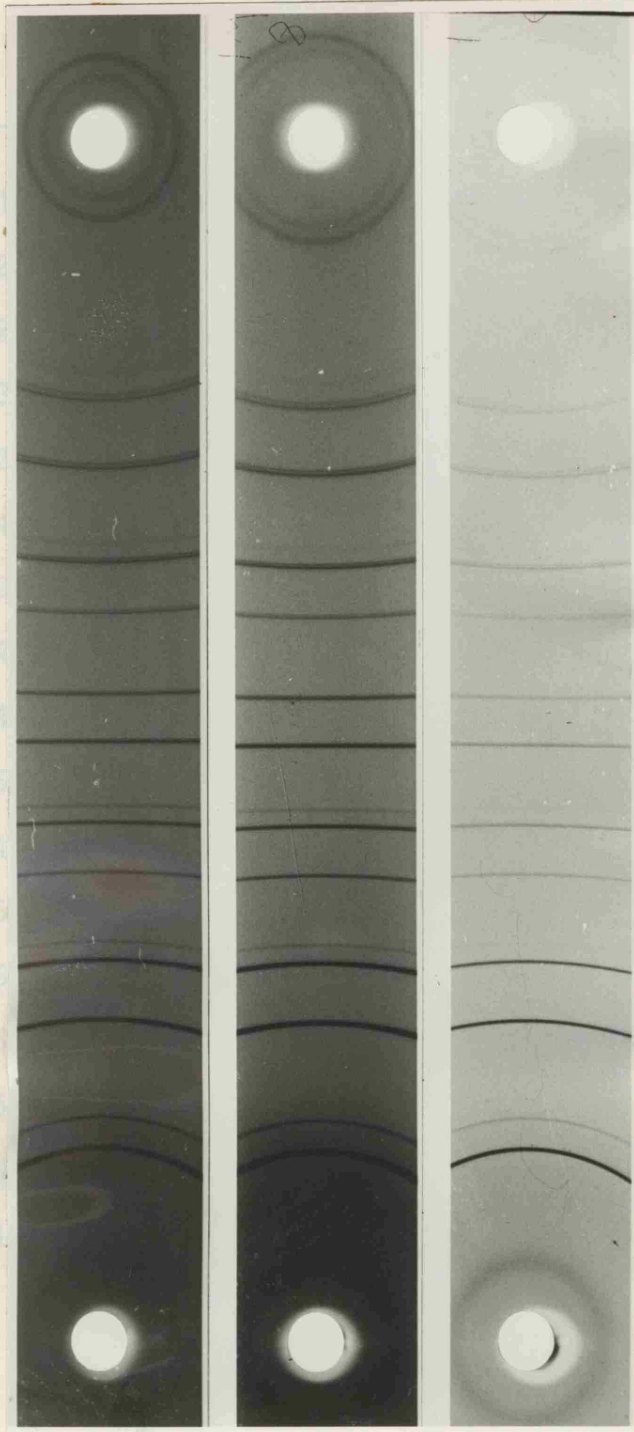


Table 5.5

$d - \lambda$	$1/d^2$
3.0494	100.00
2.6839	20.49
1.8976	80.00
1.6104	55.60
1.5495	6.79
1.3419	21.56
1.2314	33.30
1.2002	6.40
1.0957	37.79
1.0330	23.48
0.9489	16.65
0.9073	24.47
0.8946	2.13
0.8437	23.06
0.8185	14.43
0.8092	1.92
0.7747	5.11

Figure 5.6 X-Ray powder photographs of the system  $(\text{CuGe}_2\text{P}_3)_{x-1}(\text{7Ge}_3\text{P}_4)_x$

Table 5.5

X-Ray powder data of CuGe<sub>2</sub>P<sub>3</sub>

<u>hkl</u>	<u>sin<sup>2</sup>θ (obs.)</u>	<u>sin<sup>2</sup>θ (calc.)</u>	<u>d → Å</u>	<u>I/I<sub>0</sub></u>
111	0.0619	0.0618	3.0991	100.00
200	0.0828	0.0825	2.6839	20.49
220	0.1655	0.1650	1.8978	60.00
311	0.2275	0.2268	1.6184	55.60
222	0.2482	0.2475	1.5495	6.79
400	0.3309	0.3300	1.3419	21.56
331	0.3928	0.3918	1.2314	33.30
420	0.4135	0.4125	1.2002	6.40
422	0.4948	0.4942	1.0957	37.79
511,333	0.5568 α <sub>1</sub>	0.5559	1.0330	23.48
440	0.6591 α <sub>1</sub>	0.6589	0.9489	16.65
531	0.7208 α <sub>1</sub>	0.7206	0.9073	26.47
600,442	0.7407 α <sub>1</sub>	0.7412	0.8946	2.13
620	0.8235 α <sub>1</sub>	0.8236	0.8487	23.06
533	0.8854 α <sub>1</sub>	0.8854	0.8185	14.43
622	0.9061 α <sub>1</sub>	0.9060	0.8092	1.92
444	0.9886 α <sub>1</sub>	0.9884	0.7747	8.11

Table 5.6

X-Ray powder data of the CuGe<sub>5</sub>P<sub>3</sub> system

<u>hkl</u>	<u>sin<sup>2</sup>θ (obs.)</u>	<u>sin<sup>2</sup>θ (calc.)</u>	<u>d → Å</u>	<u>I/I<sub>0</sub></u>
111	0.0599	0.0598	3.1512	100.00
200	0.0799	0.0798	2.7290	02.77
220	0.1599	0.1595	1.9297	54.76
311	0.2197	0.2194	1.6456	44.28
222	-	0.2394	1.5756	00.47
400	0.3195	0.3191	1.3645	12.85
331	0.3792	0.3790	1.2517	19.50
420	-	0.3989	1.2205	00.00
422	0.4793	0.4787	1.1141	21.42
511,333	0.5380 $a_1$	0.5377	1.0504	11.42
440	0.6376 $a_1$	0.6372	0.9648	06.19
531	0.6971 $a_1$	0.6970	0.9225	10.40
600,442	-	0.7169	0.9097	00.00
620	0.7966 $a_1$	0.7966	0.8630	09.52
533	0.8564 $a_1$	0.8563	0.8323	05.23
622	-	0.8762	0.8228	00.00
444	0.9559 $a_1$	0.9559	0.7878	02.38

the second phase for  $\text{CuP}_2$ . Another unknown second phase was formed on the top of the sample, appearing as single crystal platelets.

In the investigation of the samples with a deviation from stoichiometry in the direction of  $\text{Ge}_3\text{P}_4$ , a wide range of solid solutions were found to exist. The lattice was zincblend, changing from 5.367 Å for  $\text{CuGe}_2\text{P}_3$  to 5.4015 Å for alloys containing about 35% (6/7)  $\text{Ge}_3\text{P}_4$ . For more excess of  $\text{Ge}_3\text{P}_4$ , the lattice remained constant and the excess  $\text{Ge}_3\text{P}_4$  remained unreacted.

The lattice parameters obeyed Vegard's law, while changes of relative X-ray intensities were small (Figure 5.6). However, the  $\text{CuGe}_2\text{P}_3$ - $\text{Ge}_3\text{P}_4$  system was reported for a wide range of existence of homogeneous phase with the sphalerite structure, with limited information [36].

Table 5.7

X-Ray powder data for the alloy 65%  $\text{CuGe}_2\text{P}_3$ -35% 6/7  $\text{Ge}_3\text{P}_4$

<u>hkl</u>	<u><math>\sin^2\theta</math> (obs.)</u>	<u><math>\sin^2\theta</math> (calc.)</u>	<u><math>d \rightarrow \text{Å}</math></u>	<u>I/I<sub>0</sub></u>
111	0.0613	0.0611	3.1185	100.0
200	0.0817	0.0814	2.7007	09.5
220	0.1633	0.1629	1.9097	76.8
311	0.2246	0.2240	1.6286	46.2
222	-	0.2444	1.5592	02.7
400	0.3269	0.3259	1.3503	09.5
331	0.3880	0.3870	1.2392	13.6
420	-	0.4073	1.2078	01.3
422	0.4898	0.4888	1.1025	19.0
511,333	0.5507	0.5499	1.0395	08.8
440	0.6515 $a_1$	0.6507	0.9548	04.7
531	0.7120 $a_1$	0.7117	0.9130	10.2
600,442	-	0.7320	0.9002	00.0
620	0.8136	0.8133	0.8540	08.1
533	0.8747	0.8743	0.8237	03.4
622	-	0.8947	0.8143	00.0
444	0.9758	0.9760	0.7796	02.7

## 5.6 The Compound $\text{CuSi}_2\text{P}_3$ and the $\text{CuSi}_2\text{P}_3$ -Si System

One of the compounds which researchers have so far failed to prepare, is  $\text{CuSi}_2\text{P}_3$ . The only known information is its lattice parameters,  $a = 5.25 \text{ \AA}$ , a zincblend structure [32]. Its atomic distribution is similar to that of  $\text{CuGe}_2\text{P}_3$ , except that germanium is replaced by silicon. The existence of this compound was reported by others with limited information [24]. DTA results on samples prepared by melt growth showed a high melting point of about  $1178 \text{ }^\circ\text{C}$ . Samples prepared by this method are polycrystalline, silvery in colour and with an X-ray analysis showing two unidentified phases, both of zincblend structure with lattice parameters about  $5.25 \text{ \AA}$  for the main phase and larger for the second. Although the surface becomes darker with time when exposed to air, X-ray films remain unchanged, while infrared reflectivity spectra showed a significant difference [118].

Tin solution growth was used as a second method for preparing this compound. The latter was used successfully previously for most high pressure and melting point compounds such as  $\text{ZnSiP}_2$ . Crystals of *ca.*  $2 \times 4 \times 8 \text{ mm}^3$  size were grown. X-Ray analysis of different crystals from the same run showed the same lattice parameters, with  $a = 5.244 \text{ \AA}$ . The latter result is smaller than the one reported earlier [32].

In order to understand more of the details of the ternary compound  $\text{CuSi}_2\text{P}_3$ , the solid solution, with its component of group IV, was tried. Alloys of  $\text{CuSi}_{2+x}\text{P}_3$  for  $x$  up to 8 were prepared, using a melt growth technique of modified Bridgman method. The results were single crystal ingots for alloys up to  $x = 3$ . X-Ray analysis showed that the alloys of  $x = 1, 2$  and  $3$  are single phase with lattice parameters from  $5.248 \text{ \AA}$  for  $x = 1$  to  $5.2923 \text{ \AA}$  for  $x = 3$  and obeying Vegard's law [Figure 5.8(a)].

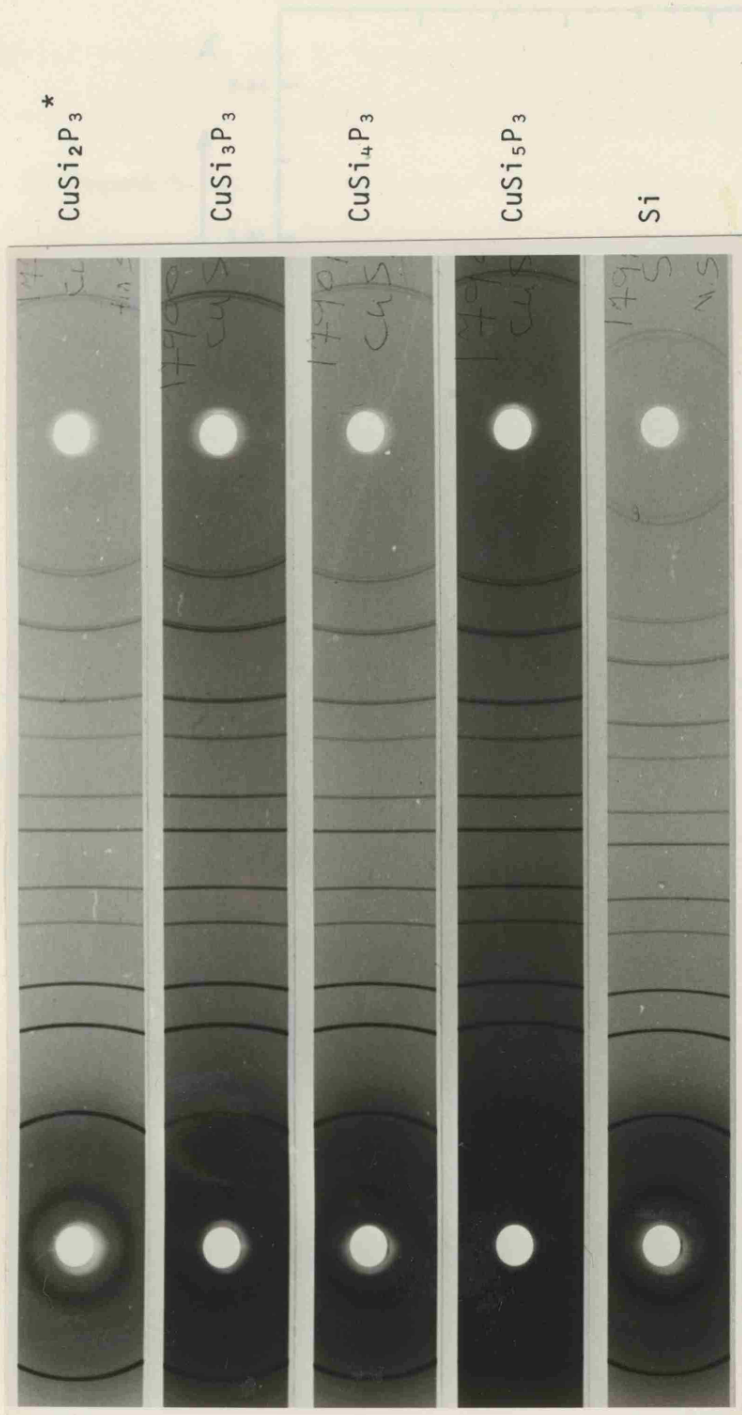


Figure 5.7 X-Ray powder photograph of the system  $\text{CuSi}_2\text{P}_3$ -Si showing single phase for all alloys prepared up to 33% of Si.

\*This sample is grown in tin solution.

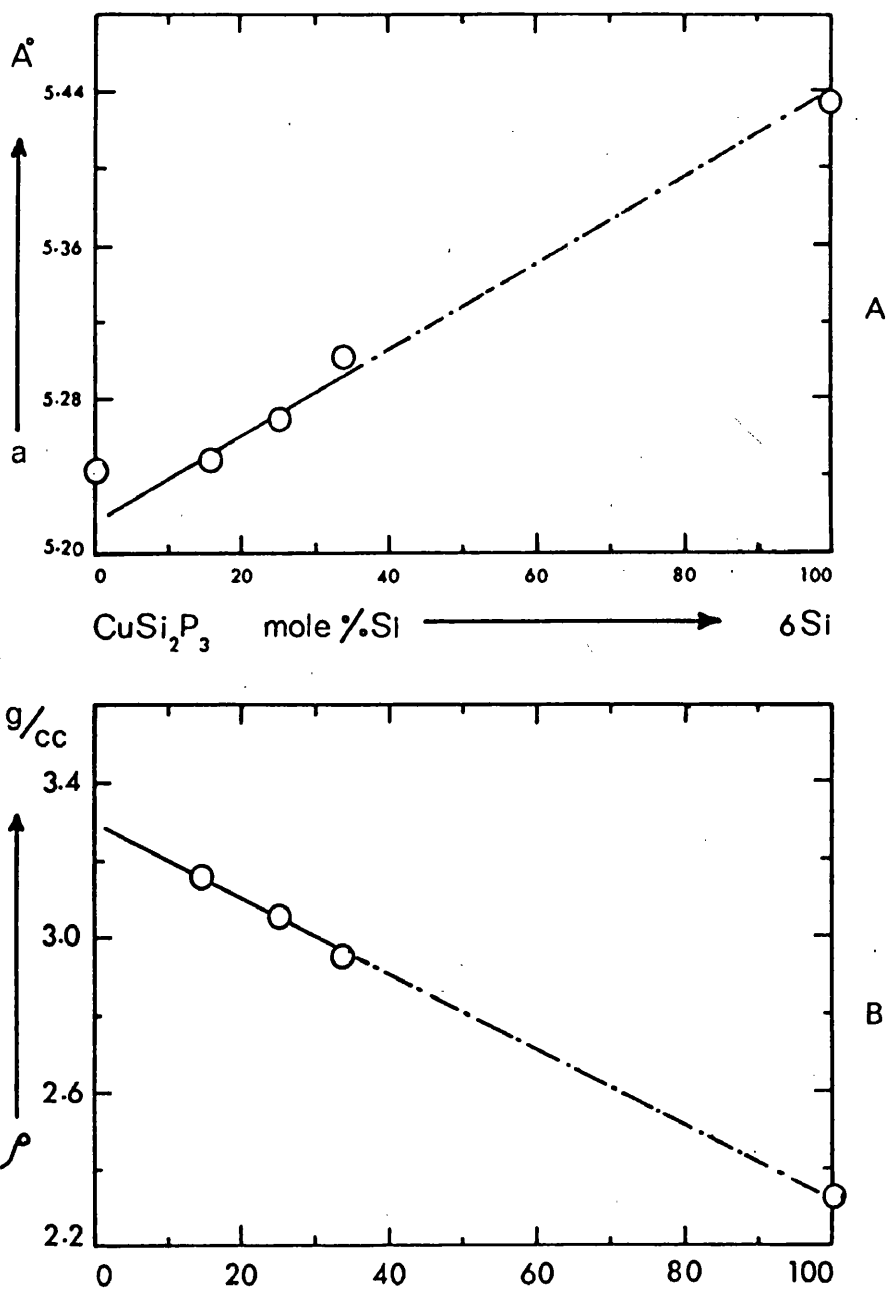


Figure 5.8 Section  $\text{CuSi}_2\text{P}_3$ -Si of the system Cu-Si-P  
A - lattice parameter for various compositions  
B - density of various compositions



However, for the alloys  $x = 4$  to  $8$ , the materials did not melt completely. The latter may be due to temperature difficulties. The expected lattice parameter for the compound  $\text{CuSi}_2\text{P}_3$  is  $a = 5.220 \text{ \AA}$ , using Vegard's law, as in Figure 5.8(a). The latter is much smaller than was found for the tin solution growth and the one reported by Folberth [32]. Adding excess silicon to  $\text{CuSi}_2\text{P}_3$  is similar to germanium excess in  $\text{CuGe}_2\text{P}_3$ . However, it would be interesting to explain the possibilities of a silicon excess in its own compound,  $\text{CuSi}_2\text{P}_3$ . The unit cell volume of silicon and  $\text{CuSi}_2\text{P}_3$  are  $166.18$  and  $142.23 \text{ \AA}^3$  respectively. If the  $\text{CuSi}_2\text{P}_3$  lattice has a suggested value of  $5.220 \text{ \AA}$ , then the difference of their volume is  $17.75 \text{ \AA}^3$ , while between germanium and  $\text{CuGe}_2\text{P}_3$  is  $26.42 \text{ \AA}^3$ . The  $\text{CuSi}_2\text{P}_3$  has larger density than silicon, while germanium has larger density than  $\text{CuGe}_2\text{P}_3$ , with less difference. Then from the density point of view,  $\text{CuSi}_2\text{P}_3$  would appear to dissolve more silicon than germanium in  $\text{CuGe}_2\text{P}_3$ , if it is not a complete solid solution.

The atomic distribution is similar to  $\text{ZnS}$ . Cu and Si occupied Zn sites in random distribution, with P atoms occupying S sites. Excess Si goes to cation and anion sites with equal probability, replacing Cu in cation sites and P in anion sites.

The Si atom is similar to P and smaller in size than Cu, while Ge atoms are bigger than P atoms and similar to Cu atoms. It is less difficult to replace P sites by Si than Cu by Si, while in the  $\text{CuGe}_2\text{P}_3$ -Ge system, replacing Cu is less difficult than P sites. However, the number of anion sites replaced by group IV excess atoms are three times more than in anion sites. Thus the existence of the solid solution in the system  $\text{CuSi}_2\text{P}_3$ -Si is expected to be more than the one found in  $\text{CuGe}_2\text{P}_3$ -Ge systems, as mentioned earlier. The relative line intensity

for the  $\langle 200 \rangle$  line is less than 2.0% for  $\text{CuSi}_2\text{P}_3$ , while the lines  $\langle 222 \rangle$ ,  $\langle 420 \rangle$ ,  $\langle 600 \rangle$  and  $\langle 622 \rangle$  are almost zero intensity. However, excess Si in the compound changes the intensity linearly with increasing Si as expected.

Table 5.8

X-Ray powder data for the tin solution growth of  $\text{CuSi}_2\text{P}_3$

<u>hkl</u>	<u><math>\sin^2\theta</math> (obs.)</u>	<u><math>\sin^2\theta</math> (calc.)</u>	<u><math>d \rightarrow \text{\AA}</math></u>	<u>I/I<sub>0</sub></u>
111	0.0653	0.0648	3.0276	100.0
200	-	0.0864	2.6220	01.4
220	0.1736	0.1728	1.8540	79.8
311	0.2389	0.2377	1.5811	44.7
222	-	0.2593	1.5138	00.0
400	0.3469	0.3457	1.3110	11.2
331	0.4119	0.4106	1.2030	17.9
420	-	0.4322	1.1726	00.0
422	0.5199	0.5186	1.0704	20.8
511,333	0.5846	0.5834	1.0092	11.9
440	0.6914 $\alpha_1$	0.6903	1.9270	07.4
531	0.7555 $\alpha_1$	0.7550	0.8863	14.1
600,442	-	0.7766	0.8740	00.0
620	0.8634 $\alpha_1$	0.8629	0.8291	14.9
533	0.9277 $\alpha_1$	0.9277	0.7997	08.2
622	-	0.9492	0.7905	00.0

## 5.7 Solid Solutions of the $\text{CuGe}_2\text{P}_3\text{-I}_2\text{-IV-VI}_3$ Systems

### 5.7.1 $\text{I}_2\text{-IV-VI}_3$ compounds

Ternary  $\text{I}_2\text{-IV-VI}_3$  compounds were first reported by Goodman [119], who synthesised  $\text{Cu}_2\text{SnSe}_3$ ,  $\text{Cu}_2\text{SiTe}_3$  and  $\text{Cu}_2\text{SnTe}_3$ . Averkieva and Vaipolin [120] studied a series of  $\text{I}_2\text{-IV-VI}_3$  compounds with  $\text{I} = \text{Cu}$ ,  $\text{IV} = \text{Sn}$  and  $\text{VI} = \text{S, Se or Te}$  and reported a sphalerite structure for all of them. The same structure was reported for compounds containing  $\text{Cu, Ge}$  and  $\text{Sn}$  in another investigation [121]. A large group of ternary chalcogenides was studied by Rivet [122] and others [33]. They synthesised the compounds by fusion of the component elements with *ca.* 1% excess sulphur, selenium or tellurium, compared with the stoichiometric amount. Thermal analysis showed that  $\text{Cu}_2\text{SiS}_3$  has two enantiotropic forms with a transition point near 840 °C. Quenching in cold water from a temperature above 840 °C produced a wurtzite-type structure in  $\text{Cu}_2\text{SiS}_3$ , but after annealing at lower temperature, the lattice is tetragonal.

The compound  $\text{Cu}_2\text{GeSe}_3$  and the possible range of solid solutions with  $\text{Ge}$  has been investigated in more detail by Sharma and others [123]. Their investigation indicated that the structure and stability of the  $\text{I}_2\text{-IV-VI}_3$  group of compounds depends on the valence state of the participating group IV elements, which are known to exhibit variable valency (tetravalency and divalency). The tetravalent state favours a more distorted, but more stable phase, while the divalent state favours a less distorted and less stable phase.

The structure of these compounds was studied in more detail by Parthe *et al.*, [124]. They reported that  $\text{Cu}_2\text{GeSe}_3$  and  $\text{Cu}_2\text{GeS}_3$  crystallise in an orthorhombic substructure of zincblend with  $z = 2$  (space group  $I mm 2$ ). An orthorhombic superstructure of wurtzite was observed with high temperature

modification of  $\text{Cu}_2\text{SiS}_3$ , space group (mc  $2_1$  with  $z = 4$ ). The two new structures belong to the normal tetrahedral structure and they thought that these structures might occur not only with  $\text{I}_2\text{-IV-VI}_3$ , but also with  $\text{I-IV}_2\text{-V}_3$  compounds. So far, no compounds of the second group have been found in these structures.

Alloys on the basis of  $\text{I}_2\text{-IV-VI}_3$  compounds have been investigated to some extent by several authors. Their study represents a matter of considerable interest, since solid solutions based on these ternary compounds may have properties which would differ in a desired manner from the properties of the original compounds.

The existence of chalcopyrite solid solutions has been established [125] in the range of compositions from pure  $\text{Cu}_2\text{GeSe}_3$  to  $2\text{Cu}_2\text{GeSe}_3\text{-Cu}_2\text{SnSe}_3$  in the system  $\text{Cu}_2\text{GeSe}_3\text{-Cu}_2\text{SnSe}_3$ . Others [120] showed that the system  $\text{Cu}_2\text{GeSe}_3\text{-Cu}_2\text{GeTe}_3$  forms non-equilibrium substitutional solid solutions throughout the whole range of compositions.  $\text{Cu}_2\text{GeSe}_3$  can also form solid solutions with gallium arsenides. Goryunova *et al.* [126] reported single crystals of an alloy consisting of 20%  $\text{Cu}_2\text{GeSe}_3$  and 80%  $3(\text{GaAs})$  in a sphalerite structure, using the method of gas transport reaction. It has been reported [127] that there is a solid solution for the system  $\text{Cu}_2\text{GeSe}_3\text{-Ga}_2\text{Se}_3$  of the range  $0.4 < x < 1$  where  $x$  is the mole fraction of  $\text{Cu}_2\text{GeSe}_3$ .

#### 5.7.2 $\text{CuGe}_2\text{P}_3\text{-Cu}_2\text{GeS}_3$ system

The ternary compound  $\text{Cu}_2\text{GeS}_3$  is reported to be an orthorhombic sub-structure type of zincblend [124], which represents a new ordered super-structure of zincblend. S atoms are occupying the former S sites, while Cu and Ge atoms are arranged in ordered fashion on the former Zn sites. Thus, both Cu and Ge atoms are each co-ordinated by 4S neighbours. The

lattice parameters were reported to be  $a = 11.321 \text{ \AA}$ ,  $b = 3.766 \text{ \AA}$  and  $c = 5.208 \text{ \AA}$ .

A monoclinic structure was reported by Avekleva [128] when observing a superstructure lattice, and with atomic distribution completely analogous to that in zincblende, with the Cu and Ge atoms replacing the Zn atoms in ordered distribution, and the S atoms retaining the S sites. Finally, tetragonal and monoclinic lattices were reported by Mohamed *et al.* [129], with tetragonal lattice of  $a = 5.31 \text{ \AA}$  and  $c = 5.219 \text{ \AA}$ . Reports of different structures for this and others in this group of compounds could be discussed by means of changing the stoichiometry of the compound, as below.

The compound  $\text{Cu}_2\text{GeS}_3$ , with excess copper, was reported to have monoclinic structure [129], while a zincblende structure was reported for a sample grown without excess S, which may mean that it is rich in germanium [130]. As this compound contains a volatile component (S), and under different growth conditions may lose a different amount of S, which can cause non-stoichiometry in the compound. Then different structures would be expected, depending on the Cu and Ge excess existing in the compound. The compound  $\text{CuGe}_2\text{P}_3$  is similar to Ge, as discussed in Section 5.5.1. The complete solid solution of  $\text{CuGe}_2\text{P}_3$  with  $\text{Cu}_2\text{GeS}_3$  was found to have the zincblende structure and lattices obeying Vegard's law [see Figure 5.10(a)].

In order to understand how the complete solid solution between the two compounds are possible, it is better to discuss the similarity of Ge with the compound  $\text{Cu}_2\text{GeS}_3$ . There are two possible lattice sites in  $\text{Cu}_2\text{GeS}_3$ , one occupied by S atoms (anion) and the other shared by Cu and Ge atoms (cation) in ordered form. The structure of pure Ge is also similar, with the difference being that both sites are now occupied by identical atoms.

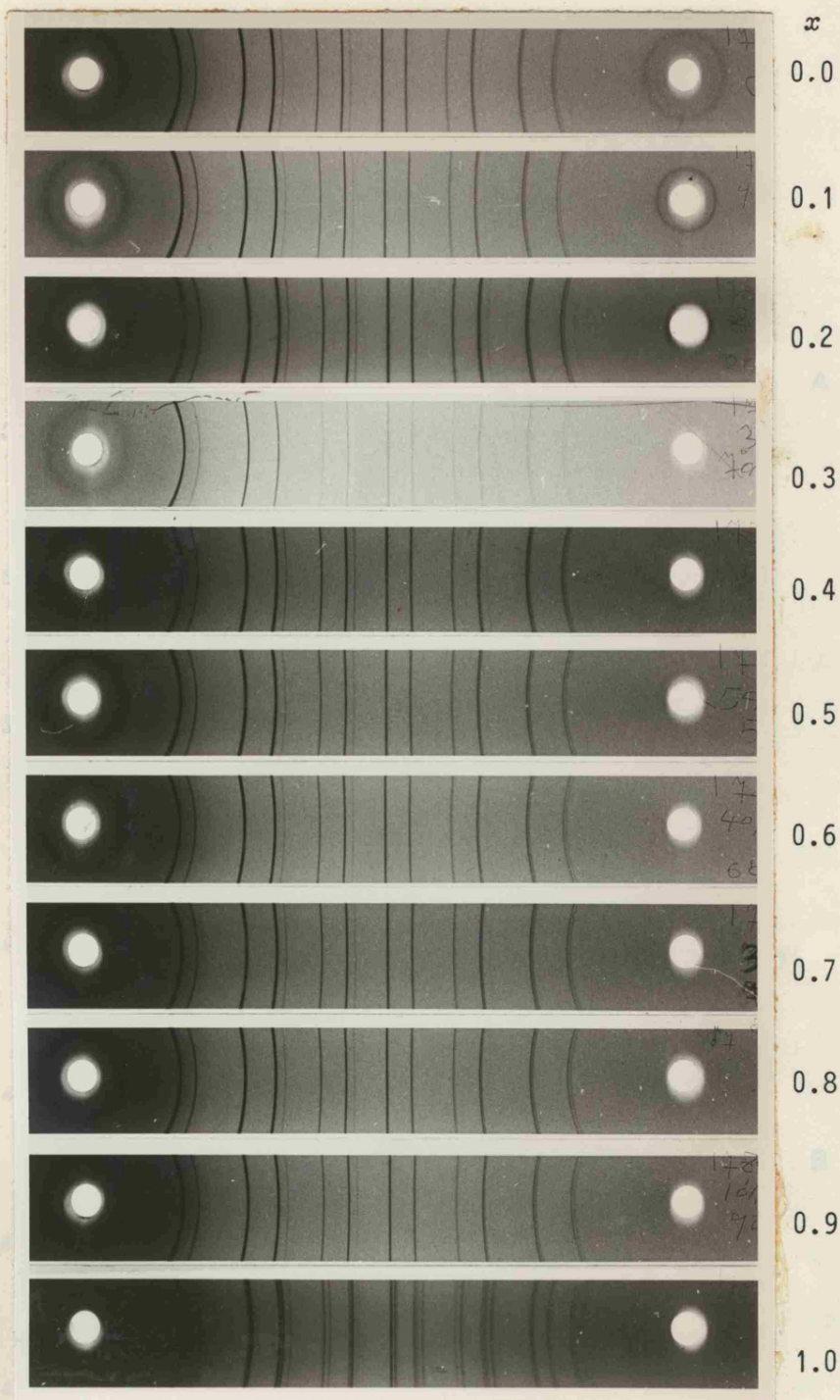


Figure 5.9 X-Ray powder photographs of the system  $(\text{CuGe}_2\text{P}_3)_{x-1}-(\text{Cu}_2\text{GeS}_3)_x$ . These show a complete solid solution between the two compounds.

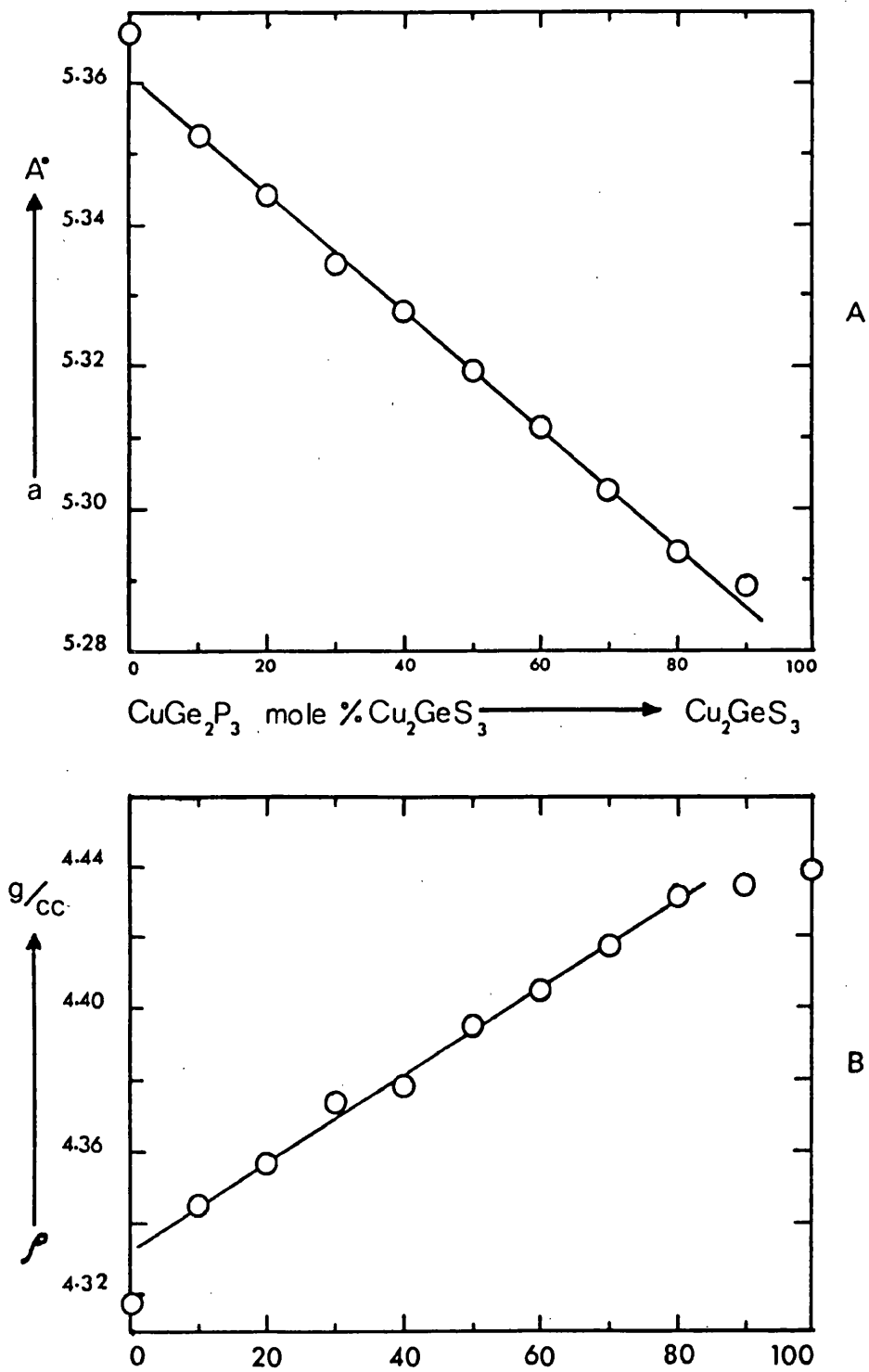


Figure 5.10 Section  $\text{CuGe}_2\text{P}_3$ - $\text{Cu}_2\text{GeS}_3$  of the system Cu-Ge-P-S  
A - lattice parameter for various compositions  
B - density of various compositions

Therefore, if the excess Ge goes substitutionally into the  $\text{Cu}_2\text{GeS}_3$  lattice, it must be replacing atoms on both sites with equal probability.

The unit cell volumes for  $\text{CuGe}_2\text{P}_3$  and  $\text{Cu}_2\text{GeS}_3$  [129] are  $154.6 \text{ \AA}^3$  and  $147.5 \text{ \AA}^3$  respectively, and bulk densities 4.317 and 4.439 g/cc respectively. It can easily be seen that the unit cell mass had a very small change. The average mass per atom for both compounds is almost the same. Thus it appears that the  $\text{CuGe}_2\text{P}_3$ - $\text{Cu}_2\text{GeS}_3$  alloy is only a substitutional solid solution.

As mentioned at the beginning of this section, there are two lattice sites for both compounds  $\text{CuGe}_2\text{P}_3$  and  $\text{Cu}_2\text{GeS}_3$ . One is occupied by P and S respectively, and the other is shared by Cu and Ge for both compounds. The cell constants are not very different (especially when  $\text{Cu}_2\text{GeS}_3$  is in the cubic form [130]). Therefore, if  $\text{CuGe}_2\text{P}_3$  is added to the  $\text{Cu}_2\text{GeS}_3$  lattice, it must be S atoms in anion sites replaced by P atoms and Cu by Ge in cation sites. The latter is due to a larger amount of Ge in  $\text{CuGe}_2\text{P}_3$  than in  $\text{Cu}_2\text{GeS}_3$ .

Another confirmation can be obtained by examining the relative line intensities of the X-ray powder pattern of the system (Figure 5.9). It has not shown significant changes. This is due to the similarity of the atomic scattering factors for atoms of Cu and Ge on one side and P and S atoms on the other. Hence the intensity pattern in the alloy system showed similarities in both compounds  $\text{CuGe}_2\text{P}_3$  and  $\text{Cu}_2\text{GeS}_3$ .



Table 5.9X-ray powder data for 50% CuGe<sub>2</sub>P<sub>3</sub> - 50% Cu<sub>2</sub>GeS<sub>3</sub>

<u>hkl</u>	<u>sin<sup>2</sup>θ (obs.)</u>	<u>sin<sup>2</sup>θ (calc.)</u>	<u>d → Å</u>	<u>I/I<sub>0</sub></u>
111	0.0633	0.0630	3.0709	100.0
200	0.0843	0.0840	2.6595	16.9
220	0.1688	0.1680	1.8805	59.3
311	0.2319	0.2306	1.6037	51.1
222	0.2529	0.2520	1.5354	04.1
400	0.3372	0.3360	1.3297	13.2
331	0.4004	0.3991	1.2202	25.5
420	0.4214	0.4201	1.1893	02.7
422	0.5048 α <sub>1</sub>	0.5033	1.0857	21.9
511,333	0.5674 α <sub>1</sub>	0.5662	1.0236	12.3
440	0.6727 α <sub>1</sub>	0.6710	0.9402	07.3
531	0.7348 α <sub>1</sub>	0.7339	0.8990	14.6
600,442	-	0.7549	0.8865	00.0
620	0.8397 α <sub>1</sub>	0.8388	0.8410	12.3
533	0.9023 α <sub>1</sub>	0.9017	0.8110	06.3
622	-	0.9227	0.8018	00.0

Table 5.10

X-ray powder data for 10% CuGe<sub>2</sub>P<sub>3</sub> - 90% Cu<sub>2</sub>GeS<sub>3</sub>

<u>hkl</u>	<u>sin<sup>2</sup>θ (obs.)</u>	<u>sin<sup>2</sup>θ (calc.)</u>	<u>d → Å</u>	<u>I/I<sub>0</sub></u>
111	0.0641	0.0637	3.0538	100.0
200	0.0853	0.0849	2.6447	15.4
220	0.1705	0.1699	1.8701	46.7
311	0.2343	0.2336	1.5948	43.5
222	0.2556	0.2548	1.5269	02.9
400	0.3408	0.3398	1.3223	13.2
331	0.4046	0.4035	1.2135	15.4
420	0.4259	0.4248	1.1827	02.5
422	0.5100 α <sub>1</sub>	0.5089	1.0797	17.0
511,333	0.5738 α <sub>1</sub>	0.5725	0.0179	09.3
440	0.6795 α <sub>1</sub>	0.6785	0.9350	06.1
531	0.7432 α <sub>1</sub>	0.7421	0.8940	09.6
600,442	-	0.7633	0.8815	00.0
620	0.8486 α <sub>1</sub>	0.8481	0.8363	08.0
533	0.9120 α <sub>1</sub>	0.9118	0.8066	04.8
622	-	0.9330	0.7974	00.0

### 5.7.3 Alloys of $\text{CuGe}_2\text{P}_3$ with other $\text{I}_2\text{-IV-VI}_3$ compounds

The system  $\text{CuGe}_2\text{P}_3\text{-Cu}_2\text{GeSe}_3$ , unlike alloys with  $\text{Cu}_2\text{GeS}_3$ , does not form a complete solid solution. The existence of the solid solution appears in the region  $0.25 \geq x \geq 0.9$  when  $x$  is  $\text{CuGe}_2\text{P}_3$  (Figures 5.11 and 5.12). The two compounds have similarities in their structure, particularly when  $\text{Cu}_2\text{GeSe}_3$  has the same structure and atomic distribution of  $\text{Cu}_2\text{GeS}_3$ , except that S sites here are occupied by Se atoms [124]. The compounds  $\text{CuGe}_2\text{P}_3$  and  $\text{Cu}_2\text{GeSe}_3$  are similar and their cation sites are occupied by P and Se atoms respectively, while their anion sites are shared by Cu and Ge randomly for  $\text{CuGe}_2\text{P}_3$  and ordered for  $\text{Cu}_2\text{GeSe}_3$ . However, they differ in their unit cell volumes, bulk densities and mass per atom. When the alloy system is based on  $\text{Cu}_2\text{GeSe}_3$ , the Se atoms will be replaced by P atoms and Cu by Ge. It is possible to replace Cu by Ge in this compound [123], but because of the difference in atomic size between P and Se, limited substitution could be expected.

The X-ray powder photographs show no significant change in their relative line intensities for alloys up to 25%  $\text{CuGe}_2\text{P}_3$  and an unknown second phase appeared.\* The lattice parameters obeyed Vegard's law [see Figure 5.12(a)]. When the solid solutions were based on  $\text{CuGe}_2\text{P}_3$ , the Ge atoms were exchanged for Cu, and P atoms for Se in their anion sites. Only up to 10%  $\text{Cu}_2\text{GeSe}_3$  was shown to be single phase. An unacceptable excess of Cu in  $\text{CuGe}_2\text{P}_3$  could be the explanation for the formation of this alloy (see Section 5.5.2).

The existence of  $\text{Cu}_2\text{SiS}_3$  and  $\text{Cu}_2\text{SiSe}_3$  in solid solution has not so far been reported. However, different structures have been reported by several people for these compounds [33,131], which were different from those found in  $\text{CuGe}_2\text{P}_3$ .

---

\*See Figure 5.11.

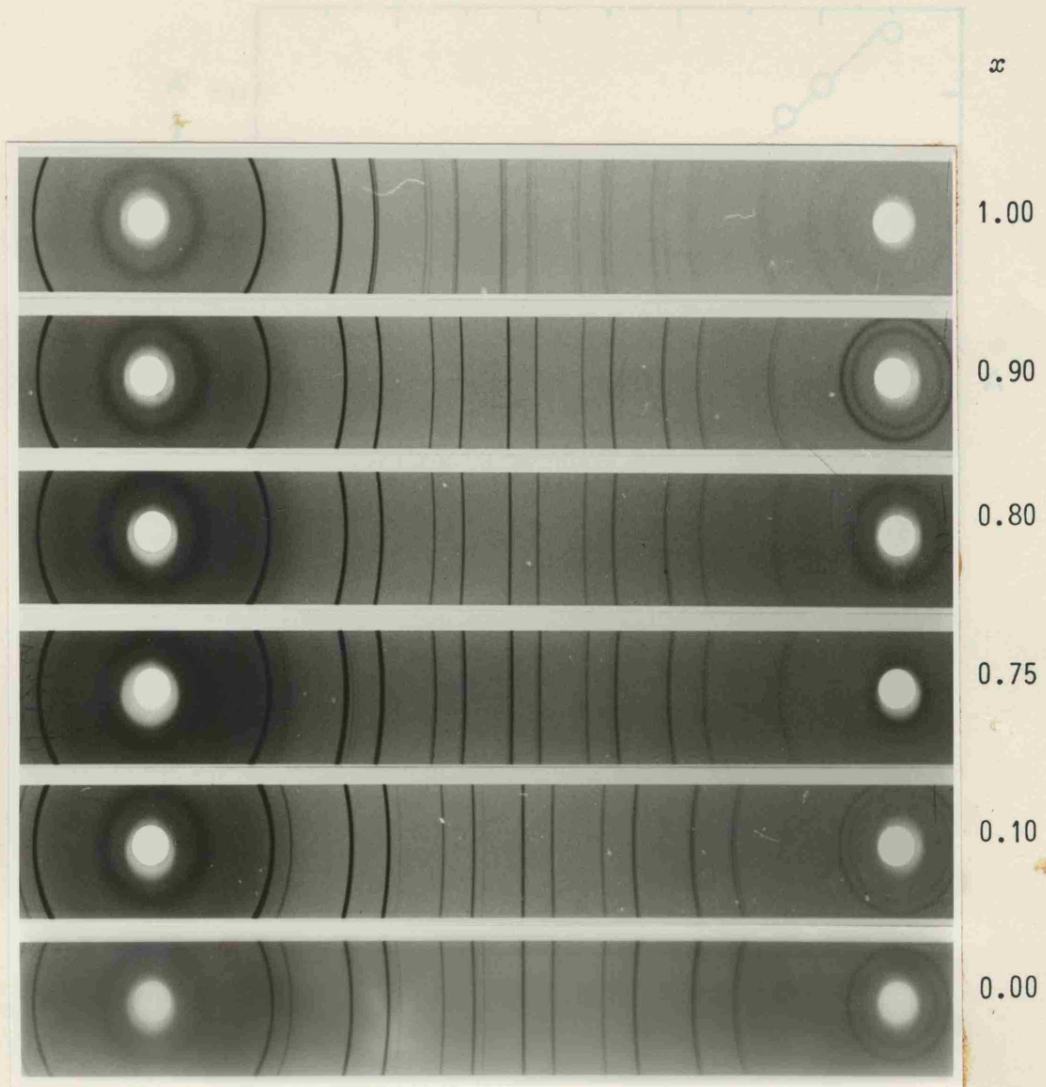


Figure 5.11 X-Ray powder photograph of the system  $(\text{CuGe}_2\text{P}_3)_{x-1}-(\text{Cu}_2\text{GeSe}_3)_x$ , showing a second phase for a sample when  $x = 0.75$

Figure 5.12 Section  $\text{CuGe}_2\text{P}_3-\text{Cu}_2\text{GeSe}_3$  of the system Cu-Ge-P-Se  
A - lattice parameter for various compositions  
B - density of various compositions

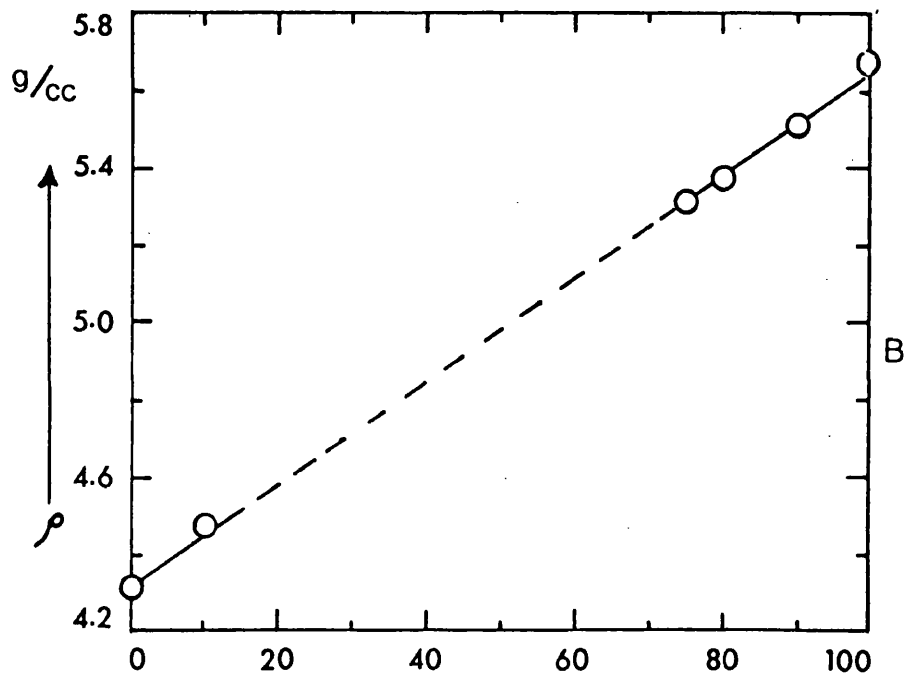
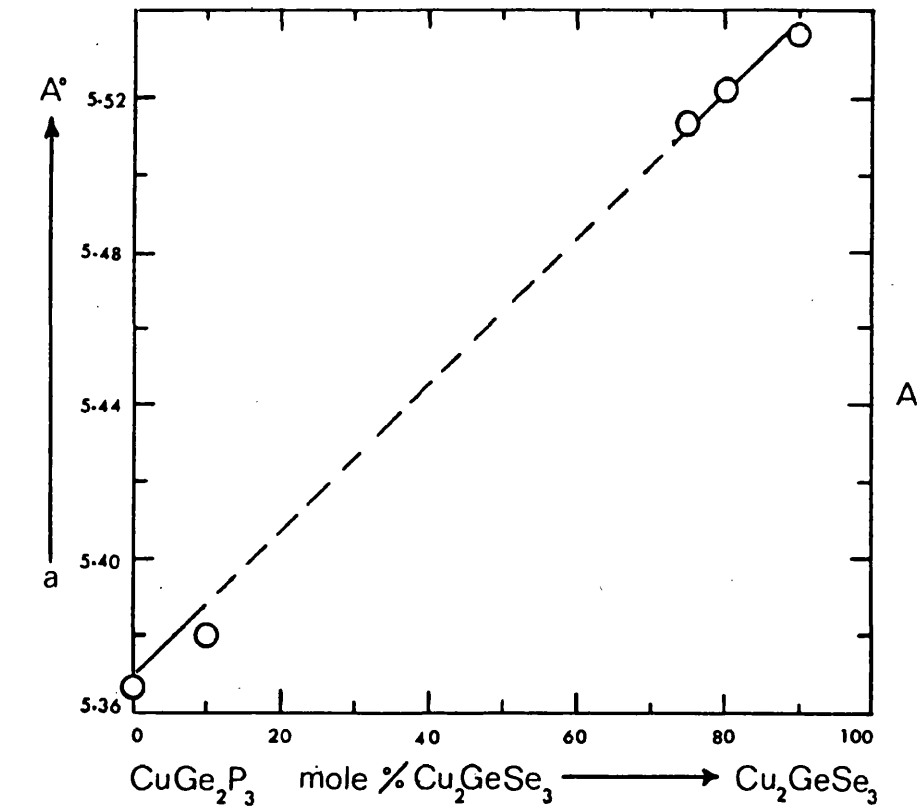


Figure 5.12 Section  $\text{CuGe}_2\text{P}_3$ - $\text{Cu}_2\text{GeSe}_3$  of the system Cu-Ge-P-Se  
A - lattice parameter for various compositions  
B - density of various compositions

Table 5.11X-ray powder data for the alloy 10% CuGe<sub>2</sub>P<sub>3</sub> - 90% Cu<sub>2</sub>GeSe<sub>3</sub>

<u>hkl</u>	<u>sin<sup>2</sup>θ (obs.)</u>	<u>sin<sup>2</sup>θ (calc.)</u>	<u>d + Å</u>	<u>I/I<sub>0</sub></u>
111	0.0586	0.0581	3.1971	100.0
200	-	0.0775	2.7688	01.5
220	0.1554	0.1550	1.9578	75.0
311	0.2138	0.2131	1.6696	67.5
222	-	0.2325	1.5985	00.0
400	0.3109	0.3100	1.3844	22.5
331	0.3692	0.3682	1.2704	38.0
420	-	0.3876	1.2382	00.0
422	0.4661	0.4651	1.1303	39.0
511,333	0.5241	0.5232	1.0657	20.0
440	0.6204	0.6191	0.9789	12.0
531	0.6778	0.6771	0.9360	20.5
600,442	-	0.6965	0.9229	00.0
620	0.7741	0.7738	0.8755	15.0
533	0.8328	0.8319	0.8444	07.5
622	-	0.8513	0.8348	00.0
444	0.9290	0.9286	0.7993	04.5
711,551	0.9864	0.9867	0.7754	12.5

### 5.8 Other Solid-Solution Systems based on $\text{CuGe}_2\text{P}_3$

The Ge excess in  $\text{CuGe}_2\text{P}_3$  was not the only group IV element which was investigated. The other one investigated was Si. The fusion method was used for preparation of the alloys. Samples of different composition up to 25% Si per mole were tried. X-Ray investigations showed complete separation between the two materials.

Investigation of the possibilities of solid-solution with compounds of groups III-V was unsuccessful. Compounds I-IV<sub>2</sub>-V<sub>3</sub> are the second most similar to III-V after II-IV-V<sub>2</sub>. Most of the latter were found to form solid-solutions with groups III-V compounds [ 37 ]. Alloys with GaP were investigated by preparing more than eight samples containing up to 50% 3GaP. X-ray results showed fast cooling materials to have two phases for the two compounds, while a complete separation was observed for slow cooled material in temperature gradients suitable for growing single crystals. Low resistivity single crystals of GaP were found on top of the  $\text{CuGe}_2\text{P}_3$  crystals. Thus p-type GaP single crystals could be grown using this method for special treatment. However, a significant interface was observed between the two compounds in a p-n junction grown by using epitaxial growth of molten  $\text{CuGe}_2\text{P}_3$  on single crystals of GaP after special treatment (see Chapter 8 for the details). Alloys with GaAs, unlike GaP, showed some kind of solid solution. X-Ray investigation showed more than 65% of zincblend structure phase with lattice parameter of  $\alpha = 5.479 \text{ \AA}$  for a system  $\text{CuGe}_2\text{P}_3$ -GaAs. So far, the other lines have not been identified. However, alloys with InP appeared in complete separation between the two compounds. Attempts to dissolve II-VI and III<sub>2</sub>-VI<sub>3</sub> compounds completely failed (see Table 5.12).

Table 5.12

Some other alloys investigated in this work

Compounds and alloys	X-Ray powder results
$\text{CuGe}_2\text{As}_3$	More than one phase
$\text{CuZnGe}_3\text{As}_5 (\text{CuGe}_2\text{As}_3 - \text{ZnGeAs}_2)$	Lines of $\text{ZnGeAs}$ appeared with unknown phases
$\text{Cu}_2\text{ZnGe}_5\text{As}_8 (2\text{CuGe}_2\text{As}_3 - \text{ZnGeAs}_2)$	Lines of $\text{ZnGeAs}$ appeared with unknown phases
$\text{AgZnGe}_3\text{P}_5 (\text{AgGe}_2\text{P}_3 - \text{ZnGeP}_2)$	Two phases were the result
$\text{Ag}_2\text{ZnGe}_5\text{P}_8 (2\text{AgGe}_2\text{P}_3 - \text{ZnGeP}_2)$	Two phases were the result
$\text{CuInGe}_2\text{P}_4 (\text{CuGe}_2\text{P}_3 - \text{InP})$	Complete separation between the two compounds
$\text{CuGe}_2\text{Ge}_2\text{P}_3\text{S}_3 (\text{CuGe}_2\text{P}_3 - \text{Ga}_2\text{S}_3)$	More than one phase
$\text{CuGa}_2\text{Ge}_2\text{P}_3\text{Se}_3 (\text{CuGe}_2\text{P}_3 - \text{Ga}_2\text{Se}_3)$	More than one phase
$\text{CuCdGe}_2\text{P}_3\text{S} (\text{CuGe}_2\text{P}_3 - \text{CdS})$	The alloy does not melt up to 1250 °C
$\text{CuCdGe}_2\text{P}_3 (\text{CuGe}_2\text{P}_3 - \text{CdSe})$	More than one phase
$\text{CuZnGe}_3\text{P}_3\text{As}_2 (\text{CuGe}_2\text{P}_3 - \text{ZnGeAs}_2)$	More than one phase
$\text{Cu}_2\text{GaGe}_2\text{P}_3\text{Se}_2 (\text{CuGe}_2\text{P}_3 - \text{CuGaSe}_2)$	The compounds are completely separated
$\text{CuInGeP}_2\text{Se} (\text{CuGe}_2\text{P}_3 - \text{CuInSe}_2 - \text{InP})$	The three compounds were shown to be completely separated.



Another interesting investigation with regard to  $\text{CuGe}_2\text{P}_3$ , which was carried out was with regard to its interaction with ternary compounds. Its alloying with two compounds of type II-IV- $\text{V}_2$  was investigated. The alloy with  $\text{ZnGeP}_2$  appeared as two phases of the two compounds with one and two parts of  $\text{CuGe}_2\text{P}_3$ . Annealing treatment for 350 h at 700 °C produced single phase material of zincblend structure with  $a = 5.40 \text{ \AA}$ , which is similar to the alloy found for  $\text{CuZnGe}_3\text{P}_5$ . However, polycrystalline single phase materials for  $\text{CuZnGe}_3\text{P}_5$  were produced by using iodine transport (see Chapter 3), with the same lattice parameter as mentioned above. The single crystals resulting from this reaction were ternary  $\text{ZnGeP}_2$  and different compositions of the Cu-Ge-P system, with unknown structures which differed from the original compound,  $\text{CuGe}_2\text{P}_3$ . Figure 5.13 shows X-ray photographs for some alloys of this type.

The final compound in this group to be investigated was  $\text{ZnGeAs}_2$ . The solid solution does show some zincblend lines, while most other lines were unidentified.

No solid-solutions were observed with compounds in group I-III- $\text{VI}_2$ , while the latter compound showed a wide range of solid-solution with binary and ternary compounds of types III-V, II-IV- $\text{V}_2$  and other binary and ternary compounds [37].

In the investigations carried out in connection with solid-solutions of  $\text{CuGe}_2\text{P}_3$  with compounds in the same ternary group,  $\text{CuGe}_2\text{As}_3$  was the only compound which showed some interaction and 80% of zincblend structure was the result. The lattice parameter was  $5.454 \text{ \AA}$  for a solution of 50%  $\text{CuGe}_2\text{As}_3$ , while complete separation was found with compounds  $\text{CuSi}_2\text{P}_3$  and  $\text{AgGe}_2\text{P}_3$ . However, alloys of compound  $\text{AgGe}_2\text{P}_3$  with II-IV- $\text{V}_2$  ternary groups have so far been unsuccessful. Thus the atomic arrangement of this compound

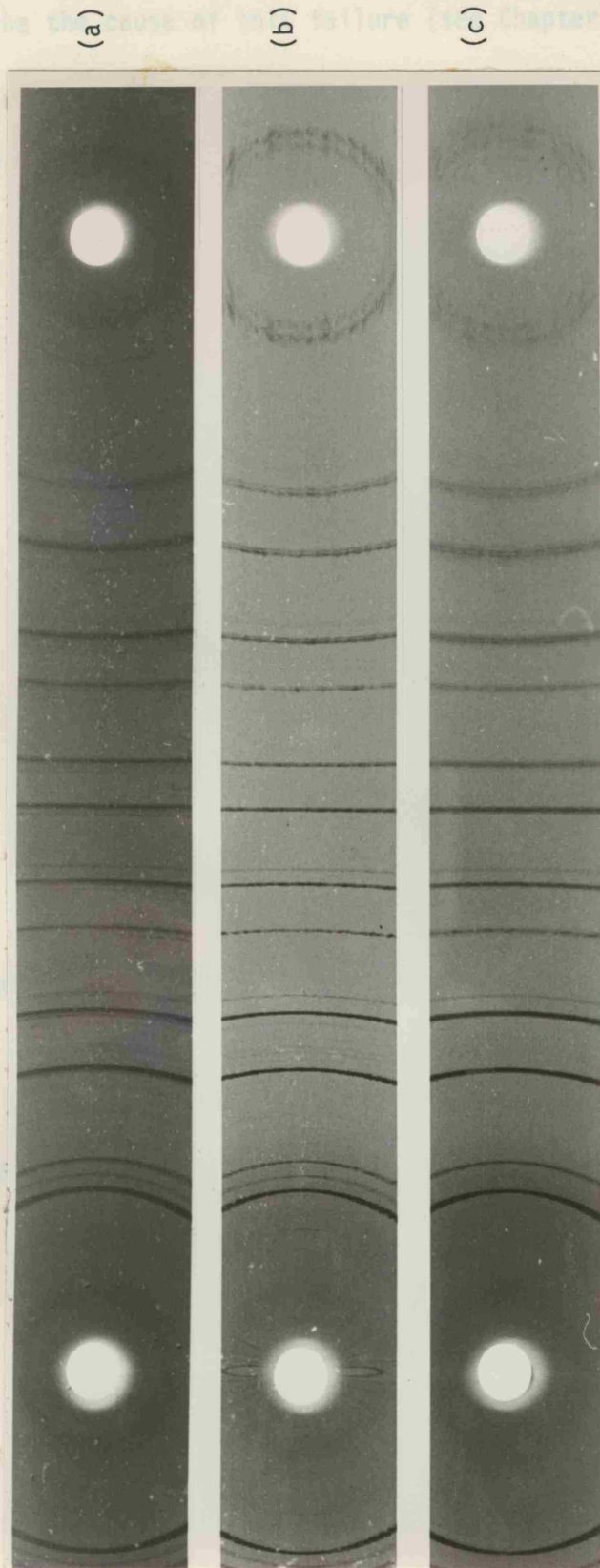


Figure 5.13 X-Ray powder photograph of (a)  $\text{Cu}_2\text{ZnGe}_5\text{P}_8$  before annealing; (b) after annealing; (c)  $\text{CuZnGe}_3\text{P}_5$  from iodine transport

could be the cause of this failure (see Chapter 2).

Table 5.12 shows the compounds and solid-solutions investigated in this work and not discussed in detail thus far.

Table 5.13

X-Ray powder data for  $\text{CuZnGe}_3\text{P}_5$

<u>hkl</u>	<u><math>\sin^2\theta</math> (obs.)</u>	<u><math>\sin^2\theta</math> (calc.)</u>	<u><math>d \rightarrow \text{\AA}</math></u>	<u><math>I/I_0</math></u>
111	0.0613	0.0611	3.1177	100.00
200	0.0818	0.0815	2.7000	29.52
220	0.1607	0.1630	1.9092	70.04
311	0.2243	0.2242	1.6281	64.47
222	-	0.2445	1.5588	6.57
400	0.3255	0.3256	1.3500	22.10
331	0.3862	0.3872	1.2388	31.15
420	-	0.4076	1.2074	5.00
422	0.4885	0.4891	1.1023	34.47
511,333	0.5484 $\alpha_1$	0.5502	1.0392	16.57
440	0.6494 $\alpha_1$	0.6521	0.9546	13.15
531	0.7101 $\alpha_1$	0.7133	0.9127	16.57
600,442	-	0.7336	0.9000	1.05
620	0.8128 $\alpha_1$	0.8152	0.8536	14.73
533	-	0.8763	0.8235	8.94
622	-	0.8967	0.8140	00.00
444	-	0.9782	0.7794	1.57

## 5.9 Discussion

The Gibbs composition triangle (Figure 3.1) is helpful in discussing the results of the present investigation. The two straight lines represent the following two conditions for the formation of tetrahedral diamond-like phases (see Chapter 2) and for the following examples [11]:-

- (i) the average number of valence electrons should be four;
- and
- (ii) all participating elements should exhibit their normal valency, *i.e.*, equal to their group number in the Periodic Table.

The first condition ensures the correct number of electrons for  $sp^3$  hybridisation. It is satisfied along the tie-line Ge-CuP<sub>3</sub>. The Ge excess phases lie on this line. The stability of tetrahedral co-ordination in these phases is possible because the average number of electrons remains four. The second condition ensures bond saturation, a necessary condition for semi-conductivity [132]. It is satisfied along the tie-line Cu<sub>3</sub>P-Ge<sub>3</sub>P<sub>4</sub>. The point of intersection of these two lines corresponds to the composition CuGe<sub>2</sub>P<sub>3</sub>, which is known to be a tetrahedral ternary semiconductor.

It was pointed out by Goryunova [36] that the ternary compounds are stable only when there is chemical interaction in the two basic binary systems (cation-anion systems). According to that author, the formation of a chemical compound in the basic system indicates the existence of the chemical interaction, while formation of a solid-solution or a eutectic indicates its absence. Goryunova also pointed out that this was a necessary, but not sufficient, condition for the actual existence of the ternary compound. However, the way this interaction influences the

stability and structure of the ternary compounds is not clear.

Investigation of  $\text{CuGe}_2\text{P}_3$  showed that  $\text{CuP}_2$  was the only second phase to exist clearly. Attempts to prepare solid-solutions with excess  $\text{Cu}_3\text{P}$  failed and  $\text{CuP}_2$  was increased. While a wide range of non-stoichiometry close to  $\text{Ge}_3\text{P}_4$  existed, the  $\text{CuP}_2$  phase began to disappear.

A second phase of  $\text{CuP}_2$ , or any others, were not observed in  $\text{CuSi}_2\text{P}_3$ . It is clear that group IV atoms decide the existence or non-existence of this phase. It has also been shown that excess Ge decreases the  $\text{CuP}_2$  phase, while a deficiency of Ge increases this phase. The information given above indicates a very strong interaction in the Cu-P system, compared with Ge-P, while the non-existence of Cu-P in  $\text{CuSi}_2\text{P}_3$  means that Si-P bonds are stronger than those of Cu-P. However, the latter could lead to the existence of a wider range of non-stoichiometries in the Gibbs triangle for  $\text{CuSi}_2\text{P}_3$ .

Solid solutions between  $\text{CuGe}_2\text{P}_3$  and Ge containing  $\text{I}_2\text{-IV-VI}_3$  compounds show interesting possibilities and similar results might be expected for  $\text{CuSi}_2\text{P}_3$  and Si containing compounds of the type  $\text{I}_2\text{-IV-VI}_3$ .

## CHAPTER 6

### Electrical Properties of I-IV<sub>2</sub>-V<sub>3</sub> Compounds

#### 6.1 Introduction

In order to understand the mechanism of semi-conductors, it is first necessary to investigate the structure of their energy bands. However, measurements of transport properties such as conductivity, Hall constant, *etc.*, can give a good idea of the utility of a material for some device applications. In this chapter, the results of Hall measurements and conductivity on some I-IV<sub>2</sub>-V<sub>3</sub> compounds after physical treatment such as annealing and doping are presented. These measurements also prove useful in helping to correlate the properties of the mixed crystals of the system Cu-Ge-P-S, as well as those of CuGe<sub>2</sub>P<sub>3</sub>-Ge and CuSi<sub>2</sub>P<sub>3</sub>-Si.

All measurements were performed on single crystals to avoid the complicated effects of structural defects such as grain boundaries.

#### 6.2 The Measuring System

##### 6.2.1 Block Diagram

A block diagram of the DC measuring system is shown in Figure 6.1. A 5<sup>1</sup>/<sub>2</sub> digital volt meter (Model Thurlby 1905a) was used for all current and voltage measurements, as well as for sample temperature.

It is known that any fluctuation in the primary current flowing through the sample will reflect as a voltage at the measuring probes. These fluctuations must therefore be kept to a minimum.

A transistorised current stabiliser Palmer 1966 [133] was used. The stabiliser places an apparent high resistance (about 50 k $\Omega$ ) in series with the sample. Any temperature, or other interference, which might induce resistance change in the sample or connecting leads, is kept to a minimum

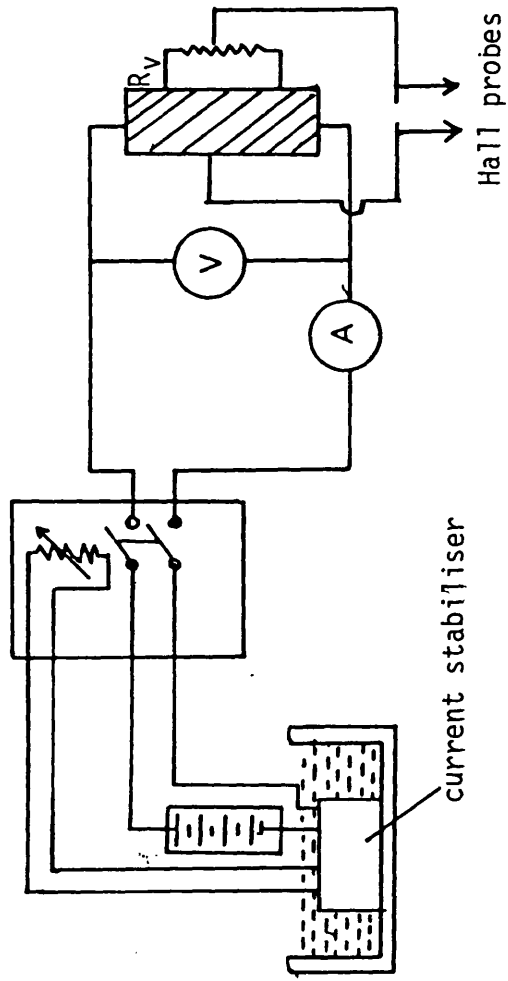


Figure 6.1 The Hall effect measuring system

in relation to the total circuit resistance and as a result the current change is very small.

To remove drifts caused by temperature changes in the stabiliser, it was completely immersed in a bath of industrial paraffin. After an initial warm-up of 1-2 h, the primary current (0.1-0.5 amps) could be held steady to better than 1 in  $10^6$  over a period of ten minutes and was quite unaffected by severe temperature changes (about 10 °C) in the sample or connecting leads.

Adjustment of the potentiometer,  $R_V$ , eliminates the zero field Hall voltage which is generally present, due to the small misalignment of essentially opposite contacts. A ten turn (Colvern Multiturn) (10 k $\Omega$ ) potentiometer was used, since this setting was quite critical.

The magnet used was a Type F, made by Newport Instruments, and calibrated by Newport Equipment Ltd., and re-calibrated in this laboratory by a gaussmeter, Type 750 (manufactured by RFL Industrial Inc., Boonton, New Jersey, U.S.A.). This instrument was capable of measuring from 0-1000 G on the low range and from 0-50000 G on the high range, with an error of less than  $\pm 1.5\%$ . A zero gauss chamber enabled instrument calibration before every measurement. Field values were always set by increasing the magnet coil current, finishing at saturation (about 16 kG).

A Cu-constantan thermocouple was used for measuring sample temperature. This type of thermocouple is suitable for measuring the temperature within 3-673 °K. One junction of the thermocouple was taped to the centre of the specimen, while the other was maintained at 0 °C in melting ice. The output from the thermocouple was led into the 5½ digital multimeter.



### 6.2.2 The Cryostat

To measure the electrical properties over the range of liquid nitrogen temperature up to 450 °K, the low temperature cryostat was used and this is illustrated in Figure 6.2.

The sample was attached to the end of a copper rod by means of a mica plate. The various electrical signals were taken through a five core (0.71 mm) copper cable. The copper rod and its carrier were fixed inside a thin copper tube on which was wound two non-inductive resistance heaters. In order to avoid burning, the heater was housed inside a secondary copper tube. The whole cryostat (heater and sample housing) was evacuated and then filled with helium gas. The helium gas was useful for transferring heat to the sample uniformly and preventing condensation of water vapour on the crystal during cooling of the system.

The tube (sample housing) was dipped into liquid nitrogen contained in a specially constructed Dewar vessel with a narrow bottom, which was supported between the pole pieces of an electromagnet.

With the tube immersed in liquid nitrogen, the crystal gradually cooled to about 78 °K in 3 h. However, temperatures between this and 450 °K were obtained by supplying current to the heater.

For measuring the Hall data, the sample temperature was cooled down, by the addition of liquid nitrogen to the Dewar, to about 78 °K. After data at this temperature had been taken, the heater was turned on for several minutes at a time, and the next readings were taken after thermal equilibrium had been reached. The sample temperature was measured at the start and finish of each series of Hall measurements, a spread of typically no more than 0.5 °K.

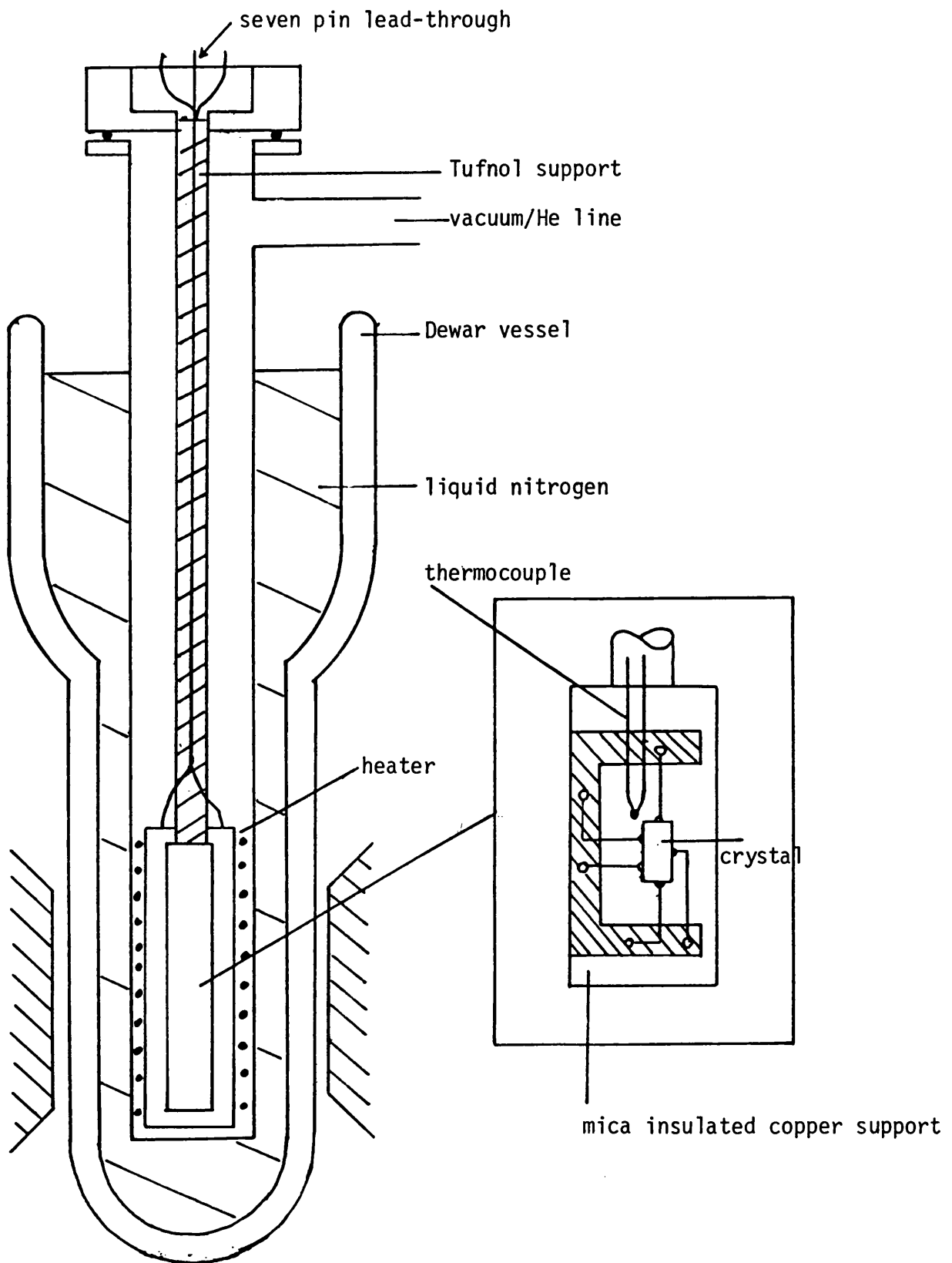


Figure 6.2 Cryostat assembly with sample holder insert

### 6.3 The Hall Effect

#### 6.3.1 Basic Theory

The electrical conductivity  $\sigma$  and the Hall coefficient,  $R_H$ , were determined for different compounds and alloys mentioned in Chapter 5, in the temperature range from liquid nitrogen to 460 °K.

Values of  $R_H$  and  $\sigma$  were derived using the following equations. If  $L$  is the length of a rectangular shaped sample and  $axb$  is the cross-section area, then:

$$\sigma = \frac{V}{I} \cdot \frac{a \cdot b}{L} (\Omega^{-1} \text{ cm}^{-1}) \quad (6.1a)$$

where  $V$  is a voltage drop along  $L$  and  $I$  is the current passing through the sample. The Hall coefficient  $R_H$  was determined from the Hall voltage  $V_H$  and the transverse magnetic field  $B$  in Tesla, from the equation:

$$R_H = \frac{V_H \cdot b}{I_x \cdot B_z} \text{ cm}^3 \text{ C}^{-1} \quad (6.1b)$$

when  $b$  is a sample thickness. The Hall mobility ( $\mu_H$ ) values were calculated from the product of (6.1a) and (6.1b). Then:

$$\begin{aligned} \mu_H &= \sigma R_H (\text{cm}^2 \text{ v}^{-1} \text{ s}^{-1}) \\ &= r\mu \end{aligned} \quad (6.1c)$$

where  $\mu$  is a drift mobility, while the carrier concentration ( $n, p$ ) is

$$p = r \cdot \frac{1}{eR_H} (\text{cm}^{-3}) \quad (6.1d)$$

The value of  $r$  depends on the scattering mechanism and  $r$  was taken here as  $3\pi/8$ , considering lattice mode scattering to be more probable than the optical mode, while  $r = 315\pi/512$  is used when ionised impurity scattering is dominant.

### 6.3.2 Hall Sample Preparation and Ohmic Contacts

The rectangular shaped samples were cut from large single crystals. Samples were finally polished by 1 micron diamond compound and washed with acetone and distilled water and then etched with HF.

Several different methods for making electrical contact were adopted with considerable success for particular materials. However, evaporated gold and copper, as well as indium, on  $\text{CuGe}_2\text{P}_3$  and the system Cu-Ge-P, did not produce good ohmic contacts before and after annealing and with the use of a different substrate temperature.

Tin gave good ohmic contacts for freshly polished samples. Indium was more successful than tin for the Cu-Ge-P-S and Cu-Si-P systems, as well as for the compound  $\text{CuSi}_2\text{P}_3$ .

No difficulties were experienced with the use of tin on  $\text{Ag}_6\text{Ge}_{10}\text{P}_{12}$  crystals, with or without polishing.

## 6.4 Hall Effect for $\text{Ag}_6\text{Ge}_{10}\text{P}_{12}$

### 6.4.1 Carrier Concentration

The temperature dependence of the carrier concentration can be expressed by the relation [134]:

$$\frac{p(p+N_D)}{(N_A+N_D-p)} = \frac{N_V}{g} \exp(-E_a/KT) \quad (6.2)$$

where  $N_A$  and  $N_D$  are the concentrations of acceptors and donors respectively,  $p$  is the Hall concentration in a non-degenerate semi-conductor,  $N_V$  is the density of states in the valence band,  $g$  is the degeneracy factor and  $E_a$  is the acceptor ionisation energy.

$$N_v = 2 \left( \frac{m_v^* KT}{2\pi\hbar^2} \right)^{3/2} \quad (6.3)$$

where  $m_v^*$  is the effective mass of holes in the valence band and is expressed in units of free electron mass  $m_0$ . Equation 6.2 is derived on the assumption that the excited states of the acceptor are far removed from the ground state. For such a simple case,  $g = 2$  [134]. However, the degenerate temperature was calculated by using the relation:

$$T_{\text{deg}} = \frac{3^{2/3} \pi^{4/3} \hbar^2 p^{2/3}}{2m_p^* k} \quad (6.4)$$

According to the relation above, all the samples tested in this work are in the degenerate region, with the exception of  $\text{Ag}_6\text{Ge}_{10}\text{P}_{12}$  (sample 4), which was non-degenerate.

Equation 6.2 was simplified for the hole concentration below 300 °K, to a formula usual for thermal excitation at single acceptor level [135]:

$$p = \frac{1}{2} (N_D + \phi) \left\{ \left[ 1 + \frac{4(N_A - N_D)\phi}{(\phi + N_D)^2} \right]^{1/2} - 1 \right\} \quad (6.5)$$

when

$$\phi = \frac{N_v}{g_v} \exp(-E_a/KT) \quad (6.6)$$

and

$$N_v = 2(2\pi m_v^* KT/\hbar^2)^{3/2} \quad (6.7)$$

The degree factor  $g$  depends upon the impurity state involved.

At low temperature ( $p \ll N_D, N_A + N_D$ ), then  $p$  in equation 6.5 will be:

$$p = \left( \frac{N_A}{N_D} - 1 \right) \phi \quad (6.8)$$

It is known that the valence (conduction) band density of states is a function of  $T^{3/2}$ ; the above equation can therefore be transformed to:

$$p = c \left( \frac{N_A}{N_D} - 1 \right) T^{3/2} \exp(-E_a/KT) \quad (6.9)$$

The activation energy,  $E_a$ , can then be calculated from the graph of  $\ln p T^{-3/2}$  vs  $\frac{1}{T}$ , where the slope will be equal to  $E_a/K$ , which gives  $E_a$  ranging from 0.004 eV to 0.0202 eV for several samples and  $m_p^* = 2.3 m_0$  [136]. Applying  $E_a$  in equation 6.9, the compensation ratio of  $N_A/N_D$  can be calculated. For different temperatures in the exhaustion range,  $N_A - N_D$  can be estimated from the limit of  $p$  in this range and  $N_A$ ,  $N_D$  can be calculated:

$$p = N_A - N_D \quad (6.10)$$

The method of least squares can then be applied to equation 6.5 to find the values of the parameters which give the best fit over the entire temperature range, as given below for sample 4 of  $Ag_6Ge_{10}P_{12}$ .

$$N_A \approx 10^{22} \text{ cm}^{-3}$$

$$\frac{N_A}{N_D} \approx 4$$

#### 6.4.2 Hall Density Analysis of $Ag_6Ge_{10}P_{12}$

It is thought that a large number of acceptors were present in the sample in the as-grown state, as can be seen in Figure 6.3. These acceptors, probably phosphorus vacancies because the compound  $Ag_6Ge_{10}P_{12}$  was expected to have covalent bonding, which means that the deficiencies of phosphorus produce the deficiencies of the bonding [28], *i.e.*, holes [137,138], while these vacancies can be regarded as donors for crystals with ionic bonds [25]. According to this model, there is

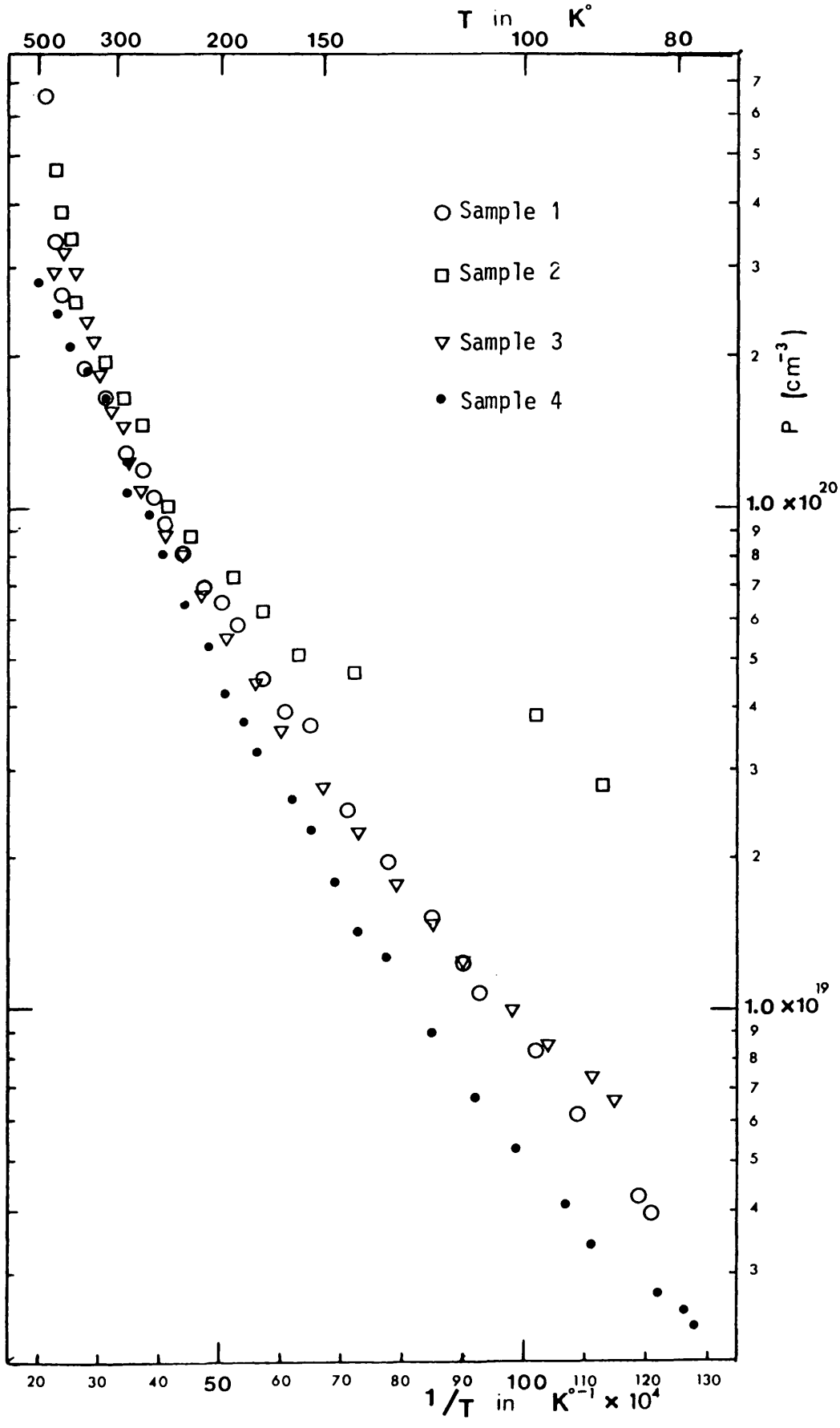


Figure 6.3 The hole density *versus* inverse absolute temperature for a single crystal of  $Ag_6Ge_{10}P_{12}$

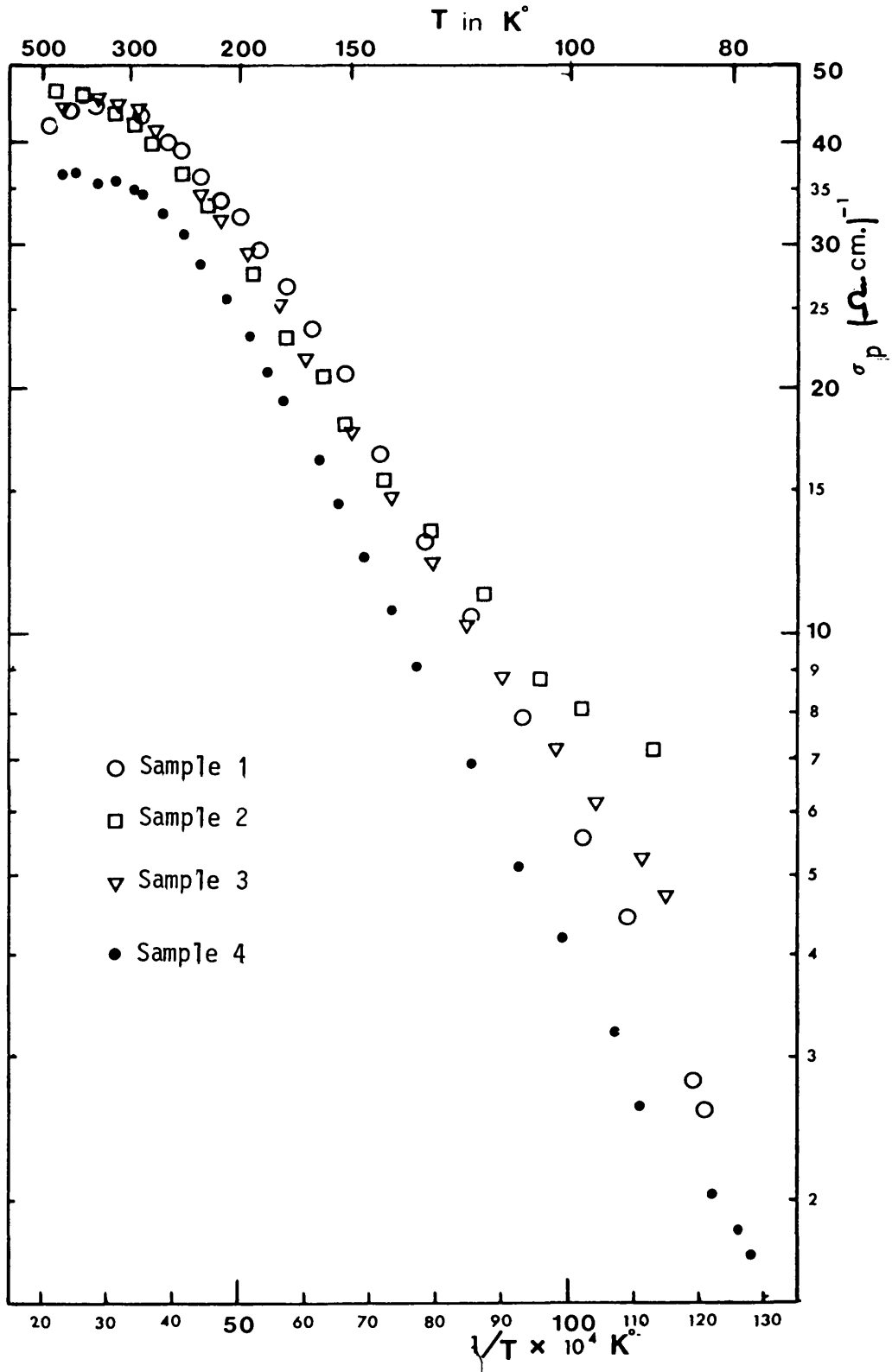


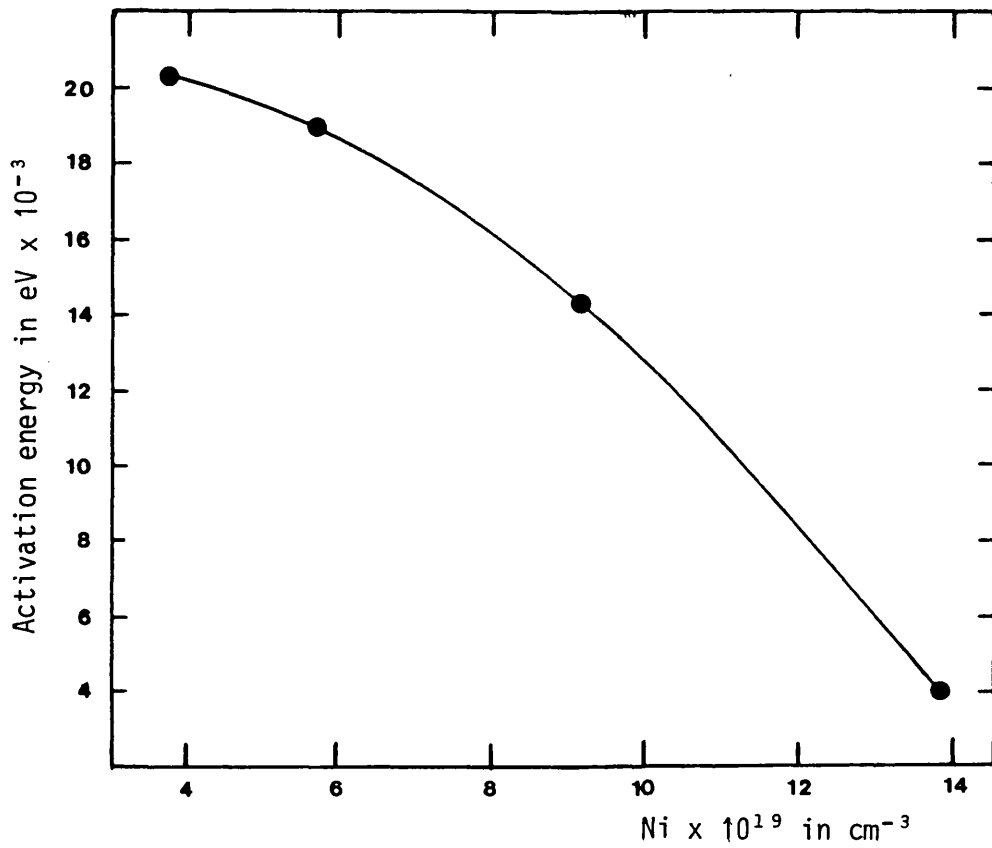
Figure 6.4 Conductivity of the compound  $\text{Ag}_6\text{Ge}_{10}\text{P}_{12}$  as a function of inverse absolute temperature



an exchange of valence electrons among the interacting atoms, in order to complete their outer shells. It is therefore logical to assume that the number of unpaired electrons is less than four, in the case of vacancies, and electrons may easily be promoted to the conduction band. However, this was not the case in our samples of  $\text{Ag}_6\text{Ge}_{10}\text{P}_{12}$ , although we suggest that the ionic bonds exist in such a compound.

If we plot  $E_A$  versus average density of ionised acceptor ( $N_i$ ) in the region from which the  $E_A$  value was obtained, then the variation of activation energy is decreasing with increasing concentration. Pearson and Bardeen [139] suggested that the decrease of activation energy with concentration is due to the potential energy of attraction between the ionised acceptors and acceptor holes. Those workers considered that this mechanism would lead to a lowering of activation energy inversely proportional to the average distance between the holes and ions, thus essentially being proportional to the third power of the density of ionised acceptors. It is apparent that this leads to a variation of activation energy with degree of ionisation. Pincherle [140] pointed out that free carriers will also give rise to decreasing activation energy by screening the field around a trapping centre. The effectiveness of screening and therefore the amount of decrease, will be greater at lower temperature and higher electron (holes) concentrations. Calculations indicated that the effect is considerable in silicon [141]. Figure 6.5 illustrates  $E_a$  vs ( $N_i$ ), the density of ionised acceptors for several samples of  $\text{Ag}_6\text{Ge}_{10}\text{P}_{12}$ .

From the  $\ln pT^{-3/2}$  versus  $\frac{1}{T}$  data, one can measure an acceptor level ( $E_a \approx 0.02$  eV), and thus the hydrogenic acceptor level can be calculated:



Ionised-impurity concentration for acceptors

Figure 6.5 Activation energy as a function of the density of ionised acceptors calculated from equation (6.12)

$$E_a = 13.6 \frac{m_p^*}{\epsilon_0^2} = 0.093 \text{ eV} \quad (6.11)$$

This does not agree with the results quoted above. Thus the uncertainty may come from low frequency dielectric constants  $\epsilon_0$ , which have been estimated [see Section 6.4.3(b)]. On the other hand,  $m_p^*$  should be diminished closer to the free electron values. The latter figure is very likely to be correct, because of the large error in its calculation [136]. However,  $m_p^*$  and  $\epsilon_0$  have shown satisfactory fitting for the mobility data, which will be described later in this chapter.

Finally, higher energy levels were found by using  $\ln \sigma T^{-3/2}$  vs  $\frac{1}{T}$  curve ( $E_a \approx 0.046$ ), which agrees better with the results calculated above.

### 6.4.3 Carrier Scattering Mechanism

There are four types of scattering processes which have been studied theoretically for semi-conductors: lattice, ionised impurity, neutral impurity and dislocation.

(a) Ionised impurity scattering. - The ionised impurity scattering results from either impurities or lattice defects generated by non-stoichiometry of the compound. This is particularly important at low temperatures, when thermal vibrations of the lattice atoms are small. Scattering by ionised impurity was first treated in a somewhat crude, essentially classical fashion. Each ion was considered to scatter independently of all the others with its scattering  $\sigma$  section arbitrarily cut off at a distance equal to half the average distance between neighbouring impurities. The latter assumption is partly justified by the screening of the impurities by the conduction (valence) electrons (holes).

Hence the mobility of holes is modified by the effect of lattice vibration and in the form of logarithmic term [142]:

$$\mu_I = \left(\frac{2}{300}\right) \frac{2^{3/2} \epsilon_0^2 (KT)^{3/2}}{\pi^{3/2} m_p^* e^3 N_j} \times \frac{1}{[\ln(1+x) - x/1+x]} \quad (6.12)$$

where

$$x = \frac{6 \epsilon_0 m_p^* K^2 T^2}{\pi \rho \hbar^2 e^2} \quad (6.13)$$

where the 2 in the numerator is due to the overlap and the 300 in the denominator is to convert to practical units ( $\text{cm}^2 \text{v}^{-1} \text{sec}^{-1}$ ), when all the parameters are entered in cgs units.

It should be noted that  $\epsilon_\infty$  (high frequency dielectric constant) has been determined for  $\text{Ag}_6\text{Ge}_{10}\text{P}_{12}$  [136] and is ( $\epsilon_\infty = 14.1$ ), whereas  $\epsilon_0$  (low frequency dielectric constant) has not, to the author's knowledge. However, Ziatkin and co-workers [143] showed  $\epsilon_0/\epsilon_\infty = 1.3$  for a zincblend structure of  $\text{ZnSnP}_2$  and between 1.15 - 1.45 for other chalcopyrite materials such as II-IV-V<sub>2</sub> and I-III-VI<sub>2</sub> compounds. Thus, in such a case,  $\epsilon_0/\epsilon_\infty = 1.3$  was chosen as a means of approximation, and  $\epsilon_0$  can be calculated for  $\text{Ag}_6\text{Ge}_{10}\text{P}_{12}$  and is equal to 18.3. Then K is a Boltzmann constant,  $m_p^*$  is the effective mass of valence holes and is  $m_p^* \cong 2.3 m_0$  [136], e is the electron charge in Coulombs and h is plank's constant in erg - sec.

Equation 6.12 will therefore be:

$$\mu_I = 8.7318 \times 10^{17} \frac{T^{3/2}}{N_j [\ln(1+x) - x/1+x]} \quad (6.14)$$

and equation 6.13 will then be:

$$x = 5.49 \times 10^{15} \frac{T^2}{\rho} \quad (6.15)$$

Then the ionised impurity concentration  $N_j$  is calculated by assuming that the maximum in  $\mu$  versus T is given by  $\mu_I \cong \mu_L \cong 2\mu$ , where  $\mu_L$  is the total lattice mobility. This is valid (in Matthiessen's approximation) if  $\mu$  is symmetrical about this maximum, which is approximately true for

the compound  $\text{Ag}_6\text{Ge}_{10}\text{P}_{12}$  ( $\mu_I \sim T^{3/2}$  and  $\mu_L \sim T^{-3/2}$ ). However,  $p$  was used as a constant in the temperature range considered.

Observation of this form of scattering is manifested by a  $T^{3/2}$  dependence of  $\mu$ . Unionised impurities and other carriers may also contribute to the scattering of carriers, although their effect will be small and only detectable at very low temperatures in the absence of ionised impurities [144].

(b) Lattice scattering mechanism.-Several theoretical treatment of scattering by lattice vibrations have been carried out, such as Bardeen and Shockley [145], but all with essentially equivalent results.

The lattice vibration of atoms deforms the potential energy configuration of the atom and leads to small variation in the energy gap. The variation in the energies of the conduction band and valence band edges resulting from the vibrational motion is localised, which creates changes in the kinetic energy of the carriers. Hence, from the Bardeen-Shockley derivation [145], the acoustic scattering is given by:

$$\mu_{ac} = \left(\frac{2}{300}\right) \frac{(8\pi)^{1/2} \hbar^4 C_{11}}{3E_{ac}^2 m_p^{5/2} (KT)^{3/2}} \quad (6.16)$$

where, again, the 2 in the numerator is due to the overlap and the 300 in the denominator is to convert to practical units ( $\text{cm}^2 \text{v}^{-1} \text{s}^{-1}$ ) when all the parameters are entered in cgs units. Here,  $C_{11}$  is the average longitudinal elastic constant and is equal to  $11.98 \times 10^{11}$  dyn/cm<sup>2</sup> for  $\text{Ag}_6\text{Ge}_{10}\text{P}_{12}$  at room temperature [146].  $E_{ac}$  is the valence bond deformation potential and the other symbols have their usual meanings.

It is usually considered that the temperature variation of  $E_{ac}$ ,  $m_p^*$  and  $C_{11}$  can be neglected, so that the principal feature of the acoustic mode scattering is a  $T^{-3/2}$  dependence of mobility.

Wiley and Didomenico [147] have combined the acoustic mode contribution with the non-polar optical mode contribution and found a combined mobility,  $\mu_{a,npo}$  given by:

$$\mu_{a,npo} = \mu_{ac} S(\phi, \eta, T) \quad (6.17)$$

where  $\phi$  is the optical phonon characteristic temperature and  $\eta = (E_{npo}/E_{ac})^2$ , where  $E_{npo}$  is the non-polar optical deformation potential. Thus:

$$S(\phi, \eta, T) \approx \{1 + (\phi/T)\eta H / [\exp(\phi/T) - D]\} \quad (6.18)$$

where H and D are constants given for each value of  $\eta$ . However, it has been satisfactorily shown that equation 6.17 explains the hole mobilities in many III-V compounds, even though the polar optical contribution has been considered to be dominant in many past studies of holes in these compounds [148]. Then Wiley has further shown that  $E_{ac} \approx 5-6$  eV in several III-V compounds and  $\eta \approx 4$  in these compounds, as well as Si and Ge [149]. The author will also assume that  $\eta \approx 4$  in  $Ag_6Ge_{10}P_{12}$  and  $E_{ac} = 5.5$  and in the present approximation we will take a simple average between some III-V compounds of  $\phi$ , so that  $\phi \approx 490$  °K [150]. In addition, for  $\eta = 4$ , we must use  $H = 1.34$  and  $D = 0.914$  [147].

When  $m_p^* = 2.4 m_0$  [136], and other symbols are used as mentioned above, equation 6.18 will be simplified to:

$$\mu_{ac} = 3.1167 \times 10^4 T^{-3/2} \text{ cm}^2 \text{ v}^{-1} \text{ sec}^{-1} \quad (6.19)$$

and equation 6.17 can be re-written as:

$$\mu_{a,npo} = 3.1167 \times 10^4 T^{-3/2} \left\{ 1 + \frac{2626}{T} \right\} / \left[ \exp\left(\frac{490}{T}\right) - 0.914 \right]^{-1} \quad (6.20)$$

Such a relation was used for CuInSe<sub>2</sub> and CuInS<sub>2</sub> materials [151,152].

Since polar optical mode scattering  $\mu_{po}$  is dominant in III-V compounds, we may expect  $\mu_{po}$  to be dominant in the ternary compound Ag<sub>6</sub>Ge<sub>10</sub>P<sub>12</sub>. The polar-optical mode scattering contribution is [135,153].

$$\mu_{po} \approx \left( \frac{2}{300} \right) \frac{8\hbar^2}{2(2\pi k)^{3/2} e \theta m_p^*} \cdot \frac{\epsilon_0 \epsilon_\infty}{(\epsilon_0 - \epsilon_\infty)} \chi(\theta/T) T^{3/2} \chi[\exp(\theta/T) - 1] \quad (6.21)$$

(cm<sup>2</sup> v<sup>-1</sup> sec<sup>-1</sup>)

where, again, the 2 in the numerator is due to the overlap integral, and  $\chi(\theta/T)$  is a slowly varying function of T, which can be approximated by  $0.48 \exp(0.18\theta/T)$ .\*  $\epsilon_0$  and  $\epsilon_\infty$  as before, are the static and high frequency dielectric constant,  $\epsilon_0 \approx 18.3$  and  $\epsilon_\infty = 14.1$  for Ag<sub>6</sub>Ge<sub>10</sub>P<sub>12</sub>, so that equation 6.21 can now be simplified as:

$$\mu_{po} = 0.42 [\exp(490/T) - 1] [\exp(88/T)] T^{3/2} \quad (6.22)$$

when  $m_p^*$  is 2.3  $m_0$

#### 6.4.4 Mobility Data Analysis of Ag<sub>6</sub>Ge<sub>10</sub>P<sub>12</sub>

Some of the values of the material parameters used in the calculations mentioned earlier, are estimated, along with those used for similar III-V compounds. Table 6.2 shows the calculated mobilities of various scattering mechanisms in all Ag<sub>6</sub>Ge<sub>10</sub>P<sub>12</sub> samples. However, the total calculated mobility ( $\frac{1}{\mu_T} = \sum \frac{1}{\mu_i}$ ) agrees well with the observed curve.

The calculated mobility curves fitted well with the experimental curve for temperatures higher than 200 °K, except for sample 2, where the curve fits at a higher temperature. Below the temperatures mentioned above,

---

\*Reference 152.

the calculated curve is well above the experimental one.

The mobilities, as expected, decrease with increasing carrier concentration, until very low temperatures are reached, where the residual impurity concentration is large enough to take over (Figure 6.6). The temperature variation of the Hall mobility for these samples shows a wide range of behavioural characteristics for different impurity concentrations. However, this is the case for most of the semi-conductors, such as silicon [141]. With increasing impurity concentration, the departure of negative slopes appears at higher temperature, which is due to the greater importance of ionised impurity scattering relative to lattice scattering.

From the low temperature dependence of mobility (Figure 6.6), it can be seen that sample 2 is changing as  $T^{+3/2}$ , while the other sample is showing slower changes, except for sample 1. However, with more data for temperatures below this range, the explanation for this expression may be clearer for those samples shown in Table 6.3.

For higher temperatures of mobility dependence, samples 1, 3 and 4 show changes as ( $T^{-1}$  to  $T^{-1.65}$ ), depending on the temperature range, while it is only  $T^{-1.5}$  for sample 2 (Table 6.3).

Since impurity scattering would only make the mobility curve less steep than  $T^{-1.5}$ , the data of section  $T^{-1.5}$ , or steeper curves, must represent lattice mobility. In this case, the theory of the preceding section predicts that  $\mu_H/\mu$  will be a constant 1.18 over the temperature range concerned for these samples. It would therefore follow that the lattice mobility varies with temperatures essentially as  $T^{-1.5}$ .



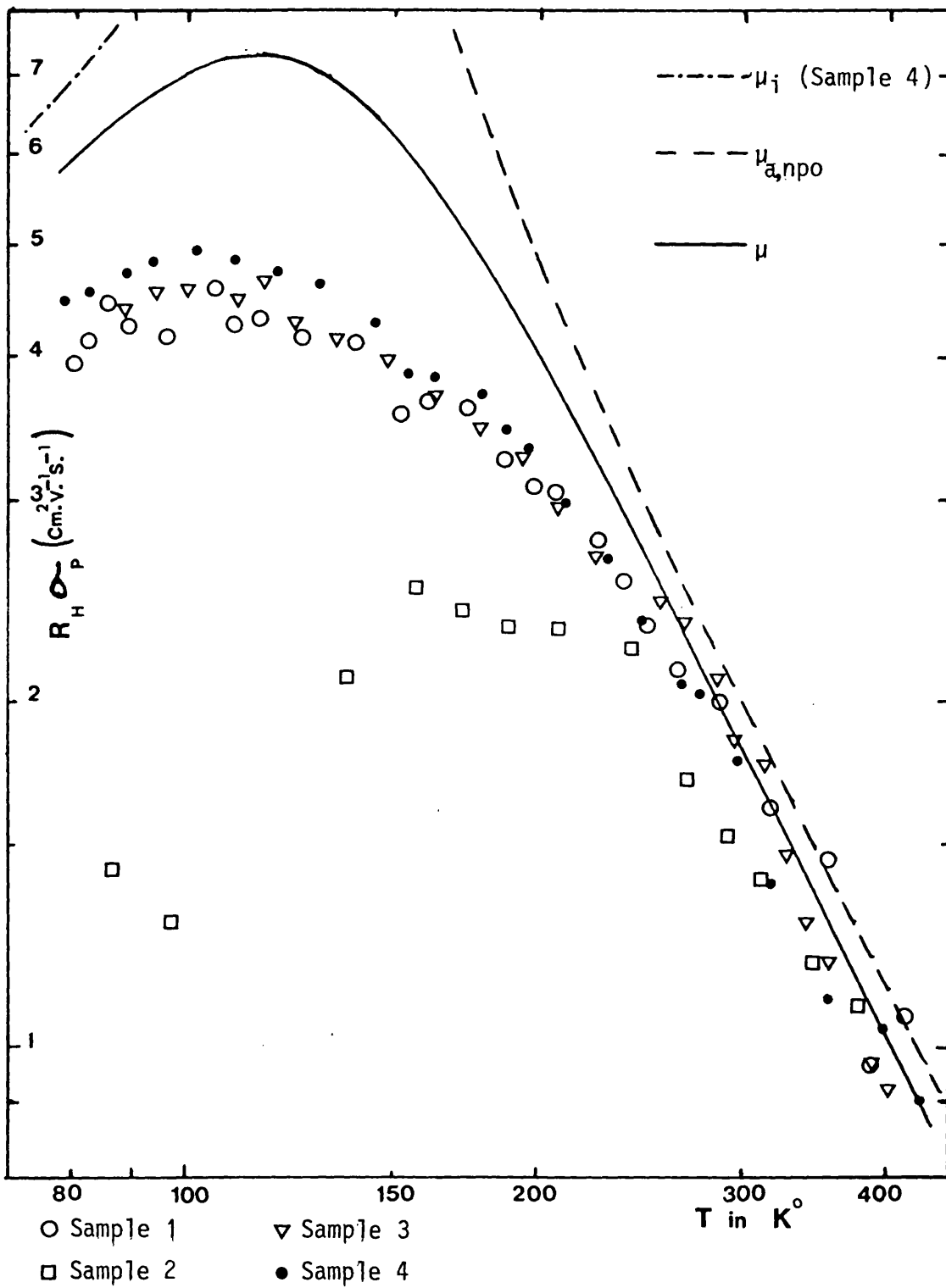


Figure 6.6 Hall mobility of  $\text{Ag}_6\text{Ge}_{10}\text{P}_{12}$  as grown crystals as a function of absolute temperature

In principle, one would expect acoustic, NPO modes and polar mode scattering to be present in the valence bands of  $\text{Ag}_6\text{Ge}_{10}\text{P}_{12}$ . However, it has been pointed out that there is no adequate theoretical expression for polar mode scattering in  $p$ -type materials of III-V compounds [147], and that the usual expression, [equation (6.21)], fails to explain the temperature dependence of the Hall mobility (Figure 6.6).

In view of the great similarities between groups IV and III-V compounds, it seems reasonable to expect that the non-polar scattering mechanisms which have been successfully treated for  $p$ -type Ge and  $p$ -type Si are also important in the III-V materials. Pursuing this analogy, it has been shown that the magnitude and temperature dependence of the Hall mobility for  $p$ -type III-V materials can be fitted. This treatment was first developed by Brown and Bray [154].

The two adjustable parameters  $E_{ac}$  and  $n = (E_{npo}/E_{ac})^2$  are quite similar for the compounds mentioned above and are physically reasonable [147]. Because of the similarity of ternary compounds of the type I-IV<sub>2</sub>-V<sub>3</sub> to those binary compounds and the fitting for  $\text{Ag}_6\text{Ge}_{10}\text{P}_{12}$  in this work, one can suggest applying such adjustable parameters to the latter group of ternary compounds are possible. However, this may fit all ternary compounds, such as II-IV-V<sub>2</sub> and I-III-VI<sub>2</sub>. Such data fitted quite reasonably to  $\text{CuInS}_2$  and  $\text{AgInSe}_2$ , as well as  $\text{AgInTe}_2$  [155].

## 6.5 Hall Effect and Conductivity Measurements for $\text{CuGe}_2\text{P}_3$ - $\text{Cu}_2\text{GeS}_3$ System

### 6.5.1 The Variation of Conductivity with Temperature

It has been found in this work that the solid-solutions of  $\text{CuGe}_2\text{P}_3$ - $\text{Cu}_2\text{GeS}_3$  are  $p$ -type for undoped materials. However,  $\text{CuGe}_2\text{P}_3$  is always reported to be  $p$ -type [157], and the same type was the result after all physical processes in this work, while  $\text{Cu}_2\text{GeS}_3$  was reported to be low

Table 6.1  
Some electrical properties of Ag<sub>6</sub>Ge<sub>10</sub>P<sub>12</sub>

Sample No.	P → cm <sup>-3</sup>	Ni → cm <sup>-3</sup>	μ <sub>I</sub> (cm <sup>2</sup> v <sup>-1</sup> s <sup>-1</sup> )	Calc. at T in °K	E <sub>a</sub> in eV		Data at T = 300 °K			Data at T = 80 °K		
					(from σ <sub>p</sub> data)	(from P data)	σ <sub>p</sub> (Ω <sup>-1</sup> cm <sup>-1</sup> )	P-cm <sup>-3</sup>	μ <sub>p</sub> (cm <sup>2</sup> v <sup>-1</sup> s <sup>-1</sup> )	σ <sub>p</sub> (Ω <sup>-1</sup> cm <sup>-1</sup> )	P(cm <sup>-3</sup> )	μ <sub>p</sub> (cm <sup>2</sup> v <sup>-1</sup> s <sup>-1</sup> )
1	1.0 × 10 <sup>19</sup>	5.72 × 10 <sup>19</sup>	9.2	110	0.046	0.0185	43.5	1.3 × 10 <sup>20</sup>	2.00	2.59	4.0 × 10 <sup>18</sup>	4.1
2	6.4 × 10 <sup>19</sup>	3.79 × 10 <sup>20</sup>	5.0	175	0.0034	0.004	42.02	1.68 × 10 <sup>20</sup>	1.56	6.6	2.8 × 10 <sup>19</sup>	1.43
3	2.0 × 10 <sup>19</sup>	9.1 × 10 <sup>19</sup>	9.0	130	0.0089	0.0143	42.8	1.86 × 10 <sup>20</sup>	1.57	4.7	6.6 × 10 <sup>18</sup>	4.4
4	5.36 × 10 <sup>18</sup>	3.74 × 10 <sup>19</sup>	9.97	100	0.015	0.0202	35.7	1.22 × 10 <sup>20</sup>	1.77	1.84	2.6 × 10 <sup>18</sup>	4.4
*							18.2	9.0 × 10 <sup>19</sup>	1.3			
†							60.6	1.0 × 10 <sup>20</sup>	2.8			

\* Data from reference 136.

† Data from reference 156.

Table 6.2

Calculated mobility in  $\text{Ag}_6\text{Ge}_{10}\text{P}_{12}$  ( $\text{cm}^2 \text{v}^{-1} \text{s}^{-1}$ )

<u>T in °K</u>	<u><math>\mu_{ac}</math></u>	<u><math>\mu_{a,npo}</math></u>	<u><math>\mu_{po}</math></u>
100	31.16	26.04	$1.35 \times 10^3$
300	6.00	1.949	40.20
450	3.26	0.851	21.35

Table 6.3

Characteristics of scattering process for samples of  $\text{Ag}_6\text{Ge}_{10}\text{P}_{12}$

Sample Number	$\mu = AT^x$	$\mu = BT^{-x}$
	$x$	$x$
1	0.825	$\frac{3}{2}$
2	1.05	$\frac{3}{2}$
3	0.255	$\frac{3}{2}$
4	0.479	$\frac{3}{2}$

mobility of  $n$ -type [129].

From equation 6.2:-

$$p = \frac{N_v}{g} \left( \frac{N_A - N_D}{N_D} \right) \exp(-E_a/KT) \quad (6.23)$$

Assuming the mobility to be relatively independent of temperature, the conductivity is simply proportional to  $P$ , So, one can modify equation 6.23 as follows:-

$$\sigma \sim cT^{3/2} \exp(E_a/KT) \quad (6.24)$$

or

$$\sigma T^{-3/2} = c \exp(-E_a/KT) \quad (6.25)$$

where the factor  $T^{-3/2}$  is from the density of states. Application of equation 6.25 reduce the expression to  $\sigma T^{-3/2}$ , which is proportional to  $E_a/KT$ , from which it is evident that plots of  $\ln \sigma T^{-3/2}$  versus  $\frac{1}{T}$  yields  $E_a$ . The impurity activation energies derived from the linear portions are listed in Table 6.4. Figure 6.7 shows  $\sigma_p$  versus  $\frac{1}{T}$  in K.

At low temperature, the impurity conductivity dominates and is different for various alloys and samples. Such conductivity is justified by the growth rate or chemical composition of the alloy, as indicated in this work. However, impurity level increased with increasing  $\text{Cu}_2\text{GeS}_3$  percentage in the alloy, or a slower cooling rate of growth.

Samples C and F have shown a single impurity level which is not far from the top of the valence band, while samples E and G show a double band of impurity levels well above the valence band. The two bands were very close for sample E, while they were well separated for sample G, which may be due to the growth effect.

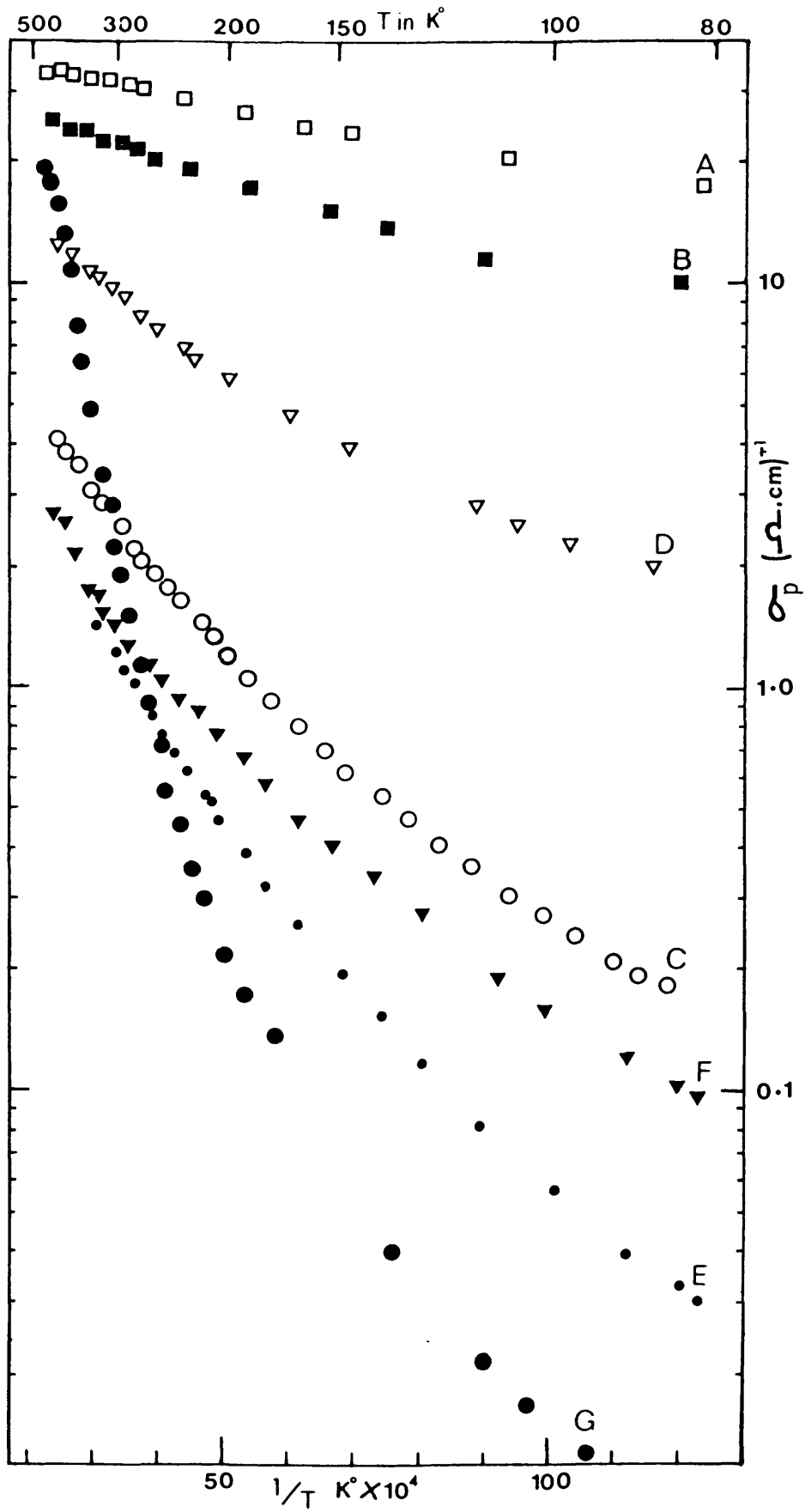


Figure 6.7 Conductivity of the system  $\text{CuGe}_2\text{P}_3\text{-Cu}_2\text{GeS}_3$  (as grown single crystals) as a function of inverse absolute temperature

The conductivity curves in the case of samples A, B and D are almost near to horizontal along the temperature range of investigation. This indicates that the acceptor levels are to be completely filled and thus lie very close to the top of the valence band, or just below it.

#### 6.5.2 The Variation of the Hall Mobility with Temperature

The Hall mobility for various compositions to 70% of  $\text{Cu}_2\text{GeS}_3$  were studied (see Section 6.8 for pure  $\text{CuGe}_2\text{P}_3$ ). The Hall voltage signal-to-noise ratio was somewhat poorer, particularly for alloys at higher sulphur composition. The temperature dependence of the Hall mobility is shown in Figure 6.8. The mobilities of all mixed crystals increase directly with temperature. For all samples, the maximum mobilities were recorded at temperatures higher than 320 °K. However, sample C does not show any decrease of mobility up to 410 °K.

When the temperature dependence of the Hall mobility is represented by:

$$\mu = AT^{\alpha} \quad (6.26)$$

The index  $\alpha$  of the temperature variation is increased with increasing sulphur in the alloys. However, the most rapid increase could be seen in sample D. Table 6.5 lists the various indices derived from the slopes of Figure 6.8. For temperatures higher than 330 °K, the mobility in samples A and B is decreasing with temperature as  $\alpha \cong -1.6$ , particularly sample A. The latter phenomenon does not appear clearly for samples C and D.

As discussed in Section 6.4.3, the temperature dependence of mobility is mainly due to ionised impurity scattering and lattice scattering.

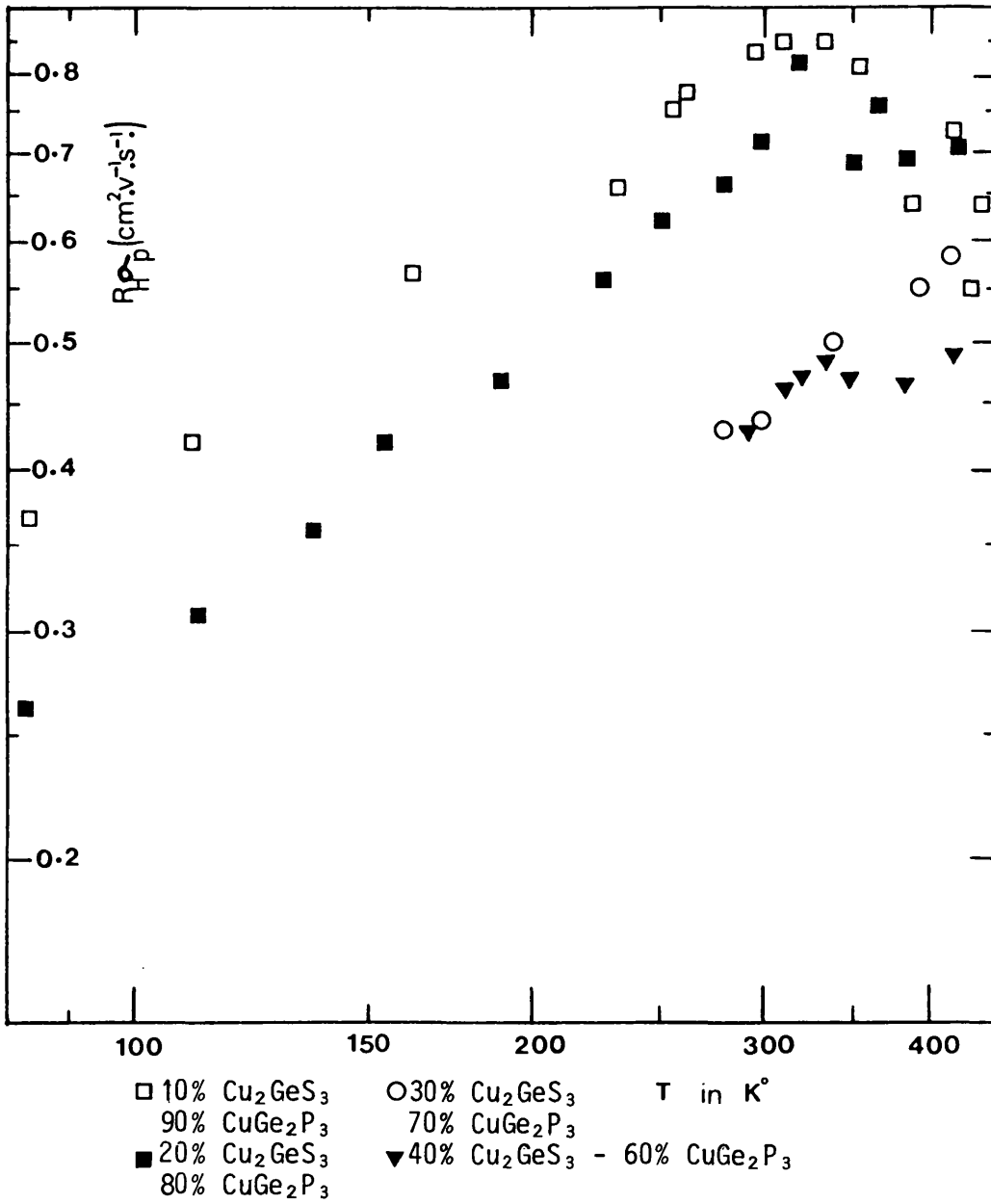


Figure 6.8 Hall mobility of  $\text{CuGe}_2\text{P}_3$ - $\text{Cu}_2\text{GeS}_3$  system as a function of absolute temperature



Table 6.4

Impurity activation energy for the system  $\text{CuGe}_2\text{P}_3$  -  $\text{Cu}_2\text{GeS}_3$

Symbols	Materials	$E_1$ - eV	$E_2$ - eV	Ret. of cooling ( $^{\circ}\text{C}/\text{hour}$ )
A	90% $\text{CuGe}_2\text{P}_3$ - 10% $\text{Cu}_2\text{GeS}_3$	-	-	2-4
B	80% $\text{CuGe}_2\text{P}_3$ - 20% $\text{Cu}_2\text{GeS}_3$	-	-	2-4
C	70% $\text{CuGe}_2\text{P}_3$ - 30% $\text{Cu}_2\text{GeS}_3$	0.0078	-	2
D	60% $\text{CuGe}_2\text{P}_3$ - 40% $\text{Cu}_2\text{GeS}_3$	-	-	2-4
E	50% $\text{CuGe}_2\text{P}_3$ - 50% $\text{Cu}_2\text{GeS}_3$	0.28	0.018	1
F	40% $\text{CuGe}_2\text{P}_3$ - 60% $\text{Cu}_2\text{GeS}_3$	0.0179	0.0105	2-4
G	30% $\text{CuGe}_2\text{P}_3$ - 70% $\text{Cu}_2\text{GeS}_3$	0.0767	-	2

The ionised impurity scattering dominates below 310 °K for all crystals except sample C. Figure 6.8 contradicts this effect, proposing instead, an increase with temperature according to:

$$\mu_H = AT^{(0.7 \text{ to } 1.46)} \quad (6.27)$$

At higher temperatures, a  $T^{-3/2}$  law is followed as acoustic mode scattering becomes dominant, particularly in sample A, while less effect was observed in sample B. The room temperature carrier mobility for all compositions investigated in this work is listed in Table 6.6. It can be seen that the room temperature mobility for these alloys is composition dependent. However, it decreases with increasing  $\text{Cu}_2\text{GeS}_3$  percentage in the crystal. All alloys investigated in this work appear to be  $p$ -type materials, while  $\text{Cu}_2\text{GeS}_3$  is reported to be low mobility  $n$ -type [129].

Table 6.5

Characterisation of the scattering process of the system  
 $\text{CuGe}_2\text{P}_3\text{-Cu}_2\text{GeS}_3$

Symbols	Materials	$\mu = AI^x$	$\mu = BT^{-x}$
		$x$	$x$
A	90% $\text{CuGe}_2\text{P}_3$ - 10% $\text{Cu}_2\text{GeS}_3$	0.7	$\sim 1.6$
B	80% $\text{CuGe}_2\text{P}_3$ - 20% $\text{Cu}_2\text{GeS}_3$	0.85	-
C	70% $\text{CuGe}_2\text{P}_3$ - 30% $\text{Cu}_2\text{GeS}_3$	$\sim 1.46$	-
D	60% $\text{CuGe}_2\text{P}_3$ - 40% $\text{Cu}_2\text{GeS}_3$	0.81	-

Table 6.6

Some room temperature electrical data for the system  $\text{CuGe}_2\text{P}_3 - \text{Cu}_2\text{GeS}_3$

Symbols	Materials	$\sigma$ ( $\Omega^{-1} \text{ cm}^{-1}$ )	$R_H$ ( $\text{cm}^3 \text{ c}^{-1}$ )	$\mu_p$ ( $\text{cm}^2 \text{ v}^{-1} \text{ s}^{-1}$ )	Carriers	
					$\text{cm}^{-3}$	type
A	90% $\text{CuGe}_2\text{P}_3$ - 10% $\text{Cu}_2\text{GeS}_3$	30.0	$2.8 \times 10^{-2}$	0.84	$2.2 \times 10^{20}$	p
B	80% $\text{CuGe}_2\text{P}_3$ - 20% $\text{Cu}_2\text{GeS}_3$	22.14	$3.2 \times 10^{-2}$	0.718	$1.9 \times 10^{20}$	p
C	70% $\text{CuGe}_2\text{P}_3$ - 30% $\text{Cu}_2\text{GeS}_3$	2.54	$1.7 \times 10^{-2}$	0.434	$3.6 \times 10^{19}$	p
D	60% $\text{CuGe}_2\text{P}_3$ - 40% $\text{Cu}_2\text{GeS}_3$	9.03	$4.7 \times 10^{-2}$	0.430	$1.3 \times 10^{20}$	p
E	50% $\text{CuGe}_2\text{P}_3$ - 50% $\text{Cu}_2\text{GeS}_3$	4.4	$7.7 \times 10^{-2}$	0.343	$8.03 \times 10^{19}$	p
F	40% $\text{CuGe}_2\text{P}_3$ - 60% $\text{Cu}_2\text{GeS}_3$	1.17	$23.3 \times 10^{-2}$	0.274	$2.65 \times 10^{19}$	p
G	30% $\text{CuGe}_2\text{P}_3$ - 70% $\text{Cu}_2\text{GeS}_3$	1.98	$15.7 \times 10^{-2}$	0.313	$3.05 \times 10^{19}$	p
	$\text{Cu}_2\text{GeS}_3$ [129]	$3.12 \times 10^{-3}$	$1.1 \times 10^3$	3.0	$8.0 \times 10^{17}$	n

## 6.6 The Hall Effect and Conductivity Measurements for the $\text{CuSi}_2\text{P}_3\text{-Si}$ System

The electrical conductivity and Hall constant were measured for undoped crystals ranged from  $\text{CuSi}_2\text{P}_3$  to  $\text{CuSi}_4\text{P}_3$  over a temperature ranging from liquid nitrogen to 450 °K. All crystals were found to be low resistivity and *p*-type materials (see Table 6.7).

The slope of the curve  $\ln \sigma T^{-3/2}$  versus  $1/T$  shows that the impurity activation energy for  $\text{CuSi}_2\text{P}_3$  is 0.0015 eV. This indicates that the energy level is very close to the top of the valence band for this material, while the impurity level appears very close to, or under, the top of the valence band for samples containing excess Si.

High carrier concentration was found for these crystals, which increases with excess Si. However, this was not the case for the system  $\text{CuGe}_2\text{P}_3\text{-Ge}$ . The author suggests that high carrier concentration is independent of group IV material in  $\text{CuSi}_2\text{P}_3$ . Such a characteristic could be due to the high melting point, since it is expected that the latter increases with excess Si in the crystal. However,  $\text{CuSi}_8\text{P}_3$  was not melted completely by a temperature as high as 1300 °C.

The mobilities of the  $\text{CuSi}_2\text{P}_3\text{-Si}$  system was measured for three crystals of different compositions, as listed in Table 6.7. A single crystal of  $\text{CuSi}_2\text{P}_3$  was grown by tin solution and polished to a rectangular shape with dimensions 4.69 x 2.15 x 0.248 mm. The mobility was found to be as low as that found for  $\text{CuGe}_2\text{P}_3$ . This could be due to the existing Cu material in those compounds. However, a low mobility is always reported for Cu compounds such as the ternary group Cu-III-VI<sub>2</sub> [ 37 ].

From the mobility curve (Figure 6.10), the ionised impurity scattering dominates at temperatures below 280 °K. The mobility was changing as slowly as  $T^{0.631}$ . The lowest mobility of  $0.346 \text{ (cm}^2 \text{ v}^{-1} \text{ sec}^{-1}\text{)}$  was registered at 87 °K. For higher temperatures, it began decreasing with temperature. This indicates the dominance of some kind of lattice scattering.

The measurement on  $\text{CuSi}_3\text{P}_3$  crystals shows higher mobility than crystals of  $\text{CuSi}_2\text{P}_3$ , where the highest was recorded to be  $5.45 \text{ (cm}^2 \text{ v}^{-1} \text{ s}^{-1}\text{)}$  at 275 °K. Below this temperature, the mobility slowly decreased with temperature as  $T^{0.244}$ . The latter figure indicates dominant ionised impurity scattering. However, screening by free carrier concentration could cause slow temperature dependence or complete disappearance of ionised impurity scattering. For temperatures higher than 275 °K, the mobility was changing as  $T^{-0.39}$ . This kind of temperature dependence is derived from a lattice scattering mechanism.

The highest mobility in this work was  $11.04 \text{ (cm}^2 \text{ v}^{-1} \text{ s}^{-1}\text{)}$ , which was recorded for a crystal of  $\text{CuSi}_4\text{P}_3$  for temperatures up to 301 °K, as  $T^{-0.431}$ . A disappearing ionised impurity scattering at low temperature for these crystals could be due to the same causes as mentioned above.

Table 6.7

Some room temperature electrical data for the system  $\text{CuSi}_2\text{P}_3\text{-Si}$

Materials	$\mu \text{ (cm}^2 \text{ v}^{-1} \text{ s}^{-1}\text{)}$	$p \text{ (cm}^{-3}\text{)}$	$\sigma \text{ (}\Omega^{-1} \text{ cm}^{-1}\text{)}$	$R_H \text{ (cm}^3 \text{ c}^{-1}\text{)}$
$\text{CuSi}_2\text{P}_3$	2.295	$1.1 \times 10^{19}$	4.2	0.55
$\text{CuSi}_3\text{P}_3$	5.357	$4.40 \times 10^{19}$	38.6	0.139
$\text{CuSi}_4\text{P}_3$	6.23	$2.14 \times 10^{20}$	213.0	0.0292

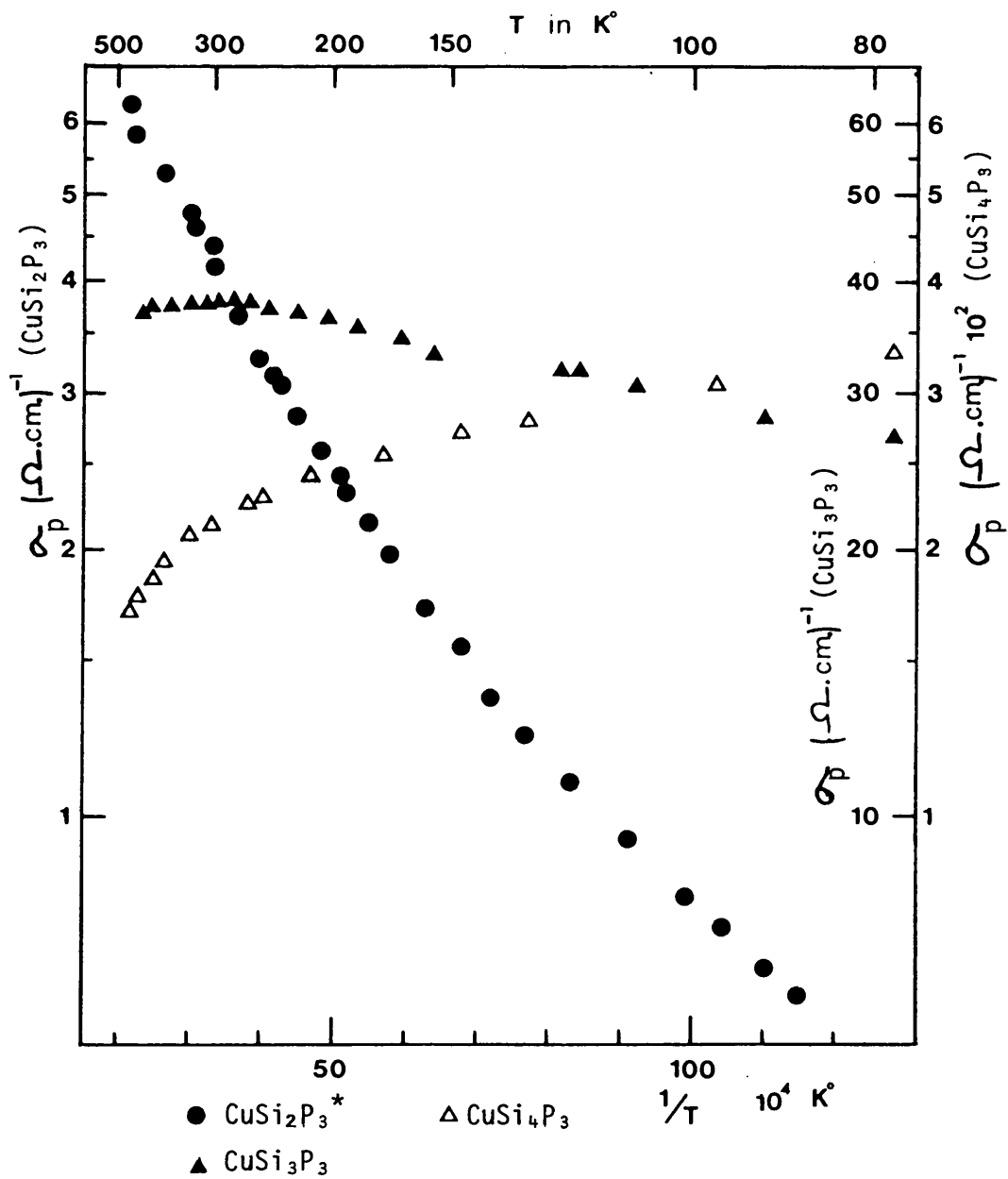


Figure 6.9 Conductivity of CuSi<sub>2</sub>P<sub>3</sub>-Si system as a function of inverse absolute temperature

\* Tin solution growth

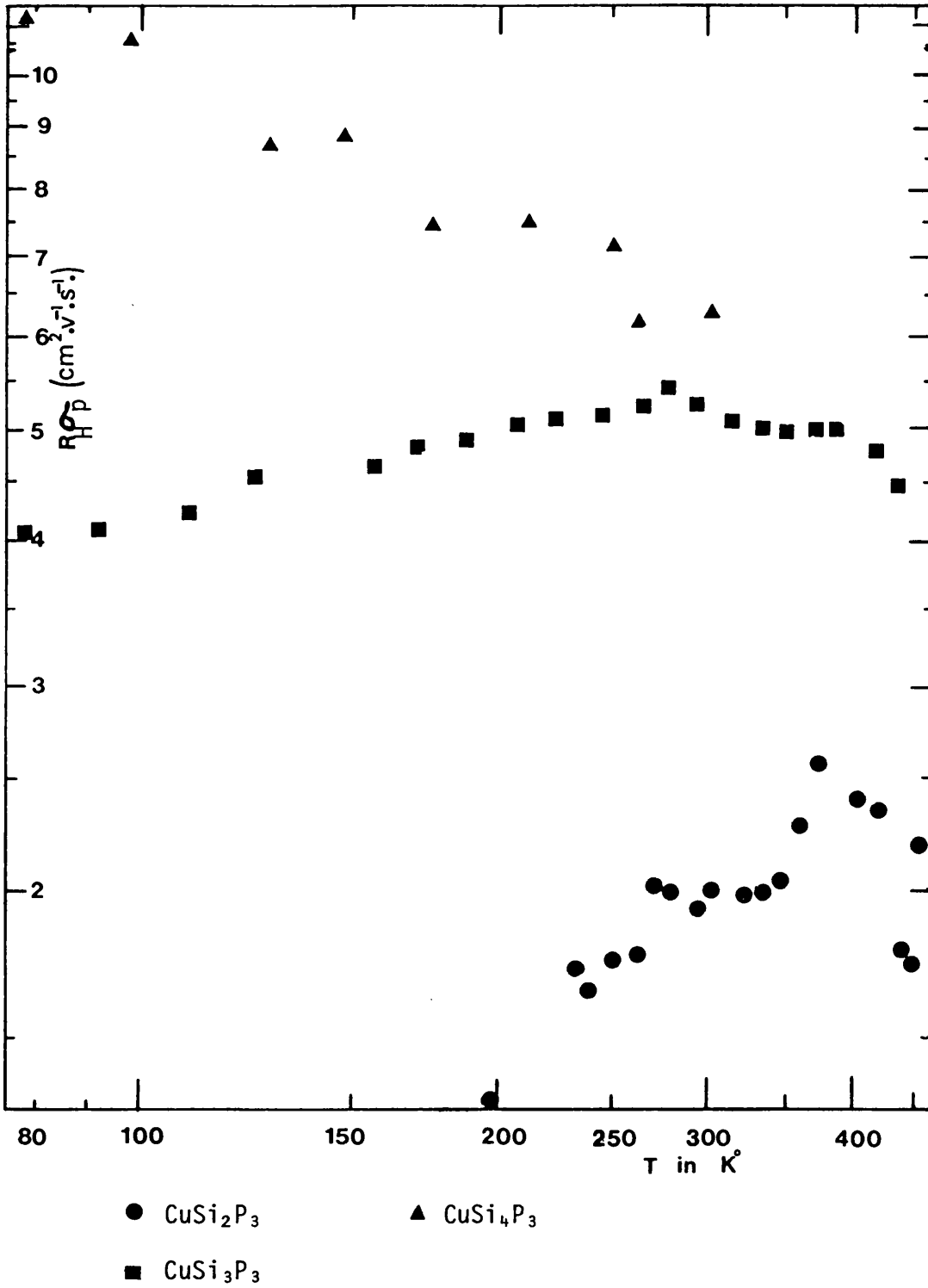


Figure 6.10 Hall mobility of CuSi<sub>2</sub>P<sub>3</sub>-Si system as a function of absolute temperature

## 6.7 Annealing and Doping Studies of $\text{CuGe}_2\text{P}_3$

The temperature dependence of conductivity and mobility of the doped crystals examined is shown in Figures 6.11 and 6.12 over a relatively high range of temperature from liquid nitrogen to above room temperature.

$\text{CuGe}_2\text{P}_3$  is a *p*-type semi-conductor in which holes are heavily produced in all circumstances, including annealing and doping with the impurities shown in Table 6.8. Attempts to compensate the *p*-type nature of the material with possible compensating donors such as Zn and the group VI elements S and Se have been inconclusive. Results are shown and given in Figures 6.11-6.14 and Tables 6.8-6.11.

Indium acts as a compensated material in Zn levels for Zn-In doping. Such a method was used to compensate Zn levels in Ge by using sufficient Sb [157].

The possible *p*-type nature of the material  $\text{CuGe}_2\text{P}_3$  might be due to a P deficiency. This idea gains credence by the appearance of a second phase,  $\text{CuP}_2$  (see Chapter 5).

The annealing in Cu-P was carried out to remove the second phase of  $\text{CuP}_2$  in the compound, but failed. The  $\text{CuGe}_2\text{P}_3$  was annealed at 700 °C with powdered Cu-P, for 7 days, then quenched in ice water. The treatment increases the hole density to about  $7.8 \times 10^{20} \text{ cm}^{-3}$ . However, higher density of holes was also the result of annealing in  $\text{CuGe}_2\text{P}_3$  powder under the same circumstances, for a period of 8 days.

It is clear from the conductivity curve (Figure 6.11), that all doped and undoped samples of  $\text{CuGe}_2\text{P}_3$  were independent of temperature, particularly for  $T < 200$  °C. This indicates a complete overlap of the acceptor impurity band with the valence band.



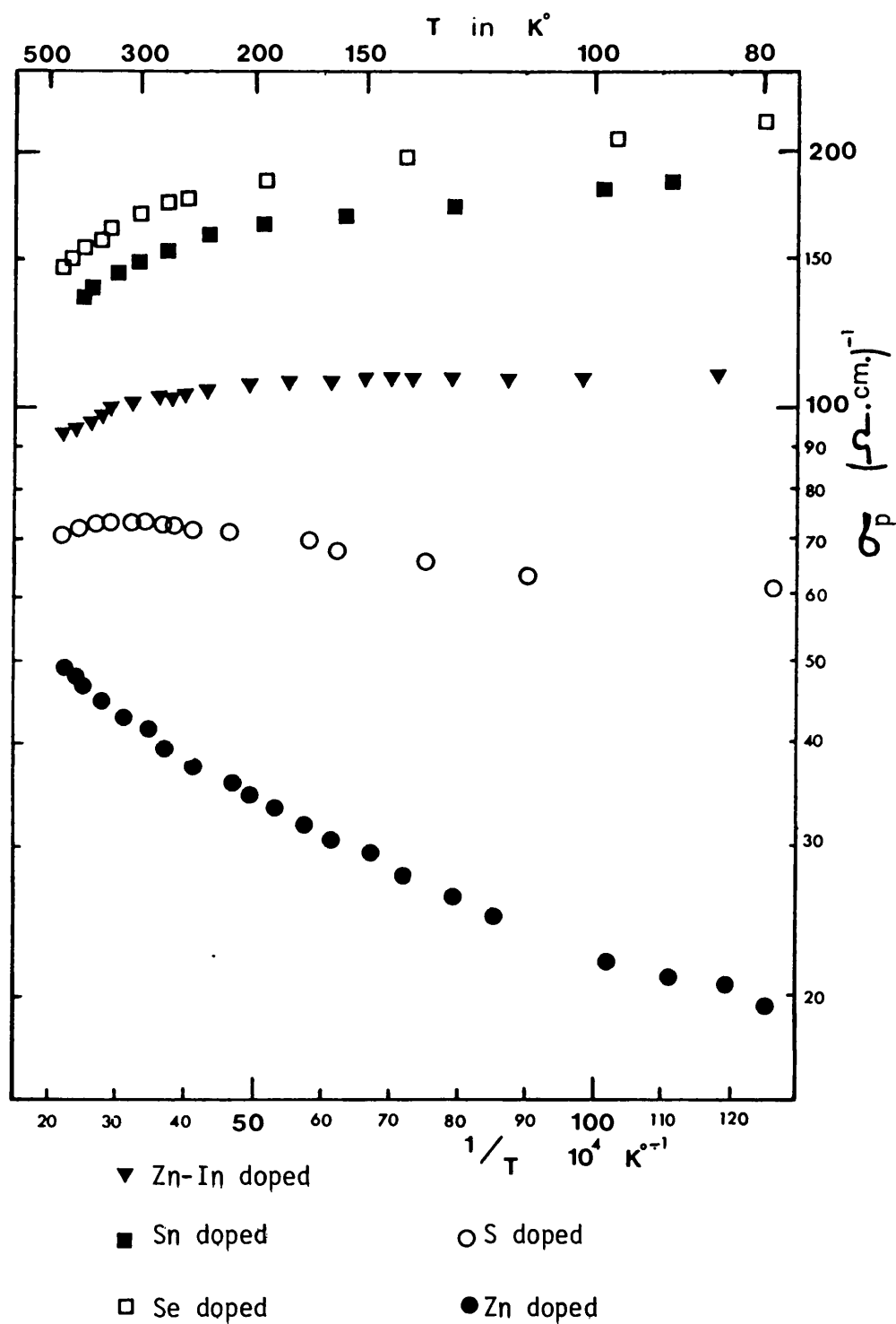


Figure 6.11 Conductivity of the compound  $\text{CuGe}_2\text{P}_3$  (doped single crystals) as a function of inverse absolute temperature

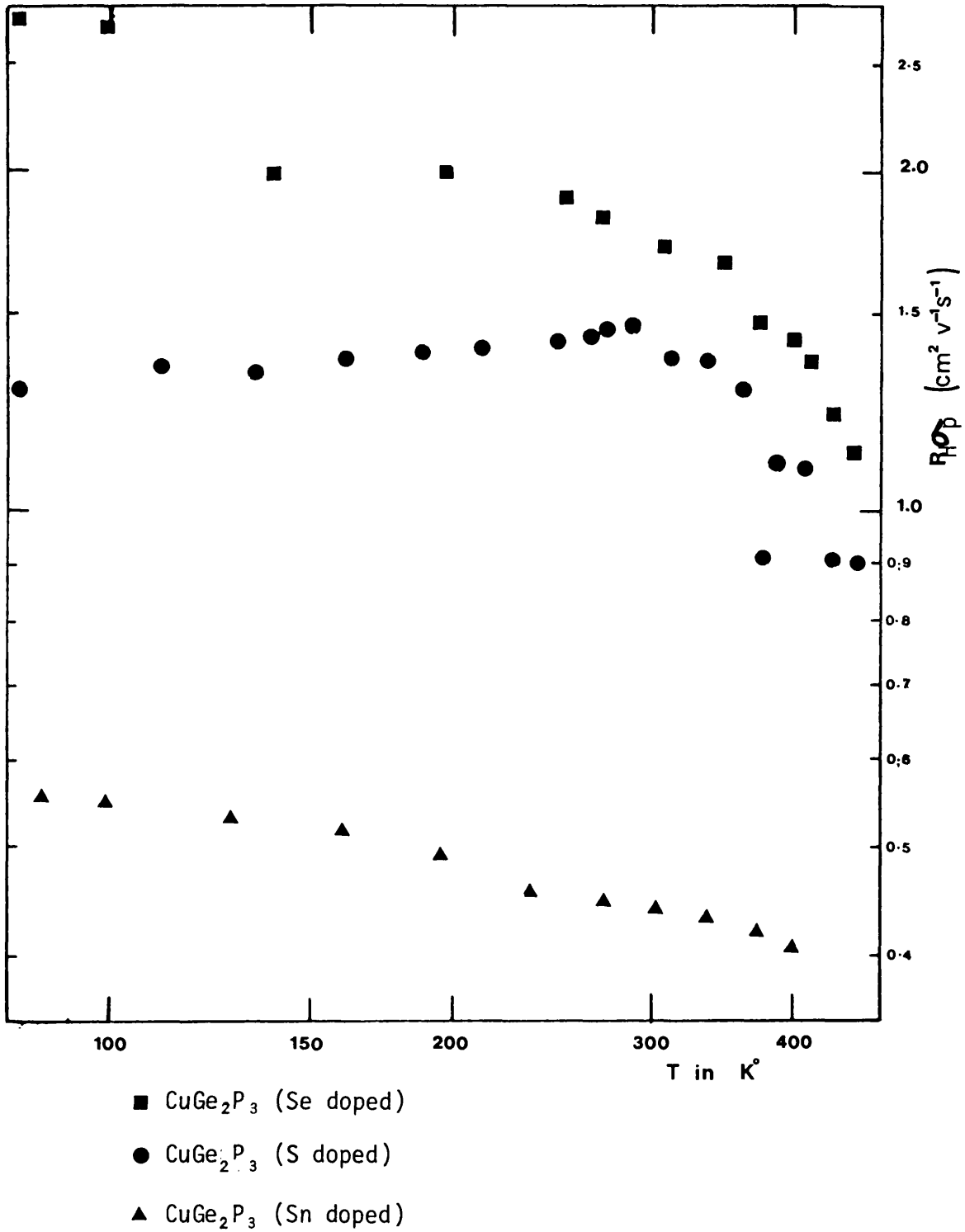


Figure 6.12(a) Hall mobility of  $\text{CuGe}_2\text{P}_3$  (doped) samples as a function of absolute temperature

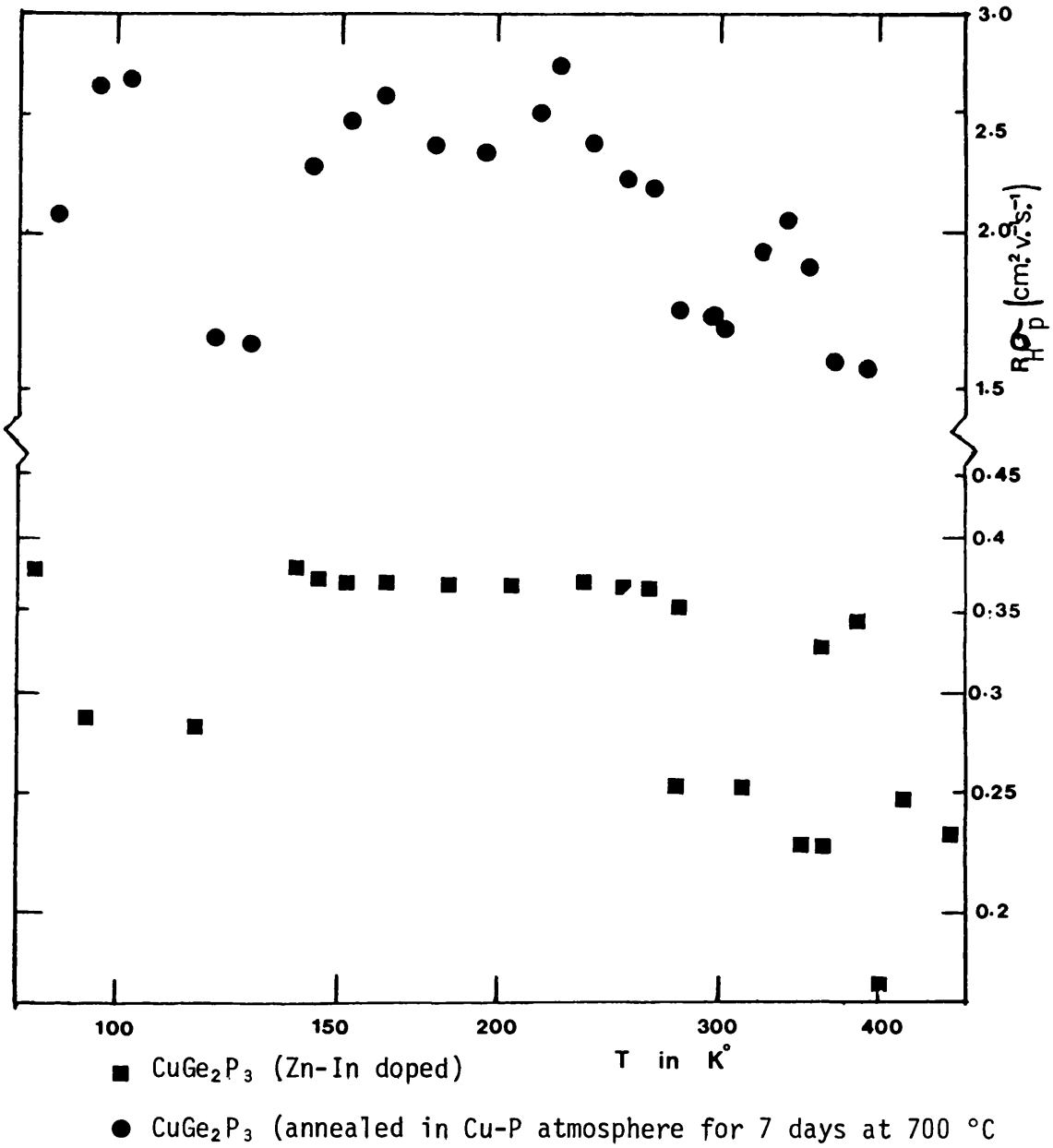


Figure 6.12(b) Hall mobility of  $\text{CuGe}_2\text{P}_3$  samples as a function of absolute temperature

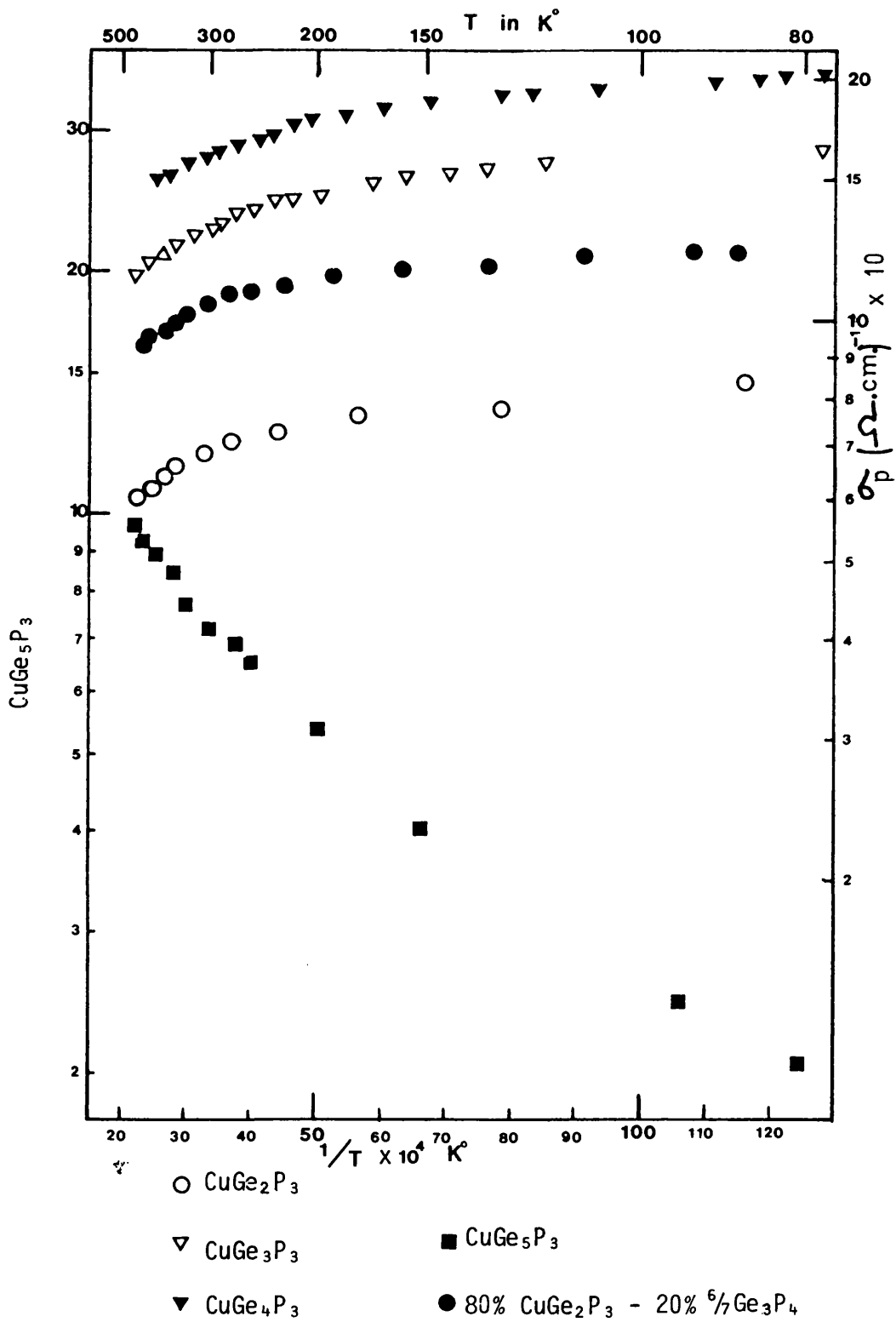


Figure 6.13 Conductivity of  $\text{CuGe}_2\text{P}_3$ -Ge system and 80%  $\text{CuGe}_2\text{P}_3$  - 20%  $\frac{6}{7}\text{Ge}_3\text{P}_4$ , as a function of inverse absolute temperature

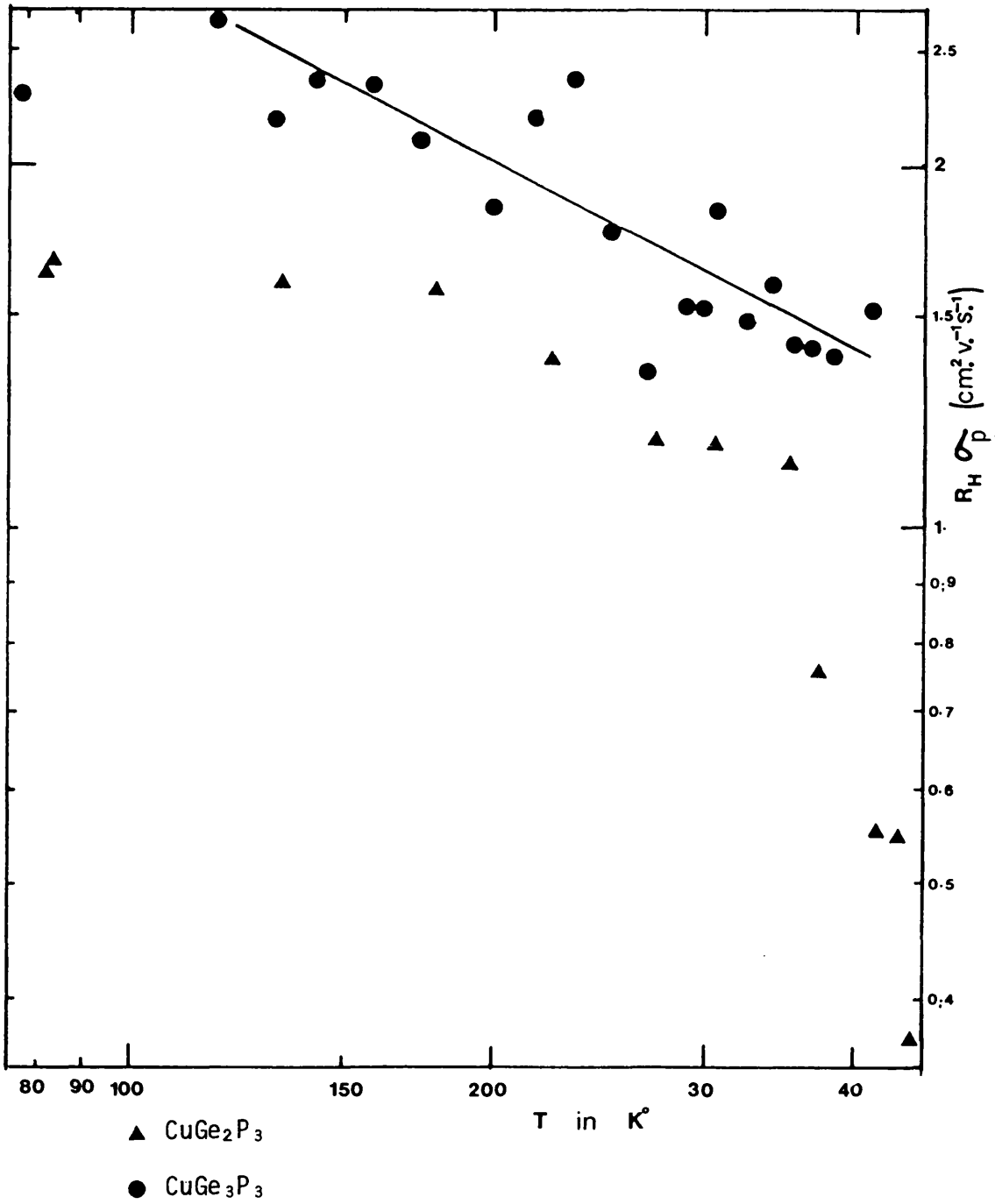


Figure 6.14(a) Hall mobility of CuGe<sub>2</sub>P<sub>3</sub>-Ge system as a function of absolute temperature

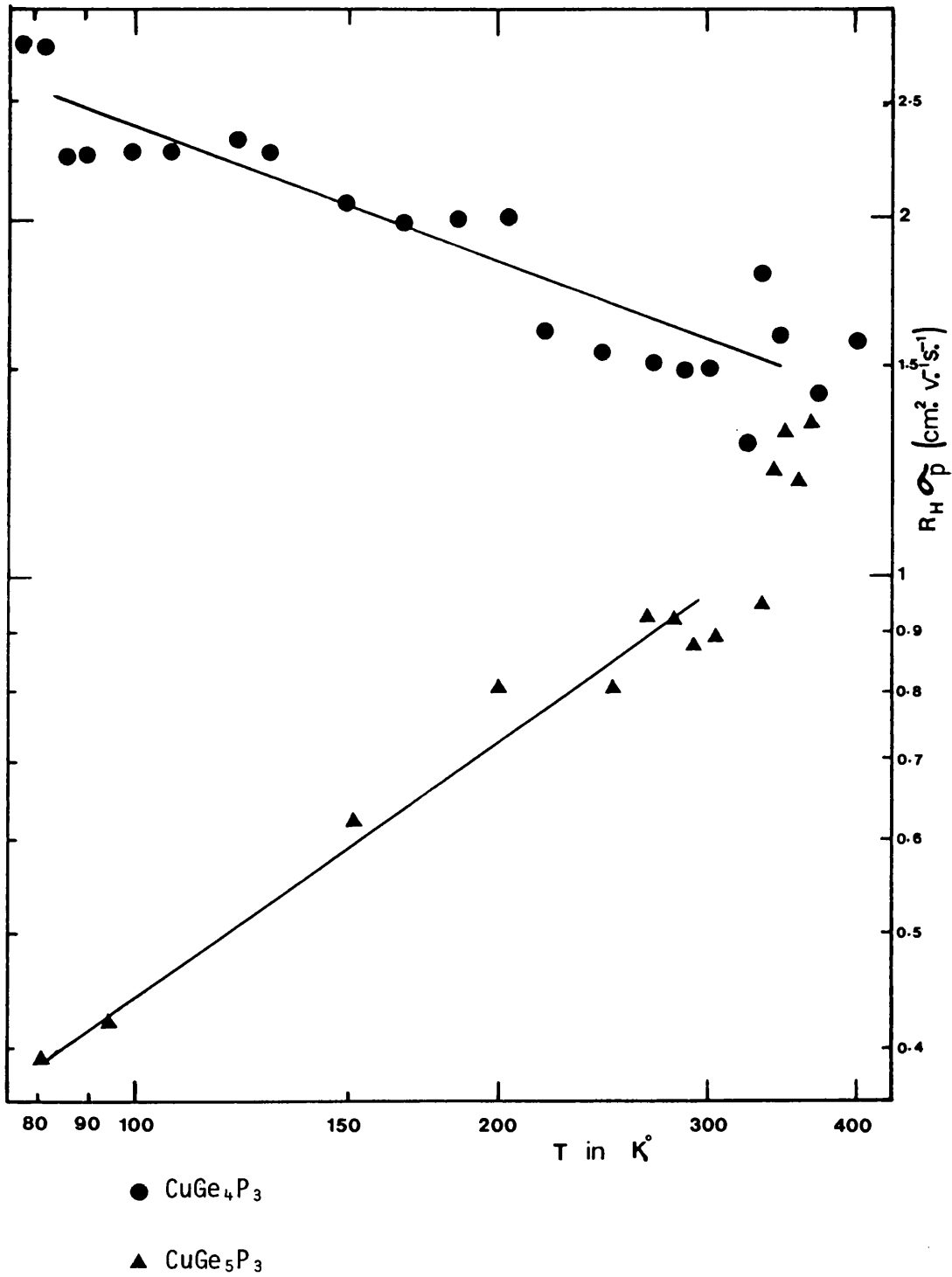


Figure 6.14(b) Hall mobility of CuGe<sub>2</sub>P<sub>3</sub>+Ge system as a function of absolute temperature

Table 6.8

Electrical data at room temperature for the doped compound  $\text{CuGe}_2\text{P}_3$

Doped elements	$R_H$ ( $\text{cm}^3 \text{c}^{-1}$ )	$\sigma_p$ ( $\Omega^{-1} \text{cm}^{-1}$ )	p-type ( $\text{cm}^{-3}$ )	$\mu_p$ ( $\text{cm}^2 \text{v}^{-1} \text{s}^{-1}$ )
Zn	0.042	41.2	$1.5 \times 10^{20}$	1.72
S	0.02	72.95	$3.14 \times 10^{20}$	1.45
Se	0.0103	174.8	$6.06 \times 10^{20}$	1.797
Sn	0.0023	147.0	$2.7 \times 10^{21}$	0.334
Zn-In	0.0032	102.0	$1.96 \times 10^{21}$	0.325
*	0.0079	216.4	$7.8 \times 10^{20}$	1.71
+	0.00594	194.2	$1.05 \times 10^{21}$	1.152

\* Sample annealed in a Cu-P atmosphere at a temperature of 700 °C for 7 days.

+ Sample annealed in  $\text{CuGe}_2\text{P}_3$  powder at a temperature of 700 °C for 8 days.

Table 6.9

Characteristics of scattering process for the doped compound  $\text{CuFe}_2\text{P}_3$

Doped elements	Ionised impurity scattering ( $\mu = AT^{-3/2}$ )	Acoustic mode scattering ( $\mu = AT^{-3/2}$ )
	$\times 10^3$	$\times 10^3$
S	0.14	1.38
Se	-	1.27
Sn	-	0.23
Zn-In	-	0.72
*	0.28	0.66

\* Sample annealed in a Cu-P atmosphere at a temperature of 700 °C for 7 days.



Table 6.10

Some electrical properties of the CuGe<sub>2</sub>P<sub>3</sub>-Ge system and 80% CuGe<sub>2</sub>P<sub>3</sub> - 20% <sup>6</sup>/<sub>7</sub> Ge<sub>3</sub>P<sub>4</sub> alloy at

Samples	room temperature				
	$R_H$ (cm <sup>3</sup> c <sup>-1</sup> )	$p$ (cm <sup>-3</sup> )	$\sigma_p$ ( $\Omega^{-1}$ cm <sup>-1</sup> )	$\mu_p$ (cm <sup>2</sup> v <sup>-1</sup> s <sup>-1</sup> )	
CuGe <sub>2</sub> P <sub>3</sub> (1)	0.0129	$4.84 \times 10^{20}$	169.2	2.181	
CuGe <sub>2</sub> P <sub>3</sub> (2)	0.0167	$3.7 \times 10^{20}$	69.44	1.159	
CuGe <sub>3</sub> P <sub>3</sub>	0.0142	$4.38 \times 10^{20}$	130.5	1.9	
CuGe <sub>4</sub> P <sub>3</sub>	0.0093	$6.7 \times 10^{20}$	160.0	1.49	
CuGe <sub>4.5</sub> P <sub>3</sub>	0.071	$8.81 \times 10^{19}$	26.6	1.9	
CuGe <sub>5</sub> P <sub>3</sub>	0.125	$4.9 \times 10^{19}$	9.0	1.13	
80% CuGe <sub>2</sub> P <sub>3</sub> - 20% <sup>6</sup> / <sub>7</sub> Ge <sub>3</sub> P <sub>4</sub>	0.016	$3.8 \times 10^{20}$	105.3	1.73	

Table 6.11

Characteristics of scattering process for the  $\text{CuGe}_2\text{P}_3$ -Ge system and  
80%  $\text{CuGe}_2\text{P}_3$  - 20%  $^{67}\text{Ge}_3\text{P}_4$  alloy at room temperature

Samples	Ionised impurity scattering	Acoustic mode scattering
	$(\mu = AT^x)$ $x$	$(\mu = AT^{-x})$ $x$
$\text{CuGe}_2\text{P}_3$ (2)	-	1.3
$\text{CuGe}_3\text{P}_3$	-	0.522
$\text{CuGe}_4\text{P}_3$	-	0.363
$\text{CuGe}_{4.5}\text{P}_3$	-	-
$\text{CuGe}_5\text{P}_3$	0.715	-
80% $\text{CuGe}_2\text{P}_3$ - 20% $^{67}\text{Ge}_3\text{P}_4$	-	0.19

The temperature dependence of the Hall mobility ( $R_H \sigma_p$  at 13.2 k gauss) for a series of doped samples was carried out, ranging from liquid nitrogen to 450 °K. All samples were shown to be heavily compensated. However, the lattice and ionised scattering were not dominating strongly.

The temperature dependence for S topped crystals shows ionised impurity scattering dominating at temperatures below 300 °K as  $T^{+0.14}$ ; for temperatures higher than those mentioned above, lattice scattering is dominated strongly as  $T^{-1.38}$ . High carrier concentration could be a reason for such low ionised scattering. However, this should also decrease lattice scattering.

Figure 6.12(b) shows the temperature dependence of mobility for a sample of Zn-In doped crystals. The mobility changed to lower than the original crystal. Such a result could be explained by the heavy compensation which comes from In atoms. Lattice scattering dominated for temperatures higher than 280 °K, while it was temperature dependent below this.

For Sn doped samples, lattice scattering was less dominant, while there was no sign of ionised impurity scattering (see Table 6.9).

Besides doping during the growth process, annealing was carried out on  $\text{CuGe}_2\text{P}_3$  crystals as well. The most interesting results were annealing in a Cu-P atmosphere. The idea was to decrease the second phase of  $\text{CuP}_2$  in the compound. The Hall mobility was temperature dependent along the temperature range from liquid nitrogen to 400 °K. Ionised impurity scattering dominated weakly at temperatures below 200 °K, while lattice scattering was dominant at higher temperatures. However, the annealing processes could be the cause of the appearance of the scattering mechanism mentioned earlier.

The mobility of a single crystal of  $\text{CuGe}_2\text{P}_3$  after annealing in its own powder was decreased. Such a process of annealing increased the mobility of some ternary ordered structure compounds, such as  $\text{CuInS}_2$  [158]. Therefore the author suggests that the mobility in this case may be dominated by atomic arrangement in the compound.

### 6.8 Electrical Properties of the $\text{CuGe}_2\text{P}_3$ -Ge system

The electrical conductivity  $\sigma_p$ , and the Hall coefficient  $R_H$ , were determined for samples of the system  $\text{CuGe}_2\text{P}_3$ -Ge, in the temperature range 80-450 °K. Values of  $R_H$  and  $\sigma_p$  were derived using the method described earlier in this chapter. However, work on thermal conductivity carried out earlier by Belger and co-workers shows it to be composition dependent [157].

Figure 6.13 shows that the conductivity for all samples up to  $\text{CuGe}_4\text{P}_3$  decreases very slowly with temperature. The explanation for this is that the acceptor levels are well below the valence band in this materials, while Figure 6.13 illustrates that for  $\text{CuGe}_5\text{P}_3$ , the acceptor level must be higher than the valence band. However the  $\ln \sigma T^{-3/2}$  versus  $1/T$  diagram shows the latter below the valence band as well.

The temperature dependence of mobility can be represented by the relation  $\mu = T^x$  where  $x$  is a scattering factor. Then in the case of  $\ln(R_H \sigma_p)$  versus  $T$ , one can obtain the value of  $x$  for all the materials. Such a diagram gives  $x$  varying from -1.3 to 0.715 (Table 6.11), for samples ranging from  $\text{CuGe}_2\text{P}_3$  to  $\text{CuGe}_5\text{P}_3$ . However, such a result could mean changing of the scattering process from lattice to ionised impurity. This clearly shows that  $x$  is composition dependent. There are no other explanations reported for these materials so far. It is quite clear that ionised impurity scattering is dominant for  $\text{CuGe}_5\text{P}_3$ .

Carrier concentration is shown to be independent of composition. However, the latter may depend on the growth rate (foundation).

Table 6.10 shows mobilities at room temperature for these alloys (as described earlier). The mobility does not exceed  $3 \text{ cm}^2 \text{ v}^{-1} \text{ s}^{-1}$ , which agrees well with measurements made by Riede and co-workers [159].

#### 6.9 Electrical Measurement for 80% $\text{CuGe}_2\text{P}_3$ - 20% $\frac{6}{7}\text{Ge}_3\text{P}_4$

The conductivity and Hall coefficient were measured along the temperature range from 89-450 °K. The conductivity curve shows much similarity to that found for the compound  $\text{CuGe}_2\text{P}_3$ . It is clear from the latter that the acceptor levels should be much below the valence band. However, that is the case for all  $\text{CuGe}_2\text{P}_3$  crystals even after different physical processes such as annealing and doping,

Very poor temperature dependence was shown for the mobility. The highest mobility registered was  $2.2 \text{ cm}^2 \text{ v}^{-1} \text{ s}^{-1}$  at 120 °K. The room temperature data are shown in Table 6.10. Figure 6.15 shows the Hall mobility as a function of absolute temperature.

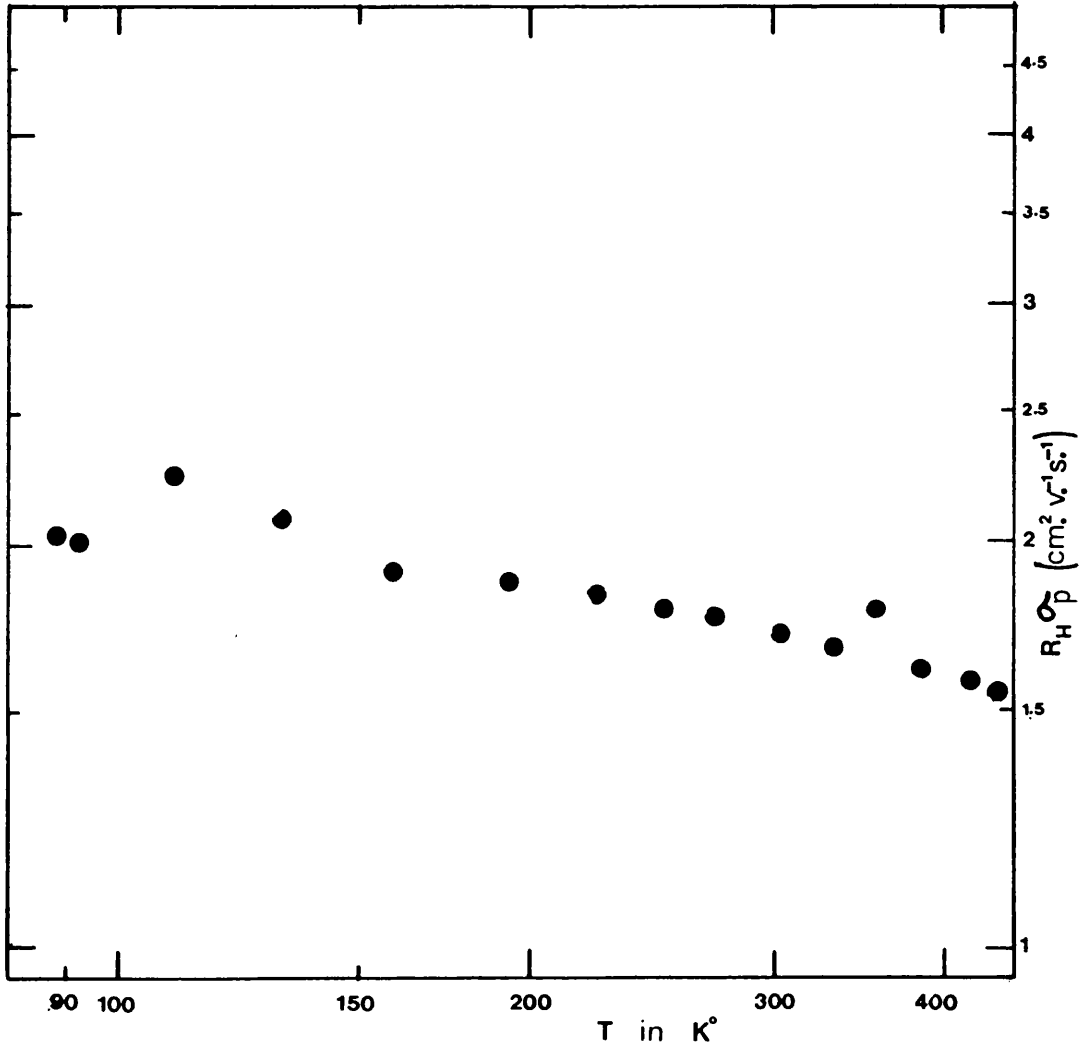


Figure 6.15 Hall mobility of 80% CuGe<sub>2</sub>P<sub>3</sub> - 20% <sup>6</sup>/<sub>7</sub>Ge<sub>3</sub>P<sub>4</sub> system as a function of absolute temperature

## CHAPTER 7

### Thin Film Preparation of $\text{CuGe}_2\text{P}_3$ and $\text{Ag}_6\text{Ge}_{10}\text{P}_{12}$

#### 7.1 Operation

The complete evaporation system is shown in schematic form in Figure 7.1, which is a type 12HG/1/103, manufactured by NGN LTA. The pumping system consisted of a high speed rotary pump, backing a 4" oil diffusion pump. Above the baffle valve was a liquid nitrogen cold trap.

The trap was for the major vapour desorbed by the chamber, namely water vapour which at the trap temperature has negligible vapour pressure and was also used to prevent contamination from back-streaming of the diffusion oil.

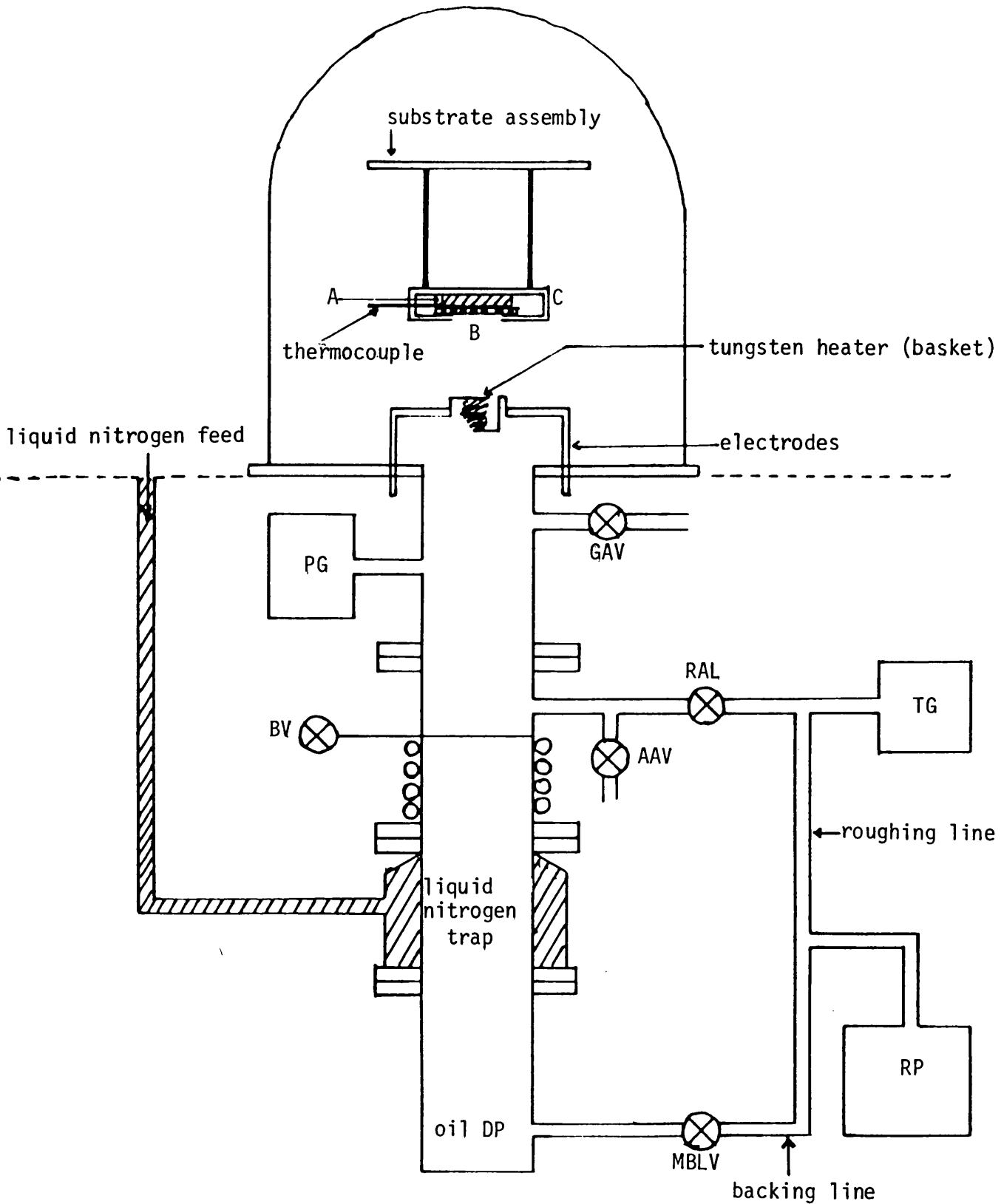
The evaporation chamber was a conventional glass dome 12" in diameter and 14.5" high, occupying a volume of approximately 22 litres.

Substrate temperature was measured using a standard chromel-alumel thermocouple, but a disappearing filament optical pyrometer was used to measure the source temperature.

The substrate was heated by a flat heater (65 watts) and was mechanically clamped to the heater, to provide good thermal contact. The source to substrate distance was 4 cm. The source heater was connected to 12 V AC through a variac, enabling the temperature to be controlled up to *ca.* 1600 °C.

#### 7.2 Film Evaporation Procedure

Films were deposited on polished quartz plates. The ingot  $\text{CuGe}_2\text{P}_3$  (single crystal) was then placed in the tungsten basket heater and the system pumped down. Usually, a minimum pressure of about  $10^{-5}$  torr only was obtained, due to the phosphorus pressure.



- |      |                             |   |                   |
|------|-----------------------------|---|-------------------|
| PG   | penning gauge               | A | resistance heater |
| TG   | thermocouple gauge          | B | silica substrate  |
| BV   | baffle valve                | C | substrate housing |
| GAV  | gas admittance valve        |   |                   |
| RLV  | roughing line valve         |   |                   |
| AAV  | air admittance valve        |   |                   |
| MBLV | magnetic backing line valve |   |                   |
| RP   | rotary pump                 |   |                   |
| DP   | diffusion pump              |   |                   |

Figure 7.1 Scheme of evaporation system



The system was flushed with argon gas to minimise oxidation problems. Liquid nitrogen was used to prevent contamination from the pump and vapour pressure. When this terminal pressure was achieved, the substrate was heated to about 220 °C, with continuous pumping down for 3-4 hours. The source material was then heated to just below the melting point, then slowly to the melting point, maintaining this temperature until all the material had melted. The temperature was then increased to about 1600 °C, when evaporation took place. During deposition, system pressure was usually between  $4-8 \times 10^{-5}$  torr, when the source material evaporated completely. The source heater was then cooled down and the substrate allowed to cool slowly in vacuum to room temperature, to prevent any pseudo-quenching effect. This is effective, especially for materials with high thermal conductivity [160]. Finally, the deposited film was removed, cut into several pieces, placed in prepared tubes for annealing and the films were then investigated with X-ray powder photography and EPMA, as well as scanning electron microscopy.

The same procedure was used for investigation of the compound  $\text{Ag}_6\text{Ge}_{10}\text{P}_{12}$ .

### 7.3 Annealing Procedure

Films were taken out from the chamber following slow cooling, cut into several pieces and put into prepared quartz ampoules for annealing. Phosphorus was added to the evacuated tubes and sealed off. The inner volume of the ampoule was made as small as possible and the ampoule was then fixed in the single zone annealing furnace. The furnace temperature was increased slowly to the annealing temperature (*ca.* 700 °C), to prevent any cracks occurring in the film. This is a reasonable temperature for carrying out this procedure. The ampoules were kept at this temperature

for different periods of time, in order to investigate annealing time dependency and second phases in the compound.

The sample slowly cooled down to room temperature and was then removed from the ampoule for testing by X-ray powder photography, Laue photographs, EPMA and scanning electron microscopy.

#### 7.4 X-Ray Powder Photography

##### 7.4.1 CuGe<sub>2</sub>P<sub>3</sub> Films

X-Ray powder photography was the best method of testing thin film preparations in this work. The powder was scratched from the silica plate and X-rayed. No crystalline material appeared for non-annealed films, except for some weak lines of Ge. The X-ray for annealed films at temperatures of about 700 °C showed crystalline material of mainly Ge, with no sign of the CuGe<sub>2</sub>P<sub>3</sub> compound.

X-Ray analysis for films annealed in an atmosphere of phosphorus showed good results. Films annealed for several minutes showed different crystalline materials, mainly consisting of Ge, CuP<sub>2</sub>, GeP<sub>3</sub> and weak lines of CuGe<sub>2</sub>P<sub>3</sub>. For annealing of 30 minutes' duration, the only second phase materials remaining were of CuP<sub>2</sub>, with lines for CuGe<sub>2</sub>P<sub>3</sub>, but these were poorly crystallised. Following longer annealing periods (ca. 2 hours), the single phase of CuGe<sub>2</sub>P<sub>3</sub> appeared as good crystalline material. The CuGe<sub>2</sub>P<sub>3</sub> lines changed, showing better crystallisation (through line intensities) after 72 hours of annealing. The films are illustrated in Figure 7.2.

The lattice parameters were calculated for several annealed films and found to be  $5.3740 \pm 0.0005 \text{ \AA}$ . This agreed with polycrystalline materials prepared by the fusion method.

The intensity of lines was measured by using a double beam recording microdensitometer. Using these results, the time dependency of the annealing procedure was calculated. The  $\langle 200 \rangle$  X-ray line intensity showed a rapid increase for the early stage of annealing, but increased slowly as the annealing time increased (see Figure 7.3).

#### 7.4.2 Ag<sub>6</sub>Ge<sub>10</sub>P<sub>12</sub> Films

The same procedure was used to evaporate this compound as was employed for CuGe<sub>2</sub>P<sub>3</sub>. The results of films before annealing were crystalline in the structure of bcc, as shown in Figure 7.4. The only second phase which appeared was GeP<sub>3</sub>, with a very low intensity and no more than three lines [110]. For films annealed in an atmosphere of phosphorus, the single phase appeared with all the X-ray lines of this compound as they appeared in single crystal material. These films are illustrated in Figure 7.4. Lattice parameters for annealed films were calculated and were found to be 10.312 Å. This agreed well with that found for single crystals grown by Bridgman's method (see Section 5.4, Chapter 5).

#### 7.5 EPMA and Scanning Electron Microscopy

These methods were used to study the surface changes and the atomic distribution of the surface of all films. Films of CuGe<sub>2</sub>P<sub>3</sub> did not show phosphorus before or after annealing in vacuum, but did reveal phosphorus after annealing in a phosphorus atmosphere, as shown in Figure 7.5. The latter result was in good agreement with X-ray powder photographs, as discussed in the previous section.

Scanning electron microscopy showed changes of the film surface as a result of increased annealing time in the phosphorus atmosphere. This improvement was also shown by the X-ray powder data.

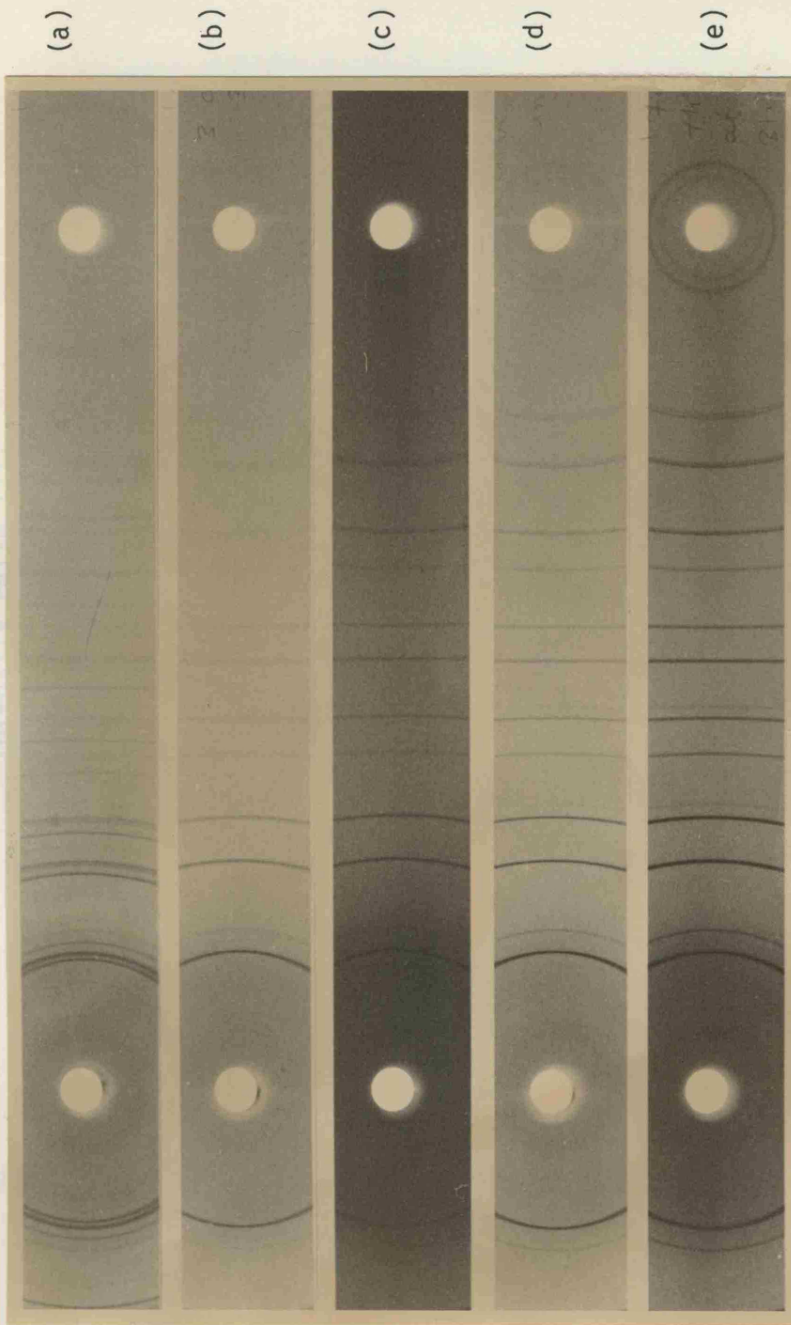


Figure 7.2 X-Ray powder photographs for annealed films in phosphorus atmosphere, showing good crystallisation for longer annealing. Annealing time: (a) 3-5 min; (b) 20 h; (c) 2 h; (d) 30 min; (e) 72 h

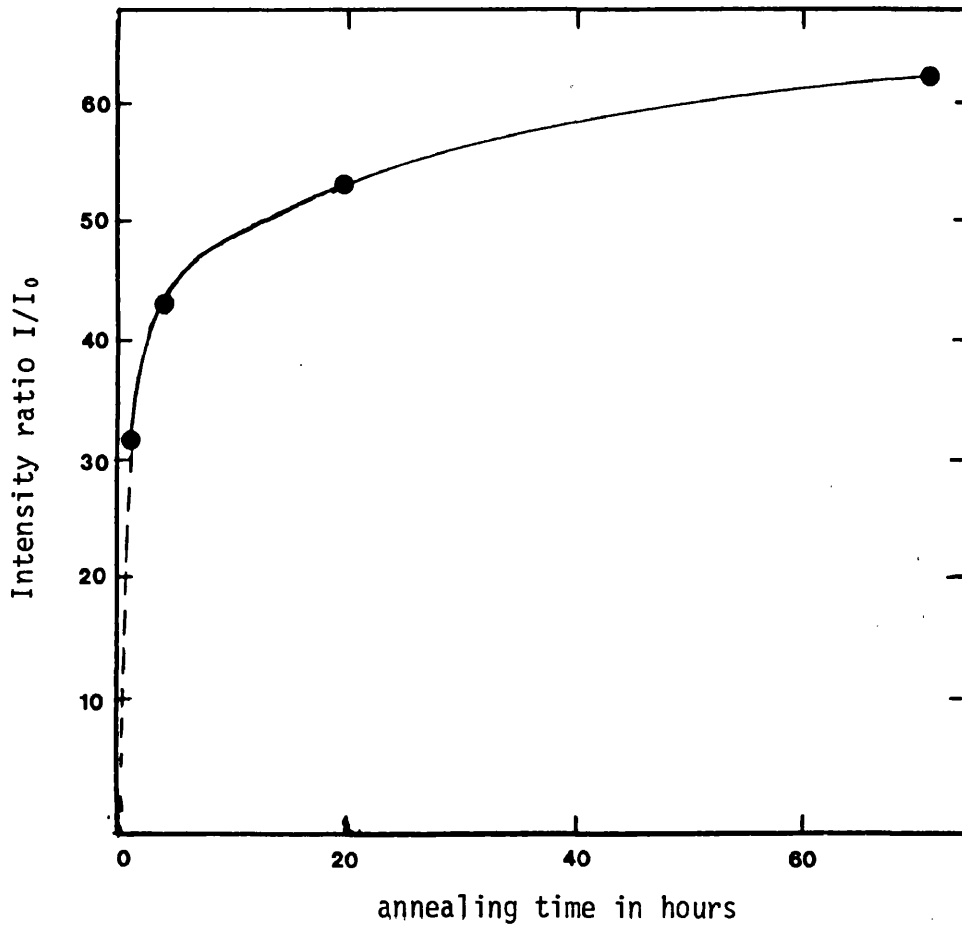


Figure 7.3 Time dependent annealing of relative intensity for a line  $\langle 220 \rangle$  of the compound  $\text{CuGe}_2\text{P}_3$  as a thin film

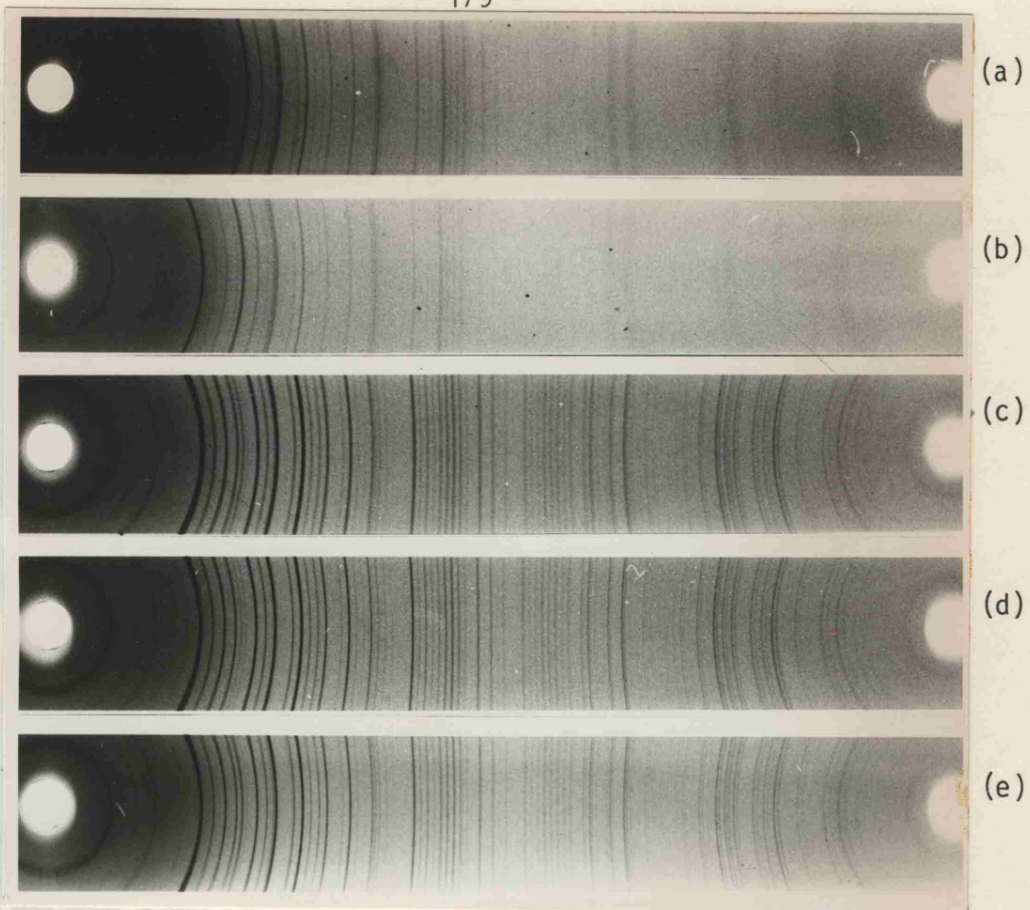


Figure 7.4 X-Ray powder photographs for annealed  $\text{Ag}_6\text{Ge}_{10}\text{P}_{12}$  thin films:

- (a) without annealing;
- (b) annealed without phosphorus atmosphere for 10 min;
- (c) annealed with phosphorus atmosphere for 10 min;
- (d) annealed with phosphorus atmosphere for 30 min;
- (e) annealed with phosphorus atmosphere for 20 h.

Figure 7.5 Scanning electron and EPMA for the surface of  $\text{CuGe}_3\text{P}_7$  films:

- (a) before annealing;
- (b) after annealing in phosphorus atmosphere (i) 30 min, (ii) 2 h, (iii) 72 h.

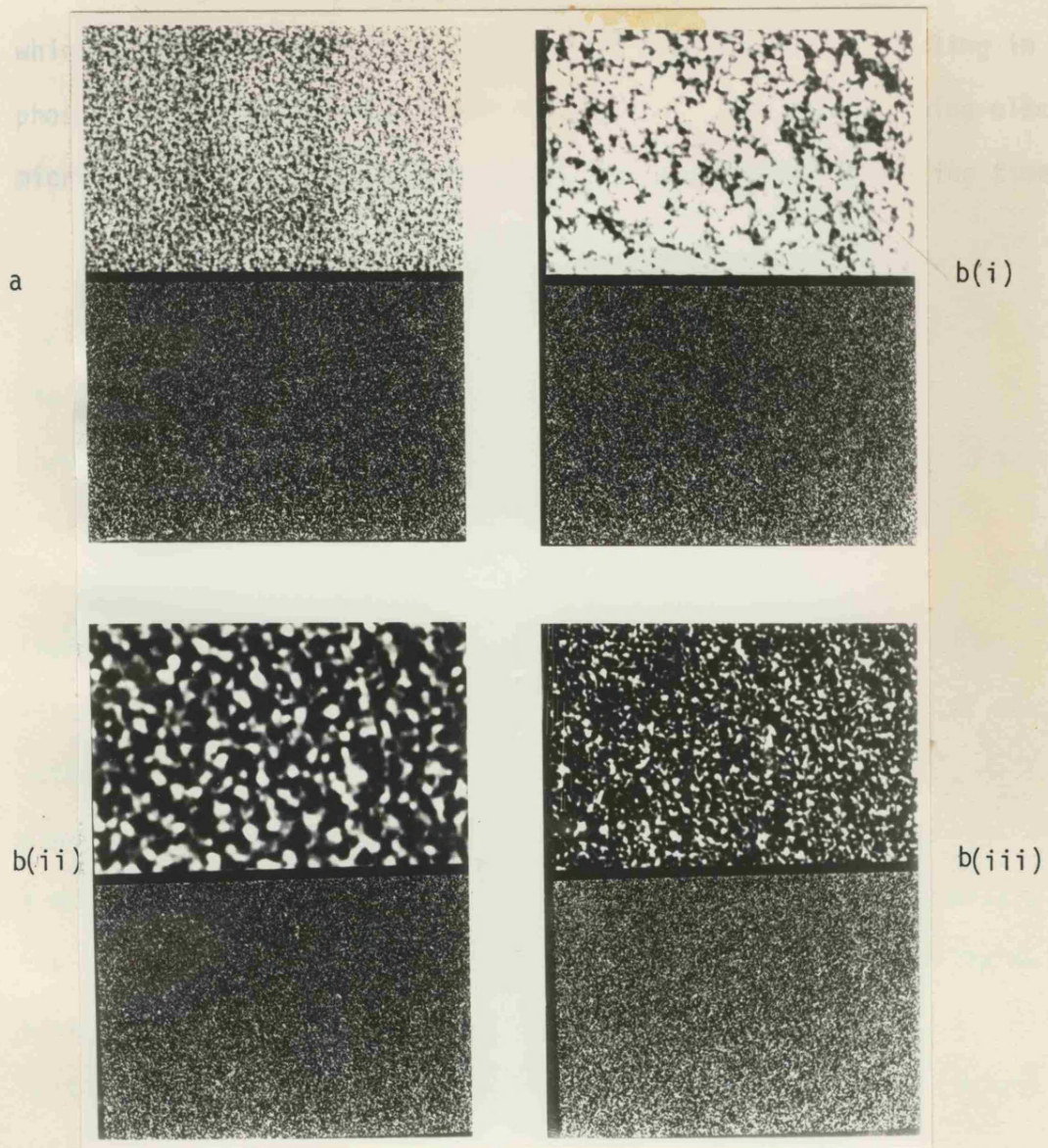


Figure 7.5 Scanning electron and EPMA for the surface of  $\text{CuGe}_2\text{P}_3$  films:  
(a) before annealing;  
(b) after annealing in phosphorus atmosphere (i) 30 min,  
(ii) 2 h, (iii) 72 h.

With regard to  $\text{Ag}_6\text{Ge}_{10}\text{P}_{12}$ , EPMA showed phosphorus before annealing, which disappeared after annealing in vacuum. However, annealing in a phosphorus atmosphere made the latter appear clearly. Scanning electron microscopy showed a uniform surface after considerable annealing time.



## CHAPTER 8

### The $p$ - $n$ Junction of $\text{CuGe}_2\text{P}_3$ -GaP

#### 8.1 Introduction

For the preparation of an epitaxial  $p$ - $n$  junction, certain similarities of physical and chemical properties between the substrate and the deposited layer need to be taken into account; such as crystal structure including lattice symmetry and spacing, thermal expansion coefficient, and the chemical interaction of the substrate with the deposited layer. The group IV semi-conductors (Si), as well as III-V (GaP) and II-VI (CdS) compounds were predicted to be good substrates for epitaxial growth of the  $\text{CuGe}_2\text{P}_3$  from the lattice symmetry and spacing point of view. For instance, in the case of GaP substrates, the lattice mismatch is 1.3% and 1.1% for Si substrates, while it is 8.0% for CdS [161]. A more critical point in achieving epitaxial growth is compatibility in the thermal expansion coefficients of the two materials. The thermal expansion coefficients of  $\text{CuGe}_2\text{P}_3$  have been measured (Chapter 3). It is quite clear that the difference in the thermal expansion coefficient is small with GaP, while it is quite large with Si and CdS [161].

Then, finally, if the two points mentioned above were satisfied, then there must be some chemical interaction between the two materials, which would increase the quality of the junction [162].

#### 8.2 Preparation of the Junction

It is well known that vapour-phase epitaxy has had a revolutionary impact on semi-conductor device technology. It is less well known that for some applications, epitaxial growth from the liquid phase can also

give excellent results. Thus liquid phase epitaxy has found important applications in the manufacture of tunnel diodes and in the fabrication of experimental GaAs laser diodes. In this work, the apparatus and processing details involved in liquid phase epitaxy are the same as those used for crystal growth and annealing processes.

The method of epitaxial growth of  $\text{CuGe}_2\text{P}_3$  on single crystals of GaP was as described below. Single crystals of GaP were polished to less than 1 micron and the single crystals were grown and polished by the Plessey Company. 1 mm thickness and area of about  $0.5 \text{ cm}^2$  was prepared, etched with dilute HF for several minutes, and washed with deionised water. This was fixed inside a prepared ampoule, then crystals of about  $1 \text{ mm}^3$  of  $\text{CuGe}_2\text{P}_3$  were arranged on the surfaces of the GaP crystal ( $\text{CuGe}_2\text{P}_3$  crystals were used immediately after cutting). Since decomposition is the main problem for both these compounds [163, 164], particularly for  $\text{CuGe}_2\text{P}_3$ , an excess of phosphorus was added to the media (see Chapter 3). The ampoule was evacuated after flushing with helium several times and was finally fixed at about  $10^{-6}$  torr. Annealing furnaces were used for heating. These furnaces could be controlled fast and accurately. To prevent phosphorus condensation on the growth material, the other side of the ampoule was cooled rapidly at between  $400\text{-}500 \text{ }^\circ\text{C}$ . These temperatures are well below the freezing point of both compounds, particularly  $\text{CuGe}_2\text{P}_3$ . After cooling to room temperature, the sample was removed from the ampoule, in order to inspect the junction area in particular. By using polishing techniques, the cross-section of the two compounds was polished up to several microns.

### 8.3 A Study of Interface Alloying

An electron probe microanalysis (EPMA) was used to determine chemical composition throughout the interface of the junction. A typical set of scans for the  $\text{CuGe}_2\text{P}_3$ -GaP couple is shown in Figure 8.2. There is no evidence of solid solubility of one phase in the other. However, attempts to form solid-solution between these two compounds failed (see Chapter 5). The results shown in Figure 8.2 can be explained by the fact that during the interface alloying a slight amount of GaP is dissolved by the compound  $\text{CuGe}_2\text{P}_3$ .

A very small diffusion (about 2 microns) is shown for Ge in GaP, but even so, the Ge can act as donor and acceptor in III-V compounds, depending on the occupying group III or V sites [111], while Ga diffused more (to about 7 microns). This could mean that the latter replaces Ge sites in  $\text{CuGe}_2\text{P}_3$ .

As Cu is the most sensitive element for *n*-type conductivity for GaP, a Cu-doped junction could be expected from the epitaxial growth junction of  $\text{CuGe}_2\text{P}_3$  on GaP crystals [165]. However, Cu was used for preparing highly sensitive GaP diodes by the diffusion method [166]. Grimmeiss [167], however, reported that diffusing Cu produced very weak *n*- and *p*-type conductivity, when he was trying to prepare high ohmic photo-conducting semi-conductor devices from GaP. In another investigation, Schulze [168], reported that only high-resistivity GaP would be produced, when Cu-doped crystals with suitable characteristics of high speed, high sensitivity photo-conductive detectors are grown from super-saturated solutions of Cu in solutions of up to 2.5 mole % and heated to 1150 °C.

In conclusion, it can be seen from the above that it is very difficult to characterise the actual *p*-type conductivity to be found in  $\text{CuGe}_2\text{P}_3$  or its Cu-doped GaP. Figure 8.3 illustrates the I-V curve for the actual junction.

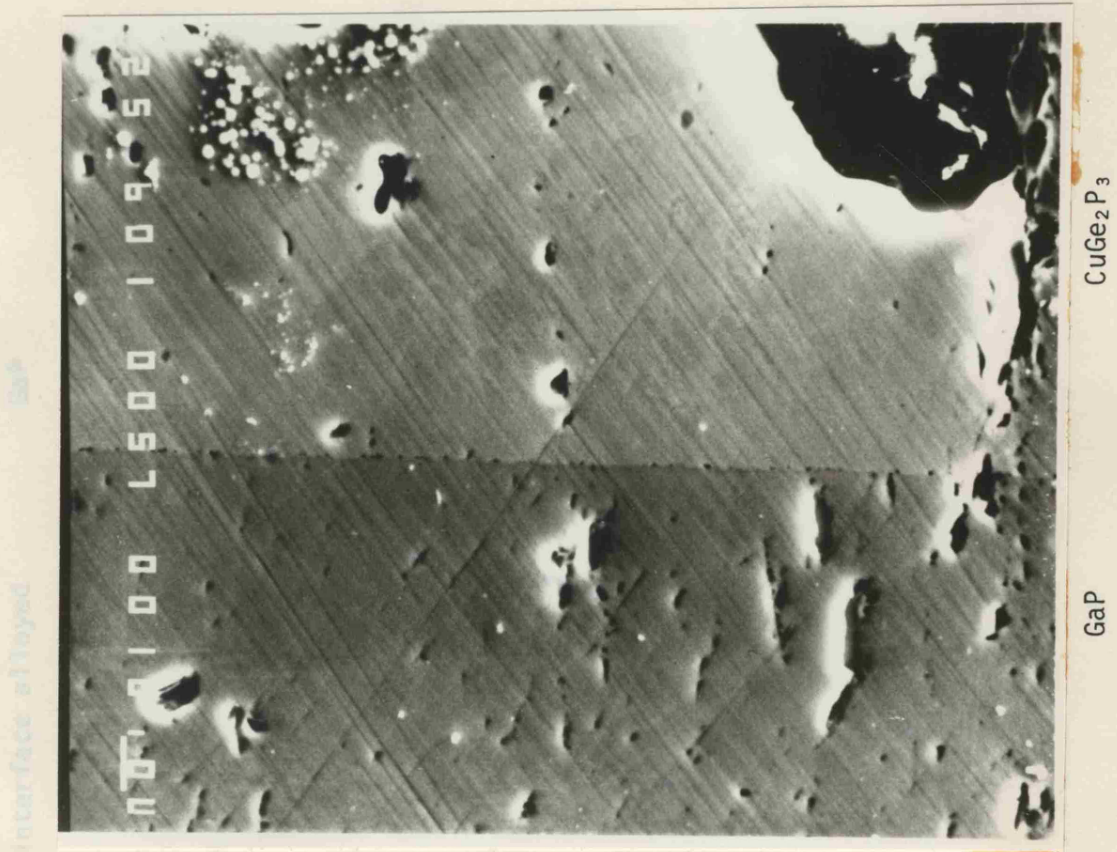


Figure 8.1 Scanning electron microscopic for the surface of a cross-section of the interface junction of  $\text{CuGe}_2\text{P}_3$ -GaP

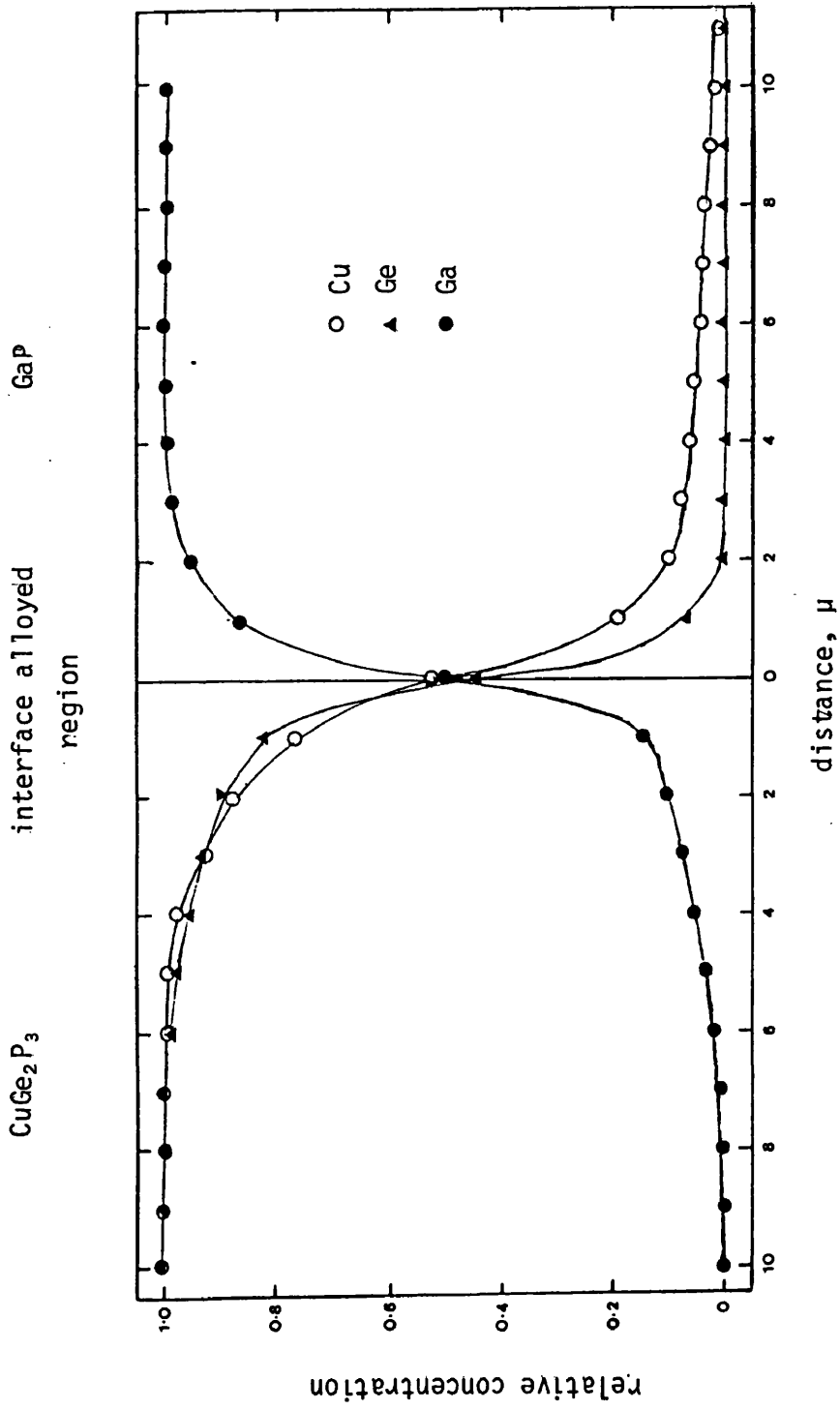


Figure 8.2 A typical electron microanalysis of CuGe<sub>2</sub>P<sub>3</sub>-GaP hetero-junction

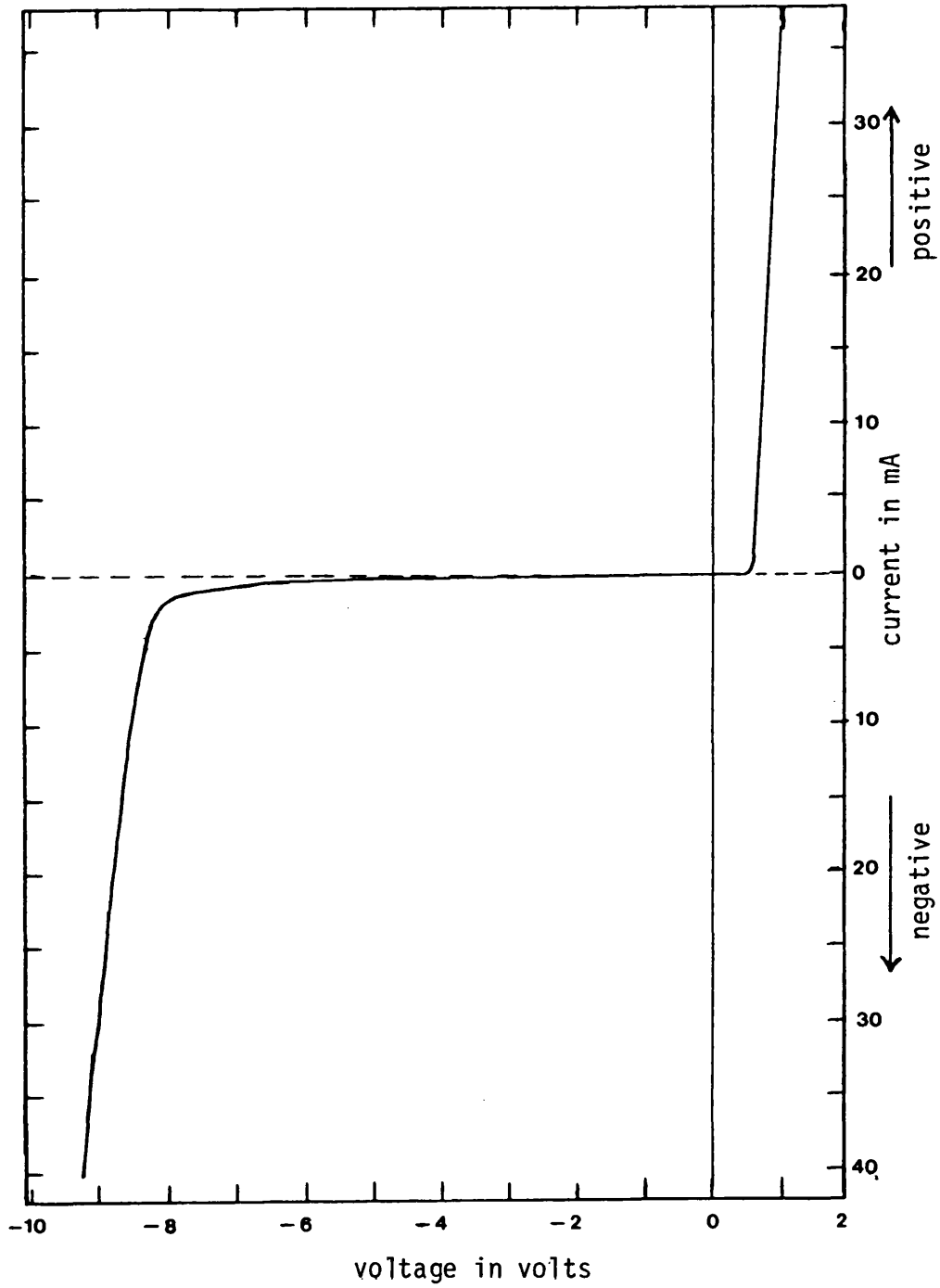


Figure 8.3 Current-voltage characteristics of typical  $\text{CuGe}_2\text{P}_3\text{-GaP}$  hetero-junction

CHAPTER 9

Conclusions and Suggestions for Further Work

9.1 Conclusions

In Chapter 2, the idea that the tetrahedral structure equation and the normal valence equation can be used to determine all possible compositions of ternary normal tetrahedral structures has been discussed. Thus the inability to prepare a ternary compound by any of the experimental methods used, does not preclude the possibility that the compound can be made. Some knowledge of the ternary phase diagrams involving the component element would, of course, be of great help in selecting the appropriate thermodynamic parameters in the preparation of these compounds.

Table 2.1 listed all the compounds of type I-IV<sub>2</sub>-V<sub>3</sub>. The compounds CuGe<sub>2</sub>As<sub>3</sub>, CuGe<sub>2</sub>P<sub>3</sub>, CuSi<sub>2</sub>P<sub>3</sub> and AgGe<sub>2</sub>P<sub>3</sub> were chosen for this investigation. Only CuGe<sub>2</sub>P<sub>3</sub> and CuSi<sub>2</sub>P<sub>3</sub> were found to be single phase, both having a zincblend structure with Cu and Ge(Si) atoms randomly arranged in Zn sites and P atoms in S sites. A third compound was found, with the composition Ag<sub>6</sub>Ge<sub>10</sub>P<sub>12</sub>, having a bcc structure with a lattice parameter of 10.312 Å.

The main emphasis was on solid solutions based on CuGe<sub>2</sub>P<sub>3</sub>. Investigations with two single component semiconductors, nine binary, ten ternary and one multi-ternary compounds were tried.

With the CuGe<sub>2</sub>P<sub>3</sub>-Ge system, it was possible to dissolve up to 33% Ge per mole, giving a zincblend structure with changing lattice parameters from 5.367 Å for CuGe<sub>2</sub>P<sub>3</sub> to 5.458 Å for CuGe<sub>5</sub>P<sub>3</sub>.



$\text{CuGe}_2\text{P}_3$  also dissolves up to 35% of  $\text{Ge}_3\text{P}_4$  per mole, maintaining the zincblend structure, with the lattice parameter increasing to  $5.4015 \text{ \AA}$  at 35%  $\text{Ge}_3\text{P}_4$  per mole.

The only ternary compound having a complete solid solution with  $\text{CuGe}_2\text{P}_3$  was  $\text{Cu}_2\text{GeS}_3$ . All the alloys up to 90%  $\text{Cu}_2\text{GeS}_3$  have a zincblend structure, while materials containing more than this were tetragonal.

The compound  $\text{Cu}_2\text{GeSe}_3$  forms a partial solid solution with  $\text{CuGe}_2\text{P}_3$  in the range  $0.1 \geq x > 0.75$ , when  $x$  is the fraction of  $\text{Cu}_2\text{GeSe}_3$ . These alloys have a zincblend structure, except that alloys containing more than 90%  $\text{Cu}_2\text{GeSe}_3$  are tetragonal.

An alloy system between  $\text{CuSi}_2\text{P}_3$  and Si was also studied. Alloys up to 33% Si per mole were obtained; results at higher Si solid solution were inconclusive. All the alloys have a zincblend structure and the lattice parameters change from  $5.244 \text{ \AA}$  for  $\text{CuSi}_2\text{P}_3$  to  $5.292 \text{ \AA}$  for 33% Si per mole.

In all the cases mentioned above, the lattice parameters obeyed Vegard's law.

The materials were initially investigated in polycrystalline form and attempts were made later to grow single crystals of the single phase materials. A simple modification was carried out on the Bridgman technique and single crystals were successfully grown. Large crystals having diameters of 1.3 cm and lengths of 3 cm were grown for  $\text{CuGe}_2\text{P}_3$ ,  $\text{Ag}_6\text{Ge}_{10}\text{P}_{12}$  and  $\text{CuGePS}$ . Iodine transport was successfully used for growing  $\text{CuZnGe}_3\text{P}_5$ , whereas for the high melting point compounds such as  $\text{CuSi}_2\text{P}_3$ , tin solution growth produced crystals of size  $0.02 \times 0.3 \times 0.5 \text{ cm}$ .

Different cooling rates between 1 and 6 °C/h produced single crystals of all materials. These cooling rates did not make remarkable changes in the physical properties of  $\text{CuGe}_2\text{P}_3$ , whereas it was very sensitive in the Cu-Ge-P-S system.

DTA results showed remarkable changes in the melting point of  $\text{CuGe}_2\text{P}_3$  between 760 and 830 °C. These melting points are thought to be pressure dependent. The measurements also showed the cooling line for the phase diagram of  $\text{CuGe}_2\text{P}_3$ -Ge to lie below the heating line. Analysis of  $\text{Ag}_6\text{Ge}_{10}\text{P}_{12}$  showed a single phase material, while more than one phase appeared for the  $\text{AgGe}_2\text{P}_3$  compound. No secondary peaks were found for  $\text{CuSi}_2\text{P}_3$ .

High temperature X-ray results showed linear thermal expansion for single crystals of  $\text{CuGe}_2\text{P}_3$  for temperatures up to the melting point, but the expansion coefficient for polycrystalline samples was temperature dependent and decomposition occurred above 620 °C.

A high carrier concentration was observed for all the crystals and analysis of the electrical properties was rather difficult. However, some results were obtained for one of the crystals of  $\text{Ag}_6\text{Ge}_{10}\text{P}_{12}$ . Acceptor levels were quite clear and obeyed the Pearson and Bardeen suggestion [139], but the activation energies were much smaller than the values calculated from the hydrogenic model. Acceptor energy levels for low carrier concentrations of sulphide alloys were calculated from conductivity data, but acceptor levels for the other materials could not be calculated. Low mobility was found for all materials. Mobility data analysis was carried out using a method similar to that successfully employed for  $\text{CuInS}_2$  and  $\text{CuInSe}_2$  [151,152].

The scattering mechanisms were determined from the temperature dependence of carrier mobilities using the standard expressions of the Brooks-Herring

theory [135]. The agreement between experimental and theoretical values is satisfactory for  $\text{Ag}_6\text{Ge}_{10}\text{P}_{12}$ , particularly for temperatures higher than 200 °K. However, liquid helium temperature would be required to gain more knowledge of the ionised and neutral scattering. The ionised impurity scattering and lattice scattering mechanisms appeared clearly in most of the mobility curves for the materials investigated.

X-Ray powder photographs showed good quality thin films of  $\text{Ag}_6\text{Ge}_{10}\text{P}_{12}$  as evaporated and of  $\text{CuGe}_2\text{P}_3$ , but only after annealing in phosphorus vapour.

Epitaxial growth of  $\text{CuGe}_2\text{P}_3$  on GaP showed results which could have applications in some devices.

## 9.2 Suggestions for Further Work

To gain more understanding of the formation of diamond-like semiconductors, new compounds and alloys will have to be prepared and examined.

Group I-IV<sub>2</sub>-V<sub>3</sub> compounds are perhaps the least studied ternary materials so far.  $\text{CuGe}_2\text{P}_3$  is the only compound in this group which has been studied in some detail. A similar investigation could be carried out on  $\text{CuSi}_2\text{P}_3$ . The various compositions of Cu-Si-P (Gibb's triangle, see Figure 3.1, Chapter 3), should be studied first in the case of  $\text{CuSi}_2\text{P}_3$ . Compositions on the tie lines of  $\text{Cu}_3\text{P}$ - $\text{Si}_3\text{P}_4$  and  $\text{CuP}_3$ -Si in the Gibb's triangle are expected to give some single phase material, while a complete solid solution could be expected towards Si and  $\text{Si}_3\text{P}_4$  from the cross-section of the two lines which intersect to form  $\text{CuSi}_2\text{P}_3$  (see Sections 5.5 and 5.9, Chapter 5).

Solid solutions with binary and ternary compounds could also be explored. Especially interesting would be solid solutions with ternary compounds of the type  $I_2$ -IV- $V_3$ , particularly when group IV is Si, such as solid solutions with  $Cu_2SiS_3$  and  $Cu_2SiSe_3$ .

Due to the high melting point of  $CuSi_2P_3$ , solution growth techniques would have to be used. Tin solution growth was used successfully to grow  $CuSi_2P_3$ , (see Section 3.5 in Chapter 3).

A study of phase diagrams of  $CuSi_2P_3$  with Sn should be undertaken to explore the possibility of using this solvent. Other possible solvents, *e.g.*, Sb, Bi and Pb could also be studied. This might lead to a better solvent for this material being found.

The  $CuSi_2P_3$  crystals prepared from tin solution may be in good quality and size, but are highly Sn doped. Iodine transport could prove to be another solution for preparing these materials.

Doping is another important aspect of the study of  $CuSi_2P_3$ . The material could be doped by the presence of suitable impurities in tin or the vapour transport chamber. A survey will have to be carried out to ascertain the percentage of the impurities introduced into the reaction region and the percentage of impurities incorporated in the material and subsequent properties. The undoped materials are heavily *p*-type, but *n*-type materials could perhaps be produced if S, Se, Te or Zn, Cd are used. This might lead to the production of a *p-n* junction.

The range of various possible compounds and solid solutions between compounds, offers considerable scope for investigation by optical techniques. For example, the high carrier concentration in our typical samples of  $CuGe_2P_3$  obscures any studies of optical properties, but investigations into the optical properties of the  $CuGe_2P_3$ - $Cu_2GeS_3$  system

might lead to some specific information on the properties of  $\text{CuGe}_2\text{P}_3$ . The results on  $\text{Cu}_2\text{GeS}_3$  and solid solutions would be of additional interest.

It would be of interest to study the Hall effect at low temperatures, to detect neutral and ionised impurities more easily, while at temperatures higher than 450 °K, some information might prove more accurate on  $N_A$  and  $N_D$  and the energy gap could be calculated. However, the latter is more interesting, particularly for the phosphide materials, due to the optical measurement difficulties.

Another field of interest would be the influence of controlled impurities upon the properties described earlier. Optical and electrical properties under high pressure could result in interesting academic investigations.

Thin films could be another interesting area to study under the various conditions mentioned earlier. Films of  $\text{Cu}_2\text{GeS}_3$  and its solution with  $\text{CuGe}_2\text{P}_3$  could be prepared using the same method as for  $\text{CuGe}_2\text{P}_3$ . Films of  $\text{CuSi}_2\text{P}_3$  are more difficult to prepare. A possible method might be to prepare a Cu-Si<sub>2</sub> alloy, which could be annealed under phosphorus pressure to produce  $\text{CuSi}_2\text{P}_3$  film.

REFERENCES

1. R.H. Wentorf and J.S. Kasper, *Science*, 1963, 139, 338.
2. F.P. Bundy and J.S. Kasper, *J. Chem. Phys.*, 1967, 46 (9), 3437.
3. H.G. Grimm and A. Sommerfeld, *Zs.Physik.*, 1926, 36, 36.
4. B.R. Pamplin, *Nature (London)*, 1960, 188, 136.
5. E. Parthe, *Z. fur Kristallographie*, 1963, 119, 204.
6. E. Parthe, "Crystal Chemistry of Tetrahedral Structures", Gordon and Breach, 1964 (English Ed.), 1972 (French Ed.).
7. B.R. Pamplin, PhD Thesis, University of Nottingham, 1960.
8. E. Mooser and W.B. Pearson, *Acta Cryst.*, 1959, 12, 1015.
9. W.B. Pearson, "Semiconducting Materials", Izd. an SSSR, (Moscow), 1960, p.249.
10. N.A. Goryunova, "Chemistry of Diamond-like Semi-conductors", Chapman and Hall Ltd., (London), 1965.
11. B.R. Pamplin, "Progress in Crystal Growth Characteristics", Pergamon Press Ltd., 1981, Vol.3, pp.179-192.
12. R. Marchand and J. Lang, *Mat. Res. Bull.*, 1971, 6, 845.
13. B.R. Pamplin, *J. Phys. Chem. Solids*, 1964, 25, 675.
14. N.A. Goryunova and E. Parthe, *Mat. Sci. Eng.*, 1967, 2, 1.
15. E.L. Amma and G.A. Jeffrey, *J. Chem. Phys.*, 1961, 34, 252
16. N.L. Smirnova, *Soviet Phys. Cryst.*, 1958, 3, 232.
17. N.L. Smirnova, *Soviet Phys. Cryst.*, 1960, 4, 10.
18. W. Schafer, K. Scheunemann and R. Nitsche, *Mat. Res. Bull.*, 1980, 15, 933.
19. A. Rabenav and P. Eckerlin, *Naturwiss.*, 1959, 46, 106.
20. P. Eckerlin, *Fortschr. Mineral*, 1961, 39, 334.

21. N.A. Goryunova and C.S. Grigoreva, *Z. Tekh. Fiz.*, 1956, 26 (10), 2157.
22. J.C. Woolley and B.A. Smith, *Proc. Phys. Soc.*, 1958, 72, 867.
23. N.A. Goryunova and V.I. Sokolova, *Izv. Moldavsk. Filiala Akad. Nauk SSSR*, 1960, 3 (69), (31), 192.
24. V.I. Sokolova and E.V. Tsvetkova, *Issled Po Poluprov.*, *Akad. Nauk Moldavsk. SSR Fiz. i Mat.*, 1964, 168.
25. N.A. Goryunova, V.M. Orlov, V.I. Sokolova, G.P. Shpenkov and E.V. Tsvetkova, *Phys. Stat. Sol. (a)*, 1970, 3, 75.
26. W. Honle and H.G.V. Schnering, VIth International Conf. on Solid Compounds of Transition Elements, Stuttgart FRG, June, 1979, pp.101-102.
27. N.N. Koshna and S.S. Tolkach, *Proc. Len. Inst.*, 1964, 16, 154.
28. H.G.V. Schnering and K.G. Hausler, *Rev. Chim. Min.*, 1976, 13, 71.
29. E.H. Werner-Koster, *Z. Met. Bd.*, 1971, 62, H11.
30. M. Bernara, *J.D.E. Phys. Coll. C<sub>3</sub>, Suppl.No.9*, 1975, 36, 1.
31. A.A. Vaipolin, N.A. Goryunova, E.O. Osmanov, Yu.V. Rud and D.N. Tretyakov, *Dokl. Chem.*, 1964, 154, 146.
32. O.G. Folberth and H. Peiester, *Acta Cryst.*, 1961, 14, 325.
33. J. Rivet, J. Flahaut and P. Laurelle, *Compt. Rend. Acad. Fr.*, 1963, 257, 161.
34. H. Hahn and A. dc Lorent, *Naturwiss.*, 1958, 24, 621.
35. S.I. Radaoutsan, *Rev. Roumaine Phys.*, 1964, 9, (3), 293.
36. L.I. Berger and V.D. Prochukhan, "Ternary Diamond-like Semi-conductors", Consultants Bureau, (New York), 1969.
37. J.L. Shay and J.K. Wörnack, "Ternary Chalcopyrite Semi-conductors", Pergamon Press, 1975.
38. V.I. Sokolova, Abstracts of Union Conf. on Semi-conducting Compounds, M. L. Lzd. an SSSR, 1961, p.60.

39. B. Chalmers, "Modern Research Techniques in Physical Metallurgy", Amer. Soc. for Metals, 1953, p.170.
40. J.W. Rutter and B. Chalmers, *Can. J. Phys.*, 1953, 31, 15.
41. W.A. Tiller, F.A. Jackson, J.W. Rutter and B. Chalmers, *Acta Met.*, 1953, 1, 428.
42. D.T. Hurlé, *J. Sol. State Electronics*, 1961, 3, 37 and 142.
43. W.A. Tiller, "The Art and Science of Growing Crystals", J. Wiley & Sons, 1966, p.294.
44. P.W. Bridgman, *Amer. Acad. Arts SCS*, 1925, 60, 303.
45. W.P. Davey, *Phys. Rev.*, 1925, 25, 243.
46. C.F. Elam, *Proc. Roy. Soc.*, 1926, A112, 289.
47. J.A. Dillon, *Rev. Sci. Instr.*, 1930, 1, 36.
48. S.L. Quimpy, *Phys. Rev.*, 1932, 39, 345.
49. D.C. Stockbarger, *Rev. Sci. Instr.*, 1936, 7, 133.
50. D.C. Stockbarger, *Disc. Faraday Soc.*, 1949, 5, 294.
51. G. Tammann, "Metallography", (trans.) Dean and Swanson, Chemical Catalogue Co., (New York), 1925, p.26.
52. J. Obreimov and L. Schubntkov, *Z. Phys.*, 1924, 25, 31.
53. M. Chesswas, B. Cockayne, D.T. Hurlé, E. Jakeman and J.B. Mullin, *J. Cryst. Growth*, 1971, 11, 225.
54. E. Buehler and J.H. Wernicr, *J. Cryst. Growth (C)*, 1971, 8, 324.
55. A.A. Vaipolin, E.O. Osmanov and D.N. Tret'yakov, *Izv. Akad. Nauk SSSR, Neorg. Mater.*, 1967, 3, (2), 260.
56. International Critical Tables, V.S. Nat. Res. Council, McGraw-Hill, (New York), 1933.
57. A.J. Springthorpe and B.R. Pamplin, *J. Cryst. Growth*, 1968, 3 (4), 313.



58. H. Schafer, "Chemical Transport Reactions", Academic Press, (New York), 1964.
59. D.K. Wickenden and R.W. Brander, "Crystal Growth from the Vapour", (Ed.) B.R. Pamplin, The General Electric Co. Ltd., (Hirst Research Centre, Wembley), 1975, p.410.
60. M.W. Richardson and B. Nolong, *J. Cryst. Growth*, 1976, 34, 198 and 205; *idem, ibid.*, 1977, 42, 90.
61. E. Wolf, H. Oppermann, G. Krabbes and W. Reichelt, "Current Topics in Material Science", (Ed.) E. Kaldis, Vol.1, North Holland, 1978, p.697.
62. M.M. Faktor and I. Garrett, "Growth of Crystals from the Vapour", Chapman and Hall, (London), 1974.
63. D.W. Show, *J. Electrochem. Soc.*, 1968, 115, 405.
64. B. Lewis, "Crystal Growth", (Ed.) B.R. Pamplin, Pergamon Press, (New York), 1972, Ch.2.
65. Yu.A. Volov, T.A. Dorazhkina and R.L. Rlechko, *Izv. Akad. Nauk SSSR, Neo. Mat.*, 1968, 14 (6), 881.
66. H.R. Widemeier and A.G. Sigai, *J. Cryst. Growth*, 1969, 6, 67.
67. H. Le Chatelier, *Compt. Rend.*, 1887, 104, 1443.
68. H. Le Chatelier, *Compt. Rend.*, 1887, 104, 1517.
69. W.C. Roberts-Austen, *Proc. Inst. Mech. Eng. (London)*, 1899, 1, 35.
70. W.J. Smothers and M.S. Chiang, "Differential Thermal Analysis", Chemical Publishing Co. Inc., (New York), 1958.
71. M. Hansen, "Constitution of Binary Alloys", McGraw-Hill Co. Inc., (New York), 1958.
72. P.L. Arens, "A Steady of DTA of Clays and Clay Minerals", Excelsiors, (The Netherlands), 1951.

73. M.D. Judd and M.I. Pope, *J. Inorg. Nucl. Chem.*, 1971, 33, 365.
74. S.L. Boersma, *J. Amer. Ceram. Soc.*, 1955, 38, 281.
75. F.H. Norton, *J. Amer. Ceram. Soc.*, 1936, 22, 54.
76. L.H. Berkelhamer, U.S. Bur. Mine Report Invest. 3762, 1944, 17pp.
77. R.W. Grimshaw, E. Heaton and A.L. Robert, *Trans. Brit. Ceram. Soc.*, 1945, 44, 76.
78. D. McConnell and J.W. Earley, *J. Amer. Ceram. Soc.*, 1951, 34, 183.
79. I.A. Berger and W.L. Whitehead, *Fuel*, 1951, 30, 347.
80. I.K. Belova, V.M. Koshkin and L.S. Palatnik, *Izv. Akad. Nauk SSSR, Neo. Mat.*, 1967, 3, (4), 617.
81. J.D. Wiley, E. Buehler, J.L. Shay and J.H. Wernick, *J. Electronic Mat.*, 1973, 2, 601.
82. L.S. Palatnik and E.K. Belova, *Izv. Acad. Nauk SSSR, Neo. Mat.*, 1967, 3, 2194.
83. E. Buehler, J.H. Wernick and J.D. Wiley, *J. Electronic Mat.*, 1973, 2, 445.
84. B.W. Neate, D. Elwell, S.H. Smith and M.D. Agostino, *J. Phys. Ed. Sci. Inst.*, 1971, 4, 775.
85. P.W. Bridgman, *Proc. Amer. Acad. Arts Sci.*, 1948, 76, 55.
86. P.W. Bridgman, *Proc. Amer. Acad. Arts Sci.*, 1929, 64, 51.
87. P.W. Bridgman, *Phys. Rev.*, 1935, 48, 893.
88. P.W. Bridgman, *Proc. Amer. Acad. Arts Sci.*, 1952, 81, 1965.
89. G.C. Kennedy and R.C. Newton, "Solids Under Pressure", (Eds) W. Paul and D.M. Warschaver, McGraw-Hill Co. Inc., (New York), 1963.
90. W. Klement, L.H. Cohen and G.C. Kennedy, *J. Phys. Chem. Solids*, 1966, 27, 155.

91. E. Raport and G.C. Kennedy, *J. Phys. Chem. Solids*, 1966, 27, 93.
92. L. Maissel, *J. Appl. Phys.*, 1960, 31, 211.
93. R. Feder and H.P. Charbnau, *Phys. Rev.*, 1966, 149, (2), 464.
94. T.B. Light, M. Berkenbit and A. Reisman, *J. Electronic Soc.*, 1968, 115, 969.
95. W.E. Schoknecht and R.O. Simmons, American Institute of Physics, Conf. Proc., 1972, 3, 169.
96. R.M. Nicklw and R.A. Young, *Phys. Rev.*, 1964, 129, 1936.
97. R.D. Fouchaux and R.O. Simmons, *Phys. Rev.*, 1964, 136A, 1664.
98. M.E. Straumanis, J.P. Krumme and M. Rubenstein, *J. Electrochem. Soc.*, 1967, 114, 640.
99. L. Bernstein and R.J. Beals, *J. Appl. Phys.*, 1961, 32, 122.
100. E.D. Pierron, D.L. Parker and J.B. McNeely, *J. Appl. Phys.*, 1967, 38, 4669.
101. V.M. Glazov, A.Ya. Nashelskii and A.D. Lyutealibekova, *Elektron. Tekh. Nauch. Tekhn. Sb. Mat.*, 1970, 5, 33.
102. I. Kudman and R.J. Paff, *J. Appl. Phys.*, 1972, 43, 3760.
103. Glen A. Slack and S.F. Bartram, *J. Appl. Phys.*, 1975, 46, 89.
104. W.B. Pearson, "Handbook of Lattice Spacing and Structure of Metals and Alloys", Vol.2, Pergamon Press, (Oxford), 1967.
105. W.L. Bragg, *Cambridge Phil. Soc.*, 1912, 17, 43.
106. P. Debye and P. Scherrer, *Phys. Zeit.*, 1916, 17, 277.
107. A.A. Vaipolin, E.O. Osmanov and D.N. Treyakov, Reports XXth Int. Congress Theo. and Appl. Chem. Yupak, Moscow, 1965.
108. N.A. Goryunova and V.D. Prochukhan, *Fiz. Tverd. Tela*, 1960, 2, 176.
109. B.B. Baronov, V.D. Prochukhan and N.A. Goryunova, *Izv. Akad. Nauk Latv. SSSR*, 1965, 3, 301.
110. P.C. Donohue and H.S. Young, *J. Solid State Chem.*, 1970, 1, (2), 143.

111. R. Solomon, *J. Electrochem. Soc.*, 1961, 108, (7), 716.
112. O.G. Folberth and H.J. Welker, *Phys. Chem. Solids*, 1959, 8, 14.
113. N.A. Goryunova, S. Mamaev, and V.D. Prochukhan, *DAN*, 1962, 112, (3), 628.
114. N.A. Goryunova and V.S. Grigoreua, *Zh. T.F.*, 1959, 26, 10.
115. N.A. Goryunova, V.I. Sokolova and Chiang Ping-Hsi, *Zh. Prikl. Khim.*, 1965, 38, 771.
116. N.A. Goryunova and Chiang Ping-Hsi, Abstracts of papers presented at the All-Union Conf. on Semi-conducting compounds, *Izd. AN SSSR*, Moscow, 1961, p.21.
117. B.B. Sharma and . Hari Singh, *J. Solid State Chem.*, 1974, 11, 285.
118. H. Neumann, W. Kissinger, Falah S. Hasoon, B.R. Pamplin, H. Sobotta and V. Riede, *J. Phys. State Solids (b)*, 1985, 127, K9.
119. C.H.L. Goodman, *J. Phys. Chem. Solids*, 1958, 6, (4), 305.
120. G.K. Averkieva and A.A. Vaipolin, Abstracts of papers presented at the All-Union Conf. on Semi-conducting compounds, *Izd. AN SSSR*, Moscow, 1961, p.4.
121. L.S. Palatnik, Yu.F. Komnik, E.K. Belova and L.V. Atroshchenko, *Ukr. Fiz. Zh.*, 1963, 8, 263.
122. J. Rivet, *Bull. Soc. Chem.*, 1963, 12, 2703.
123. B.B. Sharma, R. Ayyar and H. Singh, *J. Phys. State Solids (a)*, 1975, 29, K17.
124. E. Parthe and J. Garin, *Monatsch. Chem.*, 1971, 102, (5), 1197.
125. N.A. Goryunova, G.H. Averkieva and Y.V. Alekseev, *Izv. Mold. Fil. Akad. Nauk SSSR*, 1960, 3, 99.
126. N.A. Goryunova, G.K. Averkieva and A.A. Vaipolin, in "Physics", Proc. 23rd Sci. Conf., Leningrad Structural Engineering Inst., 1965, p.52.
127. R.A. Maslyanko and M.M. Markus, *Issled. Slozhn. Poluprov.*, 1970, 154.

128. G.K. Avekiva, A.A. Vaipolin and N.A. Goryunova, "Soviet Research in New Semi-conductor Materials", Consultants Bureau, (New York), 1965, 26.
129. M. Kaanafer, O. Gorochov and J. Rivet, *Mat. Res. Bull.*, 1974, 9, 1543.
130. L.S. Palatnik, V.M. Koshkin, L.P. Galchinetskii, V.I. Kolesnikov and Yu.F. Komnik, *Fiz. Tverd. Tela*, 1962, 4, 1430.
131. H. Kingen, W. Ness and H. Schulze, *Naturwiss.*, 1966, 53, 18.
132. W.B. Pearson, *Acta Cryst.*, 1964, 17, 1.
133. T.M. Palmer, *Elect. Eng.*, 1966, 38, 467.
134. J.S. Blakemore, "Semi-conductor Statistics", Pergamon Press, 1962.
135. E.H. Putley, "The Hall Effect and Related Phenomena", Butterworth, (London), 1960.
136. H. Neumann, E.U. Ried, H. Sobotta, M.S. Omar and B.R. Pamplin, *Solid State Commun.*, 1985, 53, (2), 155.
137. B.R. Pamplin, T. Kiyosawa and K. Masumoto, *Progr. Cryst. Growth Character*, 1979, 1, 331.
138. H. Neumann, *Cryst. Res. Technol.*, 1983, 18, 483.
139. G.L. Pearson and J. Bardeen, *J. Phys. Rev.*, 1949, 75, 825.
140. L. Pincherle, *Proc. Phys. Soc. (London)*, 1951, A64, 663.
141. D. Long and J. Myers, *Phys. Rev.*, 1959, 115, 5.
142. E. Conwell and V.F. Weisskopf, *Phys. Rev.*, 1950, 77, 388.
143. L.B. Ziatkin, Y.F. Markova, A.I. Stekhanov and M.S. Shur, *Phys. State Solids*, 1969, 32, 473.
144. H. Fritzsche and K. Lark-Horovitz, *Physica XXth Amsterdam Conf. on Semi-conductors*, 1954, pp.834-844.
145. J. Bardeen and W. Shockley, *Phys. Rev.*, 1950, 80, 72.
146. J.E. MacDonald and G.A. Saunders, in the press.
147. J.D. Wiley and M. Didomenico Jr., *Phys. Rev. B*, 1970, 2, 427.

148. C. Hilsum and A.C. Rose-Innes, in "Semi-conducting III-V Compounds", Pergamon Press, (New York), 1961.
149. J.D. Wiley, *Solid State Commun.*, 1970, 8, 1865.
150. D.L. Rode, *Phys. Rev. B*, 1970, 2, 4036.
151. Taizo Irie, Saburo Endo and Shigeo Kimora, *J. Appl. Phys.*, 1979, 7, 1303.
152. D.C. Look and J.C. Manthuruthil, *J. Phys. Chem. Solids*, 1976, 37, 173.
153. H. Ehrenreich, *J. Phys. Chem. Solids*, 1959, 8, 130.
154. D.M. Brown and R. Bray, *Phys. Rev.*, 1962, 127, 1593.
155. R. Vaidhyathan, PhD Thesis, Indian Institute of Technology, Madras, 1984.
156. K. Kohler, H.J. Queisser, W. Honle, H.G. Von Schnering and M.C. Bohm, in the press.
157. W.W. Tyler and H.H. Woodburn, *Phys. Rev.*, 1956, 102, 3.
158. N. Avagerions, PhD Thesis, University of Salford, 1984.
159. V. Riede, H. Neumann, W. Sobotta, W. Kissinger, M.S. Omar and B.R. Pamplin, *Phys. State Solids (b)*, 1984, 123, K119.
160. M.V. Below and C.M. Wayman, *J. Appl. Phys.*, 1967, 38, 5119.
161. H. Neumann, G. Kühn and B. Schumann, "Progress of Crystal Growth Characteristics", Vol.3, Pergamon Press, 1981, pp.157-178.
162. R.H. Rediker, K. Stopek and J.H.R. Ward, 1964, 7, 621.
163. O.G. Folberth, *Halbleiterprobleme*, 1960, 5, 40.
164. C.J. Frosch and L. Derick, *J. Electrochem. Soc.*, 1961, 103, (2), 251.
165. J.W. Allen and R.J. Cherry, *J. Phys. Chem. Solids*, 1962, 23, 509.
166. H.G. Grimmeiss and G. Olofsson, *J. Appl. Phys.*, 1969, 40, 2526.
167. H.G. Grimmeiss and H. Scholz, US Patent 3,261,080, July, 1966.
168. R.G. Schulze and P.E. Petersen, US Patent 3,915,754, October, 1975.